A. Barucci, R. Carpi, A. Ciccarone,
M. Esposito, M. Olmastroni, G. Zatelli

Magnetic Resonance Spectroscopy
Data Analysis for Clinical Applications

IFAC
Book Series

A. Barucci, R. Carpi, A. Ciccarone,
M. Esposito, M. Olmastroni, G. Zatelli

MAGNETIC RESONANCE SPECTROSCOPY

DATA ANALYSIS FOR CLINICAL APPLICATIONS

A. Barucci, R. Carpi, M. Esposito, M. Olmastroni, G. Zatelli

MAGNETIC RESONANCE SPECTROSCOPY

DATA ANALYSIS FOR CLINICAL APPLICATIONS

IFAC

Book Series

INDEX

PREFACE

This text is taken from the postgraduate thesis, which one of the authors (A.B.) developed for the degree of Medical Physicist in the School on Medical Physics of the University of Florence.

The text explores the feasibility of quantitative Magnetic Resonance Spectroscopy as a tool for daily clinical routine use. The results and analysis comes from two types of hyper spectral images: the first set are hyper spectral images coming from a standard phantom (reference images); and hyper spectral images obtained from a group of patients who have undergone MRI examinations at the Santa Maria Nuova Hospital.

This interdisciplinary work stems from the IFAC-CNR know how in terms of data analysis and nanomedicine, and the clinical expertise of Radiologists and Medical Physicists.

The results reported here, which were the subject of the thesis, are original, unpublished, and represent independent work.

Chapter 1

INTRODUCTION

Proton magnetic resonance spectroscopy (MRS) is provided as an option by most manufacturers and is becoming more common in clinical practice, particularly for prostate and neurological applications. Although MRS can be performed on nuclei such as ^{31}P and ^{13}C, proton (^{1}H) MRS is the easiest and least expensive spectroscopy for all MRI system because requires only a test phantom and a common software package which automate acquisition sequences and post-processing for metabolites quantification. Non-proton spectroscopy indeed requires radio frequency (RF) coils tuned to the Larmor frequency of other nuclei plus matching preamplifiers, hybrids, and a broadband power amplifier. Sometimes however, the efficient implementation of MRS acquisition protocols is beyond the expectations for most MR technologists, therefore MR physicists are often called in to perform MRS procedures to evaluate whether problems with proton MRS are due to equipment malfunctions, software problems, or operator errors.

In this thesis we focus on some of these problems.

1.1 - Single Voxel Spectroscopy

Techniques for quantitative localized *in vivo* magnetic resonance spectroscopy (qMRS) have been available for 30 years and were used in countless research projects [Ref. 91, 136, 218 - 219]. The potential value of qMRS in a clinical setting has especially been demonstrated in the characterization of pathologic tissue changes, where the diagnosis is not evident in MR imaging and in tissues that are not readily available to biopsy (e.g., intracerebral tumors) [Ref. 220]. Despite the fact that localized *in vivo* MR spectroscopy is noninvasive, and produces quantitative biochemical information [Ref. 137], its use in clinical routine examinations is still very limited. There are several reasons for this.

First, as MR images are closely linked to anatomical structures, their interpretation is for clinical radiologists much more intuitive than that of MR spectra. To interpret MR spectra correctly, knowledge about the signal acquisition and signal artifacts is mandatory. To obtain this knowledge, training is required with experienced spectroscopists, which is not possible in most clinical centers. Furthermore, background knowledge about cellular metabolism is also necessary in order to meaningfully interpret the limited number of metabolites in MR spectra. Compared to the immense amount of different structural proteins, enzymes, and metabolites of a human cell, the very few substances that can be measured using MR spectroscopy yield a low specificity and sensitivity in the context of pathologic tissue changes.

Second, clinical MR scanners and manufacturer's spectroscopy postprocessing software have greatly improved and became user-friendly in the recent years. However, most of them do not offer the possibility to quantify the measured metabolites in units of amount (expressed in mole) per unit volume. This implies that the user can only interpret peak area ratios, which is for some applications sufficient, but not for all. The inherent weaknesses of using peak area ratios [Ref. 137], is that the total number of quantifiable

metabolites decreases by one, and alterations in the peak ratio cannot be assigned unambiguously to changes in the concentration of the numerator or denominator. More serious are the indications that peak area ratios may introduce larger errors than qMRS [Ref. 221, 222]. In order to calculate ''absolute'' quantities of measured substances in a clinical setting, freely available quantification methods like AMARES, AQSES, QUEST, TDFDFIT [Ref. 74, 128, 149, 150, 223, 224], the free software package jMRUI [Ref. 145], or commercially available software like LC-Model can be used [Ref. 75]. Most of these applications have no, or only very rudimentary image display possibilities, preventing the study of MR spectra together with MR images of the same examination. As the currently available offline applications for qMRS do not support DICOM network transfer functionality, the acquired spectral data need to be exported manually from the main MR console (or satellite workstation), to a computer for quantification having one of the above mentioned programs installed. Additionally, none of the applications for qMRS offer any DICOM-typed reporting functionality, and therefore, reporting of quantitative results is normally done by the creation of text/html files and/or images (e.g., jpg, gif), or by manual insertion of screenshots of reports into a picture archiving and commu- nication system (PACS). Overall, in order to do clinical qMRS, most data handling has to be done manually, which is time consuming, and prone to errors. The time and financial cost of additional personnel makes qMRS unattractive in centers with intense workload, and prevents its use on a larger scale.

Third, qMRS of pathologic tissues requires the availability of normal values for comparison. Normal values, even within an organ (e.g., brain tissue), depend on voxel localization and subject age [Ref. 225 - 227]. Moreover, as large voxel sizes are needed for qMRS due to low signal-to-noise ratio, there is always partial volume effect of tissues with different MR spectroscopic profiles. The high variability of MR spectroscopic results further decrease the specificity and sensitivity of this method for the use in clinical routine. To minimize this variability, patient MRS results have to be compared to valid reference concentrations, and multiple databases per organ and age must be available. The currently available software packages do not offer any possibility of building up and using normal value databases, which prevents simple and easy to use comparison of patient data with reference data.

1.2 - Aim of this thesis

The aim of this thesis is to make quantitative MRS a more valuable and attractive tool for daily clinical routine use.

In the first part of this thesis we will give a brief overview of clinical proton MRS, discussing some common clinical MRS problems. In the second part we will focus on developing a standard protocol to confront the accuracy of different MR scanners from different vendors, analyzing water signals with the open source software package jMRUI – v5.0.

Then we will discuss some examples of T1, T2 estimation of water and metabolites at the 3T MR scanner of A.O.U. Meyer using the Siemens phantom aimed to quantitation of metabolites concentration. Some examples of quantitation coming from S.G.D. and S.M.N. hospital will be described too.

In the final part some examples of *in vivo* prostate cancer spectroscopic data analysis will be described, illustrating the potential of MRS, the differences between Philips data

analysis software and jMRUI-v5.0, and showing the problems in the daily clinical routine acquisitions too. These MRS data have been acquired at Philips Achieva 1.5 T (S.M.N. hospital).

As a future development we will describe an interesting application of PMMA and gold nanoparticles to MR, using the know-how coming from biophotonics research at IFAC-CNR.

Chapter 2

MAGNETIC RESONANCE SPECTROSCOPY

Usually the principal application of MR is imaging, but a very important and promising application is the Magnetic Resonance Spectroscopy. This section is a short review of proton magnetic resonance spectroscopy based on the Report of AAPM MR Task Group #9 [Ref. 13]. More details about the theory and principles of MRI can be found in [Ref. 9, 10, 11, 12].

2.1 - Larmor equation

If all the proton nuclei in a mixture of molecules had the same Larmor frequency, magnetic resonance spectra would be limited to a single peak. However, the magnetic B_0 field "seen" by a nucleus is shielded by the covalent electron structure surrounding the nucleus. Therefore, nuclei with different chemical neighbors will have slightly different resonance frequencies (f) given by

$$f = \gamma B_0 (1 - \sigma_{cs})$$

where σ_{cs} is a screening constant ($\sigma_{cs} \ll 1$). This small change in the resonance frequency is the basis for magnetic resonance spectroscopy. Note that both the overall molecular structure and the proton(s) position within the molecule will determine σ_{cs} or f.

2.2 - Magnetic resonance signal

In spectroscopy, the strength of the MR signal is proportional to the number of protons at that frequency. While spectroscopy can be described in the time domain, MRS data are usually displayed in the frequency domain. In the frequency domain, the area under a specific peak is proportional to the number of protons precessing at that frequency.

2.2.1 - Parts per million (ppm) scale

Although one could use a frequency axis to display spectra, two problems arise with this type of display. One, the axis is proportional to B_0 which means that peak locations on an axis will depend on the B_0 field used for the measurement. Second, there is no natural material to represent zero frequency. To overcome these problems, NMR chemists mix the substance to be measured with a reference, then express the frequency difference between the substance and the reference as a dimensionless quality, δ_{cs} (in parts per million), given by

$$\delta_{cs} = \frac{f_s - f_{ref}}{f_{ref} \times 10^{-6}}$$

where f_s is the frequency of the substance (laboratory frame) and f_{ref} is the frequency of the reference (laboratory frame). The reference used in proton spectroscopy is TMS (tetramethyl-silane, $(CH_3)_4Si$), and its single peak is assigned a chemical shift of 0.0 ppm. Another reference used is DSS (2,2-dimethyl-2-silapentane-5-sulfonate), and its major peak is at 0.0 ppm.

Since TMS and DSS are toxic, they are not used in *in vivo* spectroscopy. When spectra are acquired without TMS or DSS, another equation for δ_{cs} is as follows:

$$\delta_{cs} = \frac{f_s}{f_{transmitter}} 10^6 + \text{offset}$$

where f_s is the frequency of the sample (rotating frame), $f_{transmitter}$ is the frequency of the transmitter (laboratory frame), and *offset* is a constant that references the ppm scale to an *in vivo* standard, which for ^{1}H brain spectroscopy, is usually the CH3 peak of N-acetyl aspartate (NAA) with a chemical shift value of 2.01 ppm. Knowing the chemical shift of a peak, the value for offset can be determined by using the measured frequency (f_s) of the peak, the chemical shift of the peak (δ_{cs}), and the transmitter frequency. Once determined, this offset can be used to change all frequencies in a spectrum from Hz to ppm. For example with δ_{cs} = 2.01 ppm, f_s =71.8 Hz, and $f_{transmitter}$ = 63 863 375 Hz, the offset is equal to 4.700 ppm. In this example the transmitter frequency was centered on water. Note that the resonance frequency of water is dependent on temperature, with frequency increasing as temperature decreases ($\Delta ppm/\Delta °C = -0.01$ ppm/°C) [Ref. 14] At   37°C, δ_{cs} of water is 4.70 ppm; at 20°C, δ_{cs} of water is 4.87   ppm. Therefore water is not a good internal standard for the ppm scale.

2.2.2 - J coupling

Another feature of spectra is peak splitting or multiplets, caused by *J* coupling (spin–spin)[Ref. 15 -18]. With *J* coupling, the nuclear magnetic energy levels are split by quantum interactions, via covalent bond electrons, with other nuclei whose magnetic moments may be parallel or antiparallel to the main magnetic field. *J* coupling can be homonuclear (e.g., [1]H - [1]H) or heteronuclear (e.g. [1]H – [13]C).

A more intuitive classical explanation of *J* coupling can be given as follows. Suppose nucleus *A* is coupled to nucleus *X* and nucleus *X* has an equal probability of being in a parallel or an antiparallel spin state. Nucleus *A* will be split into two equal peaks. The peak of nucleus *A* that is coupled to nucleus *X* parallel to the main field will have higher frequency; the peak of nucleus *A* that is coupled to nucleus *X* antiparallel to the main field will have lower frequency. For lactate, the CH_3 nucleus at 1.31 ppm is coupled to the CH nucleus at 4.10 ppm, and the CH_3 nucleus is split into two equal peaks (doublet) separated by 6.93 Hz [Ref. 15]. Peak splitting from *J* coupling has the same absolute value in Hz, regardless of the main magnetic field strength.

In [Ref. 15, 19] have a list of *J* coupling constants for other metabolites. *J* coupling also causes phase evolutions that cause peak and baseline distortions that vary with echo time (TE, Ref. 16 -18) and field strength. *J* coupling explains the wellknown observation that the lactate doublet has negative peaks (180° out of phase) at TE 140 ms for a PRESS sequence. Less known is that *J* coupling also causes overlapping multiplet peaks within individual metabolites and between metabolites to cancel each other due to dephasing at

later echo times under typical *in vivo* field homogeneities. For this reason, metabolites such as glutamine (Gln), glutamate (Glu), and gamma-Aminobutyric acid (GABA) cannot be measured using long echo times ($T_E > 50$ ms) with *in vivo* proton spectroscopy [Ref. 19], although Ref. 20 uses a CPMG type sequence to overcome this problem. Some spectroscopy techniques use *J* coupling to eliminate overlapping peaks, in order to quantify concentrations of an underlying peak allowing the *in vivo* measurement of metabolites such as GABA [Ref. 21-23].

2.2.3 - Spectral resolution

The acquisition time depends on spectral resolution:

$$\Delta f = \frac{1}{T_{\text{Acq}}} = \frac{BW}{ns}$$

where T_{Acq} is the acquisition time, *BW* the bandwidth and *ns* the number of samples.

2.2.4 - Brain metabolites

Metabolites containing protons that can be measured in the brain at 1.5 Tesla include N-acetyl aspartate (NAA), considered to be present only in neurons and dendrites; N-acetylaspartylglutamate (NAAG), suggested to be involved in excitatory neurotransmission; creatine/phosphocreatine (Cr), a reservoir for high energy phosphate for generation of adenosine triphosphate (ATP); choline/phosphocholine/glycerophosphorylcholine (Cho), associated with glial cell membrane integrity; GABA, glutamate, and glutamine, important in neurotransmission, but very difficult to quantify *in vivo* due to multiplets and *J* coupling effects; myo-inositol (M-Ins), important in cell growth and possibly a glial cell marker; and sometimes lactate, indicative of anaerobic metabolism. Although NAA is considered a neuronal marker, changes in NAA from normal may reflect reversible changes in neuronal metabolism rather than irreversible changes in neuronal density. Ross *et al.* have a good discussion on neurometabolism and the clinical application of *in vivo* ^{1}H MRS [Ref. 24, 25].

2.2.5 - Prostate metabolites

Prostate cancer is the most prevalent non-cutaneous cancer in men and the second leading cause of cancer-related death in western countries [Ref. 26]. The use of MR in prostate cancer management is emerging, and the demand from patients and clinicians is increasing as a result of the growing number of men suspected of having prostate cancer due to the uptake of blood tests for prostate-specific antigen.

In vivo the detection of molecules is limited to those present at tissue levels of more than 0.5–1 mM. The first metabolite studied with *in vivo* was citrate, and a decrease in its resonances' amplitude was observed in prostate cancer patients compared with healthy controls [Ref. 27]. Next, the choline methyl resonance gained attention as an increase in this signal in prostate cancer was observed [Ref. 28, 29]. Due to frequency-selective water and lipid suppression, only signals of major metabolites between approximately 2.2 and 3.8 ppm

remain in prostate spectra, which also includes those of creatine and polyamines. Because the choline and creatine methyl signals are only separated by a relatively small chemical shift difference, a non-optimal B_0 homogeneity, causing line broadening, will lead to signal overlap. The presence of polyamine signals between these two metabolite signals further complicate their separation. This potential overlap led to the introduction of the signal ratio of choline plus creatine divided by citrate (Cho+Cr)/Cit [Ref. 28, 30] and its inverted counterpart [Ref. 29] as a marker for prostate cancer.

In this thesis, the major variables that can influence the (Cho+Cr)/Cit ratio are discussed. An overview of the main metabolites detectable in the commonly obtained MR spectra of the prostate, their function, and the acquisition parameters that influence their appearance in the spectrum will be provided. These metabolites form the basis for the (Cho+Cr)/Cit ratio, of which the intensity not only depends on the underlying physiology, metabolism, and anatomy, but also on the acquisition parameters. This latter aspect is particularly relevant for the citrate and polyamine signals.

Although ^{1}H-MRSI has great potential in prostate cancer management, its use in routine clinical practice is limited. A major hurdle toward clinical use is that several acquisition and processing steps still rely on manual procedures, in particular post-processing of the data, including quality control, and displaying easily visualized and interpretable results [Ref. 31]. A generalized classification scheme for prostate MRS to assist in prostate cancer management is not available. In the last part of this thesis some examples of *in vivo* measurements ratio will be discussed, looking for the introduction of a protocol-dependent classification scheme that could increase the clinical usability of the metabolite ratio for prostate cancer management.

The main metabolite signals in commonly obtained ^{1}H-MRSI spectra of the prostate are choline, creatine, polyamines and citrate.

Choline

Different compounds containing a choline moiety can contribute to the main peak at about 3.2 ppm in in vivo [1]H-MR spectra. These are free choline, glycerophosphocholine, and phosphocholine, but also contributions from protons in taurine, ethanolamines and myo-inositol may be present at this spectral position [Ref. 32]. As convenient shorthand, we refer to this composite resonance as the "choline" signal. Choline-containing metabolites are precursors and breakdown products of the phospholipid phosphatidylcholine, a major cell membrane compound [Ref. 33]. In prostate cancer cell lines, an increase in choline is observed due to an altered phospholipid metabolism [Ref. 34]. This alteration is probably due to an increased expression and activity of choline-kinase, a higher rate of choline transport, and an increased phospholipase activity [Ref. 33, 34].

The choline moiety has nine chemically equivalent protons of three methyl groups resonating as a singlet around 3.19 ppm and two methylene groups, resulting in two multiplets at 4.05 and 3.50 ppm [Ref. 15]. Because the intensity of these multiplets is very low in *in vivo* MR spectra of the prostate, it is common to only evaluate the nine-proton singlet at 3.19 ppm.

Creatine

Both creatine and phosphocreatine contribute to the methyl resonance observed at about 3.0 ppm in ^{1}H-MRS of the prostate (referred to, in combination, as the creatine signal

in this thesis). Creatine plays a crucial role in the energy metabolism of tissues [Ref. 35], as phosphocreatine acts as a spatial and temporal buffer to maintain constant adenosine triphosphate levels in tissue through the creatine-kinase reaction. The stromal cells consist predominantly of smooth muscle cells [Ref. 36], which are expected to contribute most to the creatine and phosphocreatine signals.

Creatine has five non exchanging protons: a methyl group resonating at 3.03 ppm and the methylene group at 3.93 ppm. The protons in each group are chemically equivalent and uncoupled, resulting in two singlets with a ratio of 3:2. The concentration of creatine was estimated with *in vivo* MRS at 4.4 ± 0.8 mM [Ref. 30] and with ex vivo high-resolution magic angle spinning spectroscopy as being between 7.6 ± 2.7 and 9.7 ± 4.4 mmol/kg for normal and cancer tissue (no significant differences) [Ref. 37].

Citrate

The production and storage of citrate is one of the main functions of the prostate. Citrate is an intermediate in the tricarboxylic acid cycle. In most organs, citrate is quickly oxidized in the tricarboxylic acid cycle and is therefore only present in low concentrations. In contrast, prostate epithelial cells actively produce citrate and store it in the luminal space, where it is one of the main components of the prostatic fluid [Ref. 38]. Prostate tissue has high levels of zinc, which inhibits mitochondrial (m-)aconitase activity. This leads to the buildup of a high concentration of citrate [Ref. 39]. In prostate cancer, a decrease in zinc levels is observed that leads to activation of m-aconitase and the consequential oxidation of citrate [Ref. 39]. At the same time, the morphology of the prostate gland changes, leading to a loss of luminal space, which might also cause a decrease in the observed (or total) citrate levels.

Citrate contains two methylene groups that are magnetically equivalent. The four protons of these groups form a strongly coupled AB spin system. The difference in chemical shifts, the midpoint of the chemical shifts, and the scalar coupling (J) of this spin system depend on pH [Ref. 40, 41] and cation concentration [Ref. 41] and are approximately 0.15 ppm, 2.61 ppm, and 16.3 Hz, respectively. Because citrate is a strongly coupled spin system, its shape depends on interpulse timing, pulse shape, T_E, and field strength [Ref. 40 - 46].

In the first *in vivo* prostate studies at 1.5T, stimulated echo acquisition mode (STEAM) and point resolved spectroscopy (PRESS) techniques were used for volume localization [Ref. 28, 47]. One advantage of the STEAM for these data is its ability to use a very short T_E (at the expense of the general loss of half of the signal in a stimulated echo). In this way, the strongly coupled protons of citrate will have limited phase evolution, which will result in an almost completely in-phase citrate signal. Integration of the area of the citrate peak(s) will then result in maximal signal intensity. For the PRESS sequence, generally longer T_E's are used for prostate MRS, and dispersive parts can be present in the spectrum that affect the peak area by cancellation with absorptive parts in simple integration. Several studies have been performed to determine the PRESS pulse timing with maximum absorptive signal at the central lines of the citrate signal [Ref. 42, 45, 48-51].

In the physiological range of pH (6.8 -7.4), variations in chemical shifts of 3.2 Hz and variations in the midpoint of the chemical shifts of 0.025 ppm were observed using a 400-MHz magnet [Ref. 40]. The changes in J are minimal in this pH range [Ref. 40, 41], but the concentrations of zinc, calcium, and magnesium also influence the value of this coupling [Ref. 41], which may have significant effects on the in vivo resonances. Ref. 52 shows that

small changes in chemical shifts and *J* can have substantial influences on the spectral shape of citrate. Although a relation was found in vitro between the spectral shape of citrate and the ion concentration or pH, variations in the spectral citrate shape *in vivo* are difficult to relate to ion concentrations or pH, as these are difficult to measure. For a good fitting, it is necessary to use a model signal that is based on values that closely resemble those present *in vivo*.

The RF pulses that are used to suppress the large lipid and water signals may adversely affect the citrate signals. Often dual frequency-selective pulses are used to suppress both these signals simultaneously, mainly by Mescher-Garwood (MEGA) [Ref. 53] or double band-selective inversion with gradient dephasing (BASING) [Ref. 54, 55] pulses. These pulses selectively invert the lipid and water resonances and are surrounded by crusher gradients. Their bandwidth and position in the frequency domain should be sufficient to invert all lipid signals, but distant enough from the chemical shift of citrate. When the bandwidth of the lipid inversion pulse is too broad, this will cause a decreased signal intensity of citrate. As a consequence, healthy spectra may get a "cancerous" profile. Therefore, a good adjustment of the dual frequency pulses is essential for obtaining consistent results. Spectrally selective refocusing pulses may be used instead of signal suppression pulses, which prevent refocusing of lipids by simultaneous volume and frequency selection [Ref. 56, 57]. Care should be taken that these pulses fully excite or refocus the citrate spins and leave the lipid signals untouched.

For proper selective suppression or spectral excitation, the homogeneity of the B_0 field is critical. Poor homogeneity will not only negatively affect spectral quality as it causes broadening of the spectral lines, it will also decrease the effectiveness of frequency selective pulses. Broadened or shifted fat and water signals can suffer from diminished suppression and components of these signals may overlap with the resonances of interest. In addition, in the case of shifted or broadened spectral lines of citrate, the metabolite can be influenced by the frequency selective pulses for lipid and water suppression leading to decreased citrate intensities.

The dependence of the citrate signals on interpulse timing can also be exploited for spectral editing. By varying this timing (at a constant T_E) in such a way that citrate is inverted in one measurement and in phase in the next measurement, uncoupled resonances can be removed from the spectrum by subtraction [Ref. 58, 59]. In this way, rapid citrate imaging without lipid suppression is possible.

Polyamines - Spermine

The tissue concentration of polyamines in the prostate is relatively high. Because spermine is the dominant polyamine in the prostate, we focus on this compound. Like citrate, polyamines are stored in the luminal space, and a very strong correlation between the citrate and spermine concentration is reported for prostatic fluid specimens [Ref. 60]. A hypothesis for the strong correlation is the formation of complexes between citrate and spermine since citrate is negatively charged, whereas spermine is positively charged. In this way ionic neutrality can be achieved [Ref. 60]. Polyamines play a role in prostatic growth and differentiation [Ref. 61]. A decrease in spermine has been suggested as a marker for prostatic malignancy [Ref. 61, 62]. In prostate cancer, a decrease in spermine or polyamine levels is observed compared with benign tissue using MRS [Ref. 62]. The incorporation of polyamine levels measured with MRS to improve detection of prostate cancer has been

proposed and has yielded an increased sensitivity at the same specificity [Ref. 63].

Spermine is a coupled spin system and, in addition to its amine groups, contains 10 methylene groups. These methylene protons consist of symmetrical pairs, giving a total of four protons that resonate approximately at 1.81 ppm with further groups of four at 2.11 ppm, 3.13 ppm, 3.12 ppm, and 3.18 ppm [Ref. 64]. These chemical shifts are pH-dependent [Ref. 65] and these quoted chemical shifts were measured at pH 7. At a higher pH, the amine groups are more protonated, and the chemical shifts are therefore more downfield [Ref. 65]. Protons near a nitrogen atom show the largest pH dependence. Spermine proton chemical shifts are also sensitive to temperature differences. For that reason, when one wants perform a phantom measurement to determine the shape of spermine (with a certain sequence), the phantom should be measured at body temperature and have a pH in the physiological range. Local chemical shift correction to improve the separation between choline and spermine is hindered by the dependence of the chemical shift of spermine on the environment. Also, usually no water reference measurement is done that could be used for this purpose. The metabolites in the prostate spectrum are unsuitable for this purpose, as the chemical shift of citrate is environment-dependent and choline is not always well separable from spermine.

As with citrate, T_E and interpulse timing influence the spectral shape of spermine and leading to dispersive components in the resonances. If dispersive parts are present in the 3.1-ppm region, this can negatively affect the apparent intensity of choline and/or creatine resonances. Furthermore, BASING and MEGA pulses that are used for simultaneous water and lipid suppression invert the 2.1- and 1.8-ppm resonances of spermine [Ref. 66]. Without these pulses and crushers, the 2.1- and 1.8- ppm resonances could be helpful for decomposition of spermine from the 3.1-ppm region. These measured spermine shapes can be used as prior knowledge for spectral fitting of the metabolites [Ref. 66]. T_1 and T_2 values of spermine reported in the literature are obtained in vitro and the T_2 values were rather short and dependent on the presence of ions and proteins [Ref. 65]. No *in vivo* data of relaxation times of spermine spins is available yet.

2.3 - Quantitative spectroscopy: evaluation of the metabolite ratio

Prostate spectra can be evaluated qualitatively or (semi-)quantitatively. Qualitative guidelines are based on visual inspection of the height of choline compared with the citrate height [Ref. 67, 68]. A more quantitative approach is the determination of metabolite concentrations in prostate spectra with the help of a reference compound. If the tissue water concentration is known in the volume of interest and the individual metabolites are fitted reliably, water can be used as an internal reference to obtain absolute prostate metabolite concentrations [e.g., Ref. 30, 69]. This requires additional time for a water reference measurement, which is often not available.

More practical, and sufficient for diagnostic purposes, is the use of the (Cho+Cr)/Cit ratio for classification. The usability of this ratio for prostate cancer localization was demonstrated in a prospective multicenter study, where an area under the receiver operating characteristic curve was obtained for discriminating normal peripheral zone tissue from cancer [Ref. 70]. Classification thresholds for the (Cho+Cr)/Cit ratio are needed to apply MR spectroscopy for prostate disease in clinical routine.

2.3.1 - Establishing the Ratio of (Cho + (Spm+) Cr)/Cit

The simplest method of calculating the [(Cho+Cr)/Cit] ratio is to use integration techniques and calculate a ratio based on these values (integral values; see Table 2, Ref. 52).

However, as discussed above, strong coupling effects and a long T_E can produce a spectral shape of citrate that has an integral close to zero, and small differences in citrate intensity will induce very variable ratios.

One way to circumvent this problem is by fitting the metabolites to a model signal. Model signals can be measured with phantom solutions [e.g., Ref. 66]. Alternatively, they can be simulated, when the chemical shifts and J-coupling constants are known for the metabolites of interest [e.g., Ref. 66, 71]. There are several software packages available that can be used to make model signals, including NMRSIM (part of Topspin, Bruker BioSpin Corporation, Billerica, Massachusetts, USA), GAMMA [Ref. 72], and its successor VeSPA (http://scion.duhs.duke. edu/vespa/), and jMRUI (java Magnetic Resonance User Interface, http://www.mrui.uab.es/mrui/). The model signals can be used to obtain fits of the metabolites in the time [Ref. 73, 74] or frequency domain [Ref. 75]. The output is typically a relative metabolite concentration value incorporating the amount of protons of the metabolite. These relative concentrations depend on the goodness of the fit and correlation between fits; for overlapping metabolites, overestimation of one metabolite at the cost of underestimation of another will result in a ratio that is unrepresentative for the tissue if the metabolites have a different amount of protons. Therefore, if the metabolites are fitted individually with such a quantification algorithm, the concentrations must be reconverted to their relative spectral amplitude prior to summation and division in the ratio. This procedure removes individual information gained from each metabolite but improves the reliability of the ratio. For spectral patterns dominated by absorption components, this amplitude ratio will give comparable results as the integral ratio. However, in contrast to the integral ratio, the amplitude ratio is less sensitive to the dispersive parts of citrate. The amplitude ratio gave good results for discrimination between different prostate tissues in a 3T study, where the spectral citrate shape had non-negligible dispersive parts [Ref. 70].

The fit of the individual metabolites has been used to derive the choline over citrate plus spermine ratio [Cho/(Cit+Spm)], a ratio that takes the counteracting effects of the increase in choline and decrease in citrate and spermine in prostate cancer into account [Ref. 66]. However, due to the inherent uncertainty in individual metabolite quantification [Ref. 76], it is usually recommended to use a [(Cho+Cr)/Cit] ratio rather than a simpler choline/citrate (or [Cho/(Cit+Spm)]) ratio. In most studies, spermine is not fitted individually [e.g., Ref. 87, 76-79], and spermine resonances are included in the creatine and choline fits [Ref. 63]. The ratio should therefore be seen as the [(Cho+(Spm+)Cr)/ Cit] ratio.

2.3.2 - Classification Thresholds for (Cho + (Spm+) Cr)/Cit Ratio

In the previous sections, the acquisition parameters that influence the prostate metabolite signals, and consequently the (Cho+(Spm+)Cr)/Cit ratio, were discussed. In principle, it is possible to correct for T_1, T_2 relaxation, and J-modulations and obtain a normalized ratio that is acquisition-independent. However, this requires knowledge of their precise values, which are not available (current reports show quite some variation in T_1, T_2), and these values may also vary for different tissue morphology (e.g., cancer, benign disease,

and normal prostate). Moreover, fitting of the individual metabolite signals is also necessary, which can be challenging due to the overlap between choline, creatine, and spermine signals. For that reason, we cannot work with a normalized ratio, and the [(Cho+Cr)/Cit] ratio thus has to be established per institution or per protocol.

The mean [(Cho+Cr)/Cit] plus two or three times the standard deviation of normal tissue was used as a cutoff value to classify voxels as cancerous [Ref. 29, 80-82]. The use of a five-point classification scale based on the mean and standard deviation of the [(Cho+Cr)/Cit] ratio of normal prostate tissue has been proposed [Ref. 68]. Because the [(Cho+Cr)/Cit] ratio is higher for normal transition zone tissue than for peripheral zone tissue, the cutoff values vary for the two tissues. Tables 2 and 3 in Ref. 52 provide an overview of reported mean [(Cho+Cr)/Cit] ratios for normal peripheral zone tissue at 1.5T and 3T. For 1.5T, the used T_E's in these studies are quite similar (120–130 ms) and often the same platform and post-processing methods are used, but there is quite some variation in the reported [(Cho+Cr)/Cit] ratios. At 3T, there are considerable differences between prostate spectroscopy packages of the vendors, with T_E's varying from 85 to 145 ms and TRs from 750 to 1300 ms (27). At 7T, optimal acquisition protocols still need to be established [Ref. 83]. The studies reporting [(Cho+Cr)/Cit] values for 3T spectra are still limited, but it can be expected that the metabolite ratios for normal tissue at 3T will be more variable among studies, and quite different [(Cho+Cr)/Cit] values would be obtained for the same patient measured on systems of different vendors. The dependency on acquisition and post-processing protocols asks for assessment of the mean and standard deviation of normal tissue per institution or per used protocol.

The derived classification thresholds are not necessarily institution-dependent. If the same acquisition protocol and post-processing method are used at different institutions, the [(Cho+(Spm+)Cr)/Cit] ratio can be compared between these institutions. Previously, no significant differences in the (Cho+Cr)/Cit amplitude ratio were found of any of the benign prostate tissues between patients among different institutions [Ref. 70]. Furthermore, the amplitude ratio gave good reproducibility in repeated measurements of the same subjects [Ref. 84].

2.4 - Magnetic field homogeneity

Spectral resolution is determined primarily by three factors. First, the transverse relaxation time (T_2) of the metabolite is inversely proportional to the ideal peak width. Second, the separation between peaks (in Hz) increases linearly with magnetic field strength. Third, the local magnetic field inhomogeneities widen and distort the spectral lines from their ideal Lorentizian forms. Maximum homogeneity is accomplished by adjusting DC currents in the gradient coils and room temperature shim coils. The name for this process is "shimming," which is a historical term that is derived from a time when magnetic resonance researchers were working on resistive pole–gap magnets and adjusted the magnetic field by placing thin brass shim stock between the magnet and pole faces to make them parallel.

Shimming

Improving magnetic field homogeneity increases *SNR* and narrows peak widths. Thus shimming improves both sensitivity and spectral resolution. Modern clinical MRI

systems use automated shimming routines to improve the homogeneity of the magnetic field by monitoring either the time-domain or frequency-domain MRS signal [Ref. 15, 88]. Note that the water signal (unsuppressed) is always used for shimming. *In vivo* a linewidth less than 0.05 ppm at 2-4 T is the requirement to perform MRS.

2.4.1 - Test Phantom

The MR system's manufacturer will supply a test phantom, usually an 18 to 20 cm diameter sphere containing metabolites. These concentrations emulate *in vivo* concentrations. Because test phantoms lack many *in vivo* metabolites, lipids, macromolecules, and susceptibility problems, they lead to well-resolved spectra with flat baselines, facilitating the detection of MRS acquisition or post- processing problems. A good MRS phantom is also required for an effective MRS quality control (QC) program.

Siemens supplies a spherical phantom, filled with a 0.1 M solution of $NaH_2C_3O_2$ (8.2g Sodium Acetate) + $C_2H_5O_3Li$ (9.6g Lithium Lactate) [Ref. 89, Siemens Manual].

The spectrum has a clean baseline. The acetate peak (about 1.9 ppm) and lactate doublet of the phantom fluid are clearly delimited and narrow.

The lactate molecule has 2 weakly coupled resonances: a doublet (split by coupling to the methine [CH] proton) at 1.31 ppm, arising from 3 magnetically equivalent methyl (CH_3) protons, and a quartet (split by coupling to the protons of the methyl group) at 4.10 ppm, arising from the methine proton, which is usually not visible in vivo. The scalar coupling gives rise to a phase evolution of the methyl doublet, which depends on the echo time (T_E). For $T_E = 144$ ms, the resonance shows a phase of 180° leading to a negative in-phase doublet, whereas $T_E = 288$ ms gives rise to a positive in-phase doublet. Since only in-phase resonances can be quantified, echo times of 144 ms and 288 ms are preferable for lactate detection and assignment. The coupling evolution can also be exploited for spectral editing techniques, increasing the sensitivity of lactate detection.

Lactate doblet and quadruplet have a *J*-coupling of 6.933 Hz.

With STEAM measurements, the lactate and acetate signals are always in phase (using $T_M = 10$ ms). With spin echo measurements, the lactate and acetate signals have an inverted pahse if $T_E = 135$ ms and are in phase if $T_E = 270$ ms.
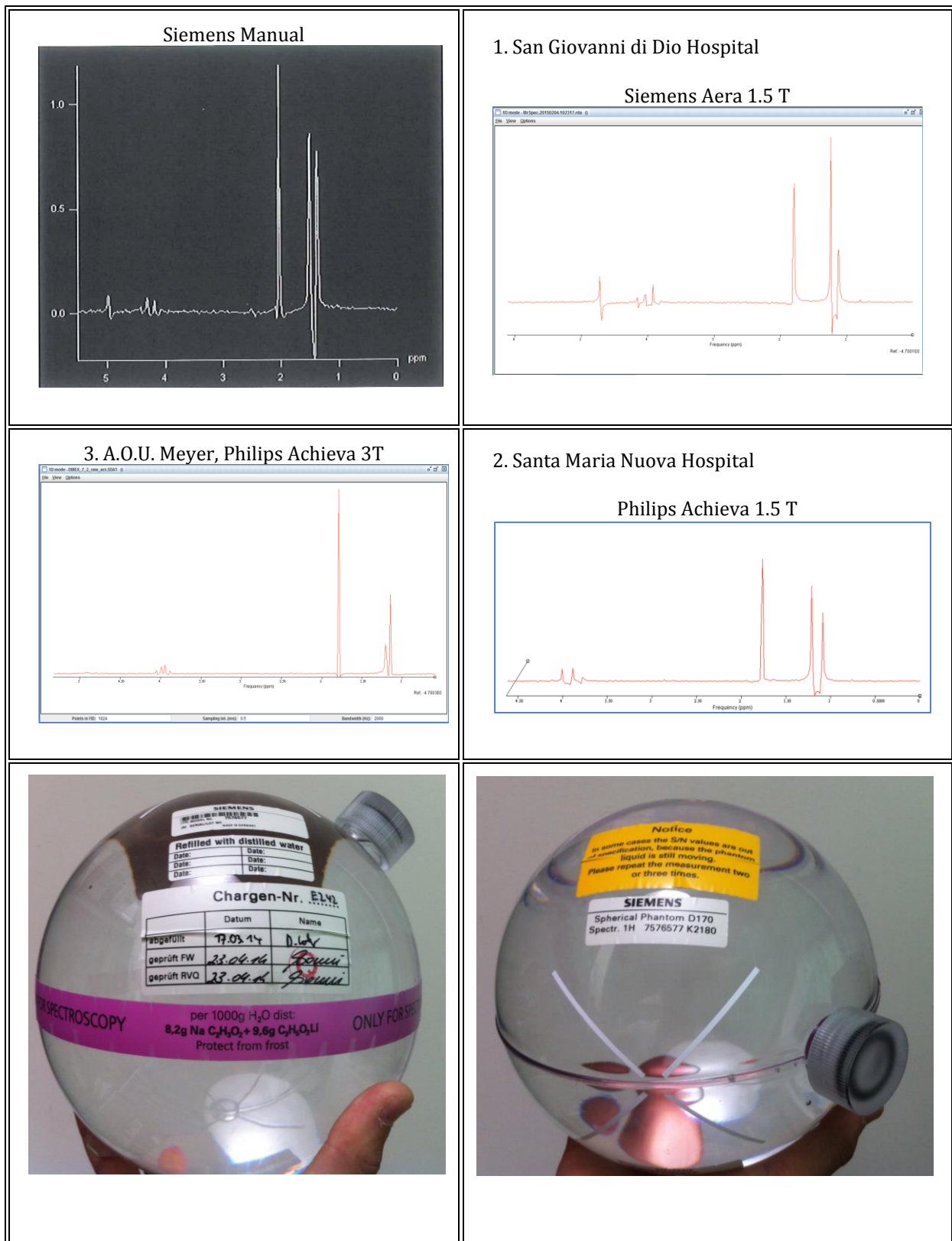
Figure 1: Siemens phantom. Top left: spectrum from Siemens Manual [Ref. 89];
top right: 1. spectrum acquisition at San Giovanni di Dio Hospital with Siemens Aera MR scanner at 1.5 T;
middle right: 2. spectrum acquisition at Santa Maria Nuova with Philips Achieva MR scanner at 1.5 T.
Left middle panel: spectrum acquisition at Meyer Philips Achieva 3 T;
Bottom left: Metabolites concentration certified from Siemens; Bottom right: ID number.
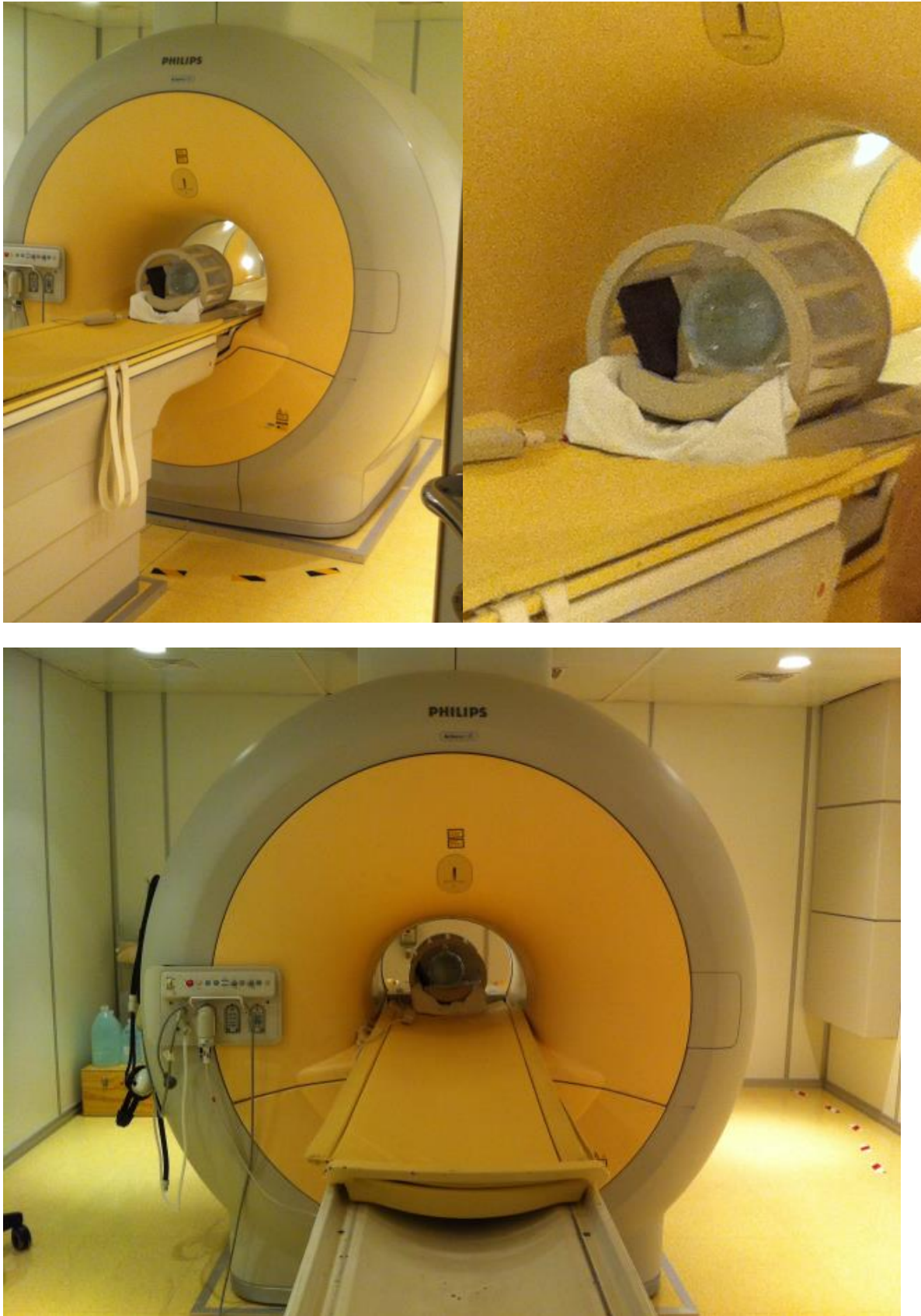
Figure 2: Siemens phantom inserted into the Philips Achieva 1.5 T MR scanner
at the Santa Maria Nuova hospital.

Chapter 3

SPECTROSCOPIC SEQUENCES

This is a short review of the principal sequences used for T_1, T_2 determination and MRS. More details can be found in Laterbour [Ref. 9], Brix G. "Basics of Magnetic Resonance Imaging and Magnetic Resonance Spectroscopy" [Ref. 90], "Quantitative MRI of the Brain" [Ref. 143], [Ref. 144].

3.1 - Standard Pulse Sequences

In an MR experiment, only the RF signal can be determined by measurement, which is induced by the rotating transverse magnetization M_{xy} in the receiver coil. Nevertheless, a large variety of MR experiments can be realized that differ in the way by which the spin system is excited and prepared by means of RF pulses before the signal is acquired. A defined sequence of RF pulses, which is usually repeated several times, is called a pulse sequence. In the following, three "classical" pulse sequences are described that are frequently used for MR experiments.

3.1.1 - Saturation Recovery Sequence

The saturation recovery (SR) sequence consists of only a single 90° pulse, which rotates the longitudinal magnetization M_z into the xy plane. The FID signal is acquired immediately after the RF excitation of the spin system. After a delay time, the repetition time T_R, the sequence is repeated. The SR sequence is described schematically by the pulse scheme (90°– AQ – T_R) (AQ =signal acquisition period).

If the repetition time T_R is long compared to T_1, the magnetization **M** relaxes back to its equilibrium state. In this case, the initial amplitude of the FID, even after repeated excitations, does only depend on the equilibrium magnetization M_0 and does not show any T_1 dependency. However, if the repetition time is shortened to a value that is comparable to T_1, the longitudinal magnetization M_z will not fully relax after excitation, and the following 90° pulse will rotate the reduced longitudinal magnetization

$$M_z(T_R) = M_0[1 - \exp(-T_R/T_1)]$$

into the xy plane. Under the assumption that the transverse magnetization after the repetition time T_R has been decreased to zero ($T_R \gg T_2^*$), the following expression is obtained for the initial amplitude S_{SR} of the FID signal:

$$S_{SR} \propto N[1 - \exp(-T_R/T_1)]$$

which exclusively depends on the relaxation time T_R and the number N of the excited spins

in the sample.

3.1.2 - Inversion Recovery Sequence

In the inversion recovery (IR) method, the longitudinal magnetization is inverted by a 180° pulse (inversion pulse), which is followed after an inversion time T_I by a 90° pulse (readout pulse). Immediately after the 90° pulse, which rotates the partially relaxed longitudinal magnetization $M_z(T_I)$ into the xy plane, the FID signal is acquired.

The IR sequence is described by the pulse scheme $(180° - T_I - 90° - AQ)$. The initial amplitude S_{IR} of the FID signal is directly proportional to the longitudinal magnetization immediately before irradiation of the read-out pulse, just as is the case in the SR method. In contrast to the SR sequence, however, the change in the longitudinal magnetization is twice as high and thus the following expression is obtained:

$$S_{IRS} \propto N[1 - 2\exp(-T_I/T_1)]$$

The derivation of this relation is based on the assumption that the spin system is in its equilibrium state before it is excited by the inversion pulse. When repeating the IR sequence, one has therefore to make sure that the repetition time T_R is markedly longer than the relaxation time T_1.

If the IR sequence is repeated several times with different inversion times T_I, it is possible to sample the temporal course of the longitudinal magnetization step by step, since the initial amplitude of the FID signal is directly proportional to the longitudinal magnetization at time T_I. This procedure is applied frequently in order to determine the relaxation time T_1 of a sample.

3.1.3 - Spin-Echo Sequence

As explained above the temporal decay of the transverse magnetization M_{xy} is caused by two effects: fluctuating local magnetic fields and spatial inhomogeneities of the magnetic field B_0. The transverse magnetization M_{xy} therefore relaxes not with the substance-specific relaxation time T_2 but rather with the effective time constant T_2^* ($T_2^* < T_2$). When determining the relaxation time T_2, it is therefore important to compensate the effect of the field inhomogeneities. This can be done, as E. Hahn has shown in 1950, by using the so-called spin- echo (SE) sequence. This sequence utilizes the fact that the dephasing of the transverse magnetization caused by B_0 inhomogeneities is reversible since they do not vary in time, whereas the influence of the fluctuating local magnetic fields is irreversible.

In order to understand the principle of the SE sequence with the pulse scheme $(90° - \tau - 180° - \tau - AQ)$, we initially neglect the influence of the fluctuating local magnetic fields and solely consider the static magnetic field inhomogeneities. Immediately after the 90° pulse, all magnetization components composing the transverse magnetization M_{xy} point along the y'-axis. Shortly afterward, some components precess faster, others more slowly around the direction of the B_0 field, so that the initial phase coherence is lost. When looking at this situation from a rotating frame, one observes a fanning out of the magnetization

components around the y'-axis. If a 180° pulse is applied after a time delay τ along the x'-axis, the magnetization components will be mirrored with respect to this axis. However, the 180° pulse does not change the rotational direction of the magnetization components, but merely inverts the distribution of the components: the faster components now follow the slower ones. After the time $t = 2\tau$, all magnetization components again point to the same direction, and the signal comes to a maximum. The 180° pulse thus induces a rephasing of the dephased transverse magnetization, which causes the MR signal to increase and to generate a spin echo. After the spin-echo time $T_E = 2\tau$, the echo decays again— as the original FID does—with the time constant T_2^*.

Due to the rephasing effect of the 180° pulse, the spin-echo signal $S_{SE}(T_E)$ is independent from the inhomogeneities of the static magnetic field: the loss of signal at the time $t = T_E$ as compared to the initial signal $S_{SE}(0)$ is determined exclusively via the substance-specific relaxation time T_2. If one irradiates a sequence of K 180° pulses at the times τ, 3τ, 5τ,..., $(2K-1)\tau$, one can detect a spin echo in between the subsequent 180° pulses. The envelope of the echo signals $S_{SE}(2\tau k)$ ($k = 1, 2, 3, ..., K$) decays exponentially with the relaxation time T_2:

$$S_{SE} \propto N\exp[-2\tau k/T_2]$$

The major advantage of this multi echo sequence consists in the fact that the T_2 decay can very effectively be detected by a single measurement.

3.2 - PRESS and STEAM

The most common *in vivo* [1]H spectroscopy acquisition techniques are STimulated Echo Acquisition Mode (STEAM, Ref. 136) and Point-RESolved Spectroscopy (PRESS Ref. 91).

The STEAM technique generates a cubic or rectangular voxel by the acquisition of three orthogonal slice selective 90-degree pulses. By using 90-degree pulses, a well-delineated voxel is created within the sample. This technique minimizes signal contamination from outside the region of interest. The second technique, PRESS, also generates a cubic or rectangular voxel by the acquisition of three orthogonal slice selective pulses, differing by using a 90-degree pulse followed by two 180-degree pulses. The voxel generated by PRESS is not as precisely defined as that of STEAM, however, the signal to noise gained by using PRESS is twice as large over STEAM.

Both STEAM and PRESS need a technique to suppress the water signal found in their voxels. A commonly used technique, CHEmically Selective Saturation (CHESS), is applied prior to the selected localization technique. Three frequency selective pulses are applied along with a dephasing gradient to suppress the water.

Both of these sequences use three slice-selective radiofrequency pulses with orthogonal magnetic field gradients where the intersection of the slices defines the volume of interest (VOI). The three RF pulses produce FIDs, multiple spin echoes (SE), and a stimulated echo (STE)[Ref. 16, 138]. Four time intervals (τ_1, τ_2, τ_3, τ_4) associated with the RF pulses are defined as follows: τ_1 is the time between the first and second RF pulses, $\tau_2 + \tau_3$ is the time between the second and third RF pulses, and τ_4 is some time period after the third RF pulse. The FID of the first RF pulse refocused by the second RF pulse [SE(1,2)] occurs at $2\tau_1$. If $2(\tau_2 + \tau_3) > 2\tau_1$, the echo SE(1,2) is refocused by the third RF pulse to produce the spin echo, SE(2,1), at $2(\tau_2 + \tau_3)$. The FID from the second RF pulse refocused by the third RF pulse [SE(2,3)] occurs at $\tau_1 + 2(\tau_2 + \tau_3)$. The FID from the first RF pulse refocused by the third RF pulse [SE(1,3)] occurs at $2(\tau_1 + \tau_2 + \tau_3)$. The stimulated echo occurs at $2\tau_1 + \tau_2 + \tau_3$. Note that all times are from the center of the first selective RF pulse.

In practice, both PRESS and STEAM use several crusher gradients after each RF pulse to dephase unwanted signals from echoes and FIDs. Although more crusher gradients can be added, this increases the probability of eddy current artifacts in the spectrum. Typical clinical *in vivo* ^{1}H-MRS acquisitions have T_E's of 20 ms with STEAM and 30 ms or 135 ms with PRESS; T_R's greater than or equal to 1.5 s; and data acquisition times of 1 s. Research MRS groups have reduced T_E from 1 to 6 ms with STEAM and to 13 ms with PRESS [Ref. 110, 139, 140].

Examples of PRESS and STEAM spectra are shown in [Ref. 13, 141]. Because STEAM uses only 90° RF pulses with a TM period, the T_E can be shorter than with a PRESS sequence, which reduces signal decay and distortion due to *J* coupling. Large and lengthy crusher gradients can be applied during the TM interval to dephase unwanted signals, which will reduce out of volume contamination [Ref. 110]. The specific absorption ratio (SAR) with PRESS is about twice that with STEAM. Finally, the effects of *J* coupling can change whether STEAM or PRESS is used, although the effects depend more on the T_M, T_E, and actual flip angles   chosen [Ref. 17, 18, 88, 101]. There is an additional complication in that the chemical shift that occurs with RF selective slices means that a particular metabolite such as lactate has coupled nuclei which are excited by one RF pulse, but not necessarily both the remaining two selective RF pulses. This can lead to signal cancellation within the voxel, which depends on both the type of sequence and the bandwidth of the RF pulses [Ref. 142].

PRESS: Point RESolved Spectroscopy

PRESS is a multi echo single shot technique to obtain spectral data. A PRESS sequence has three slice-selective RF pulses with the form of:

$$90° - \tau_1 - 180° - (\tau_2 + \tau_3) - 180° - \tau_4 - SE(2,1)$$

Usually in a PRESS sequence, $\tau_1 = \tau_2$ and $\tau_3 = \tau_4$. The T_E of the SE(2,1) in this PRESS sequence is equal $\tau_1 + \tau_2 + \tau_3 + \tau_4$.

The 90° RF rotates the spins in the xy-plane, followed by the first 180° pulse (spin rotation in the *xz*-plane) and the second 180° pulse (spin rotation in the *xy*-plane), which gives the signal.

With the long echo times used in PRESS, there is a better visualization of metabolites with longer relaxation times. Many of the metabolites depicted by stimulated echo technique are not seen on point resolved spectroscopy, but PRESS is less susceptible to motion, diffusion, and quantum effects and has a better SNR than STEAM.

STEAM: STimulated Echo Acquisition Mode

A STEAM sequence has three slice-selective RF pulses with the form of:

$$90° - \tau_1 - 90° - (\tau_2 + \tau_3) - 90° - \tau_4 - STE.$$

For the STEAM sequence, τ_1 is equal to τ_4 , $\tau_1 + \tau_4$ is the echo time, and $\tau_2 + \tau_3$ is called the mixing time (TM). An important feature of STEAM is that only half of the transverse magnetization prepared by the first 90° pulse is transformed into longitudinal magnetization by the second 90° pulse, decreasing SNR by a factor of 2. During the TM period, longitudinal magnetization decays with T_1 rather than T_2. The third RF pulse transforms the longitudinal magnetization stored by the second RF pulse back into the transverse plane to form the stimulated echo.
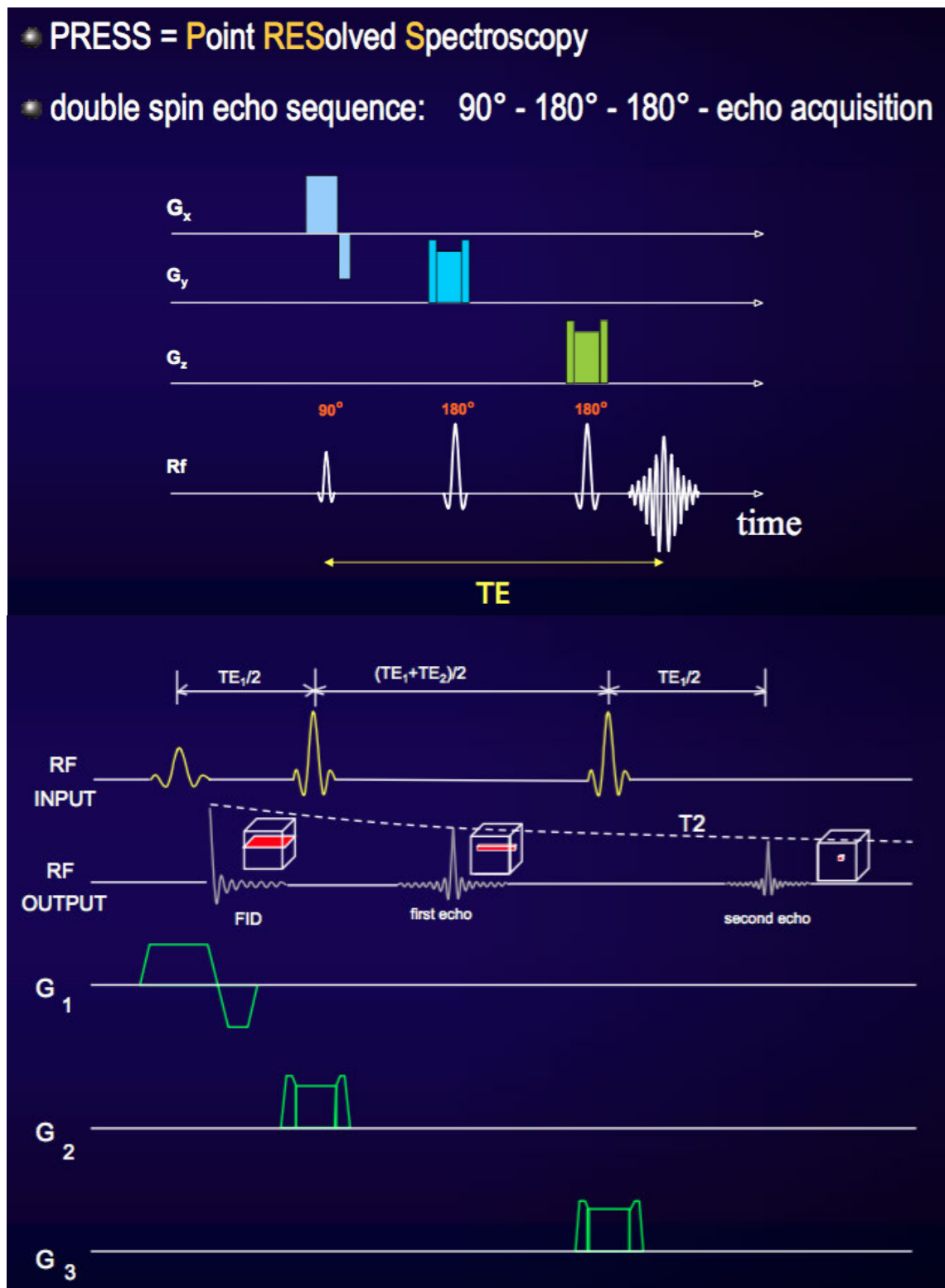
Figure 1: PRESS – Point RESolved Spectroscopy sequence scheme. Images reprinted from "Basic of MR Spectroscopy I, Imaging Science Educational Workshop 2008, Ulrike Dydak"

3.3 - Chemical shift imaging

MR Spectroscopic Imaging (MRSI, Ref. 1) is a widely available routine clinical imaging tool and clinical research tool for spatially mapping and characterizes multiple tissue metabolites signals *in vivo*. This technology, which is available on many clinical MR scanners, has reached a remarkable degree of maturity in recent years and has stimulated considerable interest in clinical applications. As most MRSI development and applications have been focused on the brain, MRSI (as well as MRS in general) is sometimes viewed as having importance only within the neuroradiological community, while many others promising clinical applications are reaching maturity.

To a large extent, MRSI technology is built upon earlier work developing localized single voxel MRS (SV-MRS). First described by Brown et al. in 1982 [Ref. 2] and further developed by Maudsley et al. in 1983 [Ref. 3], MRSI increasingly is supplanting SV-MRS for clinical applications and research due to its ability to rapidly and simultaneously assess tissue spatial heterogeneity of chemical concentrations. However, several technical challenges currently limit more widespread clinical acceptance of MRSI. Furthermore, MRSI historically has required a high degree of user training and integration into clinical routine is nontrivial.

In general terms, MRSI uses the same phase encoding procedures that are used in MRI to map the spatial distribution of MR signals. In the case of ^{1}H-MRSI, proton MR signals produced by metabolites within the tissue produce the signals that are imaged. The molecular concentrations of these metabolites are at least 10.000 times lower than water and metabolites produce correspondingly much lower signal strengths than does water, which is used to form conventional MR images. To detect enough signal above noise for quantification ^{1}H-MRSI must use much larger voxel sizes in comparison to MRI. Voxel volumes on the order of 0.3 cc can be readily measured at 3T [Ref. 4, 5] and the use of surface coils and array coils allows much smaller voxel volumes on the order of 0.1 cc [Ref. 6], or smaller. The lower spatial resolution of MRSI compared with anatomical imaging makes consideration of the spatial point spread function (PSF), correspondingly more important. The PSF expresses the fact that the combination of the phase-encoded imaging process and the image reconstruction process cause metabolite signals that are produced by one tissue voxel to bleed into the surrounding voxels, producing a blurring effect. This is conceptually not different from conventional MRI, but is expressed on a larger spatial scale. The PSF can be responsible for spectral artifacts and significant partial volume effects. Spatial filtering is used in the reconstruction process to reduce between-voxel signal bleeding and to increase the signal-to-noise ratio (SNR), but increases the effective voxel size. MRSI can be time consuming to acquire, making it sensitive to motion artifacts, which in contrast to MRI are distributed across all acquired spatial dimensions.

MRSI is also highly sensitive to macroscopic magnetic field inhomogeneity within a voxel and across the volume of interest, which introduces regionally varying spectral line broadening. Typically, a spectral line width of less than 0.1 part per million (ppm) is required for quantifiable MRSI data. Accordingly, MRSI studies may require sacrificing coverage of some anatomical regions having strong magnetic field inhomogeneity. Unacceptable field homogeneity is usually present at tissue-bone or tissue-air interfaces and such regions are difficult to study with MRSI. In these regions SV-MRS may be the only choice.

In ^{1}H-MRSI there are often artifacts related to water and lipid signals that are related

to field inhomogeneity and the PSF. Water produces a much larger signal than the target metabolites, requiring the use of frequency selective RF pulses to presaturate the water signal. However magnetic field inhomogeneity associated with interfaces can produce water signal that is frequency shifted and the water suppression process will not suppress water signal being produced by interface regions. Furthermore, water signal produced by such regions is broadened as well, which makes signal contamination due to the blurring effect difficult to identify. In tissue with a large fraction of adipocytes, a lipid signal that are as much as 1000 times stronger than metabolite signals can be produced, producing problematic in terms of bleeding into nearby voxels. Because the problem of lipid and water signal bleeding can be so significant in ^{1}H-MRSI, very precise spatial localization methods are required. Most ^{1}H-MRSI pulse sequences use volume excitation procedures analogous to those used in SV-MRI to select a box shaped tissue region over which the field homogeneity is excellent and that does not contain adipose tissue. Alternatives are to presaturate regions that would produce large lipid signal, or to use lipid nulling using the Short T_1 Inversion Recovery (STIR) [Ref. 7]. While improving overall results quality, prelocalization of a box-shaped region inside the organ of interest can result in considerable loss of volume coverage in peripheral regions of the organ. Furthermore, the majority of ^{1}H-MRSI studies to date are still performed using intermediate to long echo time (T_E) to attenuate lipid signals due to short lipid signal T_2 values. This is in part due to the difficulties of quantifying strongly overlapping multiplet resonances at short T_E. However, the use of long T_E results in substantially decreased sensitivity to the metabolite signals due to T_2 loss and J-modulation of multiplet resonances. Improved localization performance now allows MRSI mapping at much shorter T_E, to measure J-coupled metabolites that have traditionally been measurable only with SV-MRS [Ref. 8]. MRSI studies involving nuclei other than protons, usually do not have problems corresponding to the lipid and water problems present in ^{1}H-MRSI, but signal strength in these studies is usually lower than in ^{1}H-MRSI and the volume resolution must be even more coarse and this engenders more concern regarding voxel signal bleeding.

STEAM or PRESS can either be used to acquire data from a single voxel or from multiple voxels using chemical shift imaging (CSI) [Ref. 2, 16, 91 - 98]. Phase encoding gradients are used in CSI spectroscopy to encode spatial information analogous to imaging. The selected CSI volume to be phase- encoded will be larger than a single volume acquisition.

3.3.1 - Single voxel versus chemical shift imaging

Proton MRS with CSI acquisition has several advantages over single voxel acquisitions (SVA).

1. CSI provides better *SNR* as compared to two or more sequential SVA since the signal from each voxel is averaged for the total data collection time with CSI.
2. The CSI grid can be shifted after data acquisition (similar to image scrolling), allowing precise positioning of a voxel after data acquisition.
3. Many more voxels of data are collected in a practical acquisition time.

There are also disadvantages of CSI compared to SVA.

1. Since with CSI only the whole CSI volume is shimmed rather than each individual voxel as in SVA, the shim for each CSI voxel is not as good as on a SVA voxel in the same location.

2. The poorer shim causes more problems with lipid contamination although additional techniques, such as outer volume suppression (OVS), can be used to reduce this problem [Ref. 92, 94, 99]. Water suppression will also vary across the CSI volume because of both changes in B_1 and magnetic field inhomogeneities.

3. Because three "slice" selective RF pulses are used to select the CSI PRESS or STEAM volume, there are imperfect slice profiles which cause problems for spectra from voxels near the outside of the CSI volume. The resulting alterations in tip angle and phase for different voxel locations will alter *J* coupling effects as a function of location that in turn will make consistent metabolite quantification more difficult. Non-optimal tip angles at the outer edges of the CSI volume also reduce *SNR* in the outer voxels.

4. The minimum CSI data collection time is determined by the required number of phase encode steps and can become long, especially if an unsuppressed water reference set is required. Time cannot be reduced by decreasing the size of *k* space since this increases lipid contamination from the CSI point spread function [Ref. 93]. The acquisition time can be reduced by 25% with a circularly bounded *k*-space acquisition [Ref. 97], a reduced FOV and number of phase encoded steps across the narrow direction of the head [Ref. 100] (similar to a rectangular field of view in imaging), or with the echo planar imaging (EPI) spectroscopy approach [Ref. 95, 96].

5. The metabolite concentrations measured from a spectrum associated with one voxel actually correspond to the integrated metabolite concentrations over the CSI point spread function. This means the measured metabolite concentrations will depend on such factors as voxel location and how quickly metabolite concentrations change spatially throughout the brain. Since the point spread function usually has negative lobes (sinc function) and spectra quantification is done in the absorption mode, metabolite peaks from adjacent voxels will be added in negative phase. This will cause peak shape distortions because adjacent voxels usually have different center frequencies than the voxel of interest.

In summary, consistent, high quality, short T_E spectra *in vivo* are best acquired with the SVA technique, but time restraints limit acquiring data from only a few VOIs. CSI is best when more VOIs are required. A long echo time (T_E >130 ms) can be used to simplify the spectra and reduce the lipid and macromolecule signal, which will make metabolite quantification reasonably consistent. However, the long T_E time reduces the number of quantified metabolites to NAA, Cho, Cr, and lactate.

3.3.2 - *Signal to noise ratio*

Since the MRS time domain signal is complex, two frequency domain signals result from the Fourier transform that are typically labeled "real" and "imaginary." These signals are linear combinations of the absorptive and dispersive components of the Lorentzian line

shape. In principle proper phase adjustments can make the "real" signal purely absorptive and the "imaginary" signal purely dispersive.

The signal from a metabolite is the area under its peak. The full-width at half-maximum value (FWHM) of the Lorentzian absorption spectral peak in Hz is defined as, $\text{FWHM} = 1/T_2^*$, where $1/T_2^* = 1/T_2 + \gamma \Delta B_0$. For an absorptive Lorentzian peak the area under the peak is equal to $\pi/2 \times \text{FWHM} \times (\text{peak height})$. For the Lorentzian dispersion component, the peak width is much broader and the area under the peak integrates to zero, so the dispersion peak is not typically used in clinical MRS analysis.

In a well-shimmed spectrum, the peak's height is an easily measured indicator of the signal. Noise in a spectrum can be evaluated by measuring the standard deviation in a region that contains no signal, therefore, *SNR* can be defined as the ratio of peak height divided by the rms noise [Ref. 101]. Different definition can be found in literature, but careful reading may be required to learn which definition a particular paper uses.

The area of a Lorentzian peak is independent of the shim quality measured by FWHM, therefore a definition involving the area under the peak is a more absolute measure of *SNR* and a better parameter for testing hardware performance on a MRS phantom, especially for quality control (QC) and for comparing different hardware. However, *in vivo*, metabolite peaks typically overlap and the precision in determining metabolite peak areas depends as much on the FWHM as on the peak area *SNR*. Therefore, our definition of *SNR* is more pertinent for comparing *in vivo* data and optimizing MRS methodology. Note, however, that metabolite concentrations are calculated from peak areas. In addition, when comparing *SNR* between two spectra, the comparison will be valid only if identical data acquisition and post-processing were used. These conditions are rarely met when spectra are collected on MR systems from two different vendors. As an example, peak area which is proportional to the amplitude of the first time domain point is usually not affected by post-processing time domain filters, but these filters reduce noise and peak heights. Therefore post-processing filters change peak area *SNR* differently than peak height *SNR*.

The magnitude of the noise is independent of the VOI size, but depends on the tissue volume detected by the RF coil, and increases with the square root of the number of signals that were added coherently (n). The magnitude of the signal is directly proportional to the volume of the VOI, proton density, and the number of averages (n). With averaging, *SNR* is proportional to $\sqrt{n}$.

Averaging is a specific example illustrating the principle that *SNR* is proportional to the square root of the total signal data acquisition time [Ref. 102]. Therefore, *SNR* (peak height) will also depend on the duration of the STEAM or PRESS echo which decays with T_2^*, assuming that the data acquisition time is $\geq 5T_2^*$ in duration. The specific value of T_2^* will depend on the shim, metabolite T_2^*, and tissue susceptibility. A good single voxel shim in the brain's parietal–occipital lobe will give a linewidth approaching 4 Hz corresponding to a T_2^* = 80 ms. *In vitro* on a spherical phantom, voxel shims below 1 Hz are typical corresponding to a $T_2^* > 318$ ms. Therefore, *in vivo*, an echo data acquisition time of 400 ms ($5T_2^*$) is sufficient, but *in vitro*, data acquisition times >1500 ms are required to maximize *SNR*. When comparing two different MR systems on *SNR*, one must ensure that both systems are using the same data acquisition time. Also, since in a typical *in vivo* *1H*-MRS acquisition T_R is $\geq$1.5 s allowing a data acquisition time $\geq$1 s, *SNR* will increase from the longer signal duration obtained with better shimming.

Depending on the system software, two of the following three parameters must be

set prior to a spectroscopy acquisition: the data acquisition time, the number of complex data points, or the sampling frequency (bandwidth) of the analog-to-digital converter (ADC). Setting two of these automatically calculates the other. Besides having a sufficiently long enough data acquisition time one must also have a high enough sampling frequency to cover the bandwidth of the desired spectrum. Note that this required bandwidth scales linearly with B_0.

SNR can be influenced by many factors, as shown in brief below.

Eddy currents

Eddy currents are induced in the magnet structure by field gradient pulses. These eddy currents create additional magnetic fields that add to the static field. Eddy currents can be classified into two categories [Ref. 103]:

      1.   zero order eddy current or time-varying B_0 offset which could be compensated with a B_0 coil

      2.   time-varying first or higher order gradient.

Zero-order eddy currents will cause a frequency-dependent phase shift during signal readout but no decrease in *SNR* from spin dephasing within the VOI. First-order eddy currents will dephase the spins within the VOI, decreasing *SNR*. Both types of eddy currents plus magnetic field inhomogeneities will distort peak shapes, making spectral quantification more difficult, especially when peak fitting to modeled line shapes. The distortion from eddy currents can be corrected by either dividing the ^{1}H spectra time domain signal by the unsuppressed water time domain signal, dubbed *QUA*ntification by converting to the *L*orentz*I*an *TY*pe (QUALITY) deconvolution [Ref. 104], or by doing a point by point phase correction of the time domain signal, again using the unsuppressed water signal as a reference often referred to as an Eddy Current Correction (ECC) [Ref. 105-106]. Note that QUALITY will correct peak distortion caused by zero- and first- order eddy currents and B_0 inhomogeneities, while ECC only corrects peak distortion for zero-order eddy currents.

Phase cycling

Physical differences between the two channels of an analog quadrature receiver can introduce artifacts into a magnetic resonance image or magnetic resonance spectrum.

There will be ghosting of the peaks mirrored about zero frequency if the phase difference between the two channels is not 90° or the amplifier gains of the two channels are not equal. This is often called a quadrature ghost. If the DC offsets of the two channels are not equal to zero, there will be a spike at zero frequency. *CYCL*ically *O*rdered *P*hase *S*equences (CYCLOPS) can be used to correct for these artifacts [Ref. 107]. CYCLOPS involves rotating the transmitter phase by 0°, 90°, 180°, and 270°, then adding and subtracting the two receiver channels. CYCLOPS is usually implemented on NMR spectrometers, but not on whole body MR scanners because image acquisitions almost never use four acquisitions. MR scanners implement a reduced version of CYCLOPS, called phase cycling that toggles the transmitter phase between 0° and 180°. The signal obtained with the transmitter phase at 180° is subtracted from the signal obtained with the transmitter phase at 0°. This adds the signal and subtracts the DC offsets. Phase cycling corrects for the DC artifact but does not correct for the quadrature ghost. Another purpose for phase cycling is the compensation for imperfect 180° flip angles in multiecho MRI acquisitions.

Modern digital receivers use only one amplifier plus ADC and are no longer plagued with unequal DC offsets, unequal gains, or non 90° quadrature, but phase cycling can still be useful. References 108 - 110 demonstrate that phase cycling can inhibit unwanted transverse magnetization and unwanted echo signals (despite gradient spoiling) from corrupting the spectra. Therefore phase cycling should be used with *in vivo* [1]H spectroscopy, when possible. Single voxel acquisitions, which normally use 16 or more data averaging, allow 8 cycle phase cycling. However, CSI acquisitions rarely have enough data averaging per phase encode step to allow full phase cycling, but even if only two data acquisitions are used at each *k* space point, it is important to phase cycle the third selective RF pulse 0 and 180 degrees to reduce the echo contamination from the third RF pulse FID. RF pulse FIDs arise from non-ideal slice profiles and imperfect RF pulse flip angles.

The problem with water

The concentration of pure water is 55.6 M or 111 M for [1]H. The water concentration in the brain, calculated from an average MR visible brain water content of 70%, is 36 M [Ref. 111]. *In vivo* [1]H spectroscopy requires water suppression because the 36 M water signal overpowers the 1–10 mM signal of the metabolites. Water suppression is normally accomplished with one or more narrow band (60 Hz) radio frequency CHemical-Shift Selected (CHESS) pulses [Ref. 112] followed by spoiling gradients at the beginning of the STEAM or PRESS acquisition. This is similar to frequency selective fat RF saturation in imaging. The quality or degree of water suppression depends on the *in vivo* shim, the stability and linearity of the RF amplifier at low power output, the severity of eddy currents, and the number and implementation of the CHESS pulses. For maximal water suppression, the transmitter voltage (flip angle) of the CHESS pulses (s) must be adjusted for each exam. Even though water suppression is optimized for the voxel or volume (CSI) of interest, the water is suppressed globally and will reduce out of volume water contamination. Normally, an unsuppressed water spectrum is acquired by turning off the water suppression RF pulse (s). This signal can then be used for an ECC or QUALITY correction as well as a reference for absolute metabolite quantification [a mode detailed bibliography can be found in Ref. 13].

The problem with lipids

Another problem associated with *in vivo* proton MR spectra is the ubiquitous presence of lipid peaks. These lipid peaks may obscure other peaks of less abundant metabolites. Lipid contamination usually arises from outside the skull due to non-ideal selective slice profiles [Ref. 114]. Often increasing T_E can reduce the spectral contribution of lipids, but this strategy also reduces the *SNR* ratio of all peaks in the spectrum. Other strategies include moving the STEAM or PRESS VOI away from the skull, outer volume saturation bands [Ref. 92, 94, 114, 115] an inversion pulse [Ref. 113] similar to Short T_I Recovery (STIR) MR imaging, and/or spatial *k*-space data processing before the CSI reconstruction. Note that STIR will also add T_1 weighting to the proton metabolites reducing metabolite *SNR*. Along with lipids, there are broad macromolecule [Ref. 113, 114, 115] peaks under the spectrum. As with lipids, these peaks are reduced with long T_E times and/or the lipid STIR technique. However unlike lipids, macromolecule peaks are a natural component of brain tissue present within the selected voxel. Therefore improved slice profiles, outer volume suppression, and improved gradient spoiling, all techniques that reduce lipid

contamination, will not reduce macromolecule peaks.

3.3.3 - Prescan adjustments

Before the spectral data are acquired, the MR system will initiate a prescan routine that is often automatic. The prescan will shim the VOI, set the RF transmitter center frequency, set the RF transmitter gain, set the receiver gain, and set the flip angle for the water suppression pulses. On some systems, the VOI will have to be shimmed manually or semi-automatically. If second order or higher resistive shims are available, optimum shim results are obtained by using the higher order shims plus linear shims in a global shim before collecting the localizer images, followed by a localized voxel shim using the linear shims only. The data acquisition without water suppression is acquired by setting the water-suppression pulses to zero flip angle, and should be obtained just before or just after the water-suppressed acquisition. The water data is used for ECC or QUALITY eddy current correction and sometimes it is used as a reference value for absolute metabolite quantification.

3.3.4 - Post-processing

There are many post-processing techniques used in proton MRS [Ref. 75, 112, 116 - 123]. The vendors of clinical MR systems usually provide post-processing software that provides a good starting. The individual steps embedded in these software packages are described below. In general, these packages fit model peaks to the observed spectrum in the frequency domain with the vendor supplying suggested starting peak templates. However, all post-processing packages will require user tweaking for each different acquisition technique. Some packages also require that the user first acquire *in vitro* data on a set of metabolites, to be used for *a priori* knowledge. The *a priori* knowledge can either be measured experimentally or simulated. This will also have to be repeated for each acquisition technique. Typically as much or more time is required to analyze spectra as is expended in developing a MRS protocol and acquiring the MRS data.

Although raw and fitted spectra are displayed in the frequency domain, fitting can be done in either the time or frequency domain. The time domain fit is inherently simpler and slightly more flexible, but the frequency domain fit will give exactly the same final result, provided that all the limitations of the discrete FT are taken into account [Ref. 126, 127, 128, 130]. We will discuss some typical techniques and provide illustrations for each step. Several references provide a general introduction to post-processing [Ref. 101, 125, 129]. The signal received in proton MRS, whether it is a free induction decay (FID) or the last half of an echo (i.e., STEAM, PRESS), can be described mathematically as either a damped complex exponential (one component) or a sum of damped complex exponentials (multiple components). The conventional display of an FID signal received in quadrature is as plots of "real" signal versus time and "imaginary" signal versus time. The conventional display of the FID in the frequency domain is as a correctly phased absorption (real) spectrum although sometimes the dispersive (imaginary) and absolute spectra are displayed as well. However, metabolite concentrations are represented by the absorption spectrum.

Zero filling

Zero filling in the time domain is equivalent to a sinc convolution (interpolation) in the frequency domain. This interpolation improves the visual display of the data in the frequency domain, although no additional information is added. This is identical to image interpolation in MRI. For example, an N point FID has N real and N imaginary, or $2N$ points sampled at Δt intervals. After Fourier transformation, there are N real and N imaginary points with frequency spacing equal to $1/(N\Delta t)$. The spectral width (SW) of the spectrum is $1/\Delta t$ with the abscissa going from SW/2 to -SW/2. Zeros can be added to the end of the FID to decrease the frequency spacing over the same bandwidth.

Apodization filter

The signal in a free induction decay contains the signal from the metabolites being studied and the noise in the detector channels. A line broadening filter decreases the received signal at the end of the sampling window, which increases the signal-to-noise ratio in a spectrum (peak area definition of *SNR)* but increases the linewidth of the peak in the frequency domain. This filter multiplies the time domain FID by the filter before transforming to the frequency domain. This weighing of the time domain data is known as apodization. A line broadening filter can also ensure that the FID is not truncated to eliminate sinc ringing (leakage). Examples can be found in [Ref. 13, 123].

Water suppression filter

Often the water suppression used with proton spectroscopy does not completely eliminate the water signal. Post-processing with a convolution difference filter can be used to eliminate any residual water signal [Ref. 101, 125, 131]. This filter applies a low-pass filter to the FID, then subtracts the filtered signal from the original data in the time domain. The low frequency component is obtained by convolution with a window function (e.g. Gaussian). Another technique to eliminate or reduce water fits a set of peaks using a linear least squares algorithm to the water peak and   subtracts this from the FID [Ref. 124].

Phasing

Whenever the initial phase of an FID is not zero, the real and imaginary channels after Fourier transform will contain mixtures of absorption mode and dispersion mode spectra. Phasing a spectrum sorts the real and imaginary channels into absorption mode and dispersion mode spectra [Ref. 13].

Phase is the sum of the zero-order phase (constant for all frequencies) and the first-order phase (linear with frequency). The zero-order phase term corrects for the initial phase of the FID. Delay in the time domain corresponds to a frequency dependent phase shift in the frequency domain. The first-order phase term is necessary whenever the start of the ADC sampling window does not start at the peak of the damped exponential.

The zero-order phase is equal to the phase of the first point in the FID (time domain). The zero-order phase is also equal to the four-quadrant arctangent of the sum of the real points and the sum of the imaginary points in the frequency domain, providing that

there were no alterations to the FID before Fourier transformation such as applying saturation pulses when acquiring a FID or shifting the time domain points after a FID is acquired (for first-order phase correction).

When correcting water-suppressed spectra for eddy currents with post-processing such as ECC, the phase of a water FID is subtracted from the phase of a water-suppressed FID. Besides linearizing the phase, this subtraction also applies a zero-order phase to the spectra because the phase offset of the water FID is equal to the phase offset of the water-suppressed FID. If the ADC sample window is placed correctly in a STEAM or PRESS sequence, first-order phasing is not required, and the eddy current corrected spectrum is properly phased.

Software post-processing usually has a left shift tool that allows one or more data points to be deleted from the beginning of the complex FID. This is equivalent to changing the delay time by 1 ADC sample point and may correct the ADC sample window position if it was positioned early. Sometimes, the first points in a FID may be corrupted and these points can be removed with the left shift tool, but first-order phasing will be required to correct for the additional delay time.

Baseline correction

The quantification of MR spectra requires evaluating the area under the peaks in the absorption mode spectrum. Distortions of the baseline around these peaks may greatly affect the accuracy of these areas. Methods for defining the baseline of a spectrum include DC offset correction, correction with linear tilts, and cubic or higher order splines. This baseline is subtracted from the spectrum before calculating the areas. Therefore, a better approach to dealing with baseline peaks is to include them in the overall metabolite fitting algorithm, either as a baseline fit [Ref. 75, 133] or to model them as peaks [Ref. 132]. Discrepancies in metabolite values between investigators [Ref. 133] often arise from differences in baseline processing.

Chapter 4

SOFTWARE FOR POST-PROCESSING

The challenge is to quantify spectra which exhibit many metabolites, and to estimate their relaxing time and concentrations. To that effect, the software package jMRUI with a Java-based graphical user interface (GUI) [Ref. 73, 135, 145 – 148, 151] is being developed for user-friendly time-domain analysis of MRS, MRSI and HRMAS-NMR signals.

Graphical user interface (GUI) in jMRUI is managed by java development kit (JDK), while native code is written in FORTRAN and ANSI C is used for the interface between the GUI and the native code. In comparison to LCModel software, jMRUI requires user interaction. jMRUI allows time-domain MRS single voxel as well as in multiple voxel data and can handle large data sets such as time resolved MRS, and MRSI data. Theoretically, signals from metabolites can be computed by quantum mechanics using NMR scope based on the product-operator formalism.

MRS data processing using jMRUI is subdivided into two stages: preprocessing and. quantitation. There are number of preprocessing steps in the time domain. HLSVD filter and HLSVDPro-filter are used for the suppression of water molecules. The time-domain QUALITY deconvolution method helps to remove magnetic field inhomogeneity, contribution to the line-shape yielding Lorenzian line shapes. The Cadzow function is used to filter the signal. jMRUI also uses gabor as a tool for peak extraction and dynamic phase correction. Mathematical operators, like addition, subtraction, multiplication of the signal with a scalar quantity, are available for the normalization of a signal or over a series of signals. It also provides the preprocessing operator to convert an echo signal into an FID signal. All the above operations are performed in time domain except the ER filter and the baseline correction, which are done in frequency domain.

jMRUI software provides for a number of quantitation methods broadly classified as black box methods like Hankel Singular Value Decomposition (HSVD)/Hankel Lanczos Singular Value Decomposition (HLSVD), Hankel Total Least Squeres (HTLS)/Hankel Lanczos Total Least Squares (HLTLS), Linear Predictive Singular Value Decomposition (LPSVD) or interactive methods like VARPRO, AMARES, QUEST and AQSES.

The black box methods are based on either LP (linear prediction) principle or state space formalism. LPSVD method is based on LP principle and uses SVD decomposition to estimate the prediction coefficients in the forward linear prediction procedure expressed as a matrix in a least squares sense. The HSVD/HLSVD and HTLS/HLTLS methods are state space based, where the data is arranged in a Hankel matrix. HSVD computes the Eigen values of the Hankel matrix which are estimates of the signal poles. The HLSVD algorithm is a computationally efficient version of HSVD, which computes only part of the SVD using the Lanczos bidiagonalization algorithm. A variant to the HSVD algorithm is the HTLS algorithm that computes the Total Least Squares (TLS) solution leading to more accurate parameter estimates. HLTLS, like the HLSVD, is a computationally efficient version of HTLS using Lanczos algorithm.

In the interactive quantitation methods the line-widths and concentrations are part of a nonlinear model and are optimized by fitting the in vivo signal with a combination of metabolite signals by nonlinear least squares techniques.

Summarizing, the jMRUI software package offers:

- Black box quantitation algorithms based on singular-value decomposition (SVD): the state space methods HSVD, HLSVD, and HTLS and the linear prediction method LPSVD. These non-interactive black box techniques are efficient for quantitating signals with good signal-to-noise ratios. They are also helpful in parametrizing signals of unknown composition and shape, but they cannot make use of all available prior knowledge.
- Nonlinear least-squares (NLLS) quantitation algorithm: AMARES and QUEST [Ref. 149, 150]. AMARES is an improved version of VARPRO enabling us to impose prior knowledge on the model-function parameters. QUEST is based on the availability of a metabolite signal basis set.
- Preprocessing algorithms such as rapid removal of dominant signals using HLSVD and HLSVD-Pro, or time–frequency analysis, the Cadzow enhancement procedure for noise reduction, the ER-filter for frequency selection, and Gabor tools for peak extraction and dynamic phase correction.
- Estimation of spectral parameters with their confidence intervals (Cramér–Rao lower bounds).
- Conversion routines for data files from most manufacturers (Bruker, General Electric, Philips, Siemens, Varian, etc). Moreover, the software package jMRUI handles the new advanced DICOM format for MRS, MRSI and MRI.
- Signal simulations from a model function.
- Quantum-mechanical signal simulator based on NMR-SCOPE [Ref. 15] that can handle various measurement protocols and enables the simulation of metabolite signal basis sets.
- The jMRUI software package works with Windows, Linux and Unix platforms.

Some details on the interactive quantification methods in jMRUI are described below.

AMARES

AMARES method performs fitting of Lorentzian, Gaussian or Voigt peaks to the signal, with the possibility of including prior knowledge about relations between peaks, such as equal line-widths, or fixed frequency shifts. It minimizes a general functional consisting of the sum of squared differences between the data and the model function. The available biochemical prior knowledge can be expressed as a set of linear relations between parameters resulting in a minimization problem with linear equality constraints. AMARES uses a singlet approach for imposition of prior knowledge. Each of the parameters can be left unconstrained or kept fixed. In AMARES, a fixed shift or ratio, or a variable shift or ratio, with respect to any unconstrained or fixed parameter of the same type can be imposed. These variable shifts or ratios can then be linked between different groups of peaks. These constraints are substituted in the original functional in order to obtain an unconstrained NLLS optimization problem. AMARES uses a modified version of NL2SOL, a sophisticated NLLS algorithm to minimize the general functional. This algorithm allows the user to specify the upper and lower bounds on the variables. This can be used to impose positive dampings, amplitudes, and upper and lower bounds on frequencies and phases based on the spectral

width. AMARES also offers the ability to fit echo signals, an echo being modeled as two FIDs back to back. The left and right parts of the echo are considered to have the same amplitudes, frequencies and phases, but different damping. The damping of the right and left parts can be linked to each other.

MRS data processed using AMARES are displayed in a table giving information about the estimated components: their frequencies, dampings, amplitudes and phases, respectively. CR lower bounds can be used as a measure of the accuracy of the calculation of the amplitude of a certain component.

QUEST: Quantitation based on Quantum ESTimation

QUEST, the most recent method, uses a basis set of metabolite signals that are combined to fit the in vivo signal. In this linear combination model, the amplitude/concentration, line-width, phase and frequency shift of each metabolite are considered as free parameters and a nonlinear least square function is min- imized with the Levenberg–Marquardt method for nonlinear optimization. All these computations are performed on both the real and imaginary parts of the FID, in the time domain, and not on the frequency domain, as opposed to the LCModel. QUEST can also accommodate a baseline (or background) coming from macromolecules, by truncating a number of points at the FID, fitting the truncated signal with the metabolite basis set, back-extrapolating the estimated model, subtracting it from the in vivo signal, and smoothening the result to yield an approximation for the baseline. The metabolite basis set .ml and the peaks file .peak can be generated using NMR scope and used as prior knowledge input for QUEST quantitation method.

NMRScope

NMRScope-B is a plugin for program jMRUI. The plugin provides the functionality useful for the simulation of coupled spin systems during the NMR experiment. In the simulation, such properties as chemical shifts, spin-spin coupling, relaxation, spatial and/or spectral excitation selectivity, and customized pulse sequences are accounted for. The primary target is to support the simulation of metabolite FIDs in biomedical MR spectroscopy, as needed for spectroscopic quantitation, but many functions are meant to support the development of methods for MR spectroscopic imaging.
Some advantages:

- Implemented model of relaxation (Redfield matrix model - including Solomon equations, T_1 and T_2 relaxation)
- Pulse sequence programming by table filling, tabular definition of phase cycles
- Protocols for more complex pulse sequences, programmable by scripts
- Pulse sequence graphs
- Full support for simultaneous activities (rf pulses incl. heteronuclear excitation, gradient pulses, observation)
- Trick operations (e.g. for modeling a perfect crusher or full relaxation)
- Faster Bloch model for isolated spin-1/2
- Spin system and pulse sequence parameter cycles

- Arbitrary observables defined by formulas
- Arbitrary observation timepoints (even during excitation)

4.1 - Absolute quantitation using jMRUI

The measured area under a spectral peak (from a known volume) is directly proportional to the concentration of the metabolite, after normalizing to the number of protons in the metabolite peak. Since spectroscopy sequences do not have $T_R = \infty$ and $T_E = 0$, the measured area must be corrected for saturation and relaxation effects [Ref. 13, 117, 134, 135].

Most clinical MRS papers do not correct for T_1 or T_2 effects since typically spectral changes are studied over time, or spectra from a group of normal subjects are compared to spectra from a group of subjects with pathology. Therefore, a constant correction term for T_1 or T_2 relaxation will not change the results. However, if metabolite levels are altered in a diseased state or over time, one can never rule out that these changes are due to changes in metabolite T_1 or T_2 relaxation times rather than actual changes in metabolite levels. Although a few authors have measured metabolite T_1 and T_2, this is a very time-consuming procedure since spectra have to be acquired at several T_R/T_E time points [Ref. 117, 119, 120]. Since the effects on peak distortions due to J coupling change with T_E, T_2 measurements become difficult for metabolites with J coupled spins [Ref. 88].

The absolute concentration of metabolites from signal intensity as derived by jMRUI can be obtaind by a simplified equation:

$$C_{\mathrm{M}} = \frac{S_{\mathrm{M}}}{S_{\mathrm{W}}} \times C_{\mathrm{W}} \times \frac{n_{\mathrm{W}}}{n_{\mathrm{M}}} \times \frac{f_{\mathrm{W}}(T_1)}{f_{\mathrm{M}}(T_1)} \times \frac{f_{\mathrm{W}}(T_2)}{f_{\mathrm{M}}(T_2)}$$

where indexes M for metabolite and W for water, C stands for concentration, S for signal intensity, n for the number of chemically equivalent protons. C_{w} stands for concentration of water about 55.5 mol/L in pure water.

$f(T_1)$ and $f(T_2)$ are correction factors for spin-lattice and spin-spin relaxation functions respectively [Ref.13, 152]:

$$
\begin{cases}
f(T_1; PRESS, Ref.135) = 1 - 2\exp\left[\frac{-\left(T_R - \frac{T_E}{2}\right)}{T_1}\right] + \exp\left(-\frac{T_R}{T_1}\right) \\[4mm]
f(T_1; STEAM, Ref.13) = \left[1 - \exp-\left(\frac{T_R - T_M - \frac{T_E}{2}}{T_1}\right)\right] \cdot \exp\left(-\frac{T_M}{T_1}\right) \\[4mm]
f(T_1; PRESS, Ref.152) = 1 - \exp\left[-\frac{T_R}{T_1}\right] - 2\exp\left[\frac{-\left(T_R - \frac{3T_E}{4}\right)}{T_1}\right] + 2\exp\left[\frac{-\left(T_R - \frac{T_E}{4}\right)}{T_1}\right] \cong (if\ T_E \ll T_R)\ 1 - \exp\left[-\frac{T_R}{T_1}\right] \\[4mm]
f(T_2) = \exp(-T_E/T_2);
\end{cases}
$$

So, in order to perform an absolute quantitation of metabolites concentration we have to

1. Evaluate T_1, T_2 of metabolites
2. Evaluate the signal of metabolites
3. Correct the signal for saturation and relaxation effects

4. Correct for the number of active protons

The receiver attenuation must be keep fixed in all measurements in order to perform an aboslute quantitation.

Error estimation in absolute quantitation

Error estimation in the metabolites absolute quantitation can be found using the error propagation formula, where contributions from signals intensity (S_M and S_W) can be usually trascurated respect to the other. C_W is usually assumed 55.5 M for distilled water without error. ΔT_1 and ΔT_2 can be estimated by the fitting procedure as shown in Chapter 7.

$$
\begin{cases}
\dfrac{\Delta C_{\mathrm{M}}}{C_{\mathrm{M}}} = \dfrac{\Delta C_{\mathrm{W}}}{C_{\mathrm{W}}} + \dfrac{\Delta S_{\mathrm{M}}}{S_{\mathrm{M}}} + \dfrac{\Delta S_{\mathrm{W}}}{S_{\mathrm{W}}} + \dfrac{\Delta f(T_1)_{\mathrm{M}}}{f(T_1)_{\mathrm{M}}} + \dfrac{\Delta f(T_2)_{\mathrm{M}}}{f(T_2)_{\mathrm{M}}} + \dfrac{\Delta f(T_1)_{\mathrm{W}}}{f(T_1)_{\mathrm{W}}} + \dfrac{\Delta f(T_2)_{\mathrm{W}}}{f(T_2)_{\mathrm{W}}} \\[3mm]
\qquad \cong \dfrac{\Delta f(T_1)_{\mathrm{M}}}{f(T_1)_{\mathrm{M}}} + \dfrac{\Delta f(T_2)_{\mathrm{M}}}{f(T_2)_{\mathrm{M}}} + \dfrac{\Delta f(T_1)_{\mathrm{W}}}{f(T_1)_{\mathrm{W}}} + \dfrac{\Delta f(T_2)_{\mathrm{W}}}{f(T_2)_{\mathrm{W}}} \\[6mm]
\dfrac{\Delta f(T_1)}{f(T_1)} = \dfrac{-2 \exp\left[\dfrac{-\left(T_R - \dfrac{T_E}{2}\right)}{T_1}\right]\left(T_R - \dfrac{T_E}{2}\right) + T_R * e^{-T_R/T_1}}{1 - 2\exp\left[\dfrac{-\left(T_R - \dfrac{T_E}{2}\right)}{T_1}\right] + \exp\left(-\dfrac{T_R}{T_1}\right)} \cdot \dfrac{\Delta T_1}{T_1^2} \\[8mm]
\dfrac{\Delta f(T_2)}{f(T_2)} = \dfrac{T_E}{T_2^2} \Delta T_2
\end{cases}
$$

Chapter 5

QUALITY CONTROL MEASURES: PARTICIPATION IN NATIONAL PROJECT FOR SPECTROSCOPY INTERCOMPARISON

Several fundamental requirements must be met so that MRI and the related techniques can be formally adopted into clinical practice. Here we report an intercomparison exercise, which has evaluated the effectiveness of 1H MRS to generate comparable data sets from different machine vendors, using the available MR scanner in the different hospital of Florence:

- Philips Achieva 3 T (Azienda Ospedaliero Universitaria Meyer)
- Philips Achieva 1.5 T (P.O. Santa Maria Nuova Azienda Sanitaria di Firenze)
- Siemens Aera 1.5 T (P.O. San Giovanni di Dio, Azienda Sanitaria di Firenze)

This intercomparison is part of a national project of AIFM for validation of MRS data.

The research will be performed analyzing the spectroscopic signal coming from a specific test phantom, as described above.

This spectroscopic data will be analized with the jMRUI software package, looking for:

- Linearity of Amplitude of water signal with VOI volume
- Independence of Linewidth of water signal with VOI volume
- T_2 of water
- Spatial homogeneity of the signals

Overall, the comparability of data sets from the participating laboratories was good.

These results demonstrate that MRS-based study can generate data that are sufficiently comparable between hospitals to support its continued evaluation for clinical studies.

5.1 - Original intercomparison protocol

Here we report in italian language the original protocol.

Istruzioni per la partecipazione all'interconfronto di Spettroscopia

Strumenti necessari: bobina head, fantoccio proprietario di almeno 10 cm di diametro (se a disposizione maggiore di 15 cm di diametro), preferibilmente sferico (non necessariamente deve essere il fantoccio dedicato alla spettroscopia).
Preparazione:

1. Lasciare il fantoccio all'interno della sala magnete almeno dal giorno prima dell'acquisizione per permettere il raggiungimento di un buon equilibrio termico

2. Posizionare il fantoccio possibilmente al centro della bobina ed effettuare il centraggio in modo che il centro del fantoccio si venga a trovare all'isocentro dello scanner.
3. Attendere 5 minuti per permettere una buona stabilizzazione del liquido
4. Registrare la temperatura all'interno della sala magnete all'inizio e alla fine dell'acquisizione.

Acquisizione:

1. Eseguire una scout
2. Eseguire, se necessario,una scansione di calibrazione della bobina(se multicanale).
3. Effettuare le seguenti acquisizioni con tecnica PRESS e con i seguenti parametri:

    a.   1. PRESS senza soppressione dell'acqua (PRESS n.1)
         i. impostare la bobina di ricezione in quadratura se possibile
         ii. dimensioni del VOI: 20x20x20 mm^3
         iii. posizionare il VOI al centro del fantoccio
         iv. T_E = 30 ms (o minimo raggiungibile se $T_{E\text{-min}}$ > 30ms)
         v. T_R = 4000ms
         vi. Numero di medie = 16
         vii. Phase cycle = 16
         viii. Fissare se possibile il guadagno
         ix. Samples = 1024
         x. Bandwidth = 1000 Hz negli scanner a 1.5T e 2000 Hz negli scanner a 3T

    b. Ripetere la misura di cui al punto 1 spostando il centro del VOI di 4 cm in direzione alto-basso e destra-sinistra (PRESS n. 2a, PRESS n. 2b)

    c. Ripetere 5 volte la misura di cui al punto 1 nella stessa posizione, cambiando ogni volta la dimensione del VOI e impostando 10, 15, 20, 25, 30 mm di lato (per la misura 20 mm può essere utilizzata l'acquisizione al punto 1) (PRESS n. 3-10, PRESS n. 3-15, PRESS n. 3-25, PRESS n. 3-30)

    d. Ripetere 5 volte la misura di cui al punto 1 modificando ogni volta il T_E e impostando T_E=30, 100, 150, 300, 400 ms (PRESS n. 4-30, PRESS n. 4-100, PRESS n. 4-150, PRESS n. 4-300, PRESS n. 4-400). Per la misura con T_E= 30 ms può essere utilizzata la misura di cui al punto 1.

    La durata delle singole acquisizioni è di circa 1 minuto (a cui aggiungere eventuali preacquisizioni di preparazione e le operazioni di shimming).

    Per valutare la riproducibilità dei dati a lungo termine è auspicabile che questo protocollo sia ripetuto più volte con cadenza più possibile regolare nel tempo. In particolare è ottimale che si acquisiscano le misure cinque volte in due mesi. A seconda delle disponibilità delle apparecchiature e delle possibilità di ciascuno dei partecipanti questo numero può essere ridotto. I dati verranno analizzati di conseguenza.

Istruzioni per l'elaborazione degli spettri

1. Esportare gli spettri secondo la modalità e il formato disponibile presso il proprio centro
2. Salvare i dati in cartelle nominate con la data delle acquisizioni.
3. Rinominare i file corrispondenti alle singole acquisizioni secondo quanto riportato tra parentesi nel paragrafo "acquisizioni" e come anche indicato nel file Excel allegato (PRESS n.1, PRESS n. 2a, PRESS n. 2b, etc...).
4. Utilizzare il programma jMRUI per le elaborazioni

   a) Lanciare Jmrui
   b) scegliere l'opzione 1D Time Series.
   c) caricare il file relativo all'acquisizione.
   d) rifasare lo spettro per verificare eventuali distorsioni da disomogeneità (eddy currents etc.) o artefatti.
   e) Selezionare quindi dalla barra del menu in alto la voce "Quantitation-SVD-Hlsvd".
      a. Inserire in "Number of components" il numero 1 e lanciare la quantificazione, premendo il tasto Hlsvd.
      b. Apparirà una finestra "Results 1d mode" nella quale si potranno leggere:
         i. la frequenza
         ii. la larghezza a metà altezza (Linewidth in Hz)
         iii. l'ampiezza (Amplitude)
         iv. la fase (Phase in deg).
      c. Da questa finestra selezionare Options "Noise from original FID" scegliere 100 punti di misura e dare l'ok.
      d. Impostare inoltre le unità di misura in Hz e scegliere Linewidth in Hz per la misura della larghezza del picco (da "Options" e poi "Units").
      e. Infine selezionare "File, Save This, Save as a Text" e salvare i risultati ottenuti in un file di testo.
   f) Nel file di testo saranno riportate delle informazioni di questo tipo:

jMRUI Results Textfile:

Filename: CQ_SPETTRO_PRESS-H2O_3_2_raw_act.SDAT

Name of Patient: / Date of Experiment: / Spectrometer:

Additional Information:

Points Samp.Int.   ZeroOrder   BeginTime   Tra.Freq.   Magn.F. Nucleus

1024   1E0   0E0   0E0   6.39E7 1.5009E0 0E0

Name of Algorithm: HLSVD
PEAK #0
Frequencies (ppm): -2.6754E-2

Standard deviation of Frequencies (ppm): 1.7517E-5

Amplitudes (-): 3.7397E0

Standard deviation of Amplitudes (-): 2.5012E-2

Linewidths (Hz): -1.1016E0

Standard deviation of Linewidths (Hz): -1.0581E-2

Phases (degrees) -1.2344E2

Standard deviation of Phases (degrees) 3.832E-1

Noise: 2.1158E-1

pH	*Standard deviation of pH*	*[Mg2+]*	*Standard deviation of [Mg2+]*
Not known	*Not known*	*Not known*	*Not known*

g) Riportare quindi questi risultati nel file Excel allegato e corrispondentemente ad ogni singola acquisizione, per la quale dovrà essere effettuato l'intero processo di elaborazione.

h) A questo punto per le acquisizioni di cui al punto 3 inserire un grafico dell'ampiezza in funzione del volume:
   a. elevare al cubo la dimensione del lato del VOI
   b. fare un fit lineare.

i) Sempre in funzione del volume riportare anche l'andamento della linewidth.

j) Per le acquisizione del punto 4 inserire un grafico dell'ampiezza in funzione del T_E e fare un fit monoesponenziale.

k) Vedi file Excel già riempito come esempio.

5.2 - Intercomparison results

Azienda Ospedaliero Universitaria Meyer
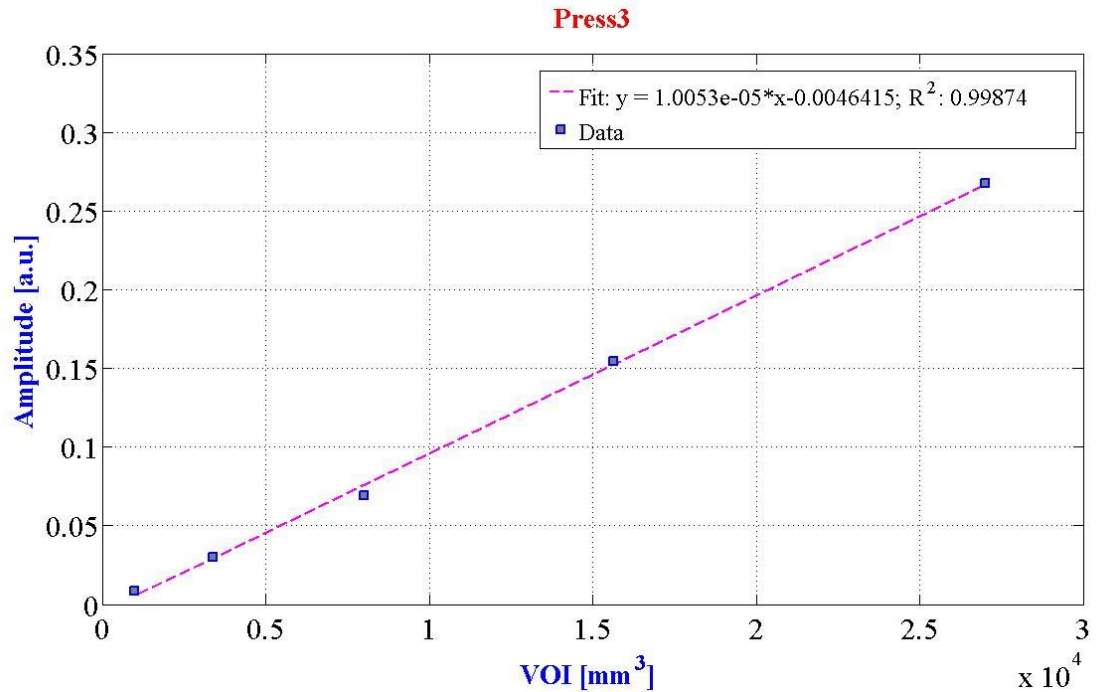
Figure 1: Meyer, Amplitude as a function of VOI volume.
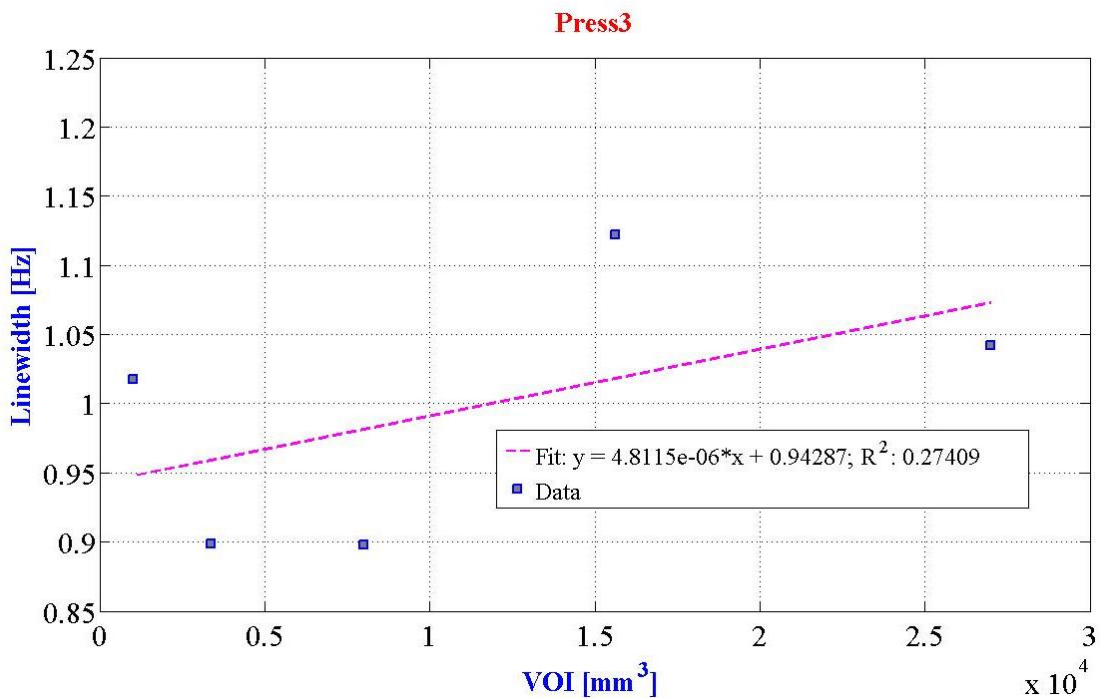
Figure 2: Meyer, Linewidth as a function of VOI volume.
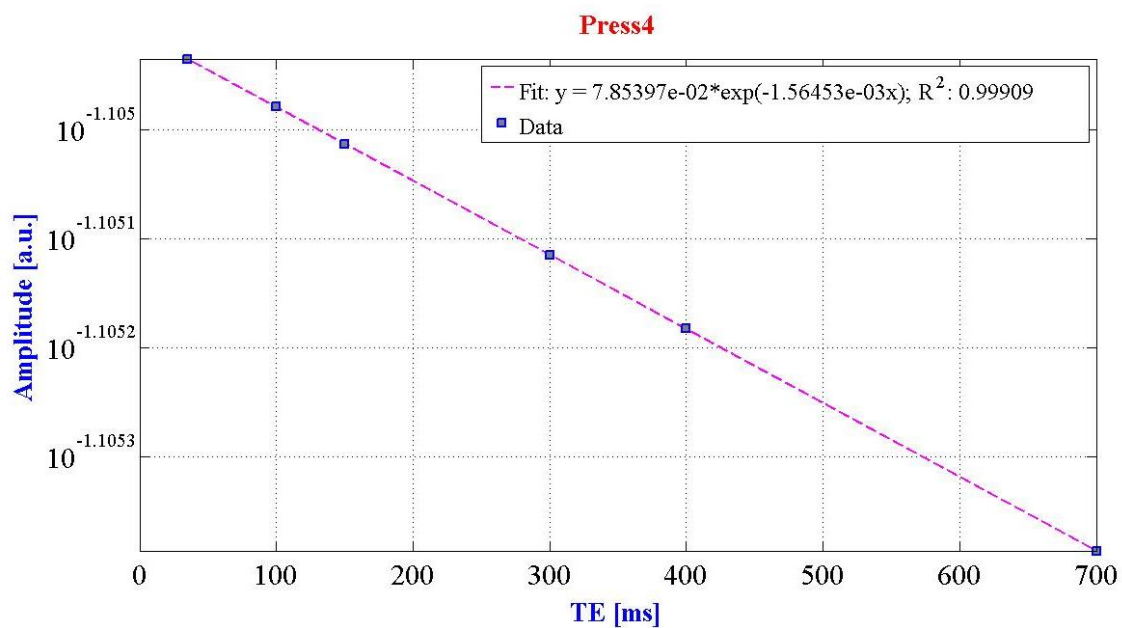
Figure 3: Meyer, Amplitude as a function of TE.

P.O. San Giovanni di Dio, Azienda Sanitaria di Firenze
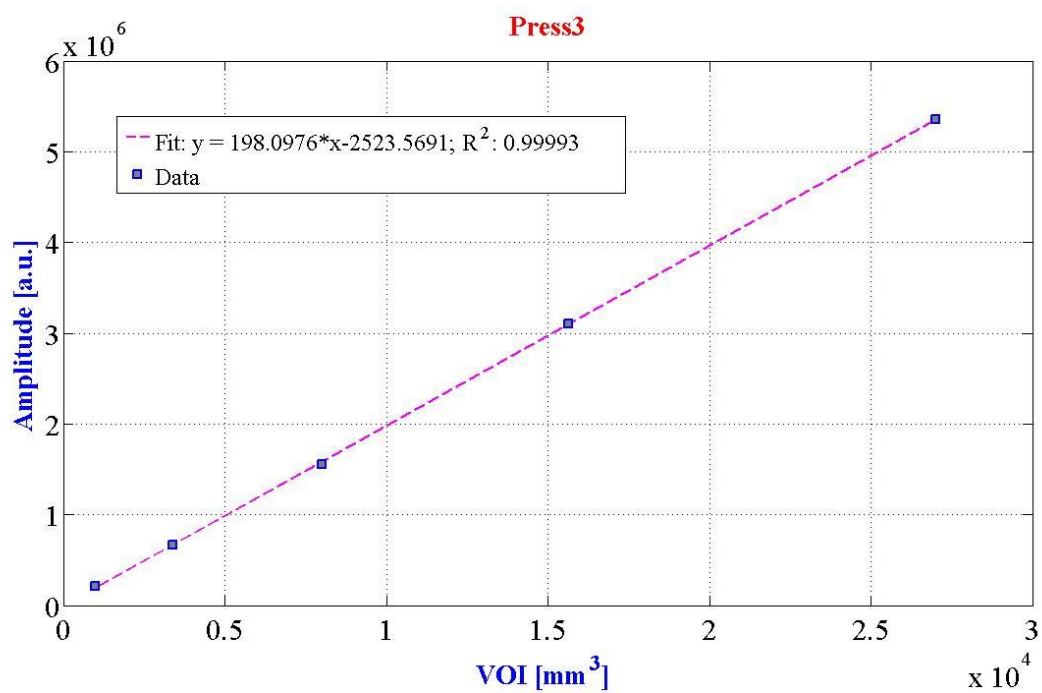
Figure 4: P.O. S.G.D., Amplitude as a function of VOI volume.
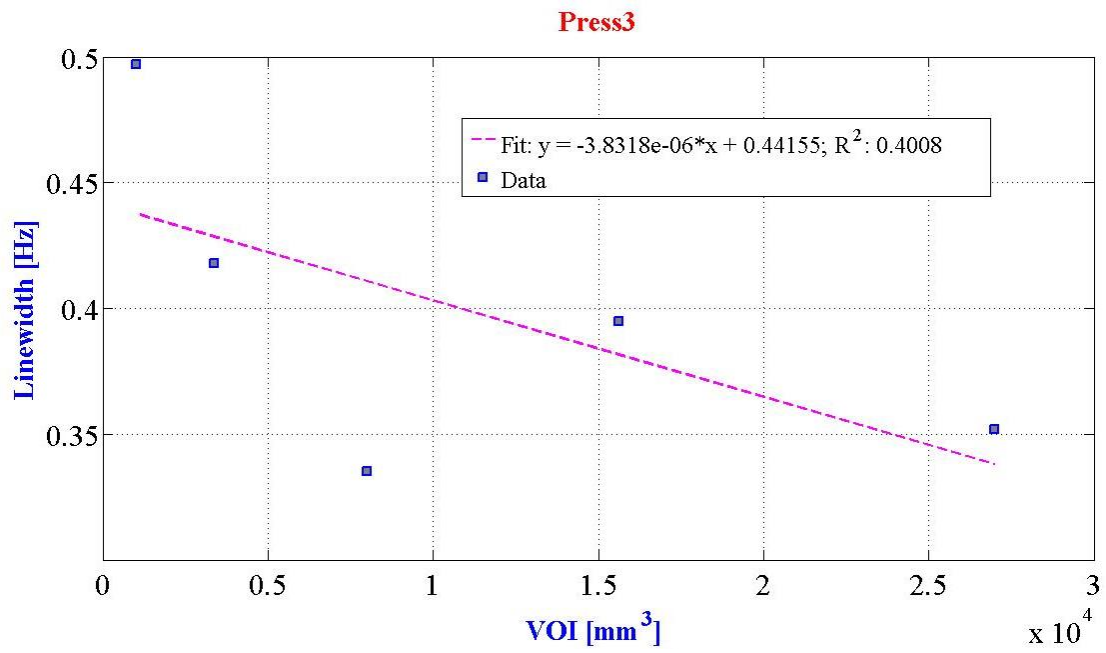
Figure 5: P.O. S.G.D, Linewidth as a function of VOI volume.
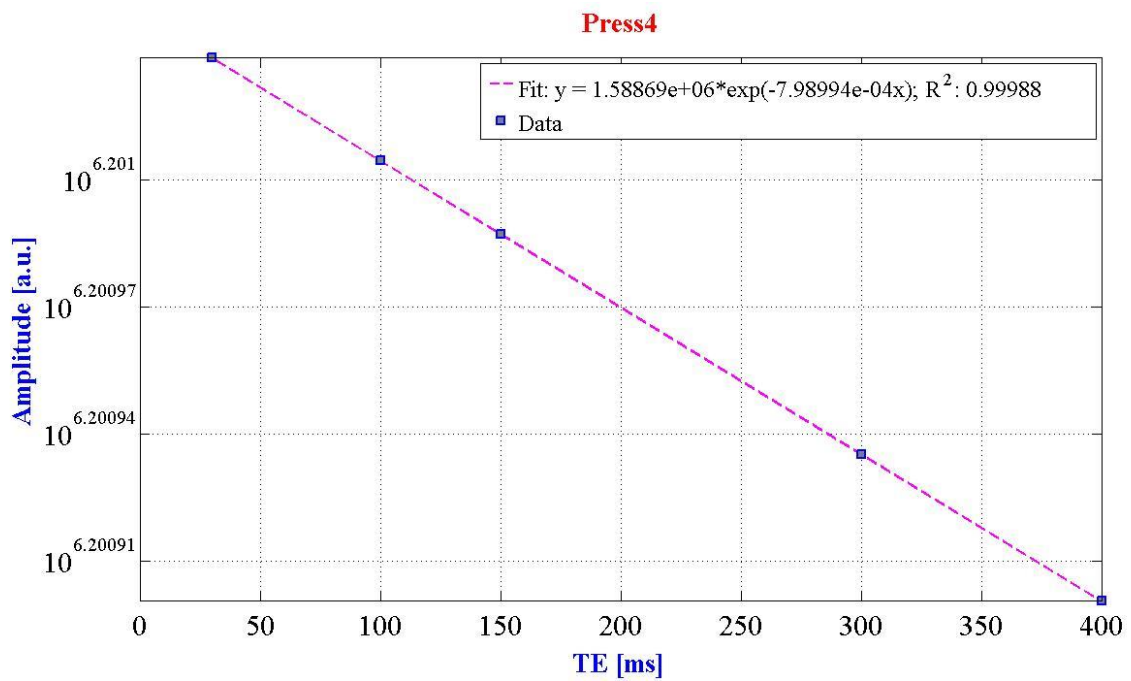
Figure 6: P.O. S.G.D., Amplitude as a function of TE.

P.O. Santa Maria Nuova Azienda Sanitaria di Firenze
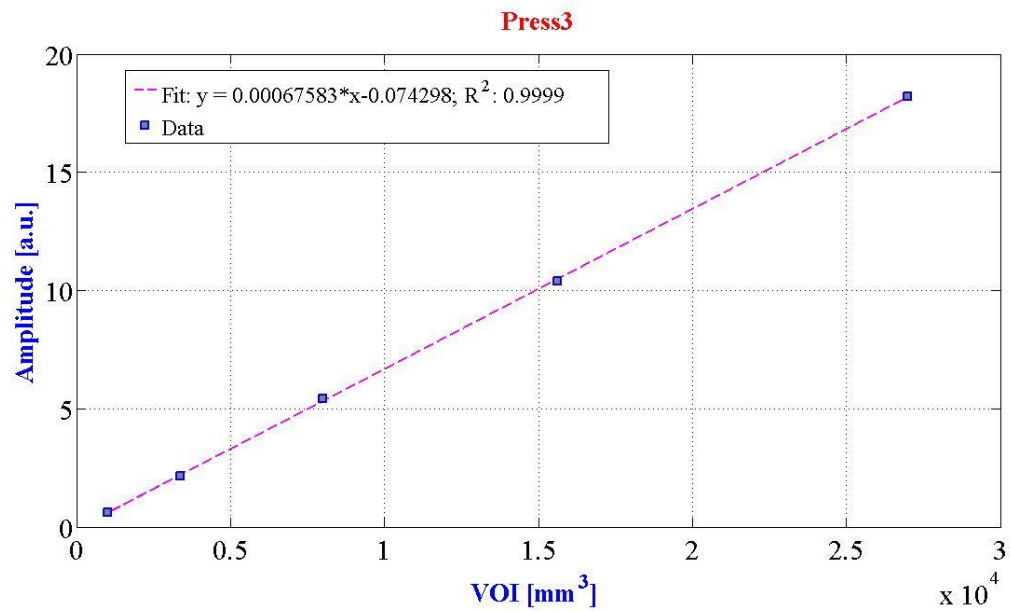
Figure 7: P.O. S.M.N., Amplitude as a function of VOI volume.
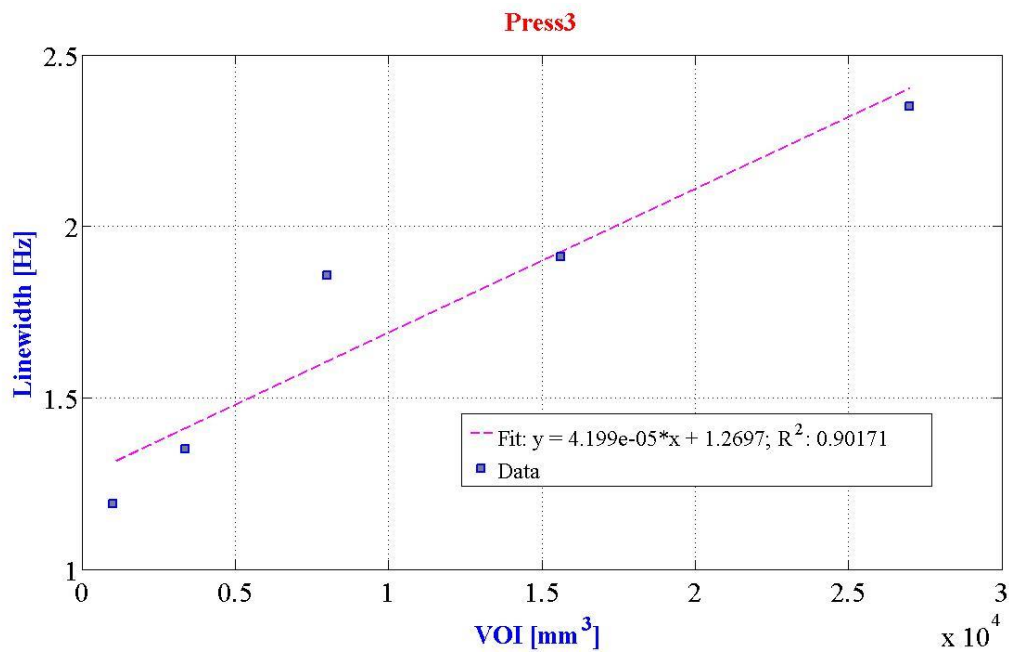
Figure 8: P.O. S.M.N., Linewidth as a function of VOI volume.
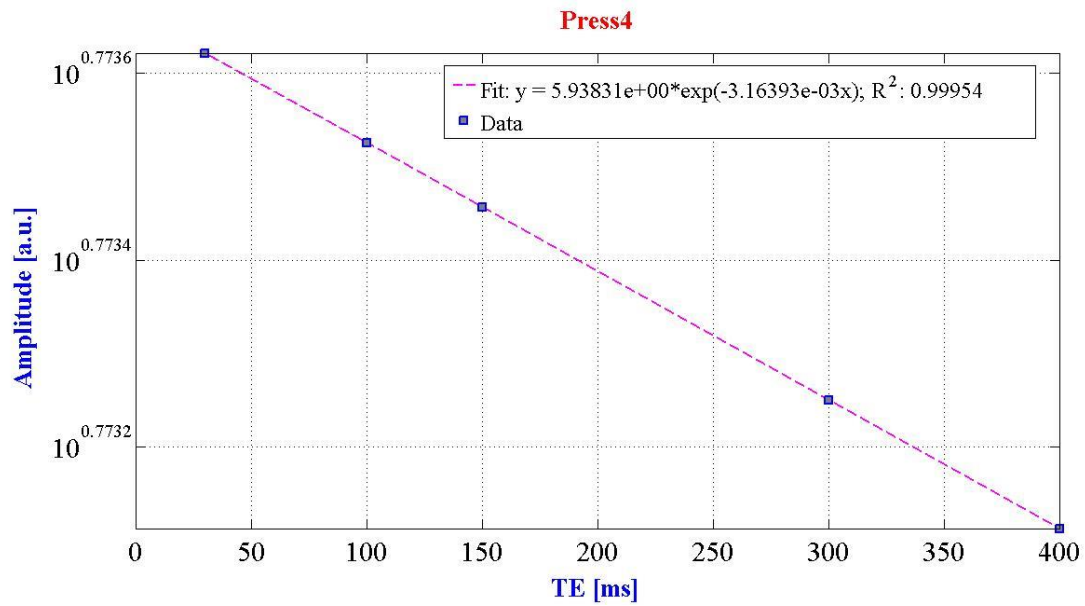
Figure 9: P.O. S.M.N., Amplitude as a function of TE.

The same analysis was performed with a difference setting of sequence parameters:

- Numberofkspacetrajectories: Press_SV_1 = 16; XX_0001 = 128

- Patientweight: Press_SV_1 = 10; XX_0001 = 20

- Transmitterfrequency: Press_SV_1 = 63.86; XX_0001 = 63.87

- suppression: Press_SV_1 = FAT; XX_0001 = NONE

- 0x2005,0x142b: Press_SV_1 = COMPLETED; XX_0001 = PARTIAL

- 0x2005,0x142c: Press_SV_1 = INITIAL; XX_0001 = PARTIAL

A different setting of sequence parameters reflects on signal amplitude and linewidth:

- Amplitude: Press_SV_1 = 2.025; XX_0001 = 5.4307

- Linewidth (Hz): Press_SV_1 = 0.9568; XX_0001 = 1.8581

Some results are shown below.
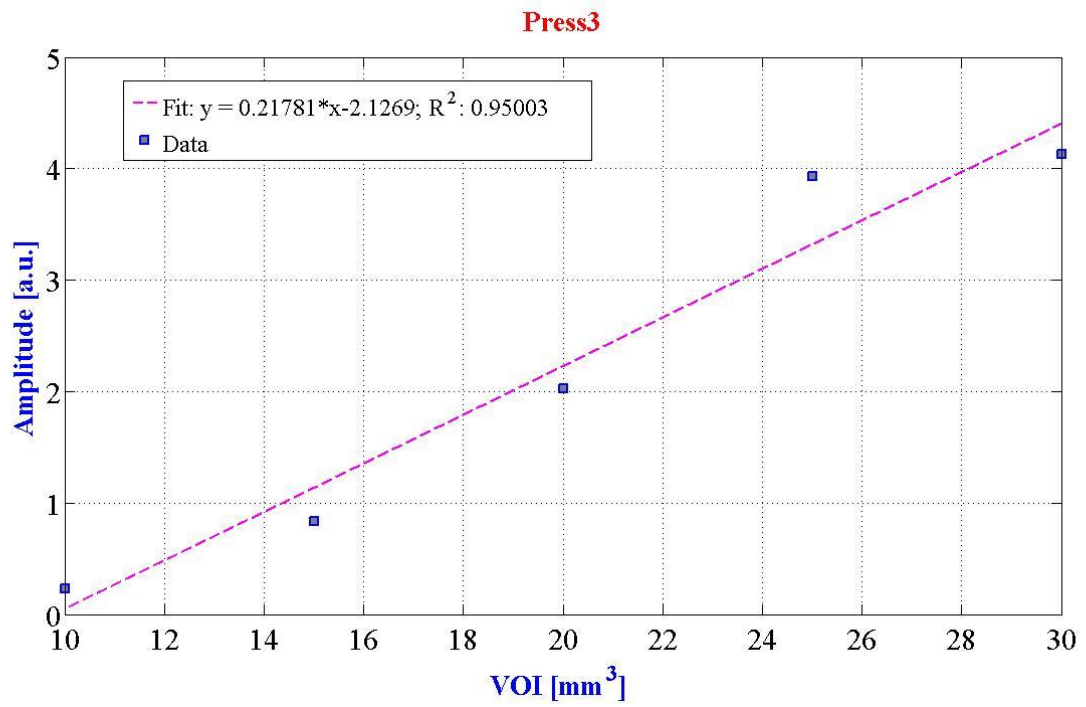
Figure 10: P.O. S.M.N., Amplitude as a function of VOI volume.
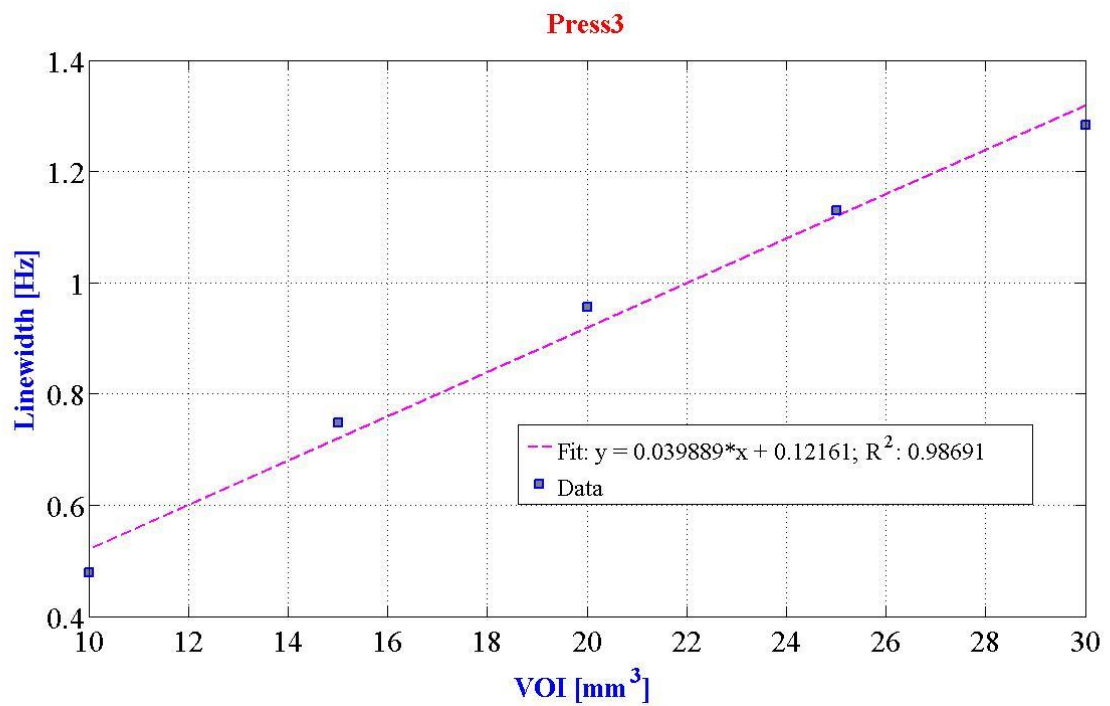
Figure 11: P.O. S.M.N., Linewidth as a function of VOI volume.

5.3 - Discussion of the results

Amplitude vs VOI volume

All hospital show a very good linearity of the amplitude of water signal as a function of VOI volume.

Linewidth vs VOI volume

Linewidth as a function of VOI volume is better for P.O. S.G.D. (0.44 Hz) than S.M.N. (1.3 Hz). Meyer has a mean linewidth of 0.94 Hz but with a static magnetic field of 3.0 T, then in relative very similar to S.G.D.

T2 of water

Meyer = 639 ms

S.G.D. = 1252 ms

S.M.N. = 316 ms

Spatial homogeneity of the signal

Meyer has a low amplitude spatial homogeniety due to the problems in shimming at 3T respect to 1.5T. Note that data are normalized to "Central position" (Figure 12).

Linewidth shows some variations with positions in particular for Meyer MR scanner at 3.0 T, still due to the problems discussed above. Please note that data from Meyer come from a 3T MR scanner, this must be taken into account when confront data coming from MR scanner at different B_0.
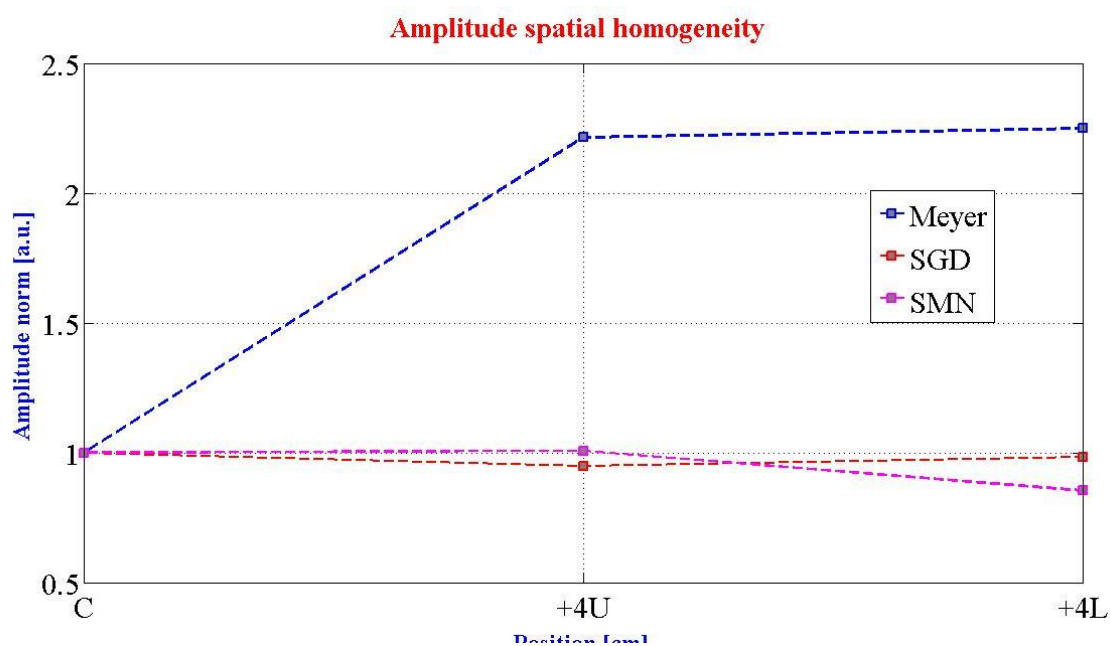
Figure 12: Amplitude spatial homogeneity. "C" means central position, "+4U" means a displacement of 4 cm upper, while "+4L" means lateral. Data are normalized to "Central position".
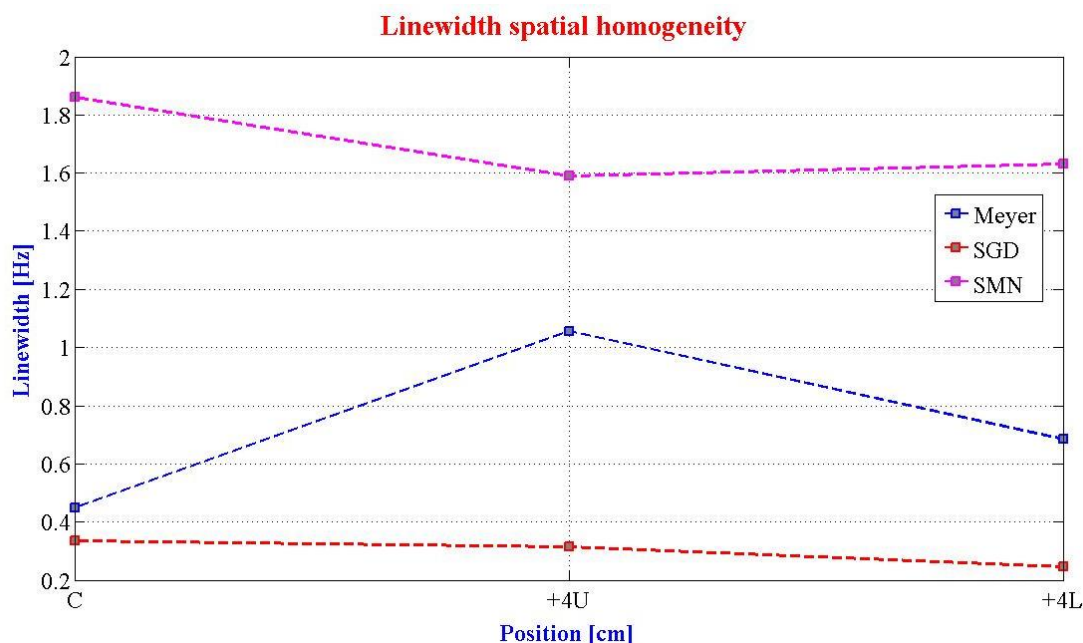
Figure 13: Linewidth spatial homogeneity. "C" means central position, "+4U"
means a displacement of 4 cm upper, while "+4L" means lateral.
For Meyer data it must be taken in account that data come from a 3T MR scanner.

Some disomogeneity effects at 3t may be interpreted by the dielectric effect [Ref. 153, 154, 155].

In MRI we often focus on magnetic fields like B_0 and B_1, so it is easy to forget that a coexisting electric field (E) is always present. As described by the Maxwell equations, B and E fields oscillate perpendicular to each other and to the direction of wave propagation. When electromagnetic waves encounter the human body, several phenomena occur: 1) the wavelength decreases; 2) electrical currents are generated; and 3) wave reflection/refraction may develop at tissue interfaces. The term dielectric effect refers to the interaction of matter with the E component of an electromagnetic field.

Abnormal bright and dark areas due to B_1 field inhomogeneity are frequently noted at very high fields (3T and above). Although the nature of these artifacts is not entirely clear, these are commonly referred to as dielectric artifacts.

The argument that these artifacts are due to dielectric effects is based on considering RF-wavelengths in tissues as a function of field strength. At fields of 1.5T and lower, RF wavelengths are long compared to the size of the body, but as the magnetic field is increased, these wavelengths become the same or smaller than the anatomic regions imaged. In theory standing wave currents might arise flowing in opposite directions from two sides of the patient creating a pattern with destructive interference (dark areas) and constructive interference (bright areas) separated by quarter wavelengths.

The degree to which significant dielectric resonances cause these bright and dark areas remain controversial. The relatively high electrical conductivity of tissues introduces a "skin-depth" term that serves to damp standing wave phenomena. Central brightening has been demonstrated in high-conductivity phantoms where dielectric resonances should be minimal.

Chapter 6

SIEMENS PHANTOM T_1 AT 3 T

In this part some results about the MRS measurements pe rformed using the Philips Achieva 3 T scanner at the Azienda Ospedaliero Universitaria Meyer are shown.

In this part we focus on the estimation of water and metabolites (Acetate, Lactate) T_1 relaxation time at 3 T.

Spectra have been acquired with the Siemens phantom using different sequences parameters, looking for the difference in the estimation. E.g. data have been acquired with different inversion bandwidth in the case of multi-inversion sequence, or using a different TE in order to highlight the behavior of Lactate. All of this will be discussed here. At the same time post-processing has been performed using different algorithms (HLSVD, AMARES and in one case QUEST), with and without apodization (lorentzian apodization with 5 Hz) of spectra and using different fit functions, looking for the difference in the estimations. A good reference to understand problems in spectra fitting can be found in Ref. 214.

6.1 - T_1 relaxation time

Measurements were performed using a inversion recovery sequences at different T_I.

Peaks area were estimated with HLSVD and AMARES (in some case with QUEST too). It is very important to highlight the importance of removing the residual water peak in the metabolites spectrum, allowing a good estimation of meatabolites peaks as small as the lactate quadrouplet.
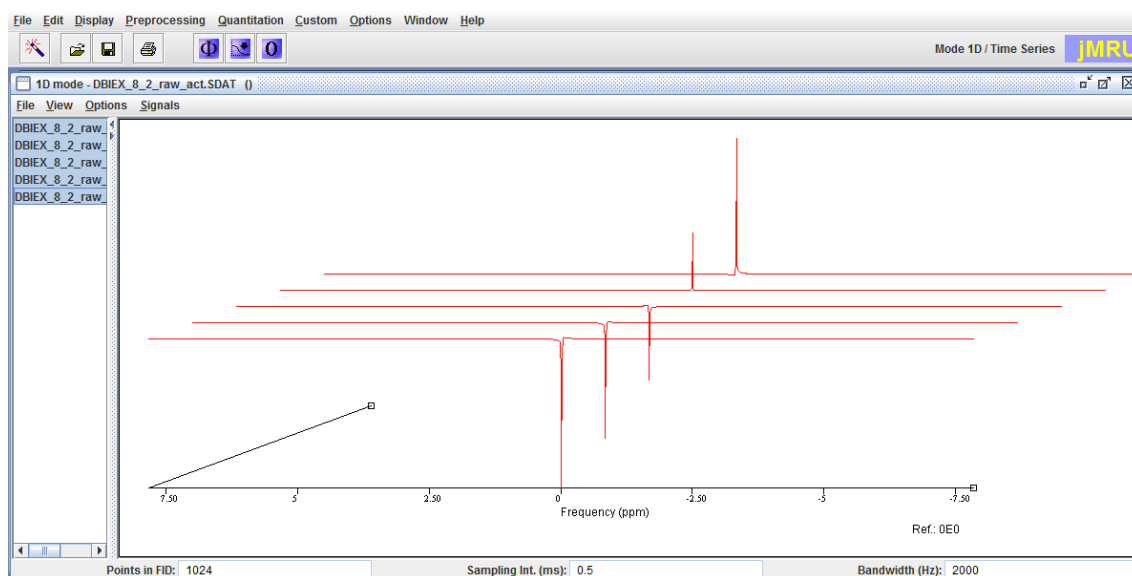
Figure 1: Example Water spectrum with multi-inversion time displayed in jMRUI. T_I(ms): 30, 250, 700, 2500, 5400. T_E = 35 ms. T_R = 6000 ms. NSA = 16, Phase cycles = 16. Inv. Bandwidth = 1500 Hz.
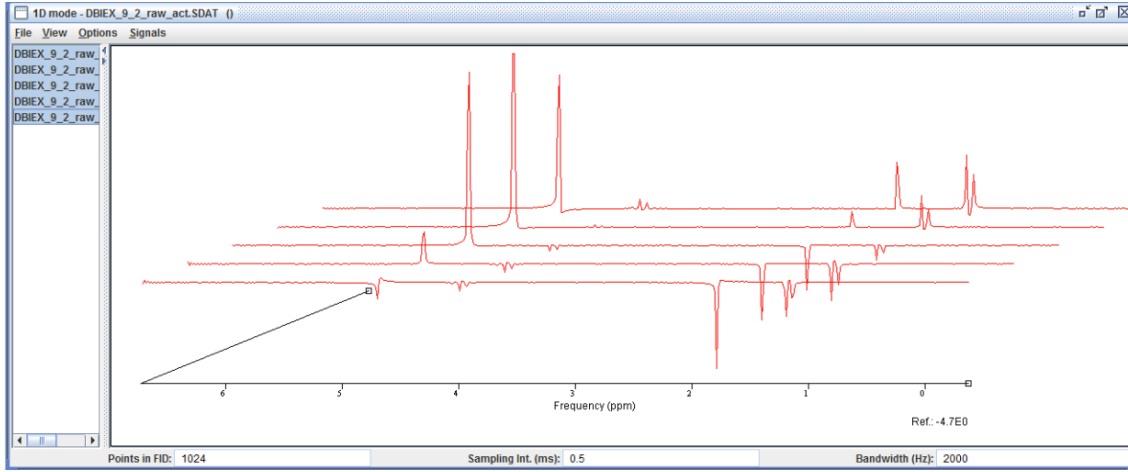
Figure 2: Example of metabolities spectrum with multi-inversion time displayed in jMRUI. The residual water peak is visible at about 4.7 ppm. Metabolites peaks: acetate at about 1.9 ppm, lactate doublet at about 1.3 ppm and lactate quadruplet at about 4.1 ppm. T_I (ms): 30, 250, 700, 2500, 5400. T_E = 35 ms. T_R = 6000 ms. NSA = 16, Phase cycles = 16. Inv. Bandwidth = 1500 Hz.

In this case the fitting were performed with three different function:

$$\begin{cases} f1(T_1) = a(1 - 2 * e^{-\frac{T_I}{T_1}}) \\ f2(T_1) = a(1 - 2 * e^{-\frac{T_I}{T_1}} + e^{-\frac{T_R - T_E}{T_1}}) \\ f3(T_1) = a(1 - (1-k) * e^{-\frac{T_I}{T_1}} + ke^{-\frac{T_R - T_E}{T_1}}) \end{cases}$$

where "a" is the signal at equilibrium magnetization, K the cosine of the effective flip angle of the inversion pulse. A perfect inversion pulse has $k = -1$.

$f1$ is an approximation of $f2$ when $T_R \gg T_1$, usually $T_R = 5T_1$, while $f3$ account for an incomplete inversion pulse.

Usually $f3$ is used when the inversion band is large (e.g. 1500 Hz for Acetate and Lactate).

A multi-inversion time inversion recovery sequences with inversion time up to 15 seconds were used to estimate T_1, allowing to evaluate the difference in fitting between $f1$, $f2$ and $f3$. Long inversion time allows to saturate the signal of metabolites, reaching a better fit estimation of the relaxation time.

A different number of NSA and phase-cycles were used in the different cases to highlight differences in the estimation, looking for criticity. A low number of NSA and/or phase cycles might reflect in some distortion in the peaks shape due to a low SNR and to eddy currents.

Using cftool toolbox in MATLAB we can find the best fit of data versus T_I, which give an estimation for the amplitude of the signal and the T_1 of water and metabolites.

Cftool uses the method of least squares when fitting data. Fitting requires a parametric model that relates the response data to the predictor data with one or more coefficients. The result of the fitting process is an estimate of the model coefficients. The supported types of least-squares fitting include Linear least squares, Weighted linear least squares, Robust least squares, Nonlinear least squares.

While water data fitting is not influenced by errors in the estimated amplitude by jmrui, metabolites fitting have many problems. Lactate quadrouplet fitting is very difficult and sometimes won't be considered.

It is usually assumed that the response errors follow a normal distribution, and that extreme values are rare. Still, extreme values called outliers do occur. The main disadvantage of least-squares fitting is its sensitivity to outliers. Outliers have a large influence on the fit because squaring the residuals magnifies the effects of these extreme data points. To minimize the influence of outliers, fit data can be performed using robust least-squares regression. The toolbox provides these two robust regression methods:

• Least absolute residuals (LAR) — The LAR method finds a curve that minimizes the absolute difference of the residuals, rather than the squared differences. Therefore, extreme values have a lesser influence on the fit.
• Bisquare weights — This method minimizes a weighted sum of squares, where the weight given to each data point depends on how far the point is from the fitted line. Points near the line get full weight. Points farther from the line get reduced weight. Points that are farther from the line than would be expected by random chance get zero weight.

For most cases, the bisquare weight method is preferred over LAR because it simultaneously seeks to find a curve that fits the bulk of the data using the usual least-squares approach, and it minimizes the effect of outliers.

Robust fitting with bisquare weights uses an iteratively reweighted least-squares algorithm. Water and metabolites fitting have been fitted with one of the previous methods always looking for the best fit in terms of Chi-square.

Errors in the estimates have been evaluated automatically by the fitting procedure.

Data on the sequences parameters can be found in Appendix 2.

6.1.1 - Water T_1 relaxation time

In Table 1 are shown results about T_1 for water. Estimation of amplitude signal and parameter K for fit function $f3$ are shown too.

Table 1: Water results for T_1.

Algorithm	T_1 [ms]	ΔT_1 [ms]	A	ΔA	K	ΔK	Date
HLSVDf1	2335	532	0.1004	0.0142			70315
HLSVDf2	3167	633	0.1123	0.0098			70315
HLSVDf3	3197	1751	0.1432	0.0684	-0.575	0.3922	70315
HLSVDAPOf1	2343	374	0.09674	0.00956		0	70315
HLSVDAPOf2	3152	282	0.1078	0.0043		0	70315
HLSVDAPOf3	2981	323	0.129	0.0122	-0.6327	0.0849	70315
AMARESf1	2333	352	0.101	0.0095		0	70315

AMARESf2	3106	418	0.1121	0.0066		0	70315
AMARESf3	2892	647	0.1315	0.0256	-0.6556	0.1808	70315
AMARESAPOf1	2344	583	0.1011	0.0156		0	70315
AMARESAPOf2	3230	668	0.1137	0.0104		0	70315
AMARESAPOf3	3389	1876	0.1514	0.0734	-0.5351	0.3706	70315
QUESTf1	2371	516	0.08714	0.01181		0	70315
QUESTf2	3232	983	0.09785	0.01305		0	70315
QUESTf3	3060	2357	0.1182	0.08	-0.6175	0.5925	70315
QUESTAPOf1	2355	333	0.09209	0.00811		0	70315
QUESTAPOf2	3169	424	0.1027	0.006		0	70315
QUESTAPOf3	2909	393	0.1197	0.0142	-0.6566	0.1098	70315
HLSVDf1	3077	142	0.1152	0.0033		0	10615
HLSVDf2	3127	169	0.1155	0.0036		0	10615
HLSVDf3	3024	335	0.1148	0.0083	-1.003	0.1	10615
HLSVDAPOf1	3105	47	0.1119	0.0011		0	10615
HLSVDAPOf2	3159	68	0.1123	0.0013		0	10615
HLSVDAPOf3	3100	118	0.1127	0.0029	-0.9858	0.0342	10615
AMARESf1	3085	149	0.1155	0.0034		0	10615
AMARESf2	3136	177	0.1158	0.0037		0	10615
AMARESf3	3031	354	0.1151	0.0087	-1.003	2.112	10615
AMARESAPOf1	3140	293	0.1131	0.0065		0	10615
AMARESAPOf2	3193	345	0.1134	0.007		0	10615
AMARESAPOf3	2946	612	0.1093	0.0149	-1.051	0.196	10615
HLSVDf1	3194	40	0.1199	9.00000E-04		0	20615
HLSVDf2	3260	60	0.1203	0.0013		0	20615
HLSVDf3	3201	102	0.1212	0.0026	-0.9797	0.0293	20615
HLSVDAPOf1	3203	22	0.1145	0.0005		0	20615
HLSVDAPOf2	3270	32	0.1149	7.00000E-04		0	20615
HLSVDAPOf3	3230	39	0.1163	9.00000E-04	-0.973	0.0112	20615
AMARESf1	3205	41	0.1186	9.00000E-04		0	20615
AMARESf2	3273	40	0.119	8.00000E-04		0	20615
AMARESf3	3248	83	0.1208	0.0021	-0.9681	0.0233	20615

AMARESAPOf1	3136	299	0.109	0.0064		0	20615
AMARESAPOf2	3192	341	0.1093	0.0067		0	20615
AMARESAPOf3	3068	725	0.1083	0.017	-1.007	0.217	20615
HLSVDf1	3294	173	0.1241	0.0041		0	30615
HLSVDf2	3370	213	0.1247	0.0045		0	30615
HLSVDf3	3243	443	0.1241	0.0117	-0.9953	0.1277	30615
HLSVDAPOf1	3262	67	0.1173	0.0016		0	30615
HLSVDAPOf2	3336	91	0.1178	0.0019		0	30615
HLSVDAPOf3	3262	175	0.1185	0.0044	-0.9801	0.0499	30615
AMARESf1	3369	225	0.1253	0.0053		0	30615
AMARESf2	3452	297	0.1259	0.0062		0	30615
AMARESf3	3152	448	0.1209	0.0119	-1.048	0.14	30615
AMARESAPOf1	3091	295	0.1137	0.0066		0	30615
AMARESAPOf2	3146	322	0.114	0.0067		0	30615
AMARESAPOf3	3149	750	0.1161	0.0183	-0.9655	0.2105	30615
HLSVDf1	3134	220	0.1179	0.0051		0	40615
HLSVDf2	3199	219	0.1183	0.0047		0	40615
HLSVDf3	3381	463	0.1253	0.0117	-0.9075	0.1175	40615
HLSVDAPOf1	3157	117	0.1129	0.0026		0	40615
HLSVDAPOf2	3222	97	0.1133	0.002		0	40615
HLSVDAPOf3	3321	174	0.118	0.004	-0.9316	0.0459	40615
AMARESf1	3132	217	0.1172	0.005		0	40615
AMARESf2	3195	221	0.1176	0.0044		0	40615
AMARESf3	3333	497	0.1234	0.0125	-0.9206	0.1284	40615
AMARESAPOf1	3184	270	0.112	0.0059		0	40615
AMARESAPOf2	3240	331	0.1123	0.0066		0	40615
AMARESAPOf3	2933	492	0.1069	0.0119	-1.07	2.301	40615
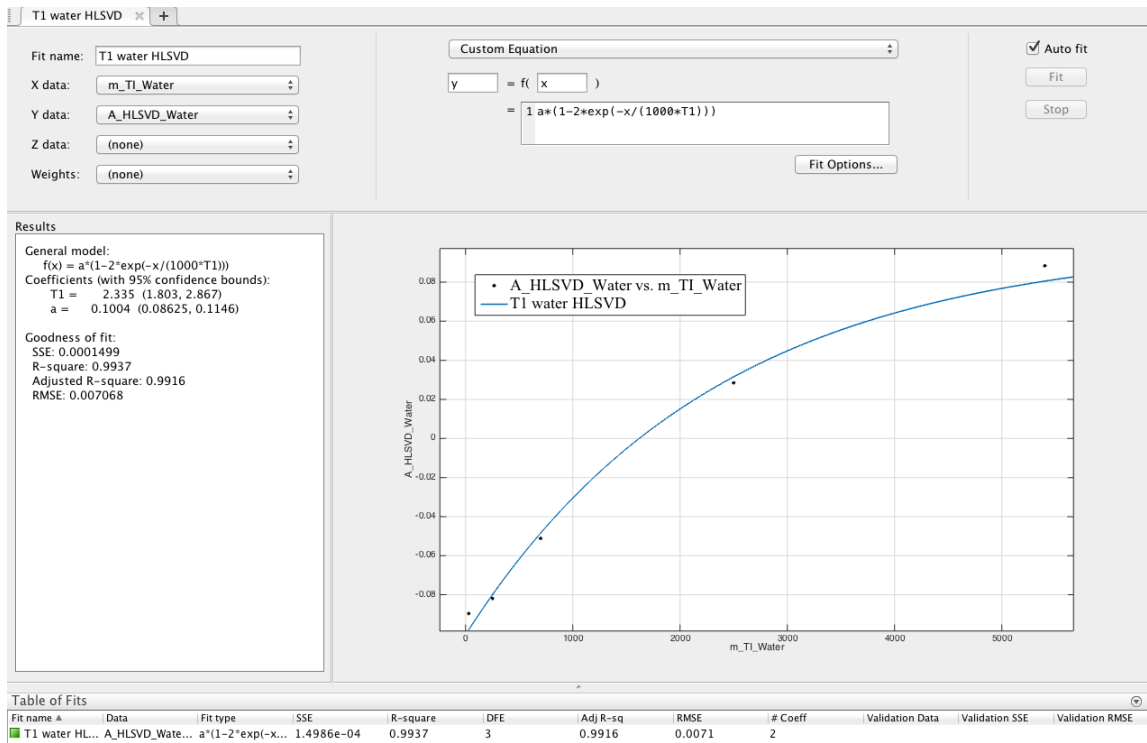
Figure 3: example of water data fitting with MATLAB-cftool using $f1$ function for fitting. Data obtained by HLSVD algorithm.

Water T1

TE: 35 ms
TR: 6000 ms
NSA: 16
Phase cycles:16
TI: 30, 250, 700, 2500, 5400
inv. bw: 1500 Hz

TE: 28 ms
TR: 15000 ms
NSA: 2
Phase cycles: 2
TI: 10, 300, 1000, 3000, 5000, 8000, 10000
inv. bw: 1500 Hz

TE: 28 ms
TR: 15000 ms
NSA: 2
Phase cycles: 2
TI: 10, 300, 1000, 3000, 5000, 8000, 10000
inv. bw: 200 Hz

	HLSVDf2	HLSVDA POf2	AMARESf 2	AMARES APOf2	QUESTf2	QUESTAP Of2	HLSVDf2	HLSVDA POf2	AMARESf 2	AMARES APOf2	HLSVDf2	HLSVDA POf2	AMARESf 2	AMARES APOf2	HLSVDf2	HLSVDA POf2	AMARESf 2	AMARES APOf2	HLSVDf2	HLSVDA POf2	AMARESf 2	AMARES APOf2
f1	2335	2343	2333	2344	2371	2355	3077	3105	3085	3140	3194	3263	3205	3136	3294	3262	3369	3091	3134	3157	3132	3184
f2	3167	3152	3106	3230	3232	3169	3127	3159	3136	3193	3260	3270	3273	3192	3370	3336	3452	3146	3199	3222	3195	3240
f3	3197	2981	2892	3389	3060	2909	3024	3100	3031	2946	3201	3230	3248	3068	3243	3262	3152	3148	3381	3321	3333	2933

7/03/15   1/06/15   2/06/15   2/06/15 2th   2/06/15 3th

Figure 4: Water $T1$ estimation at different time with different sequence parameters, algorithms (HLSVD, AMARES and QUEST). Apodization has been tested for all the algorithms. Error bars have been estimated automatically by the fitting procedure with MATLAB-cftool.

Function fitting f1 is too aproximated for short T_R, while f3 is too complex, however giving estimates very similar to f2.

The best estimates are choosen as average and standard deviation for f2 function fitting in dependence of different sequence parameters.

Table 2: Water T_1 average and std for the different sequences.
The estimate have been evaluated with f2 fit function.

	T_1 [ms]	ΔT_1 [ms]
7/03/15	3176	44
1/06-2/06-2/06 2th	3243	99
2/06 3th	3214	18

6.1.2 - Acetate T_1 relaxation time

Table 3: Acetate T_1 results.

Algorithm	T_1 [s]	ΔT_1 [s]	A	ΔA	K	ΔK	Date
HLSVDf1	2.60E-00	5.14E-01	3.65E-04	4.80E-05	0.00E+01	0.00E+01	70315
HLSVDf2	4.14E-00	4.23E-01	4.42E-04	2.14E-05	0.00E+01	0.00E+01	70315
HLSVDf3	3.86E-00	5.00E-01	5.72E-04	6.61E-05	-4.91E-01	8.18E-02	70315
HLSVDAPOf1	2.62E-00	5.51E-01	3.42E-04	4.78E-05	0.00E+01	0.00E+01	70315
HLSVDAPOf2	4.28E-00	3.24E-01	4.19E-04	1.54E-05	0.00E+01	0.00E+01	70315
HLSVDAPOf3	4.06E-00	4.25E-01	5.55E-04	5.22E-05	-4.67E-01	6.30E-02	70315
AMARESf1	2.61E-00	5.05E-01	3.66E-04	4.71E-05	0.00E+01	0.00E+01	70315
AMARESf2	4.15E-00	6.19E-01	4.44E-04	3.16E-05	0.00E+01	0.00E+01	70315
AMARESf3	3.81E-00	9.86E-01	5.67E-04	1.31E-04	-5.01E-01	1.66E-01	70315
AMARESAPOf1	2.63E-00	5.51E-01	3.43E-04	4.79E-05	0.00E+01	0.00E+01	70315
AMARESAPOf2	4.28E-00	3.20E-01	4.22E-04	1.52E-05	0.00E+01	0.00E+01	70315
AMARESAPOf3	4.05E-00	1.65E-01	5.60E-04	2.04E-05	-4.66E-01	2.44E-02	70315
HLSVDf1	3.47E-00	3.41E-01	4.15E-04	3.37E-05	0.00E+01	0.00E+01	200515
HLSVDf2	3.95E-00	3.53E-01	4.23E-04	2.24E-05	0.00E+01	0.00E+01	200515
HLSVDf3	4.12E-00	8.14E-01	4.94E-04	7.43E-05	-7.25E-01	1.79E-01	200515
HLSVDAPOf1	3.54E-00	2.52E-01	3.90E-04	2.32E-05	0.00E+01	0.00E+01	200515

HLSVDAPOf2	4.06E-00	1.78E-01	3.98E-04	1.03E-05	0.00E+01	0.00E+01	200515
HLSVDAPOf3	4.09E-00	4.08E-01	4.55E-04	3.50E-05	-7.50E-01	9.40E-02	200515
AMARESf1	3.55E-00	2.67E-01	4.19E-04	2.62E-05	0.00E+01	0.00E+01	200515
AMARESf2	4.07E-00	2.14E-01	4.27E-04	1.32E-05	0.00E+01	0.00E+01	200515
AMARESf3	4.10E-00	4.93E-01	4.90E-04	4.55E-05	-7.47E-01	1.13E-01	200515
AMARESAPOf1	3.56E-00	2.62E-01	3.93E-04	2.40E-05	0.00E+01	0.00E+01	200515
AMARESAPOf2	4.10E-00	1.38E-01	4.01E-04	8.00E-06	0.00E+01	0.00E+01	200515
AMARESAPOf3	4.17E-00	3.09E-01	4.64E-04	2.66E-05	-7.36E-01	6.88E-02	200515
HLSVDf1	3.80E-00	1.38E-01	4.30E-04	1.34E-05	0.00E+01	0.00E+01	10615
HLSVDf2	3.97E-00	1.12E-01	4.34E-04	9.00E-06	0.00E+01	0.00E+01	10615
HLSVDf3	4.08E-00	3.06E-01	4.62E-04	2.70E-05	-8.84E-01	7.69E-02	10615
HLSVDAPOf1	3.77E-00	1.95E-01	4.32E-04	1.90E-05	0.00E+01	0.00E+01	10615
HLSVDAPOf2	3.93E-00	1.71E-01	4.35E-04	1.40E-05	0.00E+01	0.00E+01	10615
HLSVDAPOf3	4.20E-00	3.71E-01	4.77E-04	3.28E-05	-8.44E-01	8.70E-02	10615
AMARESf1	3.80E-00	2.60E-01	4.50E-04	2.64E-05	0.00E+01	0.00E+01	10615
AMARESf2	3.95E-00	2.75E-01	4.53E-04	2.33E-05	0.00E+01	0.00E+01	10615
AMARESf3	4.18E-00	8.18E-01	4.93E-04	7.52E-05	-8.53E-01	1.95E-01	10615
AMARESAPOf1	3.85E-00	1.21E-01	4.17E-04	1.13E-05	0.00E+01	0.00E+01	10615
AMARESAPOf2	4.02E-00	1.39E-01	4.20E-04	1.08E-05	0.00E+01	0.00E+01	10615
AMARESAPOf3	3.97E-00	3.99E-01	4.35E-04	3.40E-05	-9.25E-01	1.07E-01	10615
HLSVDf1	3.95E-00	1.82E-01	4.14E-04	1.66E-05	0.00E+01	0.00E+01	2.06E+04
HLSVDf2	4.16E-00	1.52E-01	4.18E-04	1.13E-05	0.00E+01	0.00E+01	2.06E+04
HLSVDf3	4.36E-00	3.91E-01	4.57E-04	3.30E-05	-8.47E-01	9.01E-02	2.06E+04
HLSVDAPOf1	3.98E-00	8.60E-02	4.00E-04	7.60E-06	0.00E+01	0.00E+01	2.06E+04
HLSVDAPOf2	4.20E-00	6.60E-02	4.04E-04	4.70E-06	0.00E+01	0.00E+01	2.06E+04
HLSVDAPOf3	4.17E-00	1.90E-01	4.23E-04	1.55E-05	-9.06E-01	4.87E-02	2.06E+04
AMARESf1	3.96E-00	2.06E-01	4.20E-04	1.90E-05	0.00E+01	0.00E+01	2.06E+04
AMARESf2	4.18E-00	1.85E-01	4.24E-04	1.39E-05	0.00E+01	0.00E+01	2.06E+04
AMARESf3	4.42E-00	4.95E-01	4.67E-04	4.22E-05	-8.37E-01	1.12E-01	2.06E+04
AMARESAPOf1	3.97E-00	1.25E-01	3.99E-04	1.10E-05	0.00E+01	0.00E+01	2.06E+04
AMARESAPOf2	4.19E-00	8.20E-02	4.03E-04	5.80E-06	0.00E+01	0.00E+01	2.06E+04
AMARESAPOf3	4.26E-00	2.33E-01	4.30E-04	1.88E-05	-8.77E-01	5.67E-02	2.06E+04

HLSVDf2	4.09E-00	3.82E-01	4.54E-04	3.14E-05	0.00E+01	0.00E+01	3.06E+04
HLSVDf3	4.25E-00	1.20E-00	4.92E-04	1.10E-04	-8.60E-01	2.85E-01	3.06E+04
HLSVDAPOf2	4.05E-00	3.82E-01	4.23E-04	2.95E-05	0.00E+01	0.00E+01	3.06E+04
HLSVDAPOf3	3.90E-00	1.05E-00	4.30E-04	9.02E-05	-9.53E-01	2.95E-01	3.06E+04
AMARESf2	4.04E-00	4.98E-01	4.63E-04	4.23E-05	0.00E+01	0.00E+01	3.06E+04
AMARESf3	4.28E-00	1.60E-00	5.08E-04	1.50E-04	-8.45E-01	3.71E-01	3.06E+04
AMARESAPOf2	3.77E-00	8.49E-01	3.88E-04	6.49E-05	0.00E+01	0.00E+01	3.06E+04
AMARESAPOf3	4.18E-00	2.85E-00	4.35E-04	2.25E-04	-8.17E-01	6.44E-01	3.06E+04
HLSVDf2	4.85E-00	5.91E-01	4.44E-04	3.90E-05	0.00E+01	0.00E+01	4.06E+04
HLSVDf3	4.38E-00	1.49E-00	4.42E-04	1.30E-04	-9.60E-01	3.99E-01	4.06E+04
AMARESf2	4.89E-00	5.75E-01	4.55E-04	3.85E-05	0.00E+01	0.00E+01	4.06E+04
AMARESf3	4.38E-00	1.41E-00	4.51E-04	1.25E-04	-9.65E-01	3.79E-01	4.06E+04
HLSVDf2	4.35E-00	4.07E-01	4.13E-04	2.81E-05	0.00E+01	0.00E+01	5.06E+04
HLSVDf3	3.71E-00	4.59E-01	3.88E-04	3.84E-05	-1.07E-00	1.54E-01	5.06E+04
AMARESf2	4.42E-00	4.75E-01	4.19E-04	3.27E-05	0.00E+01	0.00E+01	5.06E+04
AMARESf3	3.69E-00	5.43E-01	3.88E-04	4.60E-05	-1.10E-00	1.88E-01	5.06E+04
HLSVDf2	4.20E-00	1.11E-01	4.25E-04	8.30E-06	0.00E+01	0.00E+01	6.06E+04
HLSVDf3	4.18E-00	3.32E-01	4.48E-04	2.86E-05	-8.96E-01	8.41E-02	6.06E+04
AMARESf2	4.21E-00	1.29E-01	4.30E-04	9.60E-06	0.00E+01	0.00E+01	6.06E+04
AMARESf3	4.23E-00	3.92E-01	4.57E-04	3.40E-05	-8.84E-01	9.71E-02	6.06E+04
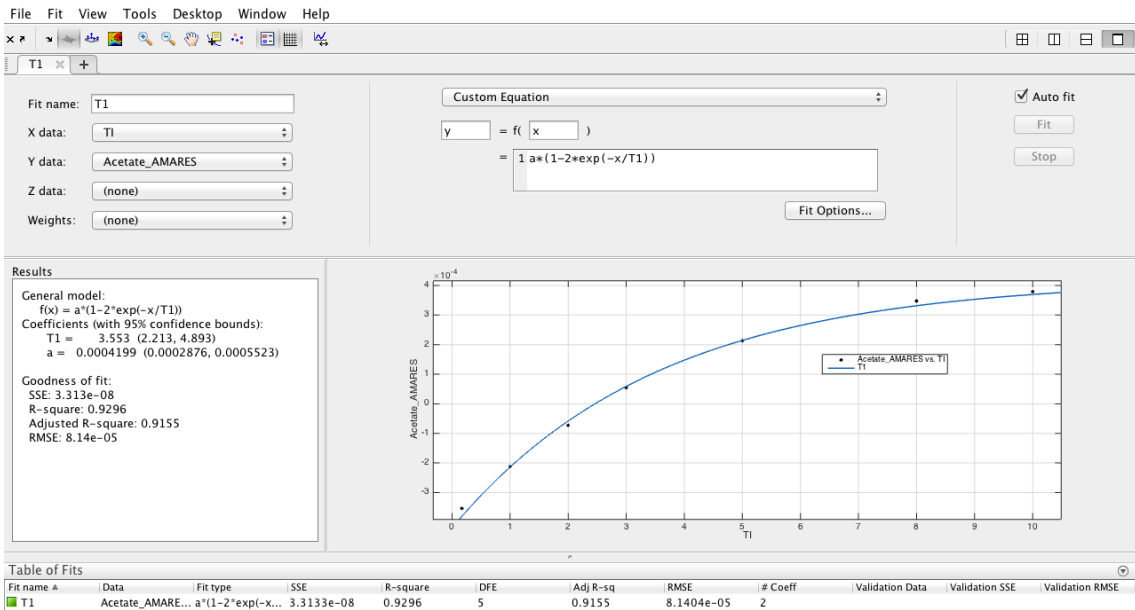
Figure 5: Example of Acetate T_1 estimation with cftool using $f1$ function for fitting. Area under the peaks have been estimated by AMARES. As shown the signal don't saturates.

Figure 6: Acetate T_1 estimation at different time with different sequence parameters, algorithms (HLSVD, AMARES). Apodization has been tested for all the algorithms. Error bars have been estimated automatically by the fitting procedure with MATLAB-cftool.

Table 4: Acetate T_1 average and std results for the different sequences parameters. The estimate have been evaluated with $f2$ fit function.

Acetate	T_1 [ms]	ΔT_1 [ms]
7/03/15	4212	77
20/05/15	4046	64
1/06 - 2/06 - 2/06 2th - 2/06 4th – 5th	4108	163
2/06 3th	4867	18

6.1.3 - Lactate T1 relaxation time

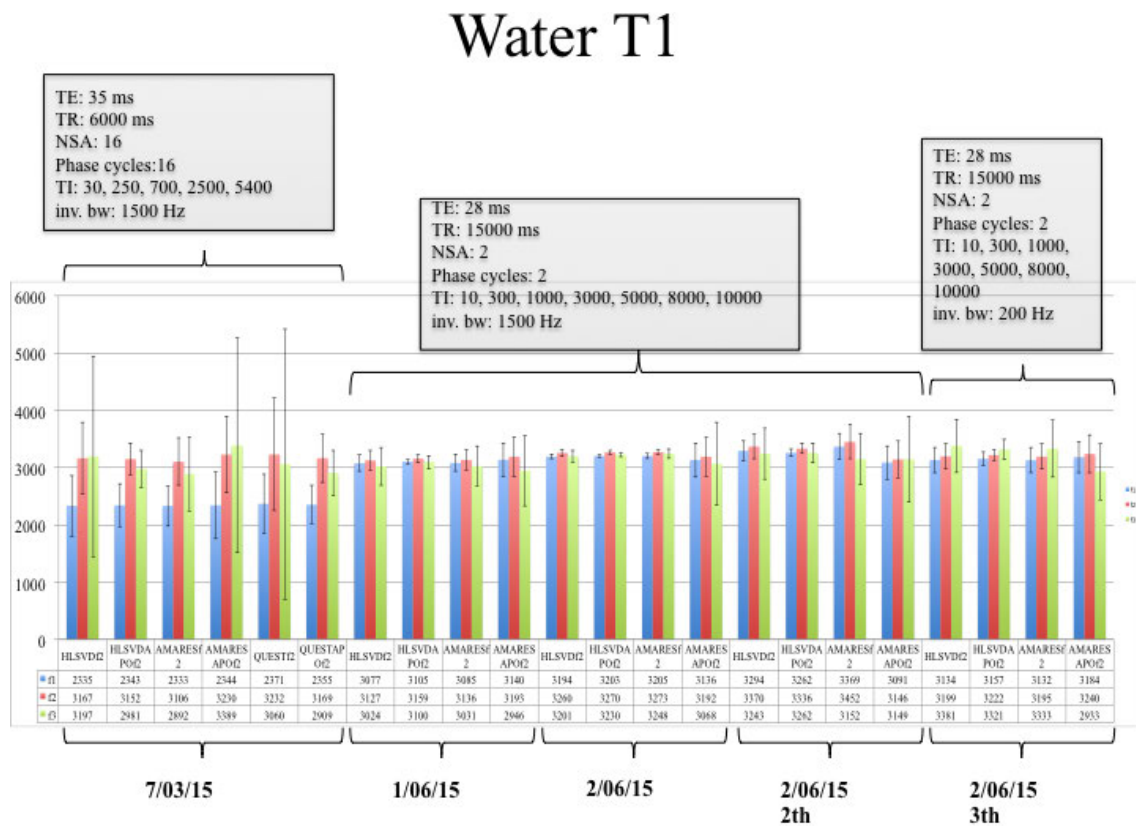Lactate estimation is complicate due to a lower SNR respect to Acetate and to a different evolution of peaks with T_E. Acquisition were performed with TE shortest (28, 30 ms) when possible, at 288 and 272 ms looking for the best SNR [Ref. 215, 216, 217].

Lactate estimation were performed with and without the quadrouplet peaks area estimation. Quadrouplet peaks area has a low SNR respect to the doublet, and many times estimation is impossible. However when possible we performed this estimation, allowing to estimate the T_1 of doublet alone and doublet and quadrouplet all together.

Table 5: Lactate doublet T_1 estimation.

Lactate doublet	T_1 [s]	ΔT_1 [s]	A	ΔA	K	ΔK	Date
HLSVDf1	1.60E-00	1.15E-01	2.84E-04	1.25E-05	0.00E+01	0.00E+01	70315
HLSVDf2	1.71E-00	5.20E-02	2.86E-04	4.30E-06	0.00E+01	0.00E+01	70315
HLSVDf3	1.74E-00	1.47E-01	3.06E-04	1.67E-05	-8.74E-01	7.54E-02	70315
HLSVDAPOf1	1.67E-00	1.56E-01	2.59E-04	1.49E-05	0.00E+01	0.00E+01	70315
HLSVDAPOf2	1.80E-00	8.40E-02	2.62E-04	5.80E-06	0.00E+01	0.00E+01	70315
HLSVDAPOf3	1.87E-00	1.73E-01	2.86E-04	1.79E-05	-8.37E-01	8.19E-02	70315
AMARESf1	1.60E-00	1.22E-01	2.60E-04	1.21E-05	0.00E+01	0.00E+01	70315
AMARESf2	1.67E-00	8.60E-02	2.62E-04	6.60E-06	0.00E+01	0.00E+01	70315
AMARESf3	1.69E-00	2.67E-01	2.78E-04	2.77E-05	-8.88E-01	1.41E-01	70315
AMARESAPOf1	1.64E-00	1.35E-01	2.39E-04	1.21E-05	0.00E+01	0.00E+01	70315
AMARESAPOf2	1.75E-00	5.90E-02	2.41E-04	3.90E-06	0.00E+01	0.00E+01	70315
AMARESAPOf3	1.80E-00	1.48E-01	2.61E-04	1.42E-05	-8.58E-01	7.36E-02	70315

HLSVDf1	1.65E-00	7.70E-02	3.01E-04	8.30E-06	0.00E+01	0.00E+01	2.01E+05
HLSVDf2	1.65E-00	7.50E-02	3.01E-04	8.00E-06	0.00E+01	0.00E+01	2.01E+05
HLSVDf3	1.72E-00	9.00E-02	3.07E-04	7.50E-06	-9.39E-01	5.27E-02	2.01E+05
HLSVDAPOf1	1.68E-00	1.23E-01	2.84E-04	1.24E-05	0.00E+01	0.00E+01	2.01E+05
HLSVDAPOf2	1.69E-00	1.24E-01	2.83E-04	1.22E-05	0.00E+01	0.00E+01	2.01E+05
HLSVDAPOf3	1.73E-00	2.34E-01	2.88E-04	1.84E-05	-9.55E-01	1.37E-01	2.01E+05
AMARESf1	1.58E-00	1.44E-01	2.78E-04	1.48E-05	0.00E+01	0.00E+01	2.01E+05
AMARESf2	1.59E-00	1.47E-01	2.78E-04	1.47E-05	0.00E+01	0.00E+01	2.01E+05
AMARESf3	1.58E-00	2.78E-01	2.78E-04	2.26E-05	-1.01E-00	1.85E-01	2.01E+05
AMARESAPOf1	1.67E-00	6.80E-02	2.66E-04	6.40E-06	0.00E+01	0.00E+01	2.01E+05
AMARESAPOf2	1.68E-00	6.60E-02	2.66E-04	6.10E-06	0.00E+01	0.00E+01	2.01E+05
AMARESAPOf3	1.75E-00	6.70E-02	2.71E-04	5.00E-06	-9.44E-01	3.88E-02	2.01E+05
HLSVDf1	1.82E-00	1.93E-01	3.52E-04	2.34E-05	0.00E+01	0.00E+01	10615
HLSVDf2	1.82E-00	1.93E-01	3.52E-04	2.33E-05	0.00E+01	0.00E+01	10615
HLSVDf3	1.97E-00	3.29E-01	3.64E-04	2.94E-05	-8.97E-01	1.58E-01	10615
HLSVDAPOf1	2.05E-00	3.63E-01	3.78E-04	4.41E-05	0.00E+01	0.00E+01	10615
HLSVDAPOf2	2.05E-00	3.66E-01	3.78E-04	4.39E-05	0.00E+01	0.00E+01	10615
HLSVDAPOf3	1.75E-00	1.21E-01	2.90E-04	9.90E-06	-1.04E-00	7.40E-02	10615
AMARESf1	1.77E-00	2.13E-01	3.25E-04	2.41E-05	0.00E+01	0.00E+01	10615
AMARESf2	1.77E-00	2.13E-01	3.25E-04	2.40E-05	0.00E+01	0.00E+01	10615
AMARESf3	1.98E-00	2.76E-01	3.40E-04	2.25E-05	-8.58E-01	1.27E-01	10615
AMARESAPOf1	1.80E-00	7.70E-02	2.93E-04	7.80E-06	0.00E+01	0.00E+01	10615
AMARESAPOf2	1.80E-00	7.70E-02	2.93E-04	7.80E-06	0.00E+01	0.00E+01	10615
AMARESAPOf3	1.75E-00	1.21E-01	2.90E-04	9.90E-06	-1.04E-00	7.40E-02	10615
HLSVDf1	1.74E-00	1.37E-01	3.11E-04	1.50E-05	0.00E+01	0.00E+01	2.06E+04
HLSVDf2	1.74E-00	1.38E-01	3.11E-04	1.50E-05	0.00E+01	0.00E+01	2.06E+04
HLSVDf3	1.79E-00	2.71E-01	3.15E-04	2.27E-05	-9.61E-01	1.51E-01	2.06E+04
HLSVDAPOf1	1.86E-00	2.39E-01	3.07E-04	2.48E-05	0.00E+01	0.00E+01	2.06E+04
HLSVDAPOf2	1.86E-00	2.40E-01	3.07E-04	2.48E-05	0.00E+01	0.00E+01	2.06E+04
HLSVDAPOf3	1.82E-00	4.70E-01	3.04E-04	3.91E-05	-1.03E-00	2.74E-01	2.06E+04
AMARESf1	1.74E-00	1.28E-01	2.95E-04	1.32E-05	0.00E+01	0.00E+01	2.06E+04
AMARESf2	1.74E-00	1.28E-01	2.95E-04	1.32E-05	0.00E+01	0.00E+01	2.06E+04

|							
AMARESf3	1.80E-00	2.45E-01	2.99E-04	1.95E-05	-9.60E-01	1.36E-01	2.06E+04
AMARESAPOf1	1.75E-00	8.60E-02	2.75E-04	8.30E-06	0.00E+01	0.00E+01	2.06E+04
AMARESAPOf2	1.75E-00	8.60E-02	2.75E-04	8.20E-06	0.00E+01	0.00E+01	2.06E+04
AMARESAPOf3	1.80E-00	1.55E-01	2.78E-04	1.14E-05	-9.63E-01	8.63E-02	2.06E+04
HLSVDf2	1.88E-00	2.74E-01	3.53E-04	3.24E-05	0.00E+01	0.00E+01	3.06E+04
HLSVDf3	2.06E-00	5.40E-01	3.67E-04	4.73E-05	-8.86E-01	2.45E-01	3.06E+04
HLSVDAPOf2	2.23E-00	5.48E-01	3.87E-04	6.40E-05	0.00E+01	0.00E+01	3.06E+04
HLSVDAPOf3	2.37E-00	1.28E-00	4.00E-04	1.17E-04	-9.20E-01	5.19E-01	3.06E+04
AMARESf2	1.86E-00	2.51E-01	3.32E-04	2.80E-05	0.00E+01	0.00E+01	3.06E+04
AMARESf3	2.04E-00	4.85E-01	3.44E-04	4.01E-05	-8.90E-01	2.23E-01	3.06E+04
AMARESAPOf2	1.84E-00	3.27E-01	3.02E-04	3.35E-05	0.00E+01	0.00E+01	3.06E+04
AMARESAPOf3	1.52E-00	1.94E-01	2.80E-04	1.83E-05	-1.27E-00	1.62E-01	3.06E+04
HLSVDf2	1.87E-00	7.20E-02	3.18E-04	7.60E-06	0.00E+01	0.00E+01	4.06E+04
HLSVDf3	1.93E-00	1.22E-01	3.21E-04	1.01E-05	-9.64E-01	6.37E-02	4.06E+04
AMARESf2	1.88E-00	6.20E-02	2.98E-04	6.20E-06	0.00E+01	0.00E+01	4.06E+04
AMARESf3	1.94E-00	9.40E-02	3.02E-04	7.30E-06	-9.60E-01	4.86E-02	4.06E+04
HLSVDf2	1.80E-00	2.36E-01	2.66E-04	2.15E-05	0.00E+01	0.00E+01	5.06E+04
HLSVDf3	1.58E-00	1.43E-01	2.52E-04	1.15E-05	-1.19E-00	1.09E-01	5.06E+04
AMARESf2	1.82E-00	2.66E-01	2.79E-04	2.53E-05	0.00E+01	0.00E+01	5.06E+04
AMARESf3	1.56E-00	1.54E-01	2.63E-04	1.30E-05	-1.22E-00	1.20E-01	5.06E+04
HLSVDf2	1.83E-00	7.80E-02	2.91E-04	7.70E-06	0.00E+01	0.00E+01	6.06E+04
HLSVDf3	1.91E-00	8.60E-02	2.97E-04	6.50E-06	-9.44E-01	4.39E-02	6.06E+04
AMARESf2	1.78E-00	1.15E-01	3.06E-04	1.22E-05	0.00E+01	0.00E+01	6.06E+04
AMARESf3	1.88E-00	1.69E-01	3.12E-04	1.36E-05	-9.31E-01	8.79E-02	6.06E+04
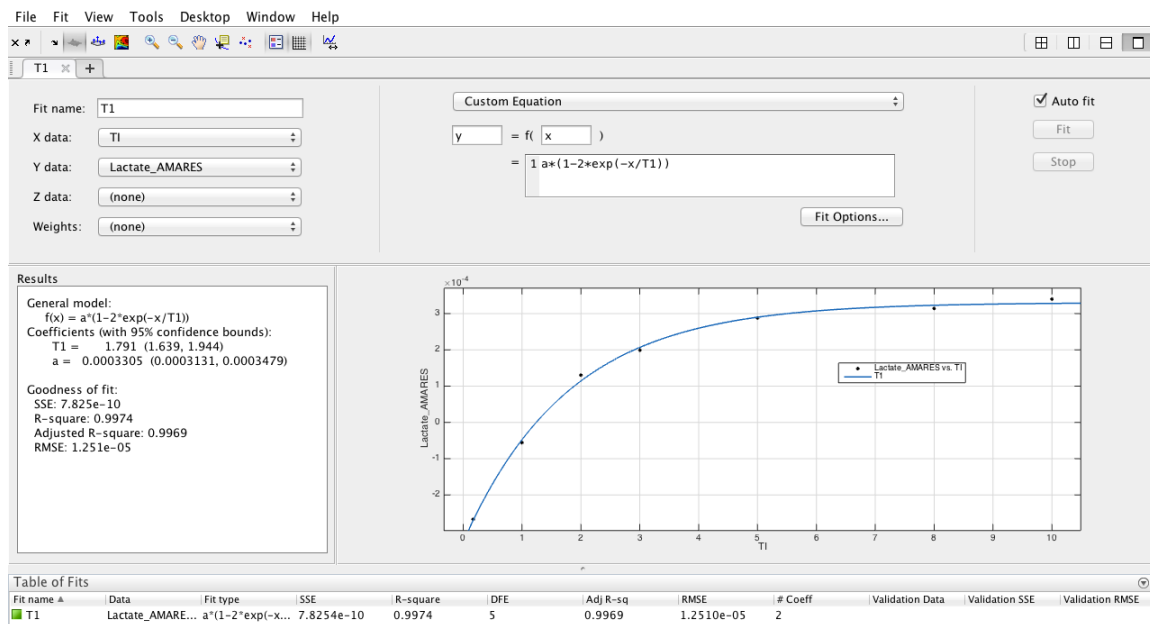
Figure 7: Example of Lactate T_1 estimation with cftool using ƒ1 function for fitting. Area under the peaks have been estimated by AMARES. As shown the signal saturates at about 8 s.
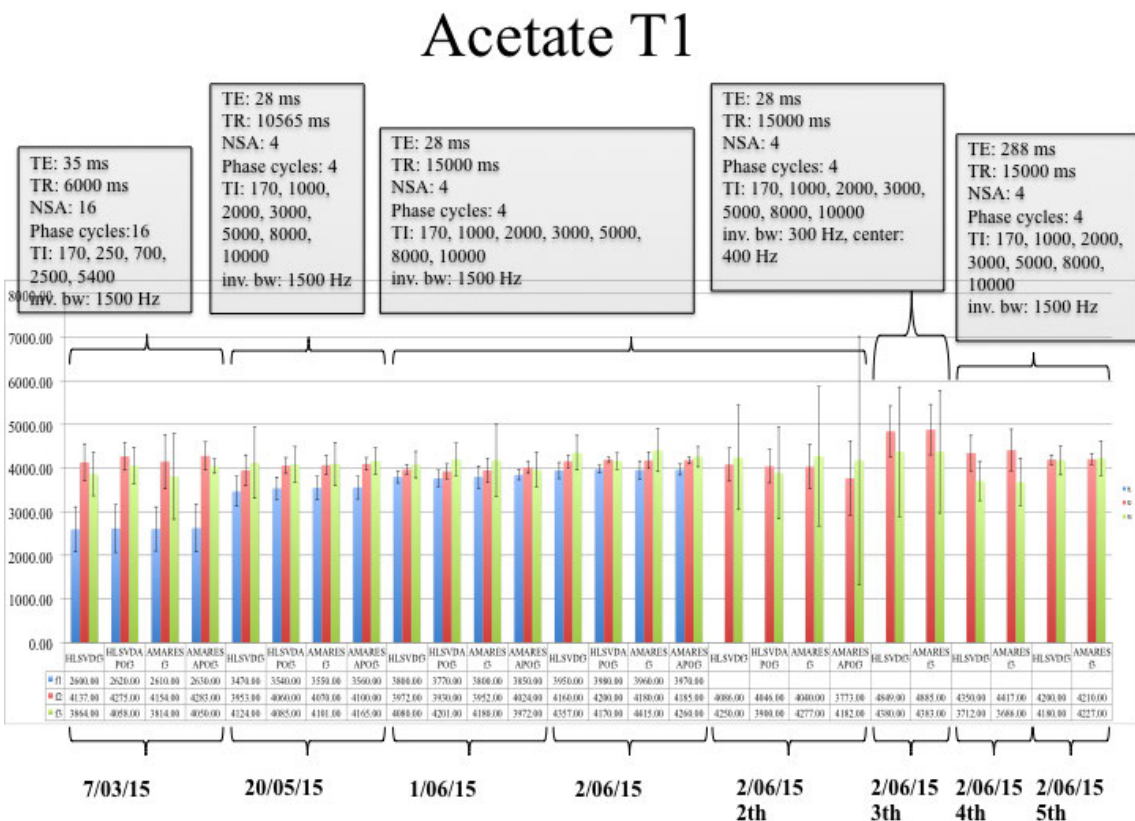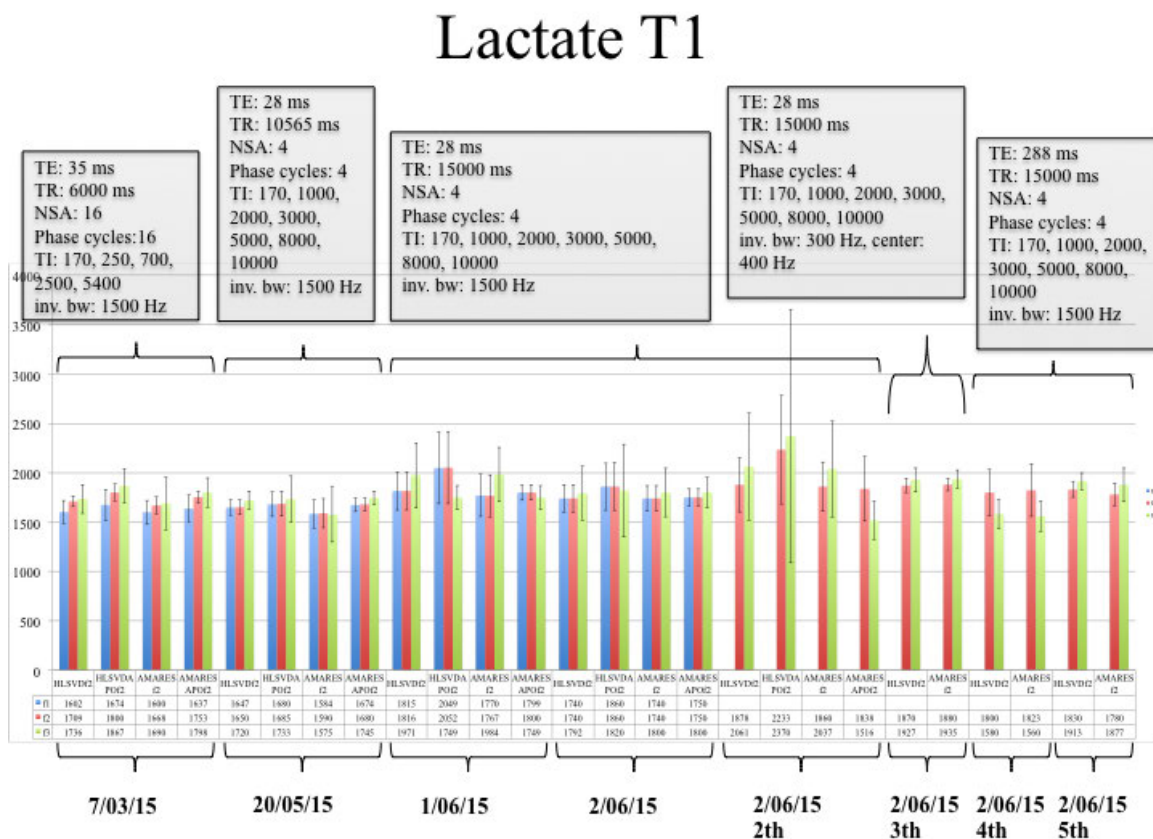

Figure 8: Lactate T_1 doublet estimation at different time with different sequence parameters, algorithms (HLSVD, AMARES). Apodization has been tested for all the algorithms. Error bars have been estimated automatically by the fitting procedure with MATLAB-cftool.

Table 6: Lactate doublet T_1 average and std results for the different sequences parameters. The estimate have been evaluated with *f*2 fit function.

Lactate doublet	T_1 [ms]	ΔT_1 [ms]
7/03/15	1732,5	57
20/05/15	1651	44
1/06 - 2/06 - 2/06 2th - 2/06 4th – 5th	1848	127
2/06 3th	1875	7

Table 7: Lactate doublet and quadrouplet T_1 estimation.

Lactate doublet and quadrouplet	T_1 [s]	ΔT_1 [s]	A	ΔA	K	ΔK	Date
HLSVDf1	1.83E-00	9.60E-02	3.53E-04	1.16E-05	0.00E+01	0.00E+01	200515
HLSVDf2	1.84E-00	9.50E-02	3.53E-04	1.09E-05	0.00E+01	0.00E+01	200515
HLSVDf3	1.90E-00	1.66E-01	3.60E-04	1.56E-05	-9.50E-01	8.84E-02	200515
HLSVDAPOf1	1.90E-00	2.16E-01	3.35E-04	2.41E-05	0.00E+01	0.00E+01	200515
HLSVDAPOf2	1.91E-00	2.25E-01	3.34E-04	2.40E-05	0.00E+01	0.00E+01	200515
HLSVDAPOf3	1.91E-00	4.47E-01	3.37E-04	4.03E-05	-9.87E-01	2.46E-01	200515
AMARESf1	1.79E-00	1.36E-01	3.31E-04	1.56E-05	0.00E+01	0.00E+01	200515
AMARESf2	1.80E-00	1.41E-01	3.30E-04	1.54E-05	0.00E+01	0.00E+01	200515
AMARESf3	1.80E-00	2.77E-01	3.32E-04	2.53E-05	-9.90E-01	1.61E-01	200515
AMARESAPOf1	1.89E-00	9.70E-02	3.13E-04	1.01E-05	0.00E+01	0.00E+01	200515
AMARESAPOf2	1.90E-00	1.02E-01	3.12E-04	1.03E-05	0.00E+01	0.00E+01	200515
AMARESAPOf3	1.88E-00	1.95E-01	3.13E-04	1.66E-05	-1.00E-00	1.10E-01	200515
HLSVDf1	2.03E-00	3.03E-01	4.36E-04	4.26E-05	0.00E+01	0.00E+01	10615
HLSVDf2	2.04E-00	3.05E-01	4.36E-04	4.25E-05	0.00E+01	0.00E+01	10615
HLSVDf3	2.26E-00	6.26E-01	4.57E-04	6.50E-05	-8.75E-01	2.55E-01	10615
HLSVDAPOf1	2.45E-00	6.27E-01	5.93E-04	1.08E-04	0.00E+01	0.00E+01	10615
HLSVDAPOf2	2.46E-00	6.40E-01	5.93E-04	1.07E-04	0.00E+01	0.00E+01	10615
HLSVDAPOf3	3.20E-00	1.64E-00	6.86E-04	2.05E-04	-7.17E-01	3.97E-01	10615
AMARESf1	1.97E-00	2.60E-01	3.93E-04	3.36E-05	0.00E+01	0.00E+01	10615
AMARESf2	1.98E-00	2.61E-01	3.93E-04	3.34E-05	0.00E+01	0.00E+01	10615

|							
AMARESf3	2.25E-00	3.95E-01	4.17E-04	3.66E-05	-8.40E-01	1.56E-01	10615
AMARESAPOf1	1.89E-00	1.99E-01	3.32E-04	2.21E-05	0.00E+01	0.00E+01	10615
AMARESAPOf2	1.89E-00	1.99E-01	3.32E-04	2.21E-05	0.00E+01	0.00E+01	10615
AMARESAPOf3	2.09E-00	2.75E-01	3.46E-04	2.25E-05	-8.76E-01	1.22E-01	10615
HLSVDf1	1.90E-00	1.98E-01	3.49E-04	2.32E-05	0.00E+01	0.00E+01	2.06E+04
HLSVDf2	1.91E-00	2.00E-01	3.49E-04	2.31E-05	0.00E+01	0.00E+01	2.06E+04
HLSVDf3	1.96E-00	4.17E-01	3.53E-04	3.76E-05	-9.65E-01	2.13E-01	2.06E+04
HLSVDAPOf1	2.17E-00	5.15E-01	3.57E-04	5.72E-05	0.00E+01	0.00E+01	2.06E+04
HLSVDAPOf2	2.17E-00	5.22E-01	3.57E-04	5.72E-05	0.00E+01	0.00E+01	2.06E+04
HLSVDAPOf3	2.02E-00	9.85E-01	3.46E-04	9.12E-05	-1.09E-00	5.44E-01	2.06E+04
AMARESf1	1.90E-00	1.81E-01	3.30E-04	1.99E-05	0.00E+01	0.00E+01	2.06E+04
AMARESf2	1.90E-00	1.81E-01	3.30E-04	1.99E-05	0.00E+01	0.00E+01	2.06E+04
AMARESf3	1.96E-00	3.73E-01	3.35E-04	3.16E-05	-9.57E-01	1.89E-01	2.06E+04
AMARESAPOf1	1.94E-00	1.60E-01	3.13E-04	1.66E-05	0.00E+01	0.00E+01	2.06E+04
AMARESAPOf2	1.94E-00	1.62E-01	3.13E-04	1.66E-05	0.00E+01	0.00E+01	2.06E+04
AMARESAPOf3	1.88E-00	3.07E-01	3.09E-04	2.56E-05	-1.04E-00	1.74E-01	2.06E+04
HLSVDf2	2.00E-00	2.42E-01	4.29E-04	3.36E-05	0.00E+01	0.00E+01	3.06E+04
HLSVDf3	2.14E-00	5.08E-01	4.42E-04	5.36E-05	-9.21E-01	2.28E-01	3.06E+04
HLSVDAPOf2	2.55E-00	8.36E-01	5.77E-04	1.33E-04	0.00E+01	0.00E+01	3.06E+04
HLSVDAPOf3	2.37E-00	1.72E-00	5.58E-04	2.37E-04	-1.08E-00	8.06E-01	3.06E+04
AMARESf2	2.09E-00	3.09E-01	4.09E-04	3.98E-05	0.00E+01	0.00E+01	3.06E+04
AMARESf3	2.35E-00	6.28E-01	4.33E-04	6.02E-05	-8.64E-01	2.42E-01	3.06E+04
AMARESAPOf2	2.04E-00	4.04E-01	3.80E-04	4.89E-05	0.00E+01	0.00E+01	3.06E+04
AMARESAPOf3	2.03E-00	8.45E-01	3.80E-04	8.21E-05	-1.00E-00	4.31E-01	3.06E+04
HLSVDf2	2.07E-00	3.99E-01	3.13E-04	3.94E-05	0.00E+01	0.00E+01	5.06E+04
HLSVDf3	1.66E-00	1.49E-01	2.84E-04	1.39E-05	-1.32E-00	1.19E-01	5.06E+04
AMARESf2	2.08E-00	3.58E-01	3.25E-04	3.66E-05	0.00E+01	0.00E+01	5.06E+04
AMARESf3	1.72E-00	2.40E-01	2.99E-04	2.25E-05	-1.26E-00	1.77E-01	5.06E+04
HLSVDf2	2.01E-00	1.80E-01	3.60E-04	2.08E-05	0.00E+01	0.00E+01	6.06E+04
HLSVDf3	2.09E-00	3.73E-01	3.67E-04	3.36E-05	-9.48E-01	1.76E-01	6.06E+04
AMARESf2	2.04E-00	1.59E-01	3.76E-04	1.90E-05	0.00E+01	0.00E+01	6.06E+04
AMARESf3	2.17E-00	2.94E-01	3.87E-04	2.70E-05	-9.20E-01	1.30E-01	6.06E+04
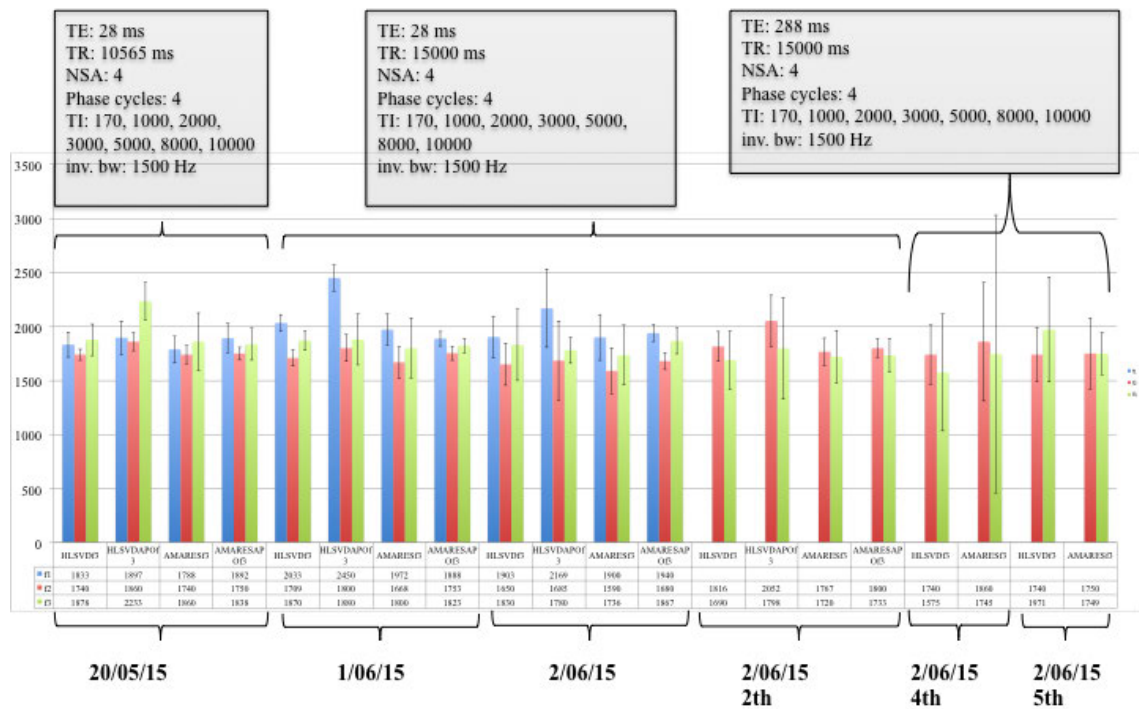
Figure 9: Lactate T_1 doublet and quadrouplet estimation at different time with different sequence parameters, algorithms (HLSVD, AMARES). Apodization has been tested for all the algorithms. Error bars have been estimated automatically by the fitting procedure with MATLAB-cftool.

Lactate estimation is complicate due to a lower SNR respect to Acetate and to a different evolution of peaks with T_E. Acquisition were performed with T_E shortest (28, 30 ms) when possible, at 288 and 272 ms looking for the best SNR [Ref. 215, 216, 217]. At 288 ms al peaks are in phase, so in this case we should have the best SNR.

Table 8: Lactate T_1 average and std results for the different sequences parameters.
The estimate have been evaluated with *f*2 fit function.

Lactate doublet + quadrouplet	T_1 [ms]	ΔT_1 [ms]
20/05/15	1861	54
1/06 - 2/06 - 2/06 2th	2080	216
2/06 4th – 5th	2049	31

6.1.4 - Understanding Acetate and Lactate T_1 estimation with AMARES

Looking at the above results on T_1 Acetate and Lactate estimation what can be surprising are the differences between estimation using different sequences parameters. In particular there is no apparent explanation at the difference between the measurements performed on 2/06/15 3th and the other. The only explanation come from the inversion bandwidth used in the sequence.

To understand this difference we decided to reanalyze these data, using AMARES, looking at the best estimation. What we found is very useful and must be taken into account for all future measurements. All estimation performed in MRS must be done with best accuracy, looking at the best fitting function. E.g. using AMARES the "Staring values" and "Prior Knowledge" must be set with the best accuracy, an error of just 0.5 Hz in the position of a spectral line, or a linewidth set too large or too narrow can change the result of the algorithm fitting, allowing or not the estimation of peaks area.

The results in table below shown the importance to use a narrow inversion bandwidth centered near the metabolites of interest. It is very important to observe how the peak area for Acetate at $T = 3000$ ms is positive for all sequences less than the sequence of 2/06/15 3th, this means that the spins inversion depends on on the inversion bandwidth, with an apparent delay in the "zero" transition of the spins between these cases.

About Lactate doublet T_1 estimation it is very important set the right "Staring values" and "Prior Knowledge" in order to have the best estimation of peaks area. The frequency difference between spectral lines must be investigated near the theoretical value, looking for the best fit.
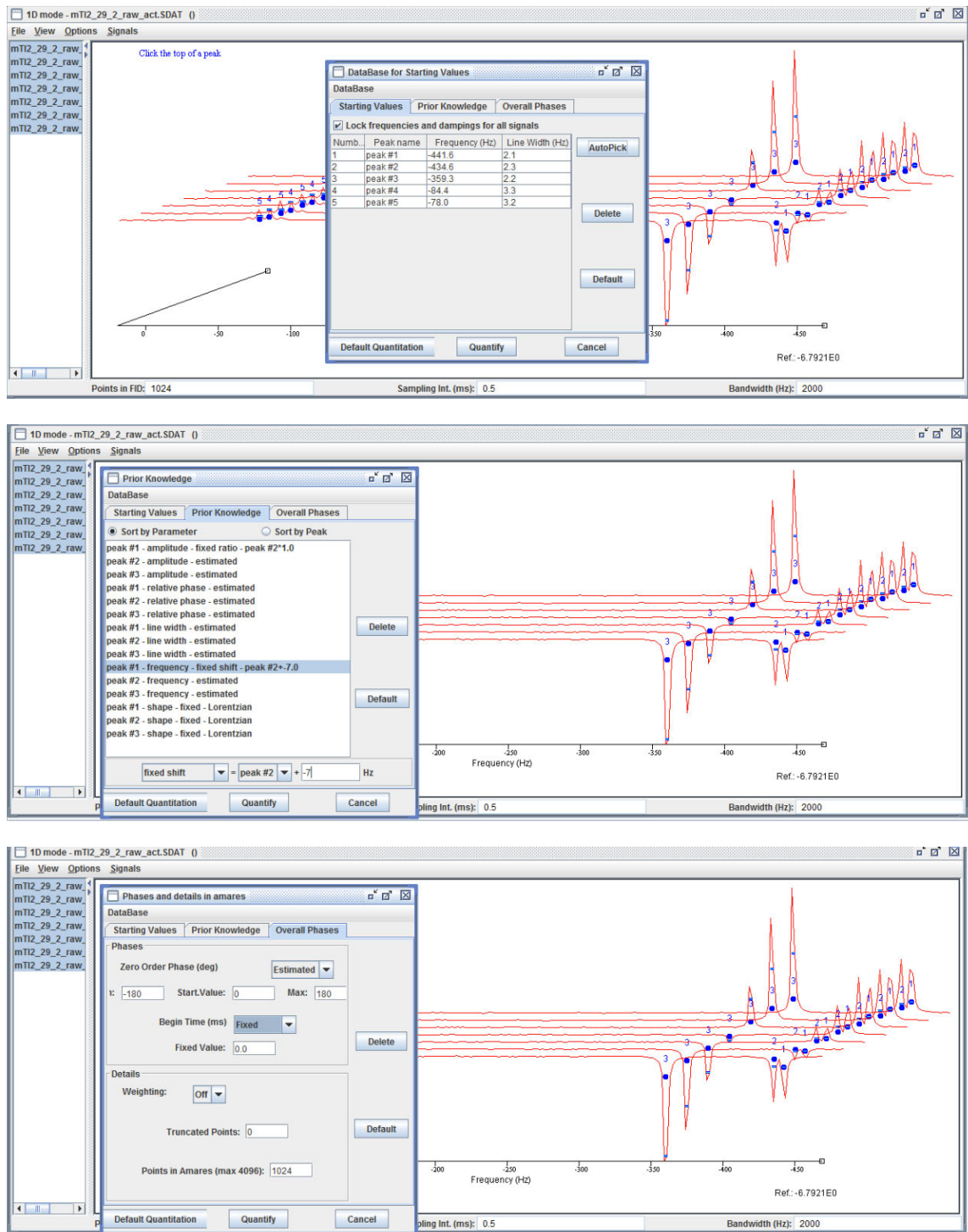
Figure 10: Example os AMARES parameters setting for Acetate and Lactate T_1 estimation. Sequence 2/06/15 3th. Inv. Bw = 300 Hz, center at 400 Hz. Lactate doublet: peaks 1, 2; Lactate quadrouplet: peaks 4, 5, the other two have a too low SNR to be estimated; Acetate: peak 3.

Table 9: AMARES results about sequence 2/06/15 3th. Inv. Bw = 300 Hz, center at 400 Hz

Acetate			
AMARES peaks setting	Manual: all parameters set manually	Autopeak, automatic linewidth estimation	Autopeak, linewidth: 2 Hz
T_I (ms) = 170 1000 2000 3000 5000 8000 10000	Peak area = -4,14E-04 -2,70E-04 -1,41E-04 -2,77E-05 1,35E-04 2,91E-04 3,53E-04	Peak area = -4,15E-04 -2,70E-04 -1,41E-04 -2,77E-05 1,35E-04 2,91E-04 3,53E-04	Peak area = -4,14E-04 -2,70E-04 -1,41E-04 -2,77E-05 1,35E-04 2,91E-04 3,53E-04
F2 fit function T_R = 15 s T_E = 28 ms	T_1 = 5.164 (5.045, 5.283) a = 0.0004633 (0.0004557, 0.0004709) R-square: 0.9998	T_1 = 5.17 (5.045, 5.294) a = 0.0004635 (0.0004557, 0.0004714) R-square: 0.9998	T_1 = 5.169 (5.05, 5.288) a = 0.0004633 (0.0004557, 0.0004709) R-square: 0.9998
$f3$ fit function T_R = 15 s T_E = 28 ms	T_1 = 5.007 (4.682, 5.332) a = 0.0004974 (0.0004685, 0.0005264) k = -0.8462 (-0.9158, -0.7765) R-square: 0.9999	T_1 = 5.017 (4.682, 5.353) a = 0.0004986 (0.0004687, 0.0005284) k = -0.8432 (-0.9147, -0.7718) R-square: 0.9999	T_1 = 5.025 (4.699, 5.351) a = 0.0004991 (0.0004701, 0.0005282) k = -0.8412 (-0.9103, -0.772) R-square: 0.9999

Lactate doublet				
T_1 (ms)	*No prior knowledge*	*Line Shift 6.9 Hz*	*Line Shift 7 Hz*	*Line Shift 7.1 Hz*
170 1000 2000 3000 5000 8000 10000	-2,44E-04 -5,55E-05 8,92E-05 1,83E-04 2,53E-04 2,97E-04 3,03E-04	-2,42E-04 -5,54E-05 8,82E-05 1,80E-04 2,52E-04 2,95E-04 3,02E-04	-2,42E-04 -5,54E-05 8,84E-05 1,81E-04 2,52E-04 2,95E-04 3,02E-04	-2,43E-04 -5,55E-05 8,86E-05 1,81E-04 2,52E-04 2,95E-04 3,02E-04
$f2$ fit function T_R = 15 s T_E = 28 ms	T_1 = 1.896 (1.826, 1.966) a = 0.0003017 (0.0002946, 0.0003088) R-square: 0.9995	T_1 = 1.9 (1.832, 1.968) a = 0.0003 (0.0002932, 0.0003068) R-square: 0.9995	T_1 = 1.9 (1.831, 1.969) a = 0.0003002 (0.0002934, 0.0003071) R-square: 0.9995	T_1 = 1.899 (1.83, 1.968) a = 0.0003006 (0.0002937, 0.0003075) R-square: 0.9995
$f3$ fit function T_R= 15 s T_E= 28 ms	T_1 = 1.94 (1.817, 2.063) a = 0.0003051 (0.0002955, 0.0003148) k = -0.966 (-1.03, -0.9024) R-square: 0.9997	T_1 = 1.96 (1.857, 2.063) a = 0.0003043 (0.0002964, 0.0003123) k = -0.96 (-1.012, -0.9076) R-square: 0.9998	T_1 = 1.956 (1.847, 2.065) a = 0.0003041 (0.0002957, 0.0003126) k = -0.9618 (-1.017, -0.9062) R-square: 0.9997	T_1 = 1.952 (1.838, 2.067) a = 0.0003043 (0.0002954, 0.0003132) k = -0.9637 (-1.022, -0.905) R-square: 0.9997

T_1 and k estimations are very accurated, with k near the "−1" value referring to perfect inversion. The MATLAB fitting of the T_1 and k must be performed with the best accuracy too, looking at the best "initial value" for the fitting algorithm, looking for the best fit by iterative trials anytime closer to the "real" values.

6.2 - Conclusions about T_1 estimation

From the results shown above we can conclude that:

1. Apparently there are no differences between HLSVD and AMARES results, so we can average all results together clustering only by sequences parameters in order to have a rough estimate;
2. AMARES must be used with accuracy in order to have the best estimation;
3. Fit function $f1$ should be used only when $T_R \gg T_1$, otherwise the estimation of T_1 is not correct;
4. Fit function $f2$ is the best fitting function in all cases;

5. Fit function $f3$ take in account for the effect of not perfect inversion, but estimation of T_1 is very similar to $f2$ but with bigger errors;

6. NSA, phase cycling don't affect results if SNR is good as in the case of phantom;

7. TE must be chosen bearing in mind the evolution of metabolites under study, as in the case of Lactate;

8. T_1 times should be chosen at the best to sample the Inversion recovery curve in order to have a good fitting;

9. The best estimation has been obtained using a sequence with an inversion bandwidth centered near the metabolites of interest;

10. With an inversion bandwidth of 1500 Hz, the estimation of T_1 is 4059 ms with an error of 172 ms.

Chapter 7

SIEMENS PHANTOM T_2 AT 3 T

In this part some results about the MRS measurements performed using the Philips Achieva 3 T scanner at the Azienda Ospedaliero Universitaria Meyer are shown.

In this part we focus on the estimation of water and metabolites (Acetate, Lactate) T_2 relaxation time at 3 T. Spectra have been acquired with the Siemens phantom using different multi-echo sequences parameters, looking for the difference in the estimation. Details are repoted in Appendix 3. E.g. data have been acquired using a different TE in order to highlight the behavior of Lactate. All of this will be discussed here. At the same time post-processing has been performed using different algorithms (HLSVD, AMARES), with and without apodization (lorentzian apodization with 5 Hz) of spectra, looking for the difference in the estimations. A good reference to understand problems in spectra fitting can be found in Ref. 214.

7.1 - T_2 relaxation time

Measurements were performed using a spin-echo sequences at different T_E. Peaks area were estimated with HLSVD and AMARES. It is very important to highlight the importance of removing the residual water peak in the metabolites spectrum, allowing a good estimation of meatabolites peaks as small as the lactate quadrouplet.

In this case the fitting were performed with the function $f(T_2) = S_2 \exp(-T_E / T_2)$, where "$S_2$" is the signal at equilibrium magnetization.

For all acquisitions, less than when we used TE multiples of 288 ms for Lactate estimation, we just estimated acetate peaks ares due to the problems with Lactate evolutions of peaks.

7.1.1 - Water T_2 relaxation time
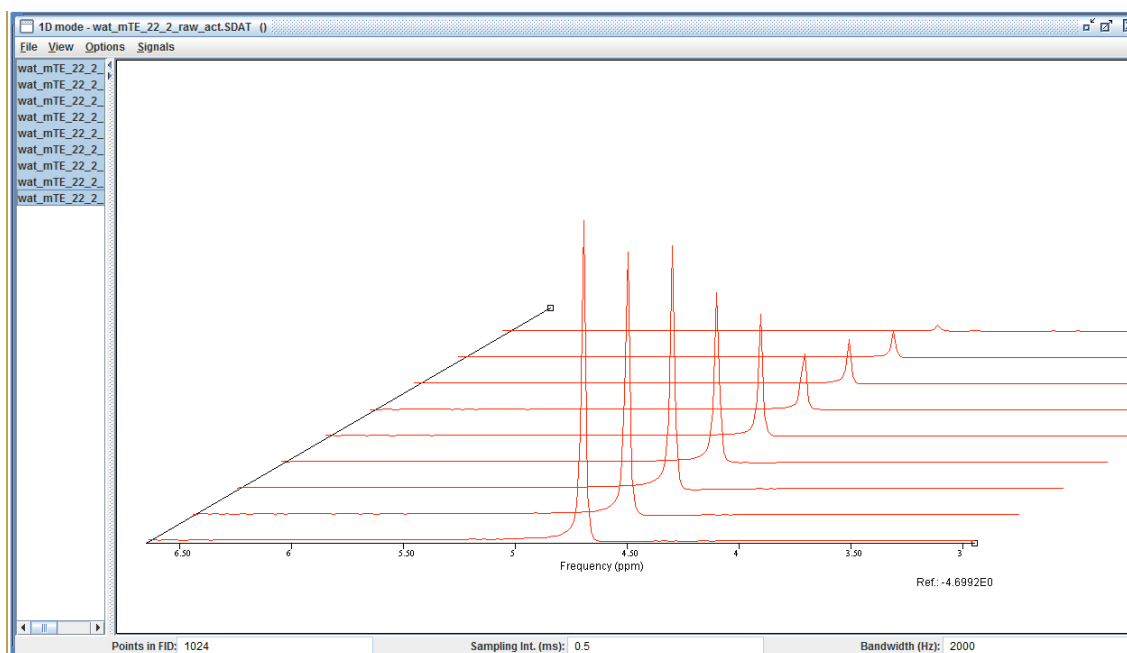
Figure 1: Example of Water multi-echo spectrum with Lorentzian apodization of 5 Hz. T_E (ms): 30, 100, 200, 400, 800, 1200, 1600, 2000, 3000. T_R = 6000 ms. NSA = phase cycles = 2.

Table 1: Water T_2 results.

Algorithm	T_2 (s)	ΔT_2 (s)	S	ΔS	Date
HLSVD	0.6391	0.0320	0.0785	0.0014	70315
AMARES	0.6280	0.0660	0.0790	0.0030	70315
HLSVD_APO5L	0.6363	0.0230	0.0748	0.0010	70315
AMARES_APO5L	0.6341	0.2634	0.0768	0.0114	70315
HLSVD	0.6058	0.0168	0.0657	0.0008	200515
AMARES	0.6058	0.0146	0.0654	0.0007	200515
HLSVD	0.7446	0.0392	0.0967	0.0021	10615
AMARES	0.7382	0.0495	0.0966	0.0027	10615
HLSVD	0.7788	0.0429	0.0995	0.0023	20615
AMARES	0.7666	0.0827	0.1003	0.0046	20615
HLSVD_APO5L	0.7760	0.0179	0.0971	0.0009	20615
AMARES_APO5L	0.8023	0.0738	0.0924	0.0036	20615
HLSVD	0.78280	0.03070	0.10170	0.00170	30615

AMARES	0.79080	0.07480	0.09917	0.00393	30615
HLSVD_APO5L	0.78600	0.01960	0.09779	0.00103	30615
AMARES_APO5L	0.79890	0.07060	0.10160	0.00380	30615
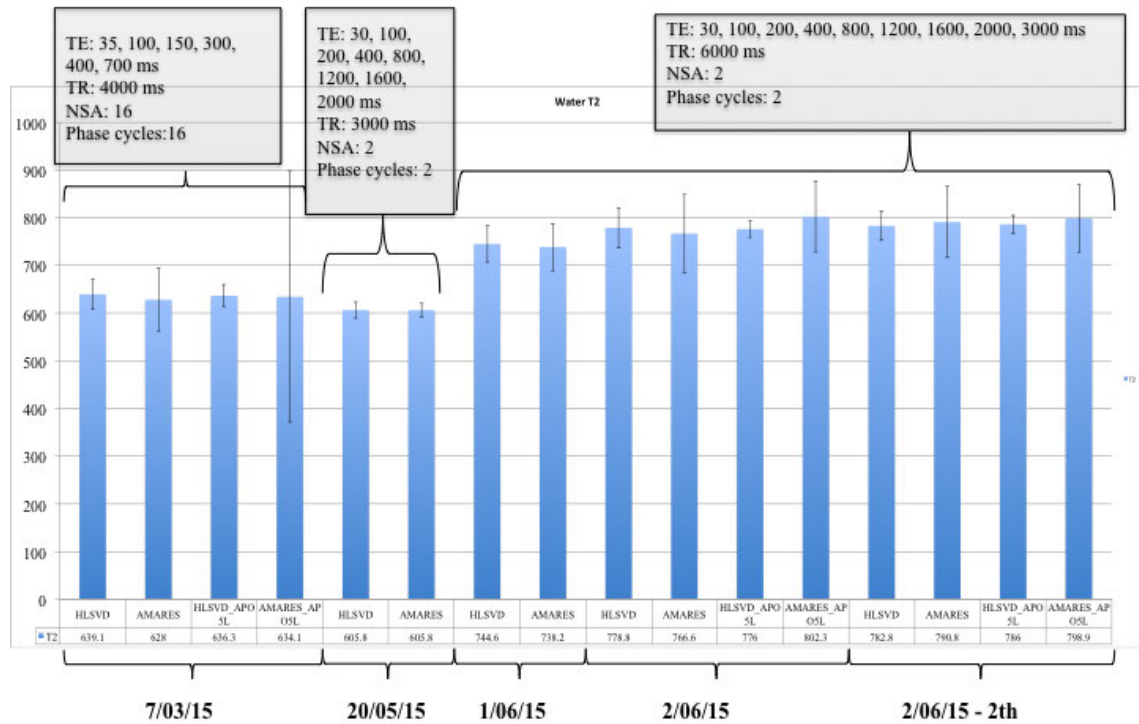
Figure 2: Water T_2

Table 2: Water T_2 average and std results for the different sequences parameters.

Water	T_2 [ms]	ΔT_2 [ms]
7/03/15	634	47
20/05/15	606	0 [no sense, only two estimations!]
1/06 - 2/06 - 2/06 2th	776,5	21

7.1.2 - Acetate T_2 relaxation time
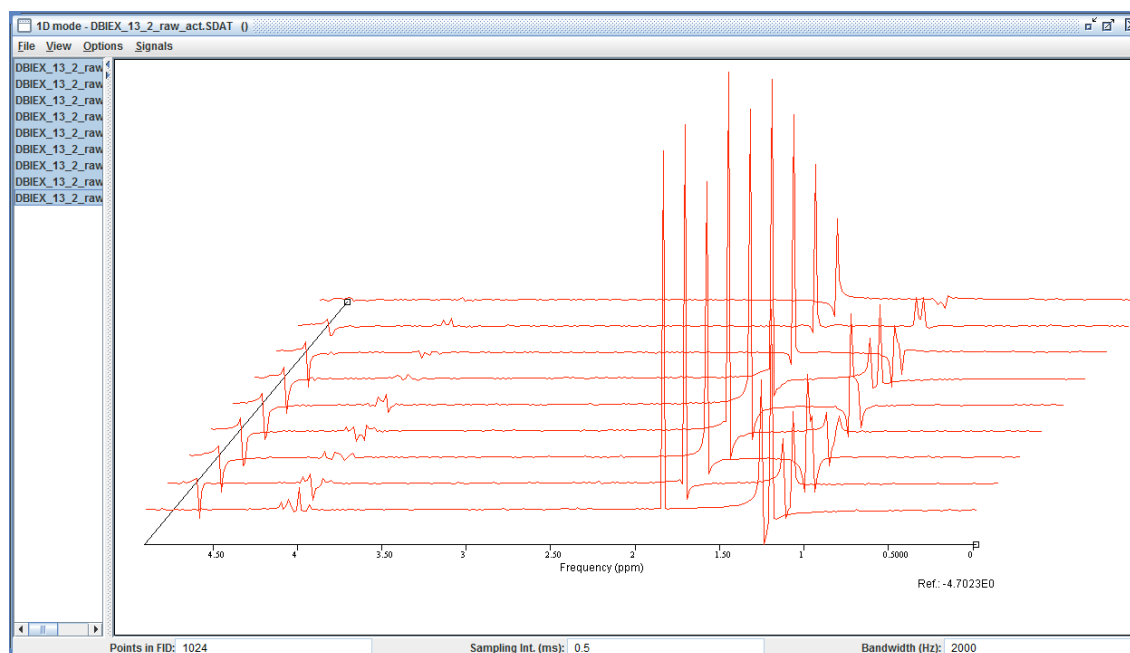
Figure 3: Example of Acetate and Lactate spectrum with multi-echo sequence. These T_E echo times are not correct for estimation of Lactate peaks area as clearly shown. TE(ms): 30, 100, 200, 400, 800, 1200, 1600, 2000, 3000. T_R = 6000 ms. NSA = phase cycles = 16.

Table 3: Acetate T_2 results.

Algoritmo	$T_2(s)$	ΔT_2 (s)	S	ΔS	Date
HLSVD	2.8000000	0.3010000	0.0002424	0.0000031	70315
AMARES	2.8140000	0.5250000	0.0002448	0.0000053	70315
HLSVD	2.0360000	0.1770000	0.0001981	0.0000056	200515
AMARES	2.1500000	0.6040000	0.0001847	0.0000164	200515
HLSVD	3.1080000	0.3490000	0.0003157	0.0000105	10615
AMARES	3.0850000	0.3530000	0.0003178	0.0000108	10615
HLSVD_APO	3.1140000	0.3210000	0.0002986	0.0000091	10615
AMARES_APO	3.0630000	0.3050000	0.0003047	0.0000090	10615
HLSVD	3.1130000	0.4540000	0.0003317	0.0000142	20615
AMARES	3.0840000	0.5850000	0.0003359	0.0000188	20615
HLSVD_APO	3.1290000	0.3460000	0.0003124	0.0000102	20615
AMARES_APO	2.8950000	0.5020000	0.0003168	0.0000169	20615
HLSVD	3.0600000	0.2900000	0.0003357	0.0000095	30615

AMARES	3.0920000	0.3150000	0.0003383	0.0000102	30615
HLSVD_APO	3.1120000	0.2880000	0.0003135	0.0000085	30615
AMARES_APO	3.1310000	0.2850000	0.0003152	0.0000084	30615
HLSVD	2.8200000	0.4080000	0.0003304	0.0000180	50615
AMARES	2.8080000	0.4130000	0.0003352	0.0000186	50615
HLSVD_APO	2.8800000	0.4120000	0.0003082	0.0000164	50615
AMARES_APO	2.8700000	0.4040000	0.0003099	0.0000163	50615
HLSVD	2.8200000	0.3760000	0.0003344	0.0000168	60615
AMARES	2.8110000	0.3740000	0.0003399	0.0000172	60615
HLSVD_APO	2.8650000	0.3710000	0.0003118	0.0000151	60615
AMARES_APO	2.8610000	0.3630000	0.0003135	0.0000149	60615
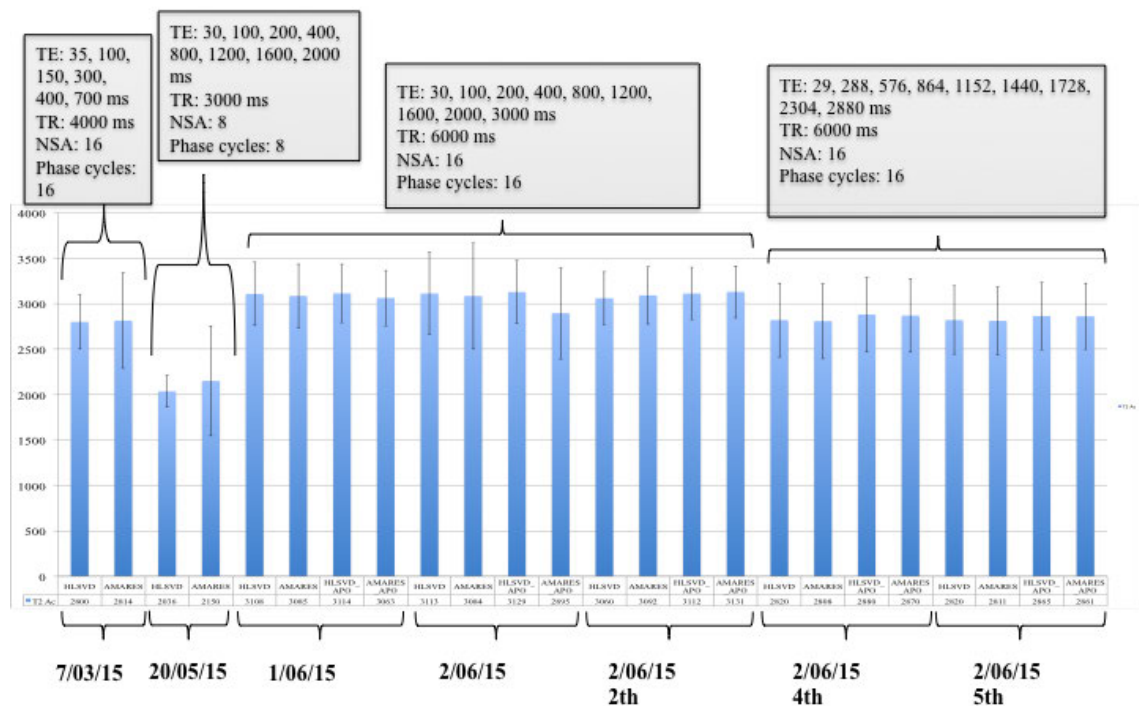
Figure 4: Acetate T_2. Error bars have been estimated automatically by the fitting procedure with MATLAB-cftool.

Table 4: Acetate T_2 average and std results for the different sequences parameters. For the last 2 sequences parameters are the same less than the sampling time T_E, so we decide in this case to average all these results.

Acetate	T_2 [ms]	$\Delta\, T_2$[ms]
7/03/15	2807	10
20/05/15	2093	8
1/06 - 2/06 - 2/06 2th	3082	63
2/06 4th - 2/06 5th	2842	30
1/06 - 2/06 - 2/06 2th - 2/06 4th - 2/06 5th	2986	131

7.1.3 - Lactate T_2 relaxation time

Lactate estimation is complicate due to a lower SNR respect to Acetate and to a different evolution of peaks with T_E. Lactate acquisitions were performed when possible with T_E multiples of 288 ms (or 272 ms) looking for the best SNR [Ref. 215, 216, 217]. At 288 ms al peaks are in phase, so in this case we should have the best SNR, but we lost SNR due to T_2 relaxation time. We tried to use multiples of 272 ms for T_E but the results is the same as with 288 ms.
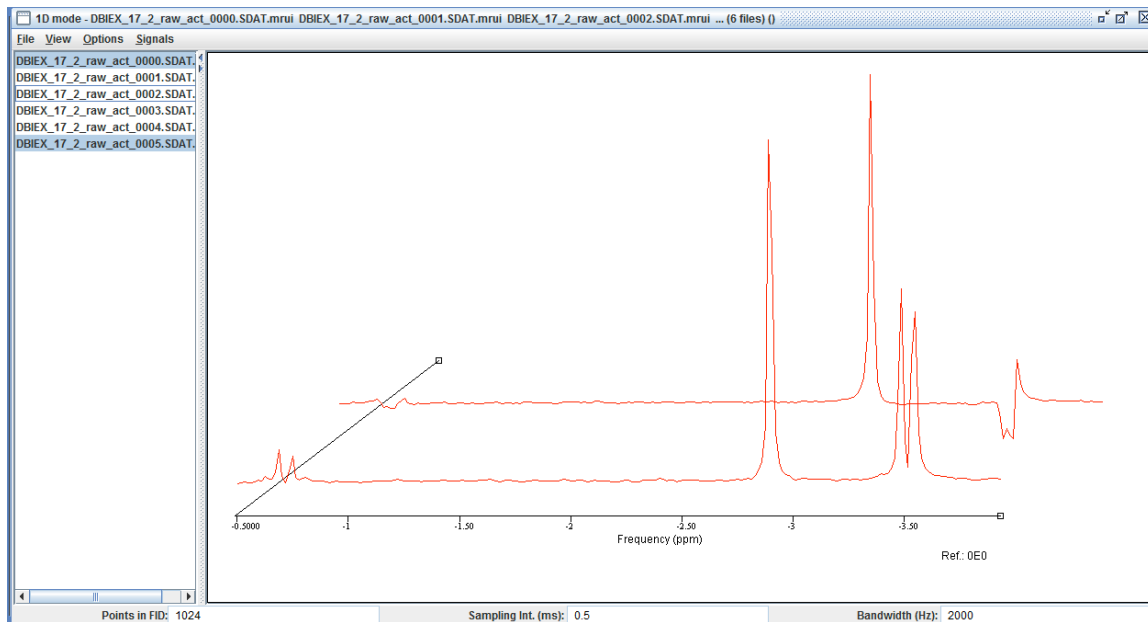
Figure 5: Lactate and Acetate peaks. Distorsions in Lactate peaks are clearly visible in the backward spectrum ($T_E = 700$ ms), while in the front spectrum ($T_E = 35$ ms) there are no distorsions.
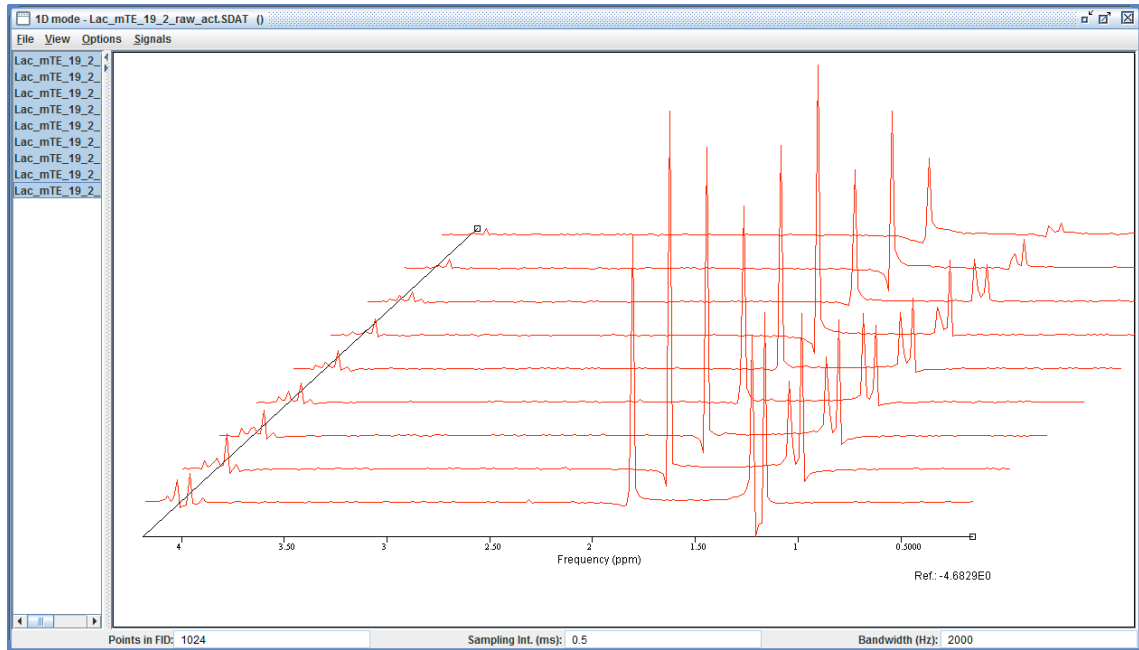
Figure 6: Acetate and Lactate spectrum with multi-echo sequence acquired with T_E multiples of 288 ms. T_E (ms) = 29, 288, 576, 864, 1152, 1440, 1728, 2304, 2880. T_R = 6000 ms. NSA = phase cycles = 16.
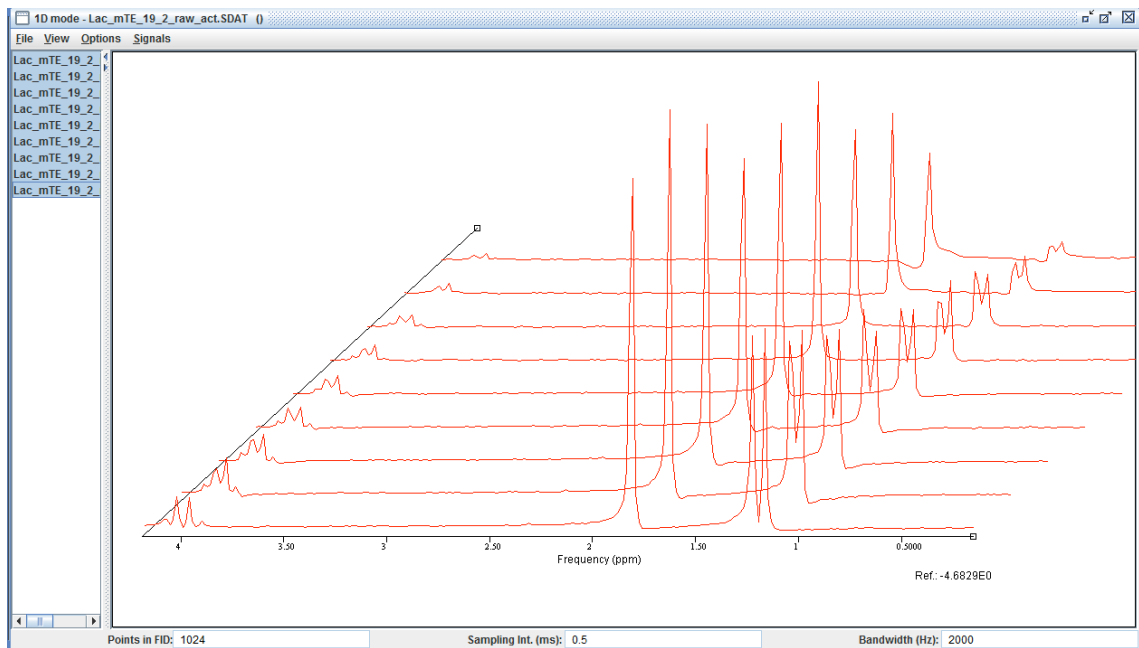
Figure 7: Acetate and Lactate spectrum with multi-echo sequence acquired with T_E multiples of 288 ms. Spectrum have been apodized with a Lorentzian of 5 Hz. T_E multiples of 288 ms.

Table 5: Lactate T_2 results.

Algorithm Lactate doublet	T_2 (s)	T_2(s)	S	ΔS	Date
HLSVD	1.4240000	0.1270000	0.0003209	0.0000149	50615
AMARES	1.3500000	0.1490000	0.0003558	0.0000210	50615
HLSVD_APO	1.3490000	0.1060000	0.0003190	0.0000133	50615
AMARES_APO	1.3520000	0.1640000	0.0003404	0.0000220	50615
HLSVD	1.3270000	0.0920000	0.0003443	0.0000128	60615
AMARES	1.3260000	0.1440000	0.0003684	0.0000215	60615
HLSVD_APO	1.3310000	0.0890000	0.0003258	0.0000117	60615
AMARES_APO	1.3310000	0.1560000	0.0003475	0.0000218	60615
Lactate doublet + quadrouplet					
HLSVD	1.3680000	0.1130000	0.0003946	0.0000172	50615
AMARES	1.3670000	0.1590000	0.0004179	0.0000257	50615
HLSVD_APO	1.3570000	0.1170000	0.0003807	0.0000175	50615
AMARES_APO	1.3640000	0.1810000	0.0004024	0.0000284	50615
HLSVD	1.328000	0.094000	0.000415	0.000016	60615
AMARES	1.339000	0.146000	0.000436	0.000026	60615
HLSVD_APO	1.323000	0.081000	0.000397	0.000013	60615
AMARES_APO	1.337000	0.160000	0.000417	0.000027	60615
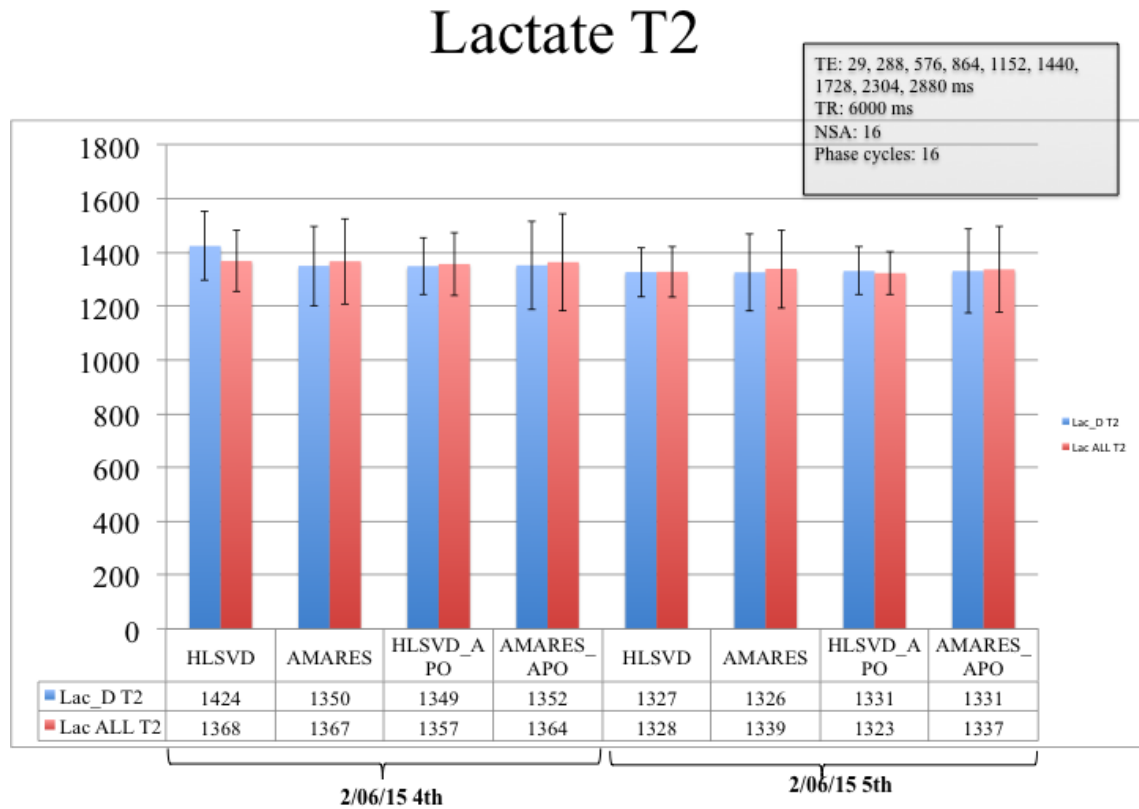
Figure 8: Lactate doublet and doublet plus quadrouplet T_2. Error bars have been estimated automatically by the fitting procedure with MATLAB-cftool.

Table 6: Lactate T_2 average and std results.

Lactate doublet	T_2[ms]	ΔT_2[ms]
2/06 4th - 2/06 5th	1349	32
Lactate doublet + quadrouplet		
2/06 4th - 2/06 5th	1348	18

7.2 - Conclusions about T_2 estimation

From the results shown above we can conclude that:
1. There are no differences between HLSVD and AMARES results, so we can average all results together clustering only by sequences parameters
2. Fit function ƒ1 should be used only when $T_R \gg T_2$, otherwise the estimation of T_2 is not correct
3. NSA, phase cycling don't affect results if SNR is good as in the case of phantom

4. T_E must be chosen bearing in mind the evolution of metabolites under study, as in the case of Lactate

5. T_E times should be chosen at the best to sample the multi-echo curve in order to ave a good fitting.

Chapter 8

SIEMENS PHANTOM: QUANTITATION OF METABOLITES CONCENTRATION

Quantitation of metabolites inside the Siemens phantom can be performed measuring the area under the peaks of metabolites and water reference. Measurements have been performed on three different hospitals.

For San Giovanni di Dio and Santa Maria Nuova we have a quantitation of metabolites concentration in Siemens phantom without $f(T_1)$ and $f(T_2)$ corrections, while for Meyer a complete characterization of the phantom has been performed so corrections for T_1 and T_2 have been evaluated.

The errors in the metabolites concentration have different components: peaks area estimations, T_1 and T_2 estimations and corrections.

8.1 - P.O. San Giovanni di Dio

8.1.1 - Quantitation with PRESS

The sequence is a PRESS with and without water suppression, with the following parameters:
- $B_0 = 1.5$ T
- VOI at the center of phantom, dimension 20x20x20 mm^3
- $T_E = 30$ ms
- $T_R = 4000$ ms
- Number of means $= 16$
- Phase cycle $= 16$
- Samples $= 1024$
- Bandwidth $= 1000$ Hz

Acetate and Lactate results are reported in Table 1. Because all area were estimated for a different number of protons, corrections are necessary.

E.g. for Lactate doublet (d) and quadruplet (q) the total number of protons is 4. Using only Lactate doublet area we have to correct for 3 protons (Area(Lac_d)/3), while if we use all areas (doublet + quadrouplet) we have to correct for 4 protons (Area(Lac_{d+q})/4). In this case we don't correct for T_1 and T_2 relaxing time.

Errors in peaks area evaluation with AMARES and HLSVD have been estimated by the "Std. Amplitude" result given by jMRUI. In this case we found an error of about 2% for Acetate area and 4% for Lactate area.

Table 1: Results of Acetate and Lactate quantitation using HLSVD and AMARES. For Lactate the Amplitude is the sum of area under all peaks corrected for the right number of protons.

	Amplitude [a.u.]				Metabolites concentration [M]	
Metabolite	Water	Acetate	Lactate D	Lactate Q	[Acetate]	[Lac D]
N° of protons	$n_W = 2$	$n_A = 3$	$n_{LD} = 3$	$n_{LQ} = 1$		[Lac D+Q]
HLSVD	1.747e6	5370	5301	654	0.114	0.112
						0.095
AMARES	1.8e6	5000	4652		0.103	0.096
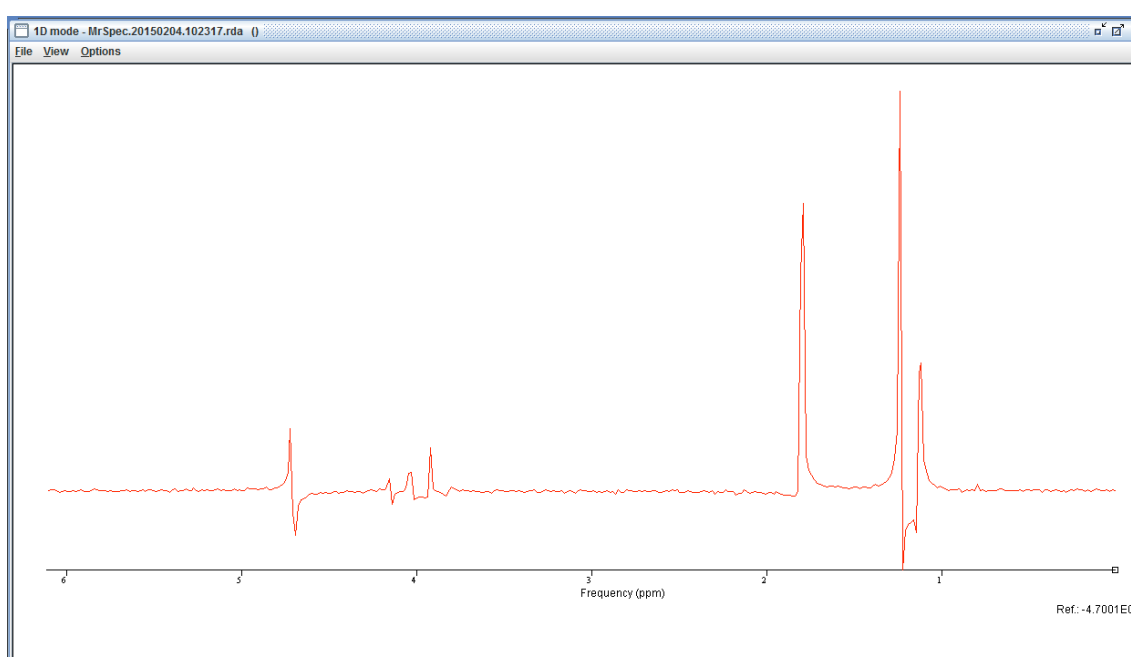
Figure 1: Metabolites spectrum from Siemens phantom acquired at SGD. Data: Spettro_04feb2015_fantoccio_Siemens"

8.1.2 - PRESS and STEAM at different echo time

Spectrum form Siemens phantom were acquired with PRESS and STEAM sequence with water suppression at multiple echo time, evaluating T_2 of metabolites. Lactate quadruplet was not considered in this case due to the associated errors in area estimation. Spectra were acquired with water suppression with the following parameters:

- Date 5 september 2014
- File name: SVS_QA_fantoccio_siemens_5set14
- Voxel 20×20×20 mm
- Number of Average: 16
- T_E PRESS: 30/135/270 ms
- T_E STEAM: 20/135/270 ms

- T_R: 1500/1500/1610 ms

T_2 estimation however is not possible due to an oscillation of the signal at time $T_E =$ 135 ms. This can be due to a change in the gain of the antennae.

Table 2: PRESS and STEAM results for the measurements performed on Siemens phantom in date 5 september 2014. Data from "SVS_QA_fantoccio_siemens_5set14"

	T_E[ms]	Acetate		Lactate d	
		HLSVD	AMARES	HLSVD	AMARES
PRESS	*30*	2.409e3	2.418e3	3.204e3	2.824e3
	135	2.466e3	2.474e3	-1921e3	n.a.
	270	2.198e3	2.194e3	2.74e3	2.722e3
STEAM	*20*	1.249e3	1.245e3	1.749e3	1.688e3
	135	1.284e3	1.296e3	n.a.	129
	270	1.177e3	1.176e3	1.458e3	1.472e3
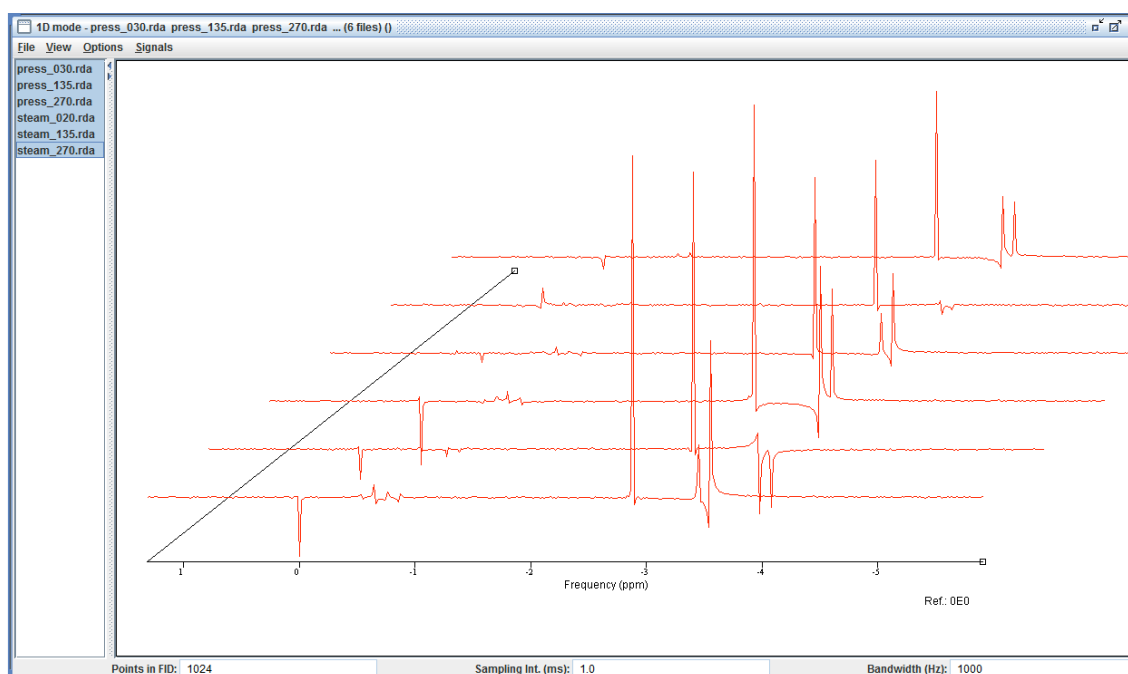
Figure 2: PRESS and STEAM spectra performed on Siemens phantom in date 5 september 2014. Data from "SVS_QA_fantoccio_siemens_5set14"

8.2 - P.O. Santa Maria Nuova

The sequence is a PRESS with and without water suppression, with the following parameters:

- B_0 = 1.5 T
- VOI at the center of phantom, dimension 20×20×20 mm³
- T_E = 30 ms
- T_R = 4000ms
- Number of means = 16
- Phase cycle = 16

- Samples = 1024
- Bandwidth = 1000 Hz

The estimated concentration evaluated using HLSVD and AMARES are reported in Table 3. In this case we don't correct for T_1 and T_2 relaxing time of water and acetate.

Errors in peaks area evaluation with AMARES and HLSVD have been estimated by the "Std. Amplitude" result given by jMRUI. In this case we found an error of about 1% for Acetate area and 10% for Lactate area.

Table 3: Results of Acetate and Lactate quantitation using HLSVD and AMARES.
For Lactate the Amplitude is the sum of area under all peaks.

Algorithm	Amplitude Water [a.u.]	Amplitude Acetate [a.u.]	Amplitude Lactate-d [a.u.]	Amplitude Lactate-d+q [a.u.]	[Acetate] estimated	[Lac-d] known	[Lac-d+q] known
HLSVD	3.78	0.0122	0.0122	0.013993	0.119	0.119	0.103
AMARES	3.89	0.0122	0.01065	0.01218	0.115	0.101	0.087
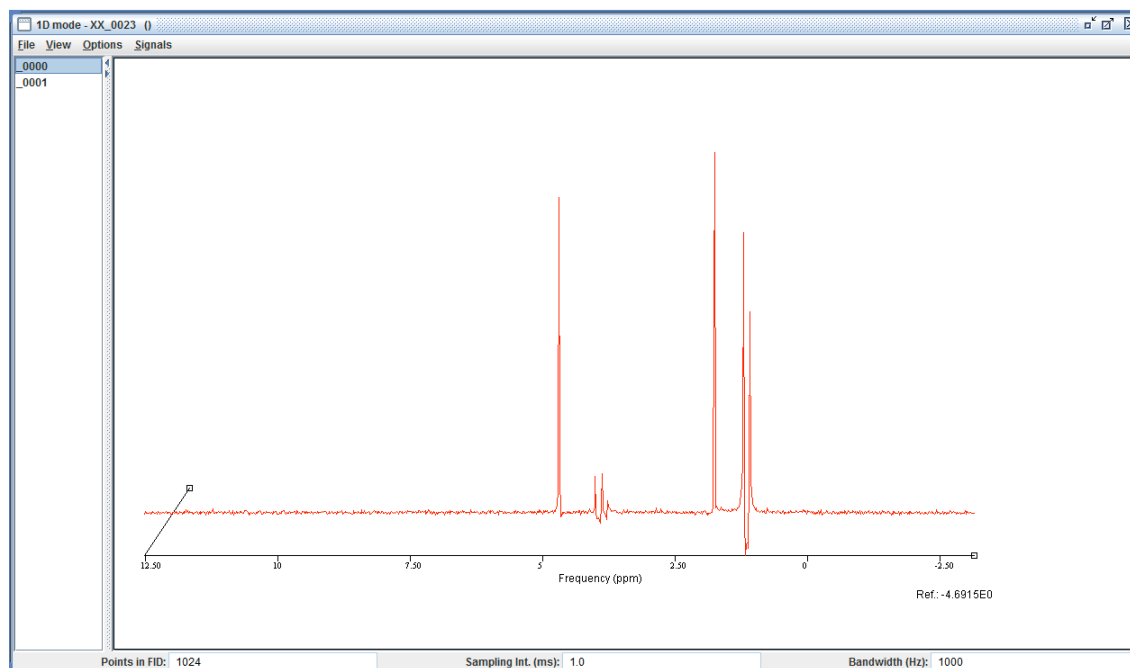
Figure 3: Siemens phantom spectrum with water suppression, acquired at SMN with PRESS sequence. T_E 30 ms. Data: "Phantom_siemens_19marzo15"

8.3 - Azienda Ospedaliera Universitaria Meyer

A PRESS sequence with and without water suppression (see Appendix 2, 3, 4) can be used to perform quantitation of Acetate and Lactate in Siemens phantom. The estimated concentration evaluated using HLSVD and AMARES are reported in In this case we correct for T_1 and T_2 of water.

Acetate and Lactate estimated by multi-inversion time and multi-echo sequences as shown in Chapter 6 and 7. Errors in peaks area evaluation with AMARES and HLSVD have been estimated by the "Std. Amplitude" result given by jMRUI. In this case we found an error of about 0.3% for Acetate area and 0.5% for Lactate area.

$$\begin{cases} f(T_1) = 1 - 2 * \exp\left(-\dfrac{T_R - \dfrac{T_E}{2}}{T_1}\right) + \exp(-T_R/T_1) \\ \qquad\qquad f(T_2) = \exp(-T_E/T_2) \end{cases}$$

Table 4: Summary of results for T_1 and T_2 at 3T.

	T_1(ms)	ΔT_1 (ms)	T_2 (ms)	ΔT_2 (ms)
Water	3214	18	776.5	21
Acetate	5169	119	2986	131
Lactate doublet	1900	68	1349	32
Lactate doublet + quadrouplet	2080	216	1348	18

Table 5: Correction factors for water and metabolites at various T_R and T_E.
Errors have been evaluated with the errors propagation formula.

	Parameters	Water	ΔW(%)	Acetate	ΔA(%)	Lactate D	ΔLD(%)	Lactate	ΔL(%)
$f(T_1)$	TR: 4000 ms	0.71	0.2	0.54	0.82	0.88	0.93	0.85	2.94
$f(T_2)$	TE: 35 ms	0.96	0.12	0.99	0.05	0.97	0.06	0.97	0.035
$f(T_1)$	TR: 15000 ms	0.99	0.026	0.94	0.38	1	0.012	1	0.062
$f(T_2)$	TE: 288 ms	0.69	1	0.91	0.42	0.81	0.51	0.81	0.29

Table 6: Errors on estimations due to $f(T_1)$, $f(T_2)$.
For metabolite the total error is the sum of water and metabolite.

Sequence parameters		ΔWater (%)	ΔAcetate (%)	ΔLactate D (%)	ΔLactate (%)
TR: 4000 ms	Δ	0.32	0.87	0.99	2.975
TE: 35 ms	Metab total Error		1.19	1.31	3.295
	Δ (Water + Metab)				
TR: 15000 ms	Δ	1.026	0.8	0.522	0.352
TE: 288 ms	Metab total Error		1.826	1.548	1.378
	Δ (Water + Metab)				

Example 1
Date: 7 march 2015
$T_R = 4000$ ms, $T_E = 35$ ms, NSA = 16, Phase cycles = 16;
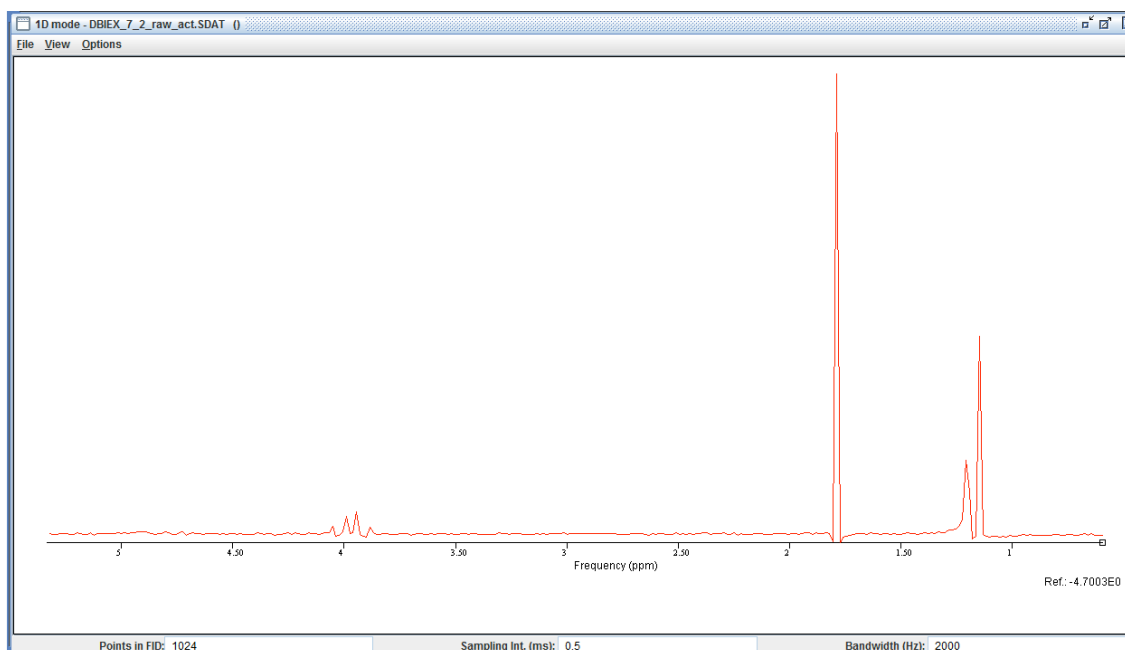
Figure 4: Spectrum of Siemens phantom. Metabolites peaks are visible. $T_R = 4000$ ms, $T_E = 35$ ms.

Table 7: Absolute quantitation results for example 1 using the same sequence with and without water suppression.

Algorithm	Amp. Water [a.u.]	Amp. Acetate [a.u.]	Amp. Lactate-d [a.u.]	Amp. Lactate-d+q [a.u.]	[Ac]	[Ac] corr	[Lac-d]	[Lac-d] corr	[Lac-d+q]	[Lac-d+q] corr
HLSVD	0.0694	2.321e-4	2.406e-4	2.7401e-4	0.124	0.159	0.128	0.1016	0.1096	0.0895
AMARES	0.0681	2.352e-4	2.263e-4	2.5838e-4	0.1277	0.163	0.143	0.1135	0.105	0.086
HLSVD_APO5L	0.0664	2.175e-4	2.253e-4	2.5459e-4	0.121	0.155	0.1255	0.0996	0.106	0.0866
AMARES_APO5L	0.0667	2.189e-4	2.087e-4	2.3601e-4	0.121	0.155	0.116	0.0921	0.0982	0.080

Table 8: Absolute quantitation results for example 1 using water reference.

Algorithm	Amp. Water [a.u.]	Amp. Acetate [a.u.]	Amp. Lactate-d [a.u.]	Amp. Lactate-d+q [a.u.]	[Ac]	[Ac] corr	[Lac-d]	[Lac-d] corr	[Lac-d+q]	[Lac-d+q] corr
HLSVD	0.0735	2.321e-4	2.406e-4	2.7401e-4	0.117	0.1495	0.121	0.096	0.1035	0.085
AMARES	0.0762	2.352e-4	2.263e-4	2.5838e-4	0.114	0.146	0.110	0.087	0.094	0.077
HLSVD_APO5L	0.0703	2.175e-4	2.253e-4	2.5459e-4	0.1145	0.1465	0.119	0.094	0.1005	0.082
AMARES_APO5L	0.0752	2.189e-4	2.087e-4	2.3601e-4	0.108	0.138	0.103	0.0815	0.0871	0.071

In the corrections the right number of protons must be taken into account, 2 for water, 3 for Acetate and Lactate doublet, 4 for Lactate in general.

The concentration of metabolites in the Siemens phantom is provided as 0.1 M, then we found an error ranging around 40% for Acetate, ranging from 4% to 20% for Lactate

doublet and from 15% to 29% for Lactate. For Lactate there is a clear indication that absolute quantitation of doublet is better than quadrouplet due to the errors in estimation of area.

For Acetate the big error could be due to a $T_R < T_1$. In this case a different formula must be used to correct. Apodization can be used to give a better estimation too.

Quantification by a sequence with and without water suppression must takes into account the "RF drive scale", which is a parameter connected to the transmitted power.

In this case 0.5362 for water and 0.5327 for water suppressed (metabolites spectrum), so just a correction of 0.6% is possible. This correction can be important when different phantoms are used for quantitation.

Example 2
Date: 2 june 2015
$T_R = 15000$ ms, $T_E = 288$ ms, NSA = 4, Phase cycles = 4;

Table 9: Metabolites quantitation results for example 2.

Algorithm	Amp. Water [a.u.]	Amp. Acetate [a.u.]	Amp. Lactate-d [a.u.]	Amp. Lactate-d+q [a.u.]	[Ac]	[Ac] corr	[Lac-d]	[Lac-d] corr	[Lac-d+q]	[Lac-d+q] corr
HLSVD	0.0875	3.94e-4	2.69e-4	3.1413e-4	0.167	0.133	0.114	0.096	0.1	0.084
AMARES	0.0913	4.013e-4	2.859e-4	3.346e-4	0.163	0.130	0.116	0.098	0.102	0.086
HLSVD_APO5L	0.0829	3.696e-4	2.563e-4	3.0338e-4	0.165	0.132	0.114	0.097	0.102	0.086
AMARES_APO5L	0.0872	3.721e-4	2.733e-4	3.2135e-4	0.158	0.126	0.116	0.098	0.102	0.087

In this case we use water reference as a measure of water instead than repeat the same measurement without water suppression.

The concentration of metabolites in the Siemens phantom is provided as 0.1 M, then we found an error ranging around 30% for Acetate, ranging around 3% for Lactate doublet and 15% for Lactate doublet and quadrouplet. For Lactate there is a clear indication that absolute quantitation of doublet is better than quadrouplet due to the errors in estimation of area. Apodization can be used to give a better estimation too.

8.3.1 - Understanding quantitation of Acetate

In the case of Acetate different results can be found using a different T_1, e.g. 4059 ms with an error of 172 ms. In this case we found correction factors $f(T_1)$ of 0.62 and 0.97 for $T_R = 4$ s and 15 s respectively.

In this case estimations are always nearest the "known" concentration of 0,1 M declared by Siemens. The error due to $f(T_1)$ and $f(T_2)$ is about 1-2%.

Table 10: Quantitation of Acetate with a T_1 of 4059 ms.

	Water "ext", T_R = 4 s	Water "REF", T_R = 4 s	Water "REF", T_R = 15 s
HLSVD	0.136	0.128	0.129
AMARES	0.140	0.125	0.126
HLSVD_APO5L	0.133	0.126	0.127
AMARES_APO5L	0.133	0.118	0.122

8.3.2 - Conclusions about quantitation at Meyer 3T

Results above shown that:

1. Acetate estimation is always bigger than theoretical value given by manifacturer
2. Lactate estimation is always lesser than theoretical value given by manifacturer
3. Lactate doublet is very near to the theoretical value given by manifacturer
4. Errors coming from correction factor $f(T_1)$, $f(T_2)$ are very small and can't take into account of the wrong estimation in concentration of metabolites
5. For the case $T_1 > T_R$ a new theoretical formula must be taken into account
6. Water acquired in the same sequence ("Water REF") gives the best estimation of water content for quantitation
7. The best estimation of metabolites concentration can be obtained taking into account all corrector factors, RF drive scale too
8. For Acetate estimation depends on the T_1, with the best estimation given by a T_1 of about 4 s. In this case we are unable to give the best result due to the different T_1 estimations with the inversion bandwidth, so we prefer give to the reader all the solutions aiming to highlight the difficulties of MRS. We are already planning new measurements in order to completely characterize the phantom.
9. A phantom with a perfectly known concentration is mandatory to understand sequence parameters influences on measurements results.

Chapter 9

IN VIVO MAGNETIC RESONANCE SPECTROSCOPY

In this part of the thesis we will explore the potential of magnetic resonance spectroscopy for the detection of prostate cancer using *in vivo* data coming from Santa Maria Nuova hospital patients. Data will be analyzed using Philips software and jMRUI-v5.0 looking for discrepancies in the metabolites ratio.

Some examples of CSI are reported too, using only the Philips software.

In vivo acquisitions are very complex due to different problems:

- *Location of the target:* a target in the center of the organ is simpler to analize than a peripherical one due to distortions from the interface between organs
- *Dimension of the target:* a small target inside a voxel can give a very small signal due to the contemporary presence of healthy and disead tissue
- *Acquisition time:* it should be shortest to prevent movement artifacts and to the confort of the patient
- *Dimension of the patient:* the physical dimension of the patient is a critical point due to the presence of fat and the distance from the antennae
- *Water and fat suppression:* great care should be taken in using suppression tecniques bacause some artifacts can be introduced in the acquired spectrum.

Before to show the results of analysis we summarize some "good practice" in accord with our and Philips experience, hoping to help people to perform *in vivo* acquistion better day by day.

Good practice for patient:
- well positioned in the center of the gantry
- fast ("digiuno")
- Cleaning of the rectum
- Empty bladder
- Buscopan for relaxation
- Biopsy at least 1-2 months before MRS to prevent contamination problems
- Breath with thorax and not with abdomen (japanese method)
- Maximum immobilization, legs too

Good practice for scanner:
- Coil: FLEX M
- Right position of the shimming volume
- No saturation bands
- Basing PULSE: FAT and WATER saturation
- VOI: only in the prostate area, avoiding air in the rectum
- Spectrum acquisition just after the survey sequence
- The area under investigation must be positioned at the center of the voxel. In this way we are very confident that signal is coming from the suspected lesion

- Sequence: SV PRESS 120, 3D PRESS 120
- Short and long TE spectroscopic sequences in order to see all metabolites
- The multivoxel sequence must be named as "AX", allowing to merge anatomical and spectroscopic images with the same axial reference system

Sequences: SV_PRESS_120 and 3D_PRESS_120

Table 1: Parameters setting for SVS and CSI sequences
for in vivo acquisitions at 1.5 T Philips of P.O. S.M.N..

SVS			CSI		
Coil selection =	"SENSE-Flex-M";		Coil selection =	"SENSE-Flex-M";	
element selection =	"12";		element selection =	"12";	
connection =	"d";		connection =	"d";	
Dual coil =		"no";	Dual coil =		"no";
VOI orientation =	"transverse";		CLEAR =		"yes";
VOI size AP (mm) =	17.2081547;		body tuned =	"no";	
RL (mm) =	18.3262787;		FOV RL (mm) =	170;	
FH (mm) =	16.7638588;		AP (mm) =	340;	
Samples =	512;		FH (mm) =	53.5499992;	
Spectral BW (Hz) =	1000;		Voxel size RL (mm) =		2.5;
Ang. AP (deg) =	0;		AP (mm) =	2.5999999;	
RL (deg) =	0;		Slice thickness (mm) =		3.5;
FH (deg) =	0;		Recon voxel size (mm) =	2.20000005;	
VOI offc. AP (P=+mm) =		12.5349264;	Fold-over suppression =	"no";	
RL (L=+mm) =	16.5764351;		Reconstruction matrix =	160;	
FH (H=+mm) =	23.2685833;		SENSE =		"no";
VOI ang. AP (deg) =	0.717895746;		Stacks =	1;	
RL (deg) =	2.6025157;		type =	"parallel";	
FH (deg) =	-0.0295728277;		slices =	14;	
Chem. shift Dir AP =	"A";		slice gap =		"default";
Chem. shift Dir LR =	"L";		slice orientation =	"transverse";	
Chem. shift Dir FH =	"F";		fold-over direction =	"AP";	
Large table movement =		"no";	fat shift direction =	"P";	
REST slabs =		2;	Stack Offc. AP (P=+mm) =	15.685936;	
shared =		"no";	RL (L=+mm) =	9.36958981;	
type =	"free", "circular",		FH (H=+mm) =	23.5021114;	
	(10) "parallel";		Ang. AP (deg) =	0.717895746;	
circular slabs =	(12) 10;		RL (deg) =	2.6025157;	
orientation =	(12) "transverse";		FH (deg) =	-0.0295728277;	
thickness (mm) =	(12) 60;		Minimum number of packages =		1;
position =		(2) "feet", (10)	Slice scan order =	"default";	
"left";			Large table movement =		"no";
gap =	(12) "default";		PlanAlign =		"no";
(mm) =		(2) 6, (10) 20;	REST slabs =	0;	
distance (mm) =	(12) 50;		Shim Size AP (mm) =		83.9444275;
Rest Offc. AP (P=+mm) =	11.4959831,		RL (mm) =	103.144699;	
	12.5349264, (10) 0;		FH (mm) =	59.3506508;	
RL (L=+mm) =	8.17602348,		Offc. AP (P=+mm) =	15.6880255;	
	16.5764351, (10) 0;		RL (L=+mm) =	9.17329025;	
FH (H=+mm) =	-21.2756672,		FH (H=+mm) =	23.1999207;	
	23.2685833, (10) 0;		Ang. AP (deg) =	0.523141384;	
Ang. AP (deg) =	-8.44129562,		RL (deg) =	2.34501886;	
	0.717895746, (10)		FH (deg) =	-0.00299369078;	
0;			Patient position =	"head first";	
RL (deg) =	-5.59742785,		orientation =	"supine";	
	2.6025157, (10) 0;		Scan type =		"Imaging";
FH (deg) =	-3.36176729,		Scan mode =		"MS";
	-0.0295728277,		technique =		"SE";
(10) 0;			Modified SE =		"no";
angulation (deg) =	(12) 0;		Acquisition mode =	"cartesian";	
FM shape =		(12) "no";	Fast Imaging mode =		"EPI";
composite elements =	(12) 1;		shot mode =		"single-shot";
correction factor =	(12) 1;		Echoes =	1;	
power =	(12) "1";		partial echo =	"no";	
target =	(12) "fat";		TE =		"shortest";
timed =	"no";		Flip angle (deg) =	90;	
start (phase) =	1;		TR =		"shortest";
stop (phase) =	2;		Halfscan =		"yes";
Patient position =	"head first";		factor =	0.616822422;	
orientation =	"supine";		Water-fat shift =		"minimum";

Scan type =	"Spectroscopy";
Scan mode =	"SV";
technique =	"ECHO";
VOI selection =	"volume";
method =	"PRESS";
Gradient Spoiling =	"no";
Fast Imaging mode =	"none";
Echo acquisition =	"half";
TE =	"user defined";
(ms) =	120;
Flip angle (deg) =	90;
RF pulse set =	"normal";
TR =	"user defined";
(ms) =	1500;
Shim =	"iterative VOI";
Shim TR =	"same";
Shim TE =	"same";
Water suppression =	"excitation";
window (Hz) =	80;
second pulse angle =	300;
WS prescan =	"auto";
BASING pulse =	"water sup.";
window (Hz) =	80;
flip angle (deg) =	180;
frequency offset =	"default";
inv. delay (ms) =	5;
Fat suppression =	"SPAIR";
inversion delay (ms) =	165;
frequency offset =	"user defined";
offset (Hz) =	40;
Pre-saturation =	"no";
SAR mode =	"high";
B1 mode =	"default";
PNS mode =	"low";
Gradient mode =	"default";
SofTone mode =	"no";
Cardiac synchronization =	"no";
Respiratory compensation =	"no";
Startup acquisitions =	2;
NSA =	256;
Phase cycles =	16;
Frequency stabilization =	"no";
Parameter series =	"no";
Manual start =	"no";
Dynamic study =	"no";
Preparation phases =	"auto";
Manual Offset Freq. =	"no";
Receiver optimization =	"ON";
Spectral correction =	"no";
Reference tissue =	"White matter";
PlanScan metabolite =	"Citrate";
Shifted metabolite displayed =	"Lactate/Lipid";
Preset window contrast =	"soft";
Save raw data =	"no";
Hardcopy protocol =	"no";
Elliptical k-space shutter =	"default";
IF_info_seperator =	1634755923;
Total scan duration =	"06:27.0";
Rel. signal level (%) =	100;
Act. TR/TE (ms) =	"1500 / 120";
Min. TR/TE (ms) =	"1133 / 117";
SPAIR TR (ms) =	1500;
SPAIR offset act./default (Hz) =	"40 [8]";
Spectral resolution (Hz/point) =	1.953125;
Readout duration (ms) =	512;
SAR / whole body =	"< 13 % / 0.5 W/kg";
Whole body / level =	"< 0.5 W/kg / normal";
B1 rms [uT] =	1.60499966;
PNS / level =	"33 % / normal";
Sound Pressure Level (dB) =	0;

Shim =	"volume";
ShimAlign =	"no";
Fat suppression =	"SPIR";
strength =	"strong";
frequency offset =	"default";
Water suppression =	"no";
BB pulse =	"no";
MTC =	"no";
Diffusion mode =	"DWI";
gradient overplus =	"yes";
nr of b-factors =	4;
b-factor order =	"user defined";
b-factors =	0, 500, 1000, 1500, (12) 0;
average high b =	"no";
SAR mode =	"high";
B1 mode =	"default";
PNS mode =	"low";
Gradient mode =	"default";
SofTone mode =	"no";
Cardiac synchronization =	"no";
Respiratory compensation =	"no";
Navigator respiratory comp =	"no";
Flow compensation =	"no";
NSA =	11;
SMART =	"no";
Manual start =	"no";
Dynamic study =	"no";
Preparation phases =	"full";
Manual Offset Freq. =	"no";
MIP/MPR =	"no";
Images =	" M", (3) " no";
Autoview image =	" M";
Calculated images =	(4) " no";
Reference tissue =	"Liver";
Preset window contrast =	"soft";
Reconstruction mode =	"real time";
Save raw data =	"no";
Hardcopy protocol =	"no";
Ringing filtering =	"rectangular";
Geometry correction =	"default";
IF_info_seperator =	1634755923;
Total scan duration =	"04:53.7";
Rel. signal level (%) =	100;
Act. TR (ms) =	"2623";
Act. TE (ms) =	"84";
ACQ matrix M x P =	"68 x 131";
ACQ voxel MPS (mm) =	"2.50 / 2.60 / 3.50";
REC voxel MPS (mm) =	"2.13 / 2.13 / 3.50";
Scan percentage (%) =	96.3235321;
Packages =	1;
Min. slice gap (mm) =	0;
Act. slice gap (mm) =	0.349999994;
EPI factor =	131;
WFS (pix) / BW (Hz) =	"19.975 / 10.9";
BW in EPI freq. dir. (Hz) =	"2001.5";
SAR / whole body =	"< 5 % / 0.2 W/kg";
Whole body / level =	"< 0.2 W/kg / normal";
B1 rms [uT] =	1.00594115;
PNS / level =	"60 % / normal";
Sound Pressure Level (dB) =	14.8767385;

Metabolites spectrum peaks info

In the prostate spectrum are usually visible these peaks:
1. Water residual from suppression at about 4.7 ppm
2. Choline, 3.19 ppm
3. Creatine, 3.03 ppm
4. CH2 NAA, Citrate doublet, 2.67 ppm
5. CH2 NAA, Citrate doublet, 2.49 ppm

9.1 - Patients info

More than 40 cases of suspected prostate cancer have been acquired at the Santa Maria Nuova Hospital. Some significative examples are reported here. All SVS spectra have been acquired using the SV_PRESS_120 sequence described above. Usually a "positive case" is when the ratio (Ch + Cr)/Citr > 0.5.

Gleason grading system

The Gleason grading system is used to help evaluate the prognosis of men with prostate cancer using samples from a biopsy. Together with other parameters, it is incorporated into a strategy of prostate cancer staging which predicts prognosis and helps guide therapy. A Gleason score is given to prostate cancer based upon its microscopic appearance. Cancers with a higher Gleason score are more aggressive and have a worse prognosis.

jMRUI and Philips software

Some examples of jMRUI-v5.0 and Philips software metabolites quantitation ratio are reported below in order to understand the differences between data elaboration. Philips software is a "black box" because user can only modify some fitting parameters, while jMRUI gives to the user more flexibility. Different estimations in the metabolites ratio have been found using the two software with discrepancies of 50% too. In these cases the clinical use of MRS is very difficult.

Some errors can be due to Philips software fitting procedure, which e.g. for Citrate use just one component for the doublet, introducing an error in the area estimation.

9.1.1 - Patient 1: Positive case

ID	Bobina & Seq	Gleason score	Diffusion	Morfological
MV	Phased array external; T_1, T_2, DWI, SV e 3D PRESS	3+3	Nella porzione periferica della ghiandola nella metà sinistra in sede medioghiandolare si evidenziano segni di restrizione dell'ADC per stipamento cellulare patologico.	Zona sospetta nella parte sinistra

Figure 1: Patient 1 CSI. Philips software.
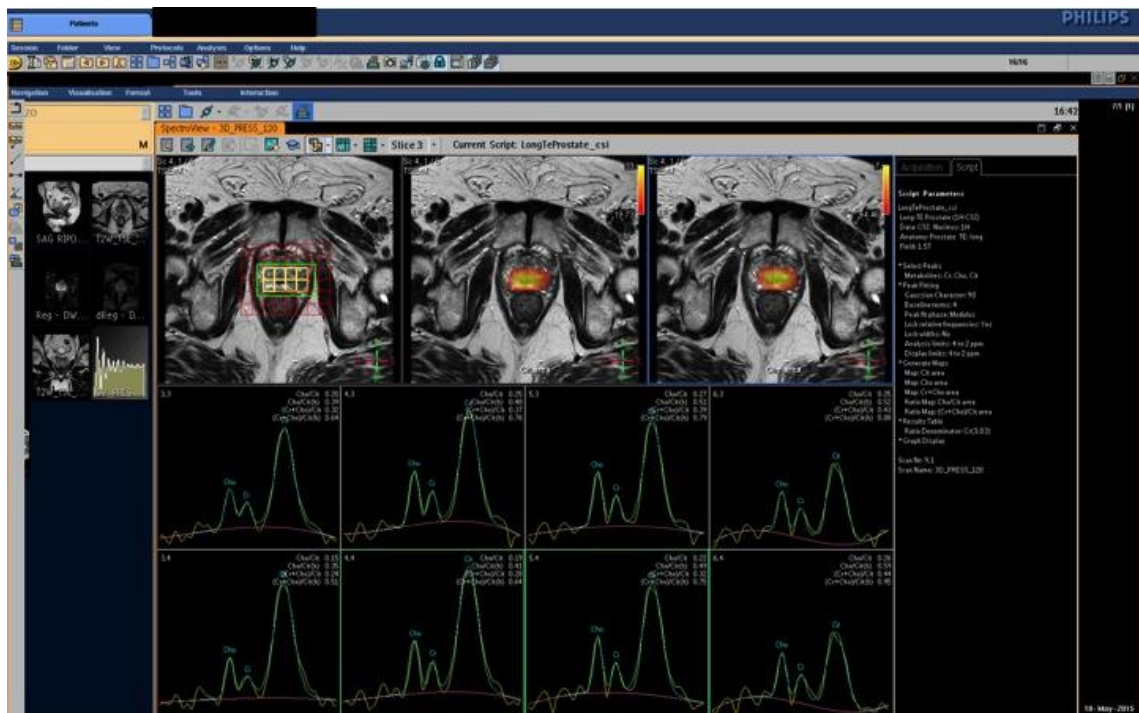
Figure 2: Patient 1 CSI. Philips software.
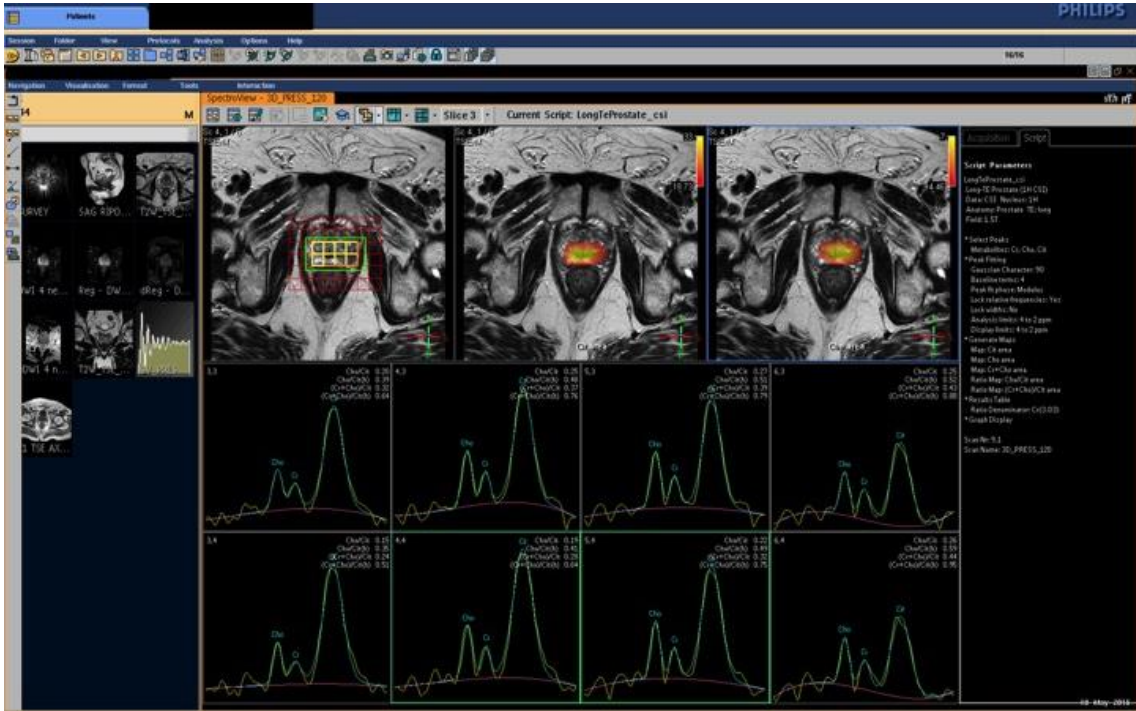
Figure 3: Patient 1 CSI. Philips software.
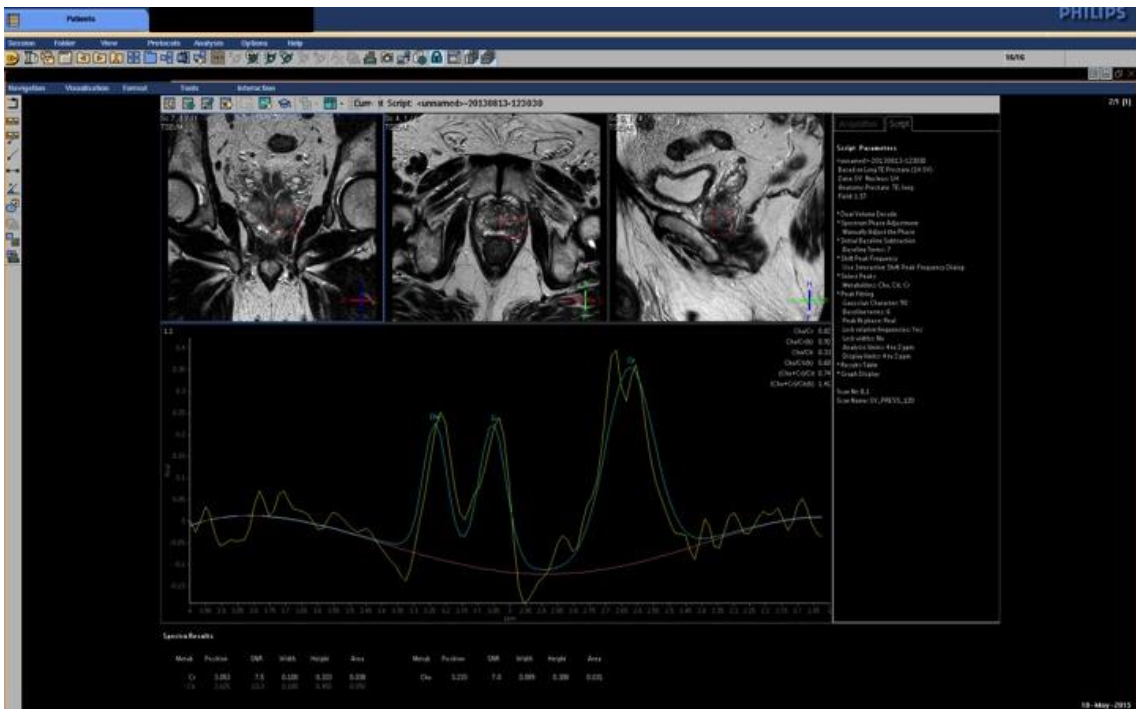
Figure 4: Patient 1. Philips software. Single-Voxel-Spectroscopy (SVS). Results with "h" are evaluated with height ratio, but won't be considered because only peak area is proportional to metabolite concentration.
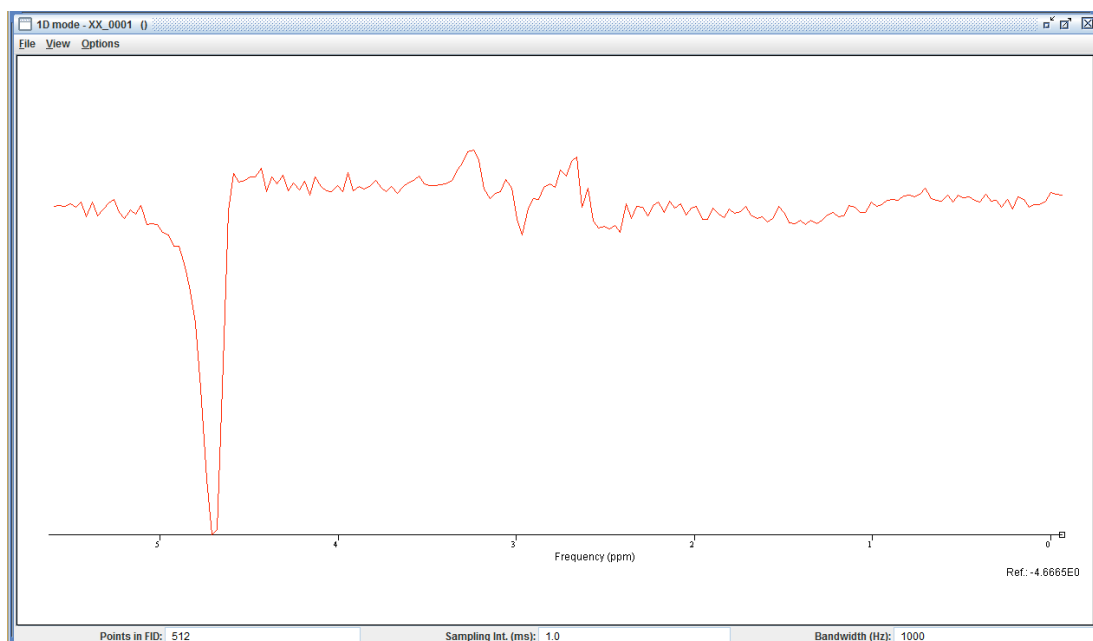
Figure 5: Patient 1, SVS. Spectrum without residual water peak removing. jMRUI software.
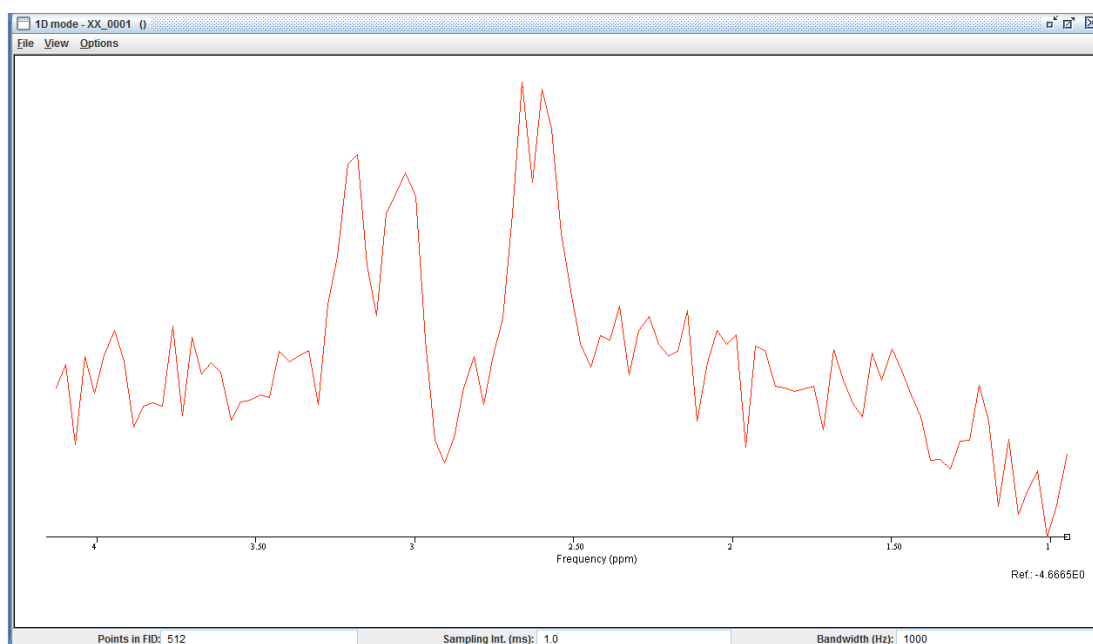
Figure 6: SVS, spectrum from Patient 1 with jMRUI software.
Choline, Creatine and Citrate doublet are clearly visible.

Table 2: AMARES results for Patient 1. (Ch+Cr)/Citrate > 0.5.

	Choline	Creatine	Ch/Cr	Citrate	Ch/Citrate	(Ch+Cr)/Citrate	Noise std
Philips	0.031	0.038	0.82	0.092	0.33	0.74	
jMRUI	7.333e-5	5.890e-5	1.24	1.428e-4	0.51	0.926	1.67e-5
Apodization Lorentzian 5 Hz	7.623e-5	5.530e-5	1.38	1.429e-4	0.53	0.92	1.47e-6

Fitting errors from AMARES have been estimated as Ch 1.3%, Cr 2.1%, Citrate 0.7%, so in the estimated ratio we have an error of about 4%.

Results from AMARES and Philips software show differences around 20% in the estimated ratio. (Ch+Cr)/Citrate>0.5 in all estimations, so this can be considered a "positive" case.

9.1.2 - Patient 2

ID	Bobina & Seq	Gleason score	Diffusion	Morfological
DeSA	Phased array external T_1, T_2, DWI, SV	4+4	Si evidenziano segni di restrizione ADC	Estesa alterazione morfo strutturale della ghiandola prostatica con estensione dell'apice fino alla base ed interessamento della porzione periferica e centrale e del fascio vescicolo-deferenziale
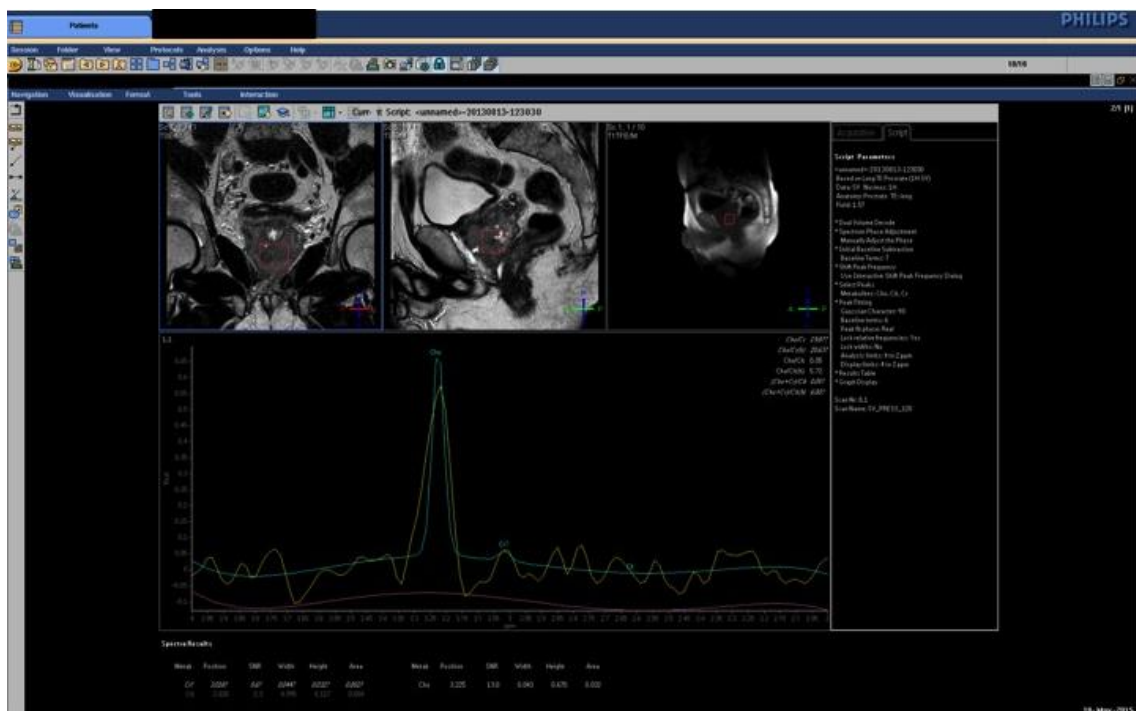
Figure 7: Patient 2, SVS from Philips software. Spectrum fit 1.
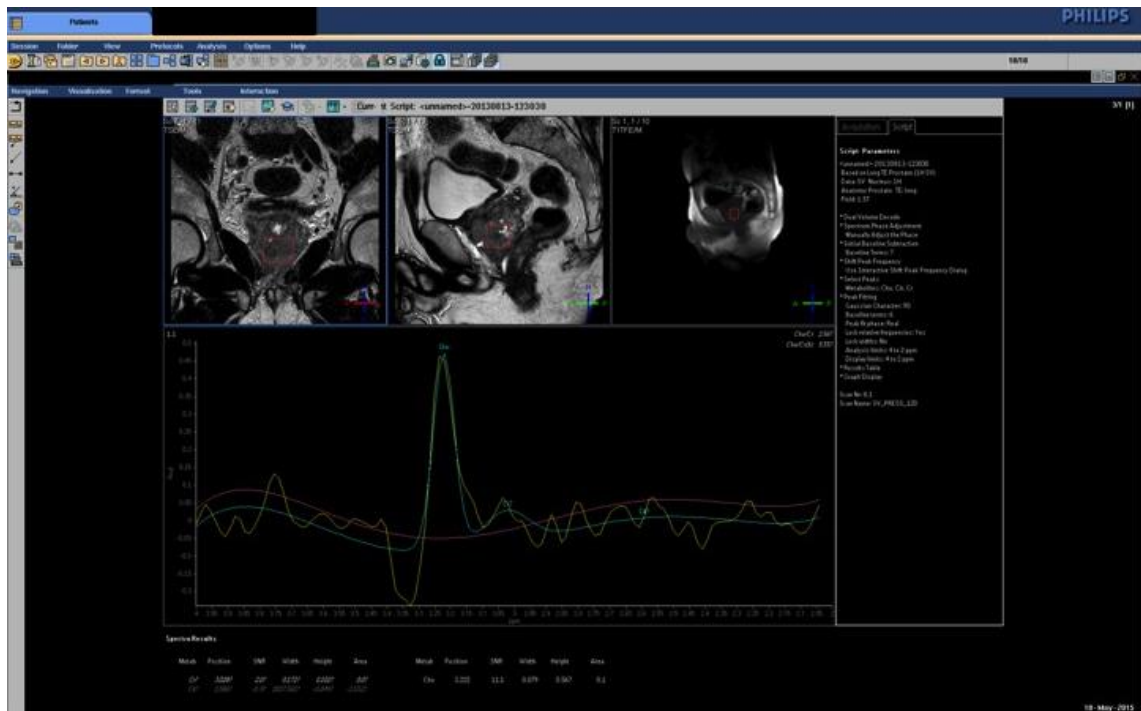
Figure 8: Patient 2, SVS. Philips software. Spectrum fit 2.
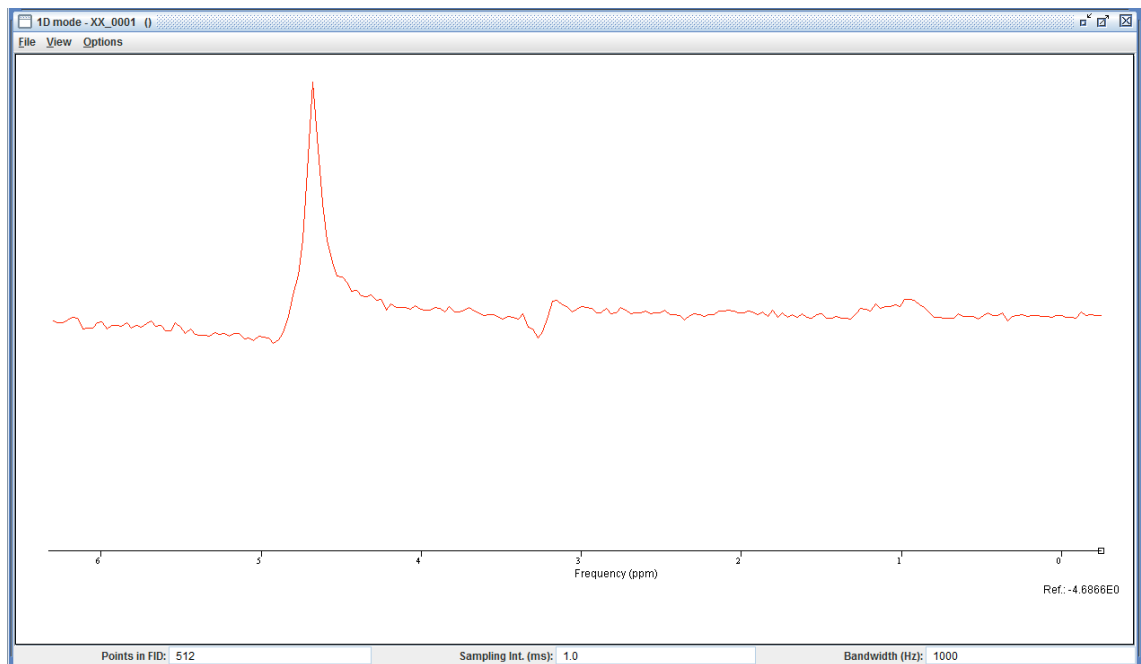
Figure 9: Patient 2, original spectrum withot removing water residual peak. jMRUI softare.
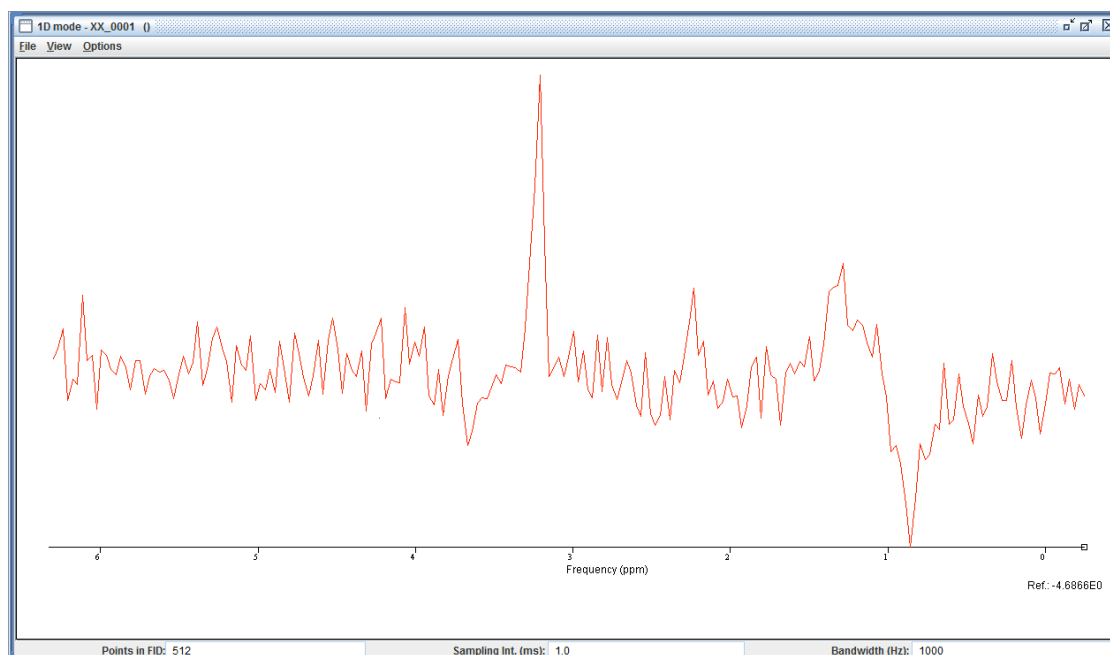
Figure 10: Patient 2, spectrum after removing water residual peak.
Choline and Citrate peaks are visible. jMRUI softare.
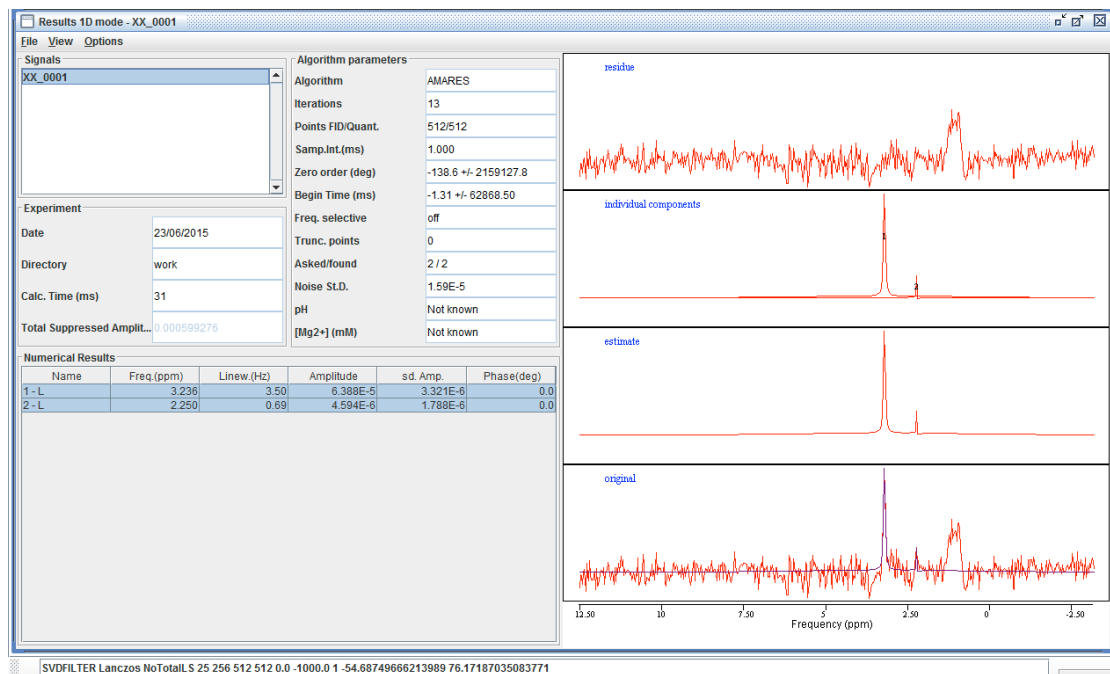
Figure 11: AMARES results for Choline and Citrate. jMRUI softare.

Table 3: AMARES results. Simbol "?" in the data means that software estimation probably is not correct.

	Choline	Creatine	Ch/Cr	Citrate	Ch/Citrate	(Ch+Cr)/Citrate	Noise std
Philips software Fit 1	0.032	0.002?	19.87?	0.654	0.05	0.05	
Philips software Fit 2	0.1	0.0?	2.56?	-1102?	Not Available	Not Available	
jMRUI	6.388e-5	Not Available	Not Available	4.594e-6?	13.9?	Not Available	1.59e-5
Apodization Lorentzian 5 Hz	5.459e-5	Not Available	Not Available	Not Available	Not Available	Not Available	1.39e-6

In this patient only Choline is estimable, apodization with a Lorentzian 5 Hz doesn't give a better estimation. Estimations from Philips software are completely wrong.

9.1.3 - Patient 3: an example of "strongly positive" case.

In this case only Choline is present.
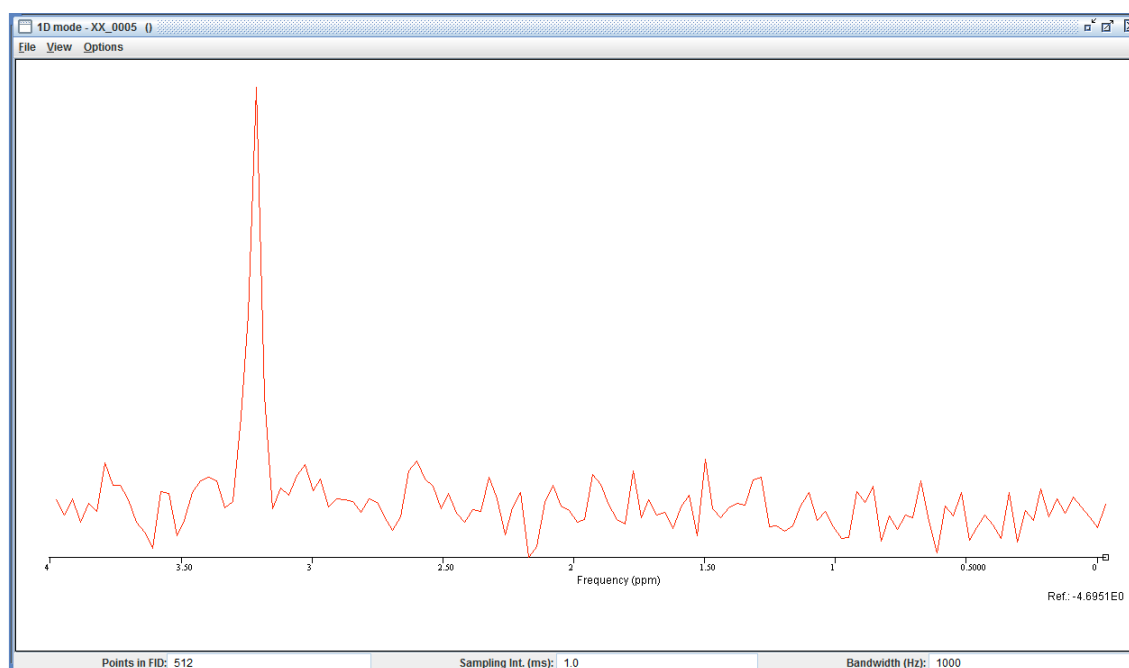
Figure 12: Patient 3, spectrum with jMRUI software. Only Choline peak is present.

9.1.4 - Patient 4: Prostata SV 27/11
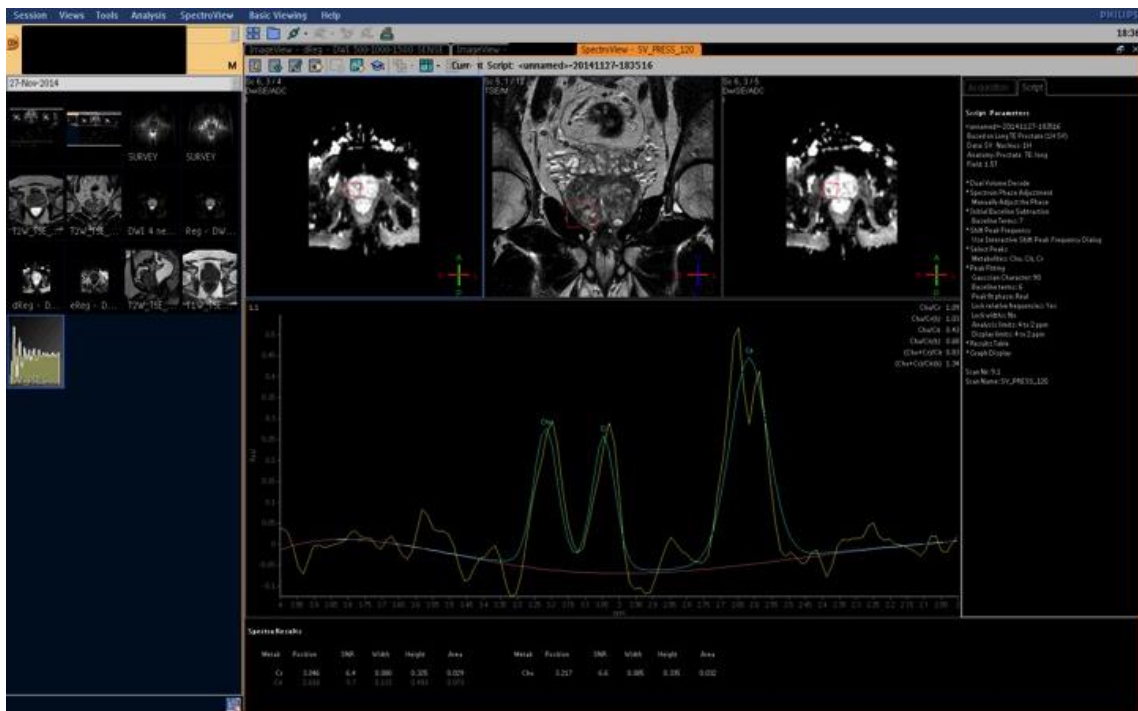
Figure 13: Patient 4, SVS. Philips software.
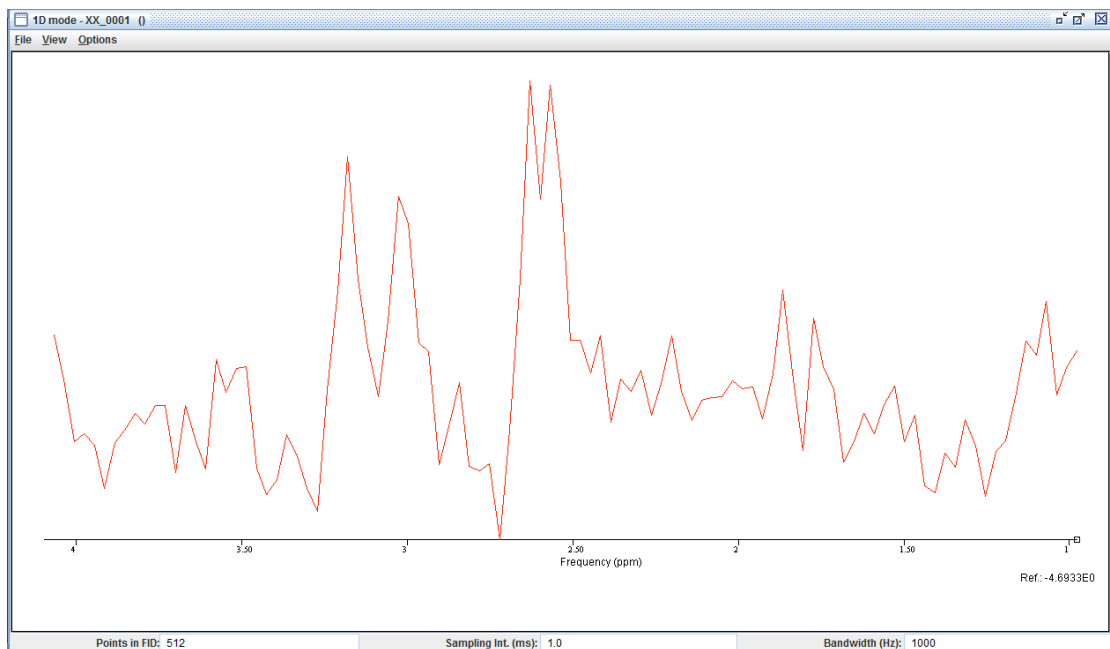
Figure 14: Patient 4. SVS, jMRUI software.
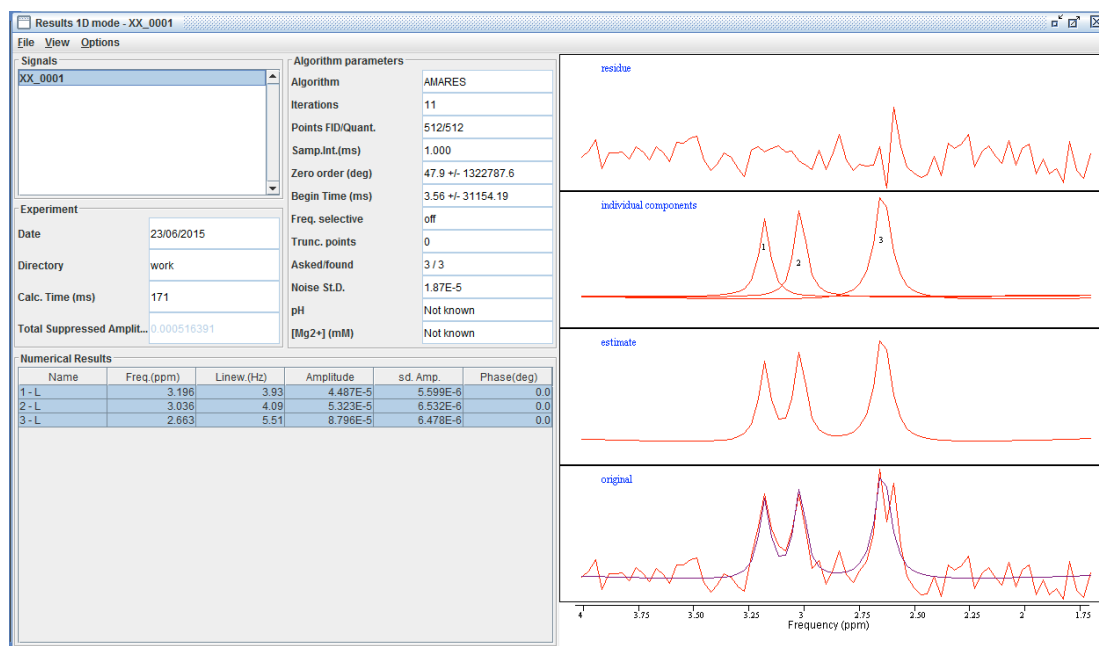
Figure 15: AMARES results. jMRUI software.

Table 4: *AMARES results for Patient 4.*

	Choline	Creatine	Ch/Cr	Citrate	Ch/Citrate	(Ch+Cr)/Citrate	Noise std
Philips Softare	0.032	0.029	1.09	0.073	0.43	0.83	
jMRUI	4.487e-5	5.323e-5	0.84	8.796e-5	0.51	1.11	1.87e-5
jMRUI with Apodization Lorentzian 5 Hz	3.876e-5	5.081e-5	0.76	9.009e-5	0.43	0.99	1.69e-6

Results from AMARES and Philips software show differences above 20% in the estimated ratio. (Ch+Cr)/Citrate >0.5, so this can be considered a "positive" case. Errors from fitting have been estimated as Ch 12%, Cr 12%, Citrate 7%, so the error in the ratio is about 30%. Then in this case Philips and jMRUI give the same estimation.

9.1.5 - Patient 5: Prostata SV2
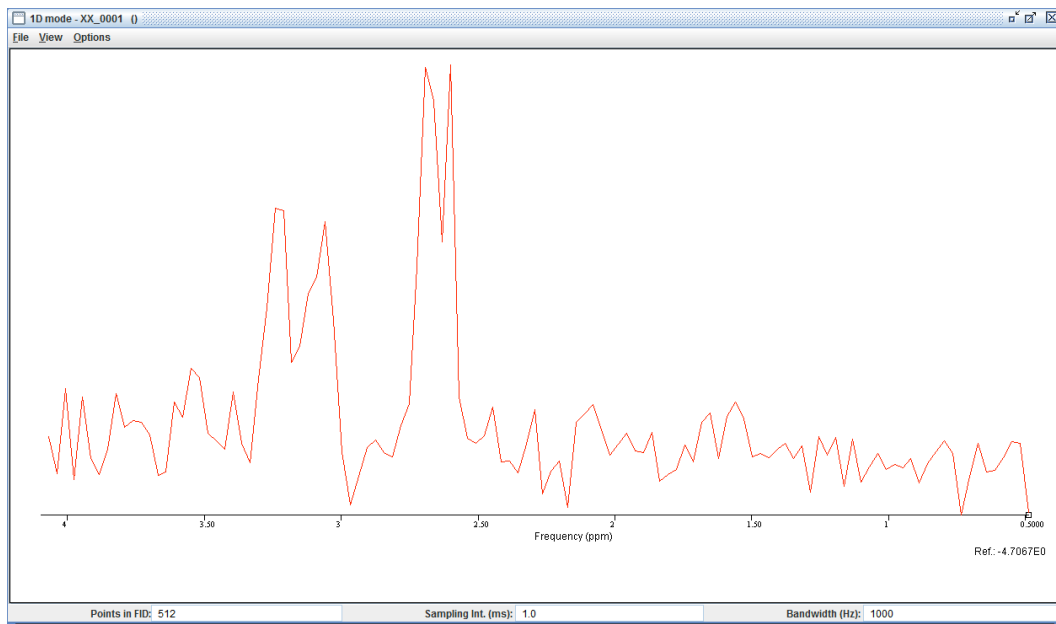
Figure 16: Patient 5 spectrum. jMRUI software.

Table 5: AMARES results for Patient 5.

	Choline	Creatine	Ch/Cr	Citrate	Ch/Citrate	(Ch+Cr)/Citrate	Noise std
jMRUI	4.985e-5	7.181e-5	0.69	1.506e-4	0.33	0.807	1.63e-5
jMRUI with Apodization Lorentzian 5 Hz	4.516e-5	6.124e-5	0.74	1.444e-4	0.31	0.74	1.44e-6

9.1.6 - Patient 6: MA5/03
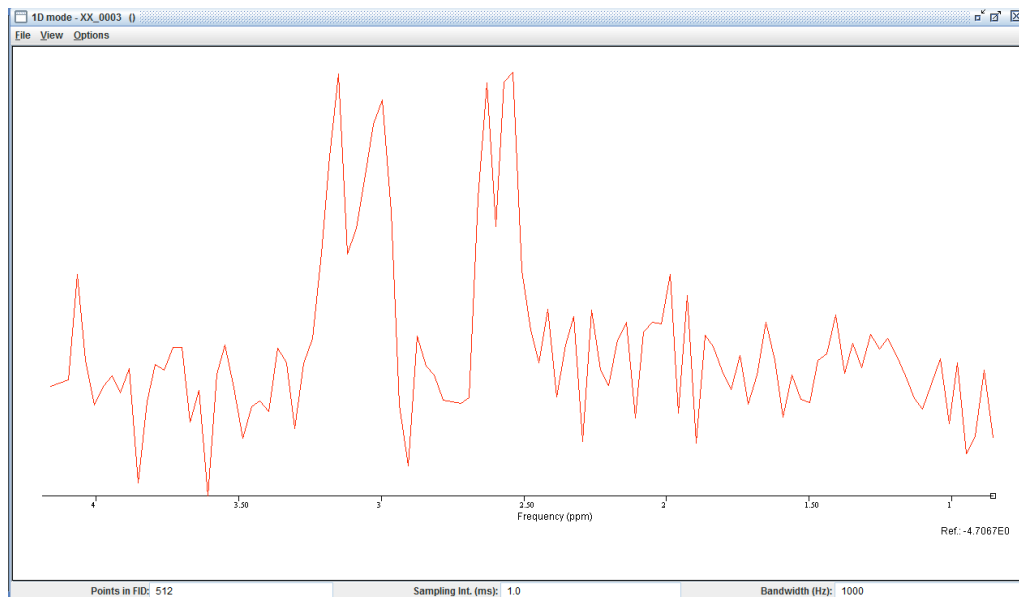
Figure 17: Patient 6. jMRUI software.

	Choline	Creatine	Ch/Cr	Citrate	Ch/Citrate	(Ch+Cr)/Citrate	Noise std
jMRUI	6.281e-5	7.997e-5	0.78	1.208e-4	0.52	1.18	1.72e-5

Table 6: AMARES results for Patient 6.

9.1.7 - Patient 7: SS, positive case post-operative.

Description: "Positivo. Prostata operata, con recidiva, si vede solo tumore." Visible only Choline peak.
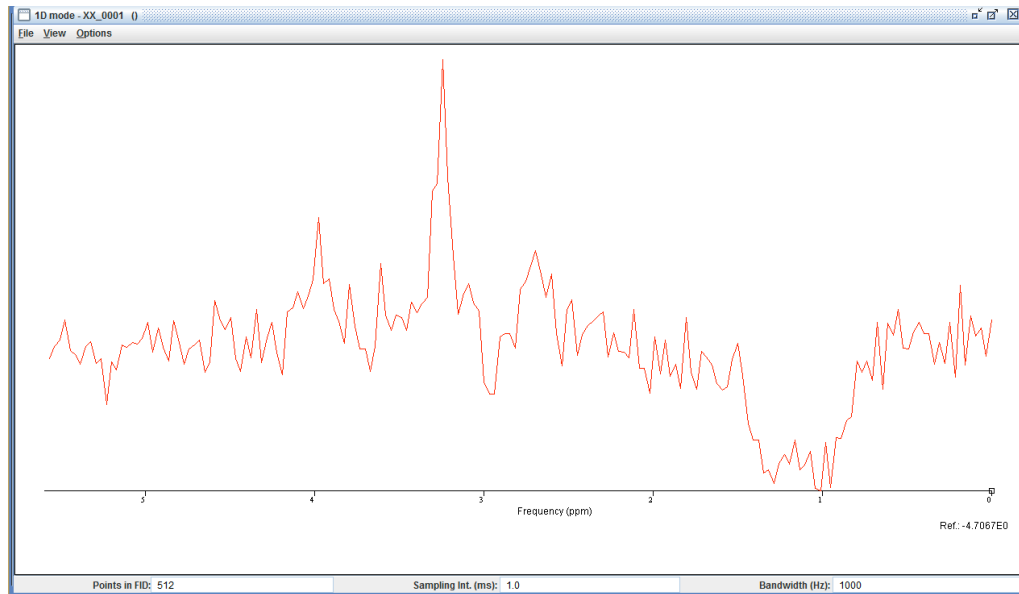
Figure 18: Patient 7. Positive case, only Choline peak is visible. jMRUI software.

9.1.8 - Patient Head 1: an example of brain spectroscopy

This is an example of brain spectroscopy performed at S.M.N. Hospital.
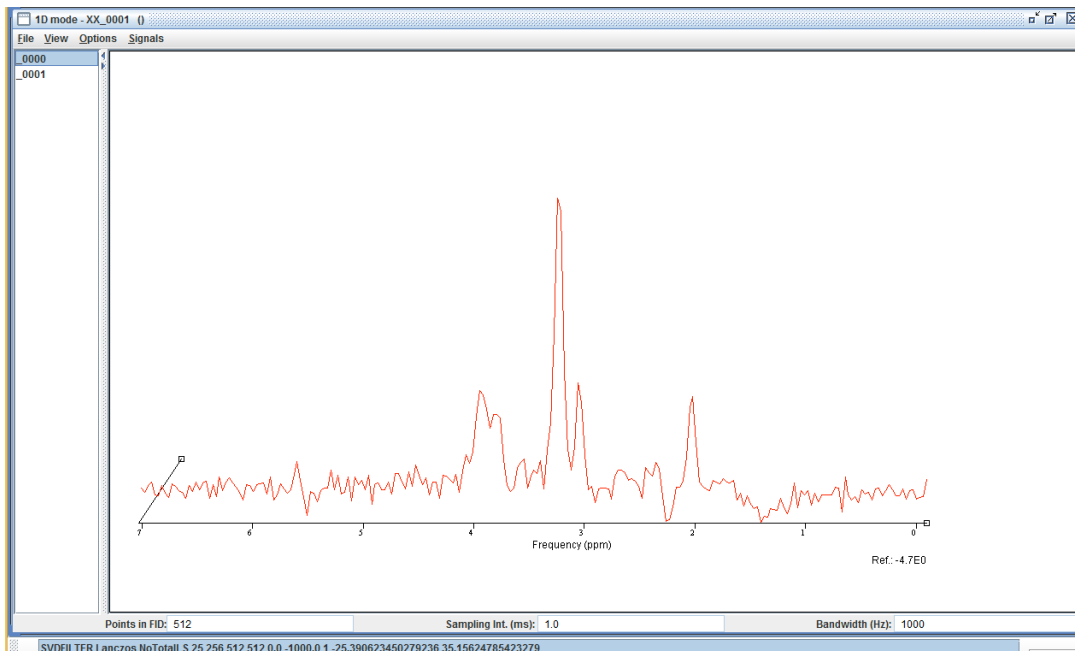
Figure 19: Patient Head 1. Spectrum demonstrates major metabolites, such as NAA peak at 2.02, Cho peak at 3.22, and Cr, which has peaks at 3 and 3.9 ppm. At short T_E, metabolites with shorter T_2 decays will be demonstrated, such as Myo at 3.6 ppm, Glx at 2.05 e 2.5 ppm, and sometimes some lipid peaks at 0.9 and 1.3 ppm.

Chapter 10

FUTURE DEVELOPMENTS:
NANOPARTICLES FOR THERANOSTIC APPLICATIONS IN MAGNETIC RESONANCE IMAGING

In this chapter, we aim to introduce some application of nanoparticles in MRI. In particular we will introduce Gold Nanoparticles (GNP) and PMMA-nanoparticles (PMMA-NP) which are already used at "Nello Carrara" Institute of Applied Physics, IFAC-CNR (via Madonna del Piano 10, Sesto Fiorentino, Firenze), Italy, for Biophotonics applications.

My idea is to use this type of nanoparticles for magnetic resonance imaging, exploring their potential as a theranostic agent. We will explore their effects in diffusion and spectroscopy, trying to characterize their behavior, opening a new scenario for their applications.

This part of my thesis has been developed in collaboration with Francesco Baldini, Ambra Giannetti, Sara Tombelli, Barbara Adinolfi, Roberto Pini, Fulvio Ratto, Sonia Centi, Lucia Cavigli, all from IFAC-CNR.

PMMA nanoparticles were supplied by ISOF-CNR (Istituto per la Sintesi Organica e la Fotoreattività, Area della Ricerca di Bologna, via P. Gobetti 101, 40129 Bologna, Italy) while Gold nanoparticles by Roberto Pini, Fulvio ratto e Lucia Cavigli from IFAC-CNR.

10.1 - Brief introduction to nanoparticles

Nanoparticles (NPs) are promising tools for applications in biology. Many innovative techniques using nanoparticles are being developed for the detection of low levels of analytes, pathogens, and cells. Nanoparticles are also being explored as delivery vehicles, imaging agents, and to better understand biology at the molecular, cellular, and tissue level. The integration of nanotechnology with biology offers many advantages that can help stimulate further biological and biomedical studies.

NPs can be engineered to possess unique compositions and functionalities to enable novel tools and techniques that have not existed previously in biomedical research.

Nanoparticles are defined as structures that are nanometers in size [Ref. 157-160]. In contrast to atoms and molecules, nanomaterials have an extensive available surface area per unit of volume and tunable optical, electronic, magnetic and biologic properties, which can be obtained, in some cases, only in nanometer scale. They can be engineered to have different sizes, shapes, chemical compositions, chemical surface characteristics, and hollow, porous or solid structures [Ref. 161, 162].

Nanoparticles can be made of materials of diverse chemical nature, the most common being metals, metal oxides, silicates, polymers, carbon, lipids and biomolecules. Nanoparticles exist in several different morphologies such as spheres, cylinders, platelets, tubes, etc. When used in living organisms, the study of these structures is known as nanomedicine. Thus, nanomedicine can be defined as the use of nanoparticles for diagnosis,

monitoring of physical and pathologic processes, for therapy and for control of biological systems [Ref. 157].

Over the last years, many studies have been reported in order to describe novel drug delivery systems. In fact, nanotechnology can be used to prepare nanostructures that will present advantages over regular chemotherapeutic agents, especially against cancer. For instance, drug carriers can be tailored to overcome some of the mechanisms conferring drug resistance to multidrug resistant cancer cells [Ref. 163]. Long-circulating nanocarriers, such as lipossomes, micells, lipid solid nanoparticles, and polymeric nanoparticles can accumulate in several affected areas where vasculature is somehow abnormal, by the EPR (Enhanced Permeability and Retention) effect. These particles, typically, display higher bioavailability and concentration in targeted tissues. Furthermore, reduced side effects compared with free drug were observed [Ref. 164].

Along with drug delivery researches other studies have been done to develop new tracers for diagnostic applications. Based on advances in molecular imaging, nanoparticles can be used to visualize, characterize and measure biological process at molecular and cellular level. Molecular imaging takes advantage of the traditional diagnostic imaging techniques and introduces molecular imaging probes to measure the expression of indicative molecular markers at different stages of diseases [Ref. 165].

Radiotracer-based imaging either using single-photon emission computed tomography (SPECT) or positron-emission tomography (PET) is particularly suited for targeted in vivo molecular imaging. The major advantages of SPECT or PET molecular imaging techniques over other approaches include high sensitivity, the ability to make quantitative measurements, and the absence of a tissue penetration limit [Ref. 166]. In addition, multimodality imaging (such as, PET/SPECT, MRI, CT, NIRF) can allow detecting the nanoparticle with various imaging techniques, providing more accurate and dependable data than SPECT or PET alone [Ref. 165].

Currently, many efforts have been made to conciliate both therapy and diagnosis properties in just one particle, leading to advantages over single approaches. The word "theranostics" refers to the simultaneous integration of diagnosis and therapy approaches [Ref. 167]. Therefore, the purpose is to diagnose and treat the diseases at their earliest stage, when the diseases are most likely curable or at least treatable. Theranostic nanomedicine shows better characteristics than other theranostics agents since they have advanced capabilities in an all-in-one single platform, which include sustained/controlled release, targeted delivery, and multimodality diagnosis and/or therapies.

Other interesting approach aims to develop multimodal nanotheranostics systems that use co-encapsulation of multiple different diagnostic modalities and therapeutic in targeting nanomedicine platforms.

As an example of studies published in recent years, we highlight the combination of a therapeutic effect of a traditional chemotherapeutic drug (i.e. paclitaxel, doxorubicin) and an excitable probes agent for imaging (i.e quantum dots, gold or metals) [Ref. 168]. In this sense, a work, conducted by Bae et al. [Ref. 169], quantum dots and paclitaxel were incorporated in solid lipid nanoparticles functionalized with siRNA aiming anticancer theranostics. The prepared solid lipid nanoparticles/siRNA complexes was efficiently delivered both paclitaxel and Bcl-2 targeting siRNA into human lung carcinoma cells and exhibited synergistic anticancer activities triggered by apoptotic mechanisms. Furthermore, the intense fluorescence of quantum dots within solid lipid nanoparticles enabled *in situ* visualization and intracellular translocation of solid lipid nanoparticles in cancer cells.

Another example of multimodality nanotheranostic system was created by Chen et al. [Ref. 170]. Nanoparticles were prepared with Doxorrubicin (DOX) conjugated to gold nanoparticles through Au-S bond by using a peptide Cys-Pro-Leu-Gly-Leu-Ala-Gly-Gly (CPLGLAGG), which is specifically cleaved by the protease. Studies conducted in tumor-bearing mice showed that after injection of the functionalized gold nanoparticles, the over-expressed protease in tumor tissue and intracellular glutathione conducted to a fast release of DOX from the functionalized gold nanoparticles, leading to enhanced efficacy on tumor growth inhibition and fluorescent imaging simultaneously.

Saho et al. [Ref. 171] introduced the concept of synergy of photothermally- activated physical and biological effects in nanoparticle-drug conjugates for theranostic objectives. The authors utilized tumor necrosis factor- alpha coated gold nanospheres (Au-TNF) heated by laser pulses. *In vivo* studies demonstrated higher therapeutic efficacy in mice, over action of laser at wavelength of 690 nm with Au–TNF conjugates. In addition, according to the authors, the photothermal activation of low toxicity Au-TNF conjugates, which are in phase II trials in humans, with a laser approved for medical applications, opens new possibilities for the development of platforms for clinically relevant nanodrugs with synergistic antitumor theranostic action.

A multifunctional pH-sensitive polymeric nanoparticle system for simultaneous tumor magnetic resonance imaging (MRI) and therapy was developed by Liu et al. [Ref. 172]. The nanoparticles were self-assembled using the multi-block polymer poly(lactic acid)-poly(ethylene glycol)- poly(L-lysine)-diethylenetriamine penta acetic acid and the pH-sensitive material poly(L-histidine)-poly(ethylene glycol)-biotin. The anti-hepatocellular carcinoma (HCC) drug sorafenib was incorporated inside the nanoparticles. Gd-DTPA complexes were distributed on the nanoparticle surface and vascular endothelial growth factor receptor (VEGFR) antibodies were linked to the surface biotin groups of nanoparticles to form the target pH-sensitive theranostic nanoparticles (TPTN). In *in vivo* anti-tumor studies, TPTN showed significantly higher antitumor effect in H22 tumor (VEGFR overexpressed cell line) bearing mice compared to free sorafenib and a positive contrast agent, with higher resolution and longer imaging time (more than 90 min) in the MRI diagnosis of tumor-bearing mice compared to Magnevist, indicated that TPTN was a promising theranostic carrier which could be a platform for the development of novel multifunctional theranostic agents.

10.2 - Types of nanoparticles

There are many types of NP platforms with differing size, shape, composition, and functionality. Furthermore, each type of NP can potentially be fabricated using different techniques, such as both nanoprecipitation and lithography for polymeric NPs. While it is not within this thesis's scope to discuss the differences in NP platforms and their fabrication in detail, we will discuss the major characteristics and functionalities of each NP that are relevant for biological research [Ref. 173], focusing on Gold and PMMA nanoparticles which are available at our research Institute.

- **Liposomes**

Liposomes were one of the first NP platforms. Liposomes were first described in 1965 as a model of cellular membranes. Since then, liposomes have moved from a model in biophysical research to one of the first NP platforms to be applied for gene and drug delivery.

Liposomes are spherical vesicles that contain a single or multiple bilayered structure of lipids that self-assemble in aqueous systems. Unique advantages imparted by liposomes are their diverse range of compositions, ability to carry and protect many types of biomolecules, as well as their biocompatibility and biodegradability. These advantages have led to the well-characterized and wide use of liposomes as transfection agents of genetic material into cells (lipofection) in biology research.

Lipofection generally uses a cationic lipid to form an aggregate with the anionic genetic material. Another major application of liposomes is their use as therapeutic carriers since their design can allow for entrapment of hydrophilic compounds within the core and hydrophobic drugs in the lipid bilayer itself. To enhance their circulation half-life and stability in vivo, liposomes have been conjugated with biocompatible polymers such as polyethylene glycol (PEG).

Liposomes can also be functionalized with targeting ligands to increase the accumulation of diagnostic and therapeutic agents within desired cells. Today, there are twelve clinically approved liposome-based therapeutic drugs.

- **Albumin-bound NPs**

Albumin-bound NPs (nab) use the endogenous albumin pathways to carry hydrophobic molecules in the bloodstream. Albumin naturally binds to the hydrophobic molecules with non-covalent reversible binding, avoiding solvent-based toxicity of therapeutics. As a result, this platform has been successfully adapted as a drug delivery vehicle. Abraxane, a 130 nm nab paclitaxel, was approved by the FDA in 2005 for the treatment of metastatic breast cancer. Abraxane concentrates in cells through albumin receptor (gp60)- mediated transport in endothelial cells. It may also target the albumin-binding protein SPARC (secreted protein acidic and rich in cysteine), which is overexpressed in certain tumors. Further understanding of the mechanism of action may lead to better targeting and development of novel therapeutics using the nab platform.

- **Polymeric NPs**

Polymeric NPs formed from biocompatible and biodegradable polymers have been extensively investigated as therapeutic carriers and contrast agent [Ref. 174 – 182, 185]. Polymeric NPs are formulated through block-copolymers of different hydrophobicity. These copolymers spontaneously assemble into a core–shell micelle formation in an aqueous environment. Polymeric NPs have been formulated to encapsulate hydrophilic and/or hydrophobic small molecule drugs, as well as proteins and nucleic acid macromolecules. The NP design can allow for slow and controlled release of drug at target sites. Polymeric NPs are usually able to improve the safety and efficacy of the drugs they carry. Functionalizing polymeric NPs with targeting ligands for improved drug delivery has been an important area of investigation since polymeric NPs are unique in their ability to be

tailored prior to particle assembly. The incorporation of targeting ligands on the NPs can lead to their increased uptake along with their cargo, leading to enhanced therapeutic outcomes.

Another type of polymeric NP is dendrimers. Dendrimers are regularly branched macromolecules made from synthetic or natural elements including amino acids, sugars, and nucleotides. They have a central core, interior layers of branches, and an exterior surface. The varied combination of these components can yield dendrimers of well-defined size, shape, and branching length/ density. As a result of their unique design, dendrimers can be developed as sensors as well as drug and gene delivery carriers. Dendrimers can be loaded with small molecules in the cavities of the cores through chemical linkage, hydrogen bond, and/or hydrophobic interaction. The exterior surface can also be readily modified to produce chemical functional groups for the attachment of molecular targeting groups, detection and imaging agents, and therapeutic agents.

- **PMMA nanoparticles in collaboration with IFAC and ISOF**

The nanoparticles used in this study consist of a core of polymethylmethacrylate surrounded by a shell bearing cationic groups (-NH4+) and amine groups with fluoresceine covalently immobilized inside the nanoparticles. NPs were kindly donated by the group of Dott. G. Varchi (ISOF, CNR, Bologna, Italy).

- **Iron oxide**

Iron oxide NPs are widely studied as passive and active targeting imaging agents since they are mainly superparamagnetic [Ref. 183 - 184]. The superparamagnetic iron oxide NPs (SPIONs) generally have an iron oxide core with a hydrophilic coat of dextran or other biocompatible compound to increase their stability. The most widely used SPIONs consist of a magnetite (Fe3O4) and/or maghemite (γFe2O3) core. These NPs exhibit size-dependent superparamagnetism, which allows them to become magnetized with the application of an external magnetic field and exhibit zero net magnetization upon removal of the magnetic field. SPIONs have been successfully used as T_2-weighted magnetic resonance (MR) contrast agents to track and monitor cells. SPIONs have several advantages over conventional gadolinium-chelate contrast agents including decreased toxicity and increased imaging sensitivity and specificity. SPIONs can also be degraded to iron and iron oxide molecules that are metabolized, stored in cells as ferritin, and incorporated into hemoglobin. Currently, two SPIO agents, ferumoxides (120–180 nm) and ferucarbotran (60 nm), are clinically approved for MRI. SPIONs have also been used in molecular imaging applications such as the detection of apoptosis and gene expression. SPIONs can be functionalized with optical and radionuclide targeting ligands for multimodal imaging. They can also potentially be used as non-invasive diagnostic tools and as drug delivery vehicles.

- **Quantum dot**

First discovered in 1980, quantum dots (QDs) are semiconductor particles that are less than 10 nm in diameter. QDs display unique size-dependent electronic and optical properties. Most QDs studied consist of a cadmium selenide (CdSe) core and a zinc selenide (ZnS) cap. The absorption spectra of these particles are very broad and emission is confined

to a narrow band. QDs can also emit bright colors, have long lifetimes and high efficiencies and are stable against photobleaching. They can be generated to have various biochemical specificities and can be simultaneously excited and detected. As a result, QDs have several significant advantages over many organic fluorophore dyes for optical applications. They are widely used in biological research as fluorescence imaging tools for applications such as cell labeling and biomolecule tracking. The small size of quantum dots also enables them to be suitable for biomedical applications such as medical imaging and diagnostics.

- **Gold**

Gold NPs offer many size-and-shape dependent optical and chemical properties, biocompatibility, and facile surface modification. Gold NPs can strongly enhance optical processes such as light absorption, scattering, fluorescence, and surface-enhanced Raman scattering (SERS) due to the unique interaction of the free electrons in the NP with light. These properties have enabled the realization of gold NPs in many applications such as biochemical sensing and detection, biological imaging, diagnostics, and therapeutic applications. Sensing techniques include the use of gold NPs in colorimetric arrays and the use of gold NPs as substrates in SERS to significantly enhance Raman scattering, allowing for spectroscopic detection and identification of proteins and single molecules at the NP surface. Gold NP probes have also been used to detect heart disease and cancer biomarkers. They can also transform absorbed light into heat and therefore have high potential for infrared phototherapy.

The intense research activities devoted to the nanotechnology led to the development of multifunctional nanoparticles which combine imaging (X-ray, CT, MRI, Optical) and therapy (phototherapy, radiotherapy, chemiotherapy, thermal therapy). There is in fact a considerable need for new functionalized NP for both imaging and therapy of cancer, in particular those that have adequate pharmacokinetic properties and low levels of non-specific accumulation in the body. The improvement of the sensitivity of magnetic resonance imaging (MRI) requires the development of original contrast agents [Ref. 186 – 189, 202], while cancer therapy requires novel agents radiosensitisers [Ref. 190 – 194, 197, 200, 201]. The experimental observation of ferromagnetic moment formation at the nanoscale in Au nanoparticles and some considerations on their intrinsic magnetic moments ocan be found in [Ref. 195, 196].

- **Gold nanoparticles in collaboration with IFAC**

GNPs were kindly donated by the group of Dott. R. Pini (IFAC, CNR, Florence, Italy) [Ref. 198, 199].

10.3 - Diffusion-MRI techniques and nanoparticles

The aim of this part of the thesis is to indroduce diffusion in MRI (d-MRI), trying to understand if nanoparticles can be revealed by d-MRI techniques, looking at the change in water motion due to the presence of nanoparticles in the environment [Ref. 203].

- **Basic diffusion**

A complete discussion of diffusion in MRI is beyond the scope of this thesis, so in this part i will briefly describe diffusion [Ref. 204, 228].

This approach is based on the measurement of Brownian motion of molecules. It has been long, but not widely, known that nuclear magnetic resonance is capable of quantifying diffusional movement of molecules. In the 1980s, a method that combines this diffusion measurement with MRI was introduced, which is now widely called *diffusion imaging.* This technique can characterize water diffusion properties at each pixel of an image. The first important application of diffusion MRI emerged at center stage of the MRI community in early 1990s when it was discovered that DWI can detect stroke in its acute phase. Around the same time, scientists had also noticed that there is a peculiar property of water diffusion in highly ordered organs such as brains. In these organs, water does not diffuse equally in all direc- tions, a property called *anisotropic diffusion.* For example, brain water diffuses preferentially along axonal fiber directions. Then molecular diffusion in tissues is not free, but reflects interactions with many obstacles, such as macromolecules, fibers, and membranes. Water molecule diffusion patterns can therefore reveal microscopic details about tissue architecture, either normal or in a diseased state.

10.3.1 - Agar Phantom for Diffusion and spectroscopy measurements in MRI

We are working on a agar phantom with some spots of nanoparticles at different concentrations.

We will look at differences in diffusion (using kurtosis too) and T_1, T_2 in respect to agar phantom without NP. We will use different kind of Gold NP and PMMA-NP.

Chapter 11

CONCLUSIONS

What emerges from this thesis is that there is no "recipe" for magnetic resonance spectroscopy data analysis. Sequences parameters must be choose very carefully and data must be analyzed from experienced Medical Physicist. Any single spectrum must be analyzed with the best accuracy. No automatic procedure is possible at moment.

At first we focused on water signals coming from different MR scanners and vendors, looking for accuracy. Good results have been found on this cases.

Then, with increasing complexity, we have focused on the Siemens phantom, characterizing its behavior at 3T Philips MR scanner, looking for the best sequence parameters and best algorithm. Results have shown the importance of the right choice of the sequence parameters in order to have a good estimation of T_1, T_2 and metabolites concentration. E.g. for T_1 estimation it is very important to have a narrow inversion band centered on the metabolite of interest. The sampling time of the sequence must be choose carefully too, bearing in mind a rough estimate of the metabolite relaxation times. T_I, T_E, T_R must be choosen very very carefully. E.g. for Lactate at 3T is very important to choose a T_E of about 288 ms or multiples. In the future we will explore different sequences, e.g. adiabatic, looking for the differences in estimated parameters.

Algorithms for peaks area estimation HLSVD and AMARES have been tested, showing no net differences between the two algorithms, although AMARES is more flexible due to the possibility in the choice of fitting parameters. About AMARES it is very important to highlight as a very good peaks area fitting estimation can be obtained only with the right choice of starting values and prior knowledge parameters, with small differences giving results completely differents.

QUEST algorithm has been tested too, and it is very interesting but it is very useful only when the real parameters of the MR scanner sequence are known.

Fitting procedure for T_1, T_2 estimation has been tested with different fitting function, showing the importance of the right choice of sequence parameters and fitting function. In particular, approximated fitting function must be choosen very carefully. Due to the use of non linear least square fitting procedure, it is very important to have a prior knowledge very accurate of the estimated parameters in order to have a good estimation.

Quantitation have been performed in detail with 3T Meyer data, showing some ciriticity about quantitation of metabolites concentration, with errors even of 40% on the estimation of the known concentration. In this case we suspect that the concentration in the Siemens phantom is not accurate, because we obtain always an overestimate for Acetate and underestimate for Lactate. In this moment we are working on a test phantom with a very accurate metabolites concentration, aimed to test again our sequences and algorithms.

In conclusion a right MRS examination requires a specific protocol for diagnostic requirements and must be evaluated patient by patient. All the recommendations discussed in the previous chapters must be taken into account too. The literature reference values are not sufficient to estimate metabolites concentration with the right precision.

MRS can become a very important diagnostic instrument for the daily clinical use of radiologists only if Medical Physicists will be part of the team.

Appendix 1

ESTIMATION BY QUEST

Acetate estimation by QUEST and NMR-Scope

In NMR-Scope we need to simulate signals one by one for every T_I. An Inversion Recovery sequence (180°-TI-90°-AQ) can be simulated with a specific T_I and for a specific metabolite as shown in Figure 2, Figure 3 for Acetate. It's very important to choose the right parameter for the simulation of the sequence, e.g. there is difference in the choice of the Phase of the Detection period.
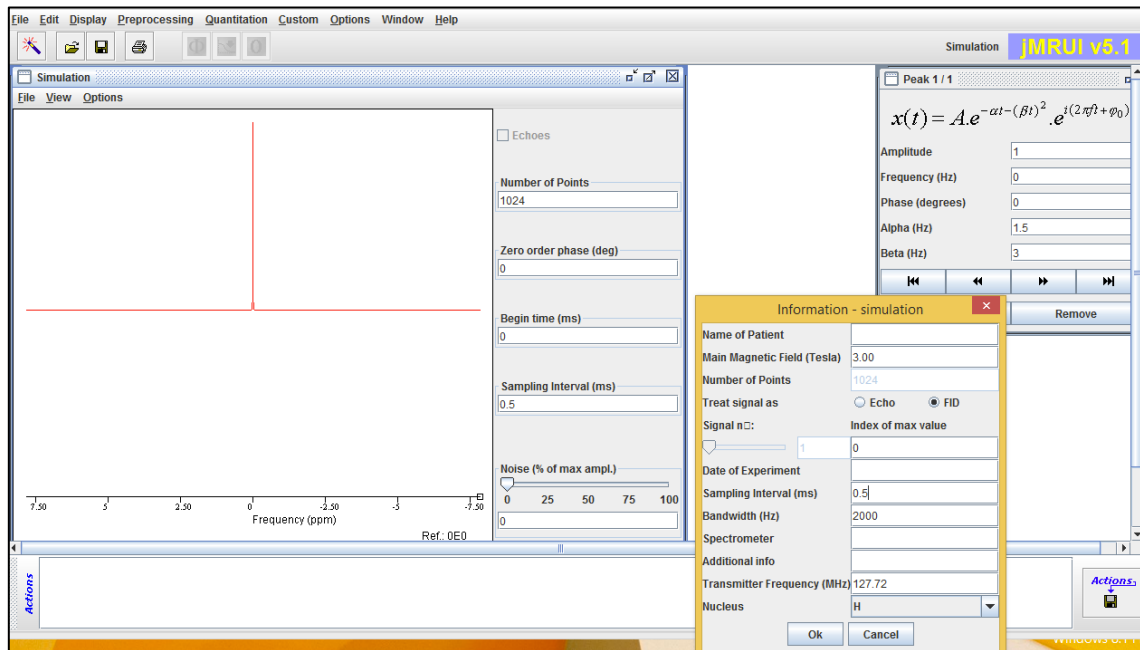
Figure 1: Example of water spectra simulation using QUEST. Scanner 3T, bandwidth 2000 Hz, sampling 0.5 ms. Alpha and Beta parameters are for a Voight curve.
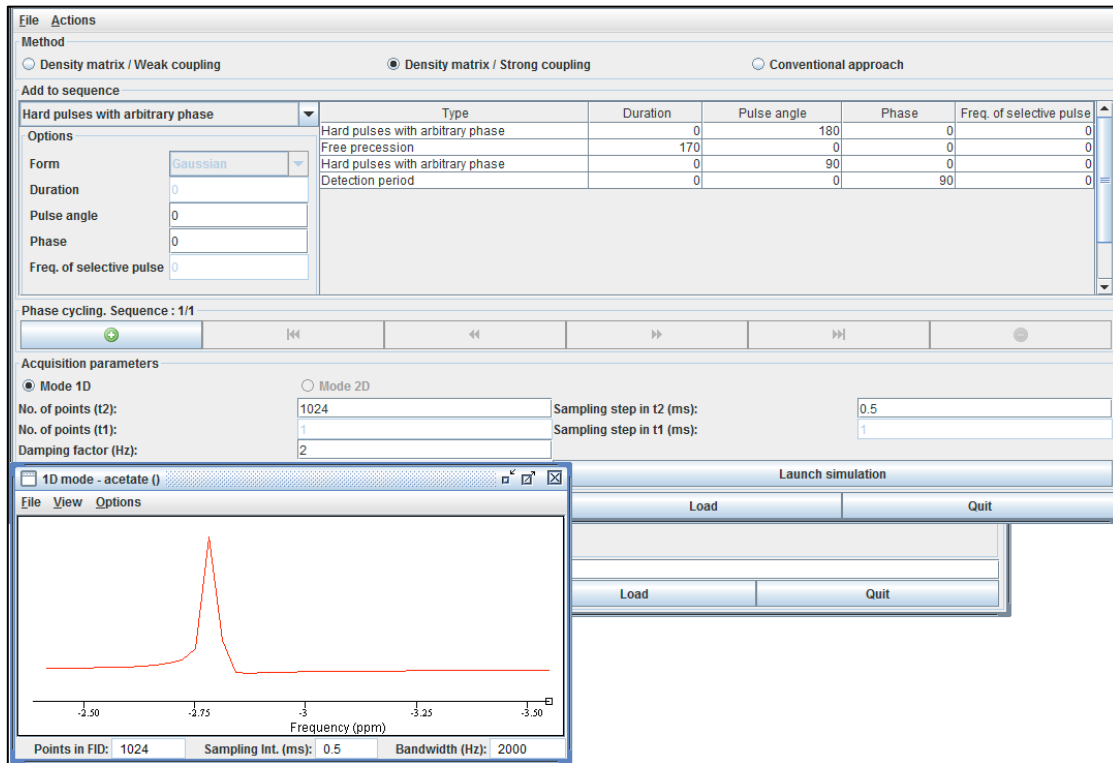
Figure 2: NMR-scope simulation Inversion Recovery sequence of Acetate at 3T with 170 ms Inversion time. Note the phase of the Detection period of 90°.
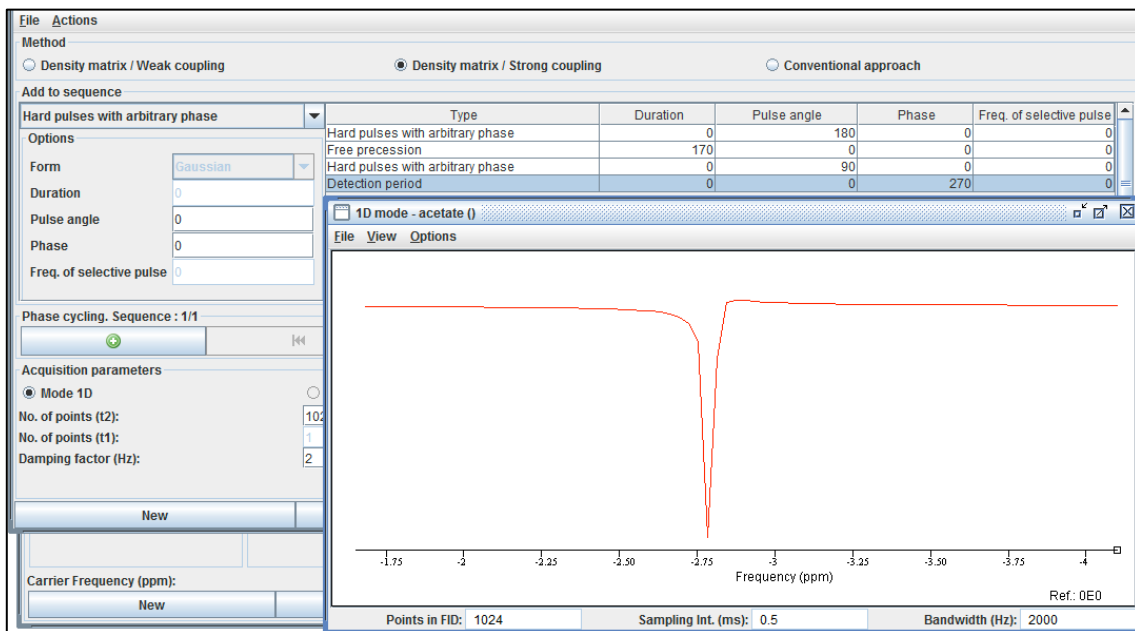
Figure 3: NMR-scope simulation Inversion Recovery sequence of Acetate at 3T with 170 ms Inversion time. Note the phase of the Detection period of 270°.

Using QUEST we can quantifies the Acetate spectrum using the simulation performed with NMR-scope.
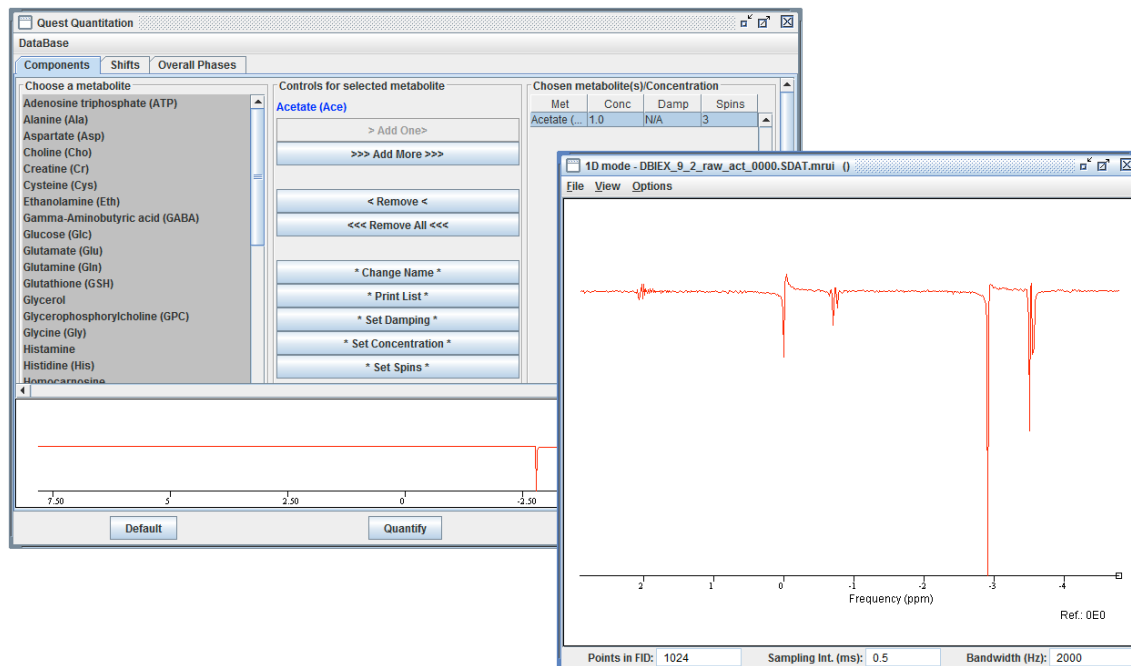
Figure 4: QUEST quantitation of Acetate. On the left side the QUEST panel, while on the right side the original signal. In this case the signal has an Inversion Recovery time of 170 ms.
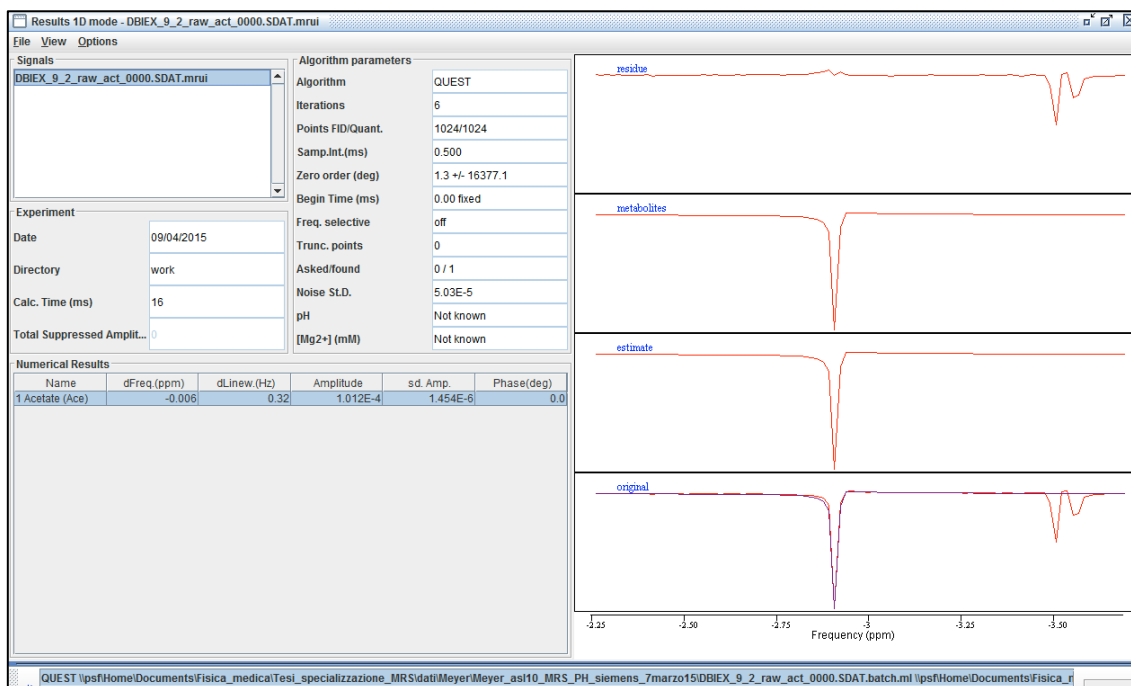
Figure 5: Result of QUEST quantification of the first Inversion Recovery signal obtained with a T_I of 170 ms.

Appendix 2

INVERSION RECOVERY SEQUENCES PARAMETERS FOR T_1 ESTIMATION

Table 1: Water sequences parameters.

7/03/15		1/06/15 - 2/06 – 2/06 2th		2/06/15 3th	
SmartSelect =		SmartSelect =		SmartSelect =	
"yes";		"yes";		"yes";	
Coil 1 (exclude) =		Coil 1 (exclude) =		Coil 1 (exclude) =	
"None";		"None";		"None";	
VOI orientation =		VOI orientation =		VOI orientation =	
"transverse";		"transverse";		"transverse";	
VOI size AP (mm) =	20;	VOI size AP (mm) =	20;	VOI size AP (mm) =	20;
RL (mm) =	20;	RL (mm) =	20;	RL (mm) =	20;
FH (mm) =	20;	FH (mm) =	20;	FH (mm) =	20;
Samples =	1024;	Samples =	1024;	Samples =	1024;
Spectral BW (Hz) =	2000;	Spectral BW (Hz) =	2000;	Spectral BW (Hz) =	2000;
VOI offc. AP (P=+mm) =		VOI offc. AP (P=+mm) =		VOI offc. AP (P=+mm) =	
-5;		0;		0;	
RL (L=+mm) =	0;	RL (L=+mm) =	0;	RL (L=+mm) =	0;
FH (H=+mm) =		FH (H=+mm) =		FH (H=+mm) =	
10;		10;		10;	
VOI ang. AP (deg) =	0;	VOI ang. AP (deg) =	0;	VOI ang. AP (deg) =	0;
RL (deg) =	-0;	RL (deg) =	-0;	RL (deg) =	-0;
FH (deg) =	-0;	FH (deg) =	-0;	FH (deg) =	-0;
Chem. shift Dir AP =	"A";	Chem. shift Dir AP =	"A";	Chem. shift Dir AP =	"A";
Chem. shift Dir LR =	"L";	Chem. shift Dir LR =	"L";	Chem. shift Dir LR =	"L";
Chem. shift Dir FH =	"F";	Chem. shift Dir FH =	"F";	Chem. shift Dir FH =	"F";
Large table movement =		Large table movement =		Large table movement =	
"no";		"no";		"no";	
REST slabs =		REST slabs =		REST slabs =	
0;		0;		0;	
Patient position =	"head	Patient position =	"head	Patient position =	"head
first";		first";		first";	
orientation =		orientation =		orientation =	
"supine";		"supine";		"supine";	
Scan type =		Scan type =		Scan type =	
"Spectroscopy";		"Spectroscopy";		"Spectroscopy";	
Scan mode =		Scan mode =		Scan mode =	
"SV";		"SV";		"SV";	
technique =		technique =		technique =	
"ECHO";		"ECHO";		"ECHO";	
VOI selection =		VOI selection =		VOI selection =	
"volume";		"volume";		"volume";	
method =		method =		method =	
"PRESS";		"PRESS";		"PRESS";	
Gradient Spoiling =	"no";	Gradient Spoiling =	"no";	Gradient Spoiling =	"no";
Fast Imaging mode =	"none";	Fast Imaging mode =	"none";	Fast Imaging mode =	"none";
Echo acquisition =	"half";	Echo acquisition =	"half";	Echo acquisition =	"half";
TE =		TE =		TE =	
"user defined";		"shortest";		"shortest";	
(ms) =	35;	Flip angle (deg) =	90;	Flip angle (deg) =	90;
Flip angle (deg) =	90;	RF pulse set =		RF pulse set =	
RF pulse set =		"normal";		"normal";	
"normal";		TR =		TR =	
TR =		"user defined";		"user defined";	
"user defined";		(ms) =	15000;	(ms) =	15000;
(ms) =	6000;	RF Shims =		RF Shims =	
RF Shims =		"fixed";		"fixed";	
"fixed";		Shim =		Shim =	
Shim =		"PB-auto";		"PB-auto";	
"PB-auto";		PB order =		PB order =	
PB order =		"second";		"second";	
"second";		Water suppression =	"no";	Water suppression =	"no";
Water suppression =	"no";	BASING pulse =		BASING pulse =	
BASING pulse =		"no";		"no";	
"no";		Research prepulse =	"no";	Research prepulse =	"no";
Research prepulse =	"no";	Pre-saturation =	"no";	Pre-saturation =	"no";
Pre-saturation =	"no";	Multi-transmit =	"yes";	Multi-transmit =	"yes";
Multi-transmit =	"yes";	Transmit channels =	"both";	Transmit channels =	"both";

Transmit channels = "both";	SAR mode =	SAR mode =
SAR mode =	"high";	"high";
"high";	B1 mode =	B1 mode =
B1 mode =	"default";	"default";
"default";	SAR Patient data = "auto";	SAR Patient data = "auto";
SAR Patient data = "auto";	PNS mode =	PNS mode =
PNS mode =	"high";	"high";
"low";	Gradient mode =	Gradient mode =
Gradient mode =	"maximum";	"maximum";
"default";	SofTone mode =	SofTone mode =
SofTone mode =	"no";	"no";
"no";	Cardiac synchronization = "no";	Cardiac synchronization = "no";
Cardiac synchronization = "no";	Respiratory compensation = "no";	Respiratory compensation = "no";
Respiratory compensation = "no";	Startup acquisitions = 2;	Startup acquisitions = 2;
Startup acquisitions = 2;	NSA =	NSA =
NSA =	2;	2;
16;	Phase cycles =	Phase cycles =
Phase cycles =	2;	2;
16;	Frequency stabilization = "yes";	Frequency stabilization = "yes";
Frequency stabilization = "yes";	Parameter series = "TI";	Parameter series = "TI";
Parameter series = "TI";	nr TIs = 7;	nr TIs = 7;
nr TIs = 5;	series spacing = "user def.";	series spacing = "user def.";
series spacing = "user def.";	TI values (ms) = 10, 300,	TI values (ms) = 10, 300,
TI values (ms) = 30, 250,		
700, 2500, 5400, (123) 0;	1000, 3000, 5000, 8000, 10000,	1000, 3000, 5000, 8000, 10000,
inv. bw (Hz) = 1500;		
inv. offset (Hz) = 0;	(121) 0;	(121) 0;
dummy scans = 1;	inv. bw (Hz) = 1500;	inv. bw (Hz) = 200;
Manual start =	inv. offset (Hz) = 0;	inv. offset (Hz) = 0;
"no";	dummy scans = 0;	dummy scans = 0;
Dynamic study =	Manual start =	Manual start =
"no";	"no";	"no";
Arterial Spin labeling = "no";	Dynamic study =	Dynamic study =
Preparation phases = "full";	"no";	"no";
Interactive F0 = "no";	Arterial Spin labeling = "no";	Arterial Spin labeling = "no";
Receiver optimization =	Preparation phases = "full";	Preparation phases = "full";
"OFF";	Interactive F0 = "no";	Interactive F0 = "no";
Receiver attenuation =	Receiver optimization =	Receiver optimization =
8;	"ON";	"ON";
Spectral correction = "yes";	Spectral correction = "yes";	Spectral correction = "yes";
spectral correction NSA = 16;	spectral correction NSA = 2;	spectral correction NSA = 2;
fat supp. on correction = "no";	fat supp. on correction = "no";	fat supp. on correction = "no";
Reference tissue = "White matter";	Reference tissue = "White matter";	Reference tissue = "White matter";
PlanScan metabolite =	PlanScan metabolite =	PlanScan metabolite =
"H20";	"H20";	"H20";
Shifted metabolite displayed =	Shifted metabolite displayed =	Shifted metabolite displayed =
"NAA";	"Lactate/Lipid";	"Lactate/Lipid";
Preset window contrast = "soft";	Preset window contrast = "soft";	Preset window contrast = "soft";
Save raw data =	Save raw data =	Save raw data =
"yes";	"yes";	"yes";
Hardcopy protocol = "no";	Hardcopy protocol = "no";	Hardcopy protocol = "no";
Elliptical k-space shutter =	Elliptical k-space shutter =	Elliptical k-space shutter =
"default";	"default";	"default";
IF_info_seperator =	IF_info_seperator =	Total scan duration =
1634755923;	1634755923;	"10:30.0";
Total scan duration =	Total scan duration =	Act. TR/TE (ms) = "15000 / 28";
"18:48.0";	"10:30.0";	Min. TR/TE (ms) = "10617 / 28";
Act. TR/TE (ms) = "6000 / 35";	Act. TR/TE (ms) = "15000 / 28";	Series TI (ms) =
Min. TR/TE (ms) = "5969 / 34";	Min. TR/TE (ms) = "10565 / 28";	
Series TI (ms) =	Series TI (ms) =	"10/300/1000/3000/5000/8000/10000";
"30/250/700/2500/5400";		"10/300/1000/3000/5000/8000/10000";	SPAIR TR (ms) =
SPAIR TR (ms) =	"10/300/1000/3000/5000/8000/10000";	14983.2227;
5983.22266;	SPAIR TR (ms) =	SPAIR inv. delay (ms) =
SPAIR inv. delay (ms) =	14983.2227;	"0.00";
"0.00";	SPAIR inv. delay (ms) =	Spectral resolution (Hz/point) =
Spectral resolution (Hz/point) =	"0.00";	1.953125;
1.953125;	Spectral resolution (Hz/point) =	Readout duration (ms) =
Readout duration (ms) =	1.953125;	512;
512;		

SAR / head =
     "< 4 %";
 Whole body / level =   "0.0 W/kg / normal";
 SED =
     " 0.0 kJ/kg";
 B1+rms / Coil Power =
     "0.46 uT / 4 %";
 Max B1+rms =
     "0.56 uT";
 PNS / level =
     "33 % / normal";
 dB/dt =   "17.0 T/s";
 Sound Pressure Level (dB) =   0;
	Readout duration (ms) =
	     512;
	 SAR / head =
	     "< 2 %";
	 Whole body / level = "0.0 W/kg / normal";
	 SED =
	     " 0.0 kJ/kg";
	 B1+rms / Coil Power ="0.29 uT / 2 %";
	 Max B1+rms = "1.19 uT";
	 PNS / level = "67 % / normal";
	 dB/dt = "37.6 T/s";
	 Sound Pressure Level (dB) = 0;
		SAR / head =
		     "< 1 %";
		 Whole body / level = "0.0 W/kg / normal";
		 SED =
		     " 0.0 kJ/kg";
		 B1+rms / Coil Power =
		     "0.24 uT / 1 %";
		 Max B1+rms = "1.19 uT";
		 PNS / level = "67 % / normal";
		 dB/dt = "37.6 T/s";
		 Sound Pressure Level (dB) = 0;

Table 2: Acetate and Lactate doublet sequences parameters.

Parameter	7/03/15	20/05/15	1/06 – 2/06 – 2/06 2th	2/06 3th	2/06 4th – 2/06 5th
SmartSelect =	"yes";	"yes";	"yes";	"yes";	"yes";
Coil 1 (exclude) =	"None";	"None";	"None";	"None";	"None";
VOI orientation =	"transverse";	"transverse";	"transverse";	"transverse";	"transverse";
VOI size AP (mm) =	20;	20;	20;	20;	20;
RL (mm) =	20;	20;	20;	20;	20;
FH (mm) =	20;	20;	20;	20;	20;
Samples =	1024;	1024;	1024;	1024;	1024;
Spectral BW (Hz) =	2000;	2000;	2000;	2000;	2000;
VOI offc. AP (P=+mm) =	-5;	0;	0;	0;	0;
RL (L=+mm) =	0;	0;	0;	0;	0;
FH (H=+mm) =	10;	0;	10;	10;	10;
VOI ang. AP (deg) =	0;	0;	0;	0;	0;
RL (deg) =	-0;	-0;	-0;	-0;	-0;
FH (deg) =	-0;	-0;	-0;	-0;	-0;
Chem. shift Dir AP =	"A";	"A";	"A";	"A";	"A";
Chem. shift Dir LR =	"L";	"L";	"L";	"L";	"L";
Chem. shift Dir FH =	"F";	"F";	"F";	"F";	"F";
Large table movement =	"no";	"no";	"no";	"no";	"no";
REST slabs =	0;	0;	0;	0;	0;
Patient position =	"head first";	"head first";	"head first";	"head first";	"head first";
orientation =	"supine";	"supine";	"supine";	"supine";	"supine";
Scan type =	"Spectroscopy";	"Spectroscopy";	"Spectroscopy";	"Spectroscopy";	"Spectroscopy";
Scan mode =	"SV";	"SV";	"SV";	"SV";	"SV";
technique =	"ECHO";	"ECHO";	"ECHO";	"ECHO";	"ECHO";
VOI selection =	"volume";	"volume";	"volume";	"volume";	"volume";
method =	"PRESS";	"PRESS";	"PRESS";	"PRESS";	"PRESS";
Gradient Spoiling =	"no";	"no";	"no";	"no";	"no";
Fast Imaging mode =	"none";	"none";	"none";	"none";	"none";
Echo acquisition =	"half";	"half";	"half";	"half";	"half";
TE =	"user defined";	"shortest";	"shortest";	"shortest";	"user defined";
(ms) =	35;				288;
Flip angle (deg) =	90;	90;	90;	90;	90;
RF pulse set =		"normal";	"normal";	"normal";	
TR =		TR =	TR =	TR =	

Column 1	Column 2	Column 3	Column 4	Column 5
"normal";	"shortest";	"user defined";	"user defined";	"normal";
TR = "user defined";	RF Shims = "fixed";	(ms) = 15000;	(ms) = 15000;	TR = "user defined";
(ms) = 6000;	Shim = "PB-auto";	RF Shims = "fixed";	RF Shims = "fixed";	(ms) = 15000;
RF Shims = "fixed";	PB order = "second";	Shim = "PB-auto";	Shim = "PB-auto";	RF Shims = "fixed";
Shim = "PB-auto";	Water suppression = "excitation";	PB order = "second";	PB order = "second";	Shim = "PB-auto";
PB order = "second";	window (Hz) = 140;	Water suppression = "excitation";	Water suppression = "excitation";	PB order = "second";
Water suppression = "excitation";	second pulse angle = 300;	window (Hz) = 140;	window (Hz) = 140;	Water suppression = "excitation";
window (Hz) = 140;	WS prescan = "auto";	second pulse angle = 300;	second pulse angle = 300;	window (Hz) = 140;
second pulse angle = 300;	BASING pulse = "no";	WS prescan = "auto";	WS prescan = "auto";	second pulse angle = 300;
WS prescan = "auto";	Research prepulse = "no";	BASING pulse = "no";	BASING pulse = "no";	WS prescan = "auto";
BASING pulse = "no";	Pre-saturation = "no";	Research prepulse = "no";	Research prepulse = "no";	BASING pulse = "no";
Research prepulse = "no";	Multi-transmit = "yes";	Pre-saturation = "no";	Pre-saturation = "no";	Research prepulse = "no";
Pre-saturation = "no";	Transmit channels = "both";	Multi-transmit = "yes";	Multi-transmit = "yes";	Pre-saturation = "no";
Multi-transmit = "yes";	SAR mode = "high";	Transmit channels = "both";	Transmit channels = "both";	Multi-transmit = "yes";
Transmit channels = "both";	B1 mode = "default";	SAR mode = "high";	SAR mode = "high";	Transmit channels = "both";
SAR mode = "high";	SAR Patient data = "auto";	B1 mode = "default";	B1 mode = "default";	SAR mode = "high";
B1 mode = "default";	PNS mode = "high";	SAR Patient data = "auto";	SAR Patient data = "auto";	B1 mode = "default";
SAR Patient data = "auto";	Gradient mode = "maximum";	PNS mode = "high";	PNS mode = "high";	SAR Patient data = "auto";
PNS mode = "low";	SofTone mode = "no";	Gradient mode = "maximum";	Gradient mode = "maximum";	PNS mode = "high";
Gradient mode = "default";	Cardiac synchronization = "no";	SofTone mode = "no";	SofTone mode = "no";	Gradient mode = "maximum";
SofTone mode = "no";	Respiratory compensation = "no";	Cardiac synchronization = "no";	Cardiac synchronization = "no";	SofTone mode = "no";
Cardiac synchronization = "no";	Startup acquisitions = 2;	Respiratory compensation = "no";	Respiratory compensation = "no";	Cardiac synchronization = "no";
Respiratory compensation = "no";	NSA = 4;	Startup acquisitions = 2;	Startup acquisitions = 2;	Respiratory compensation = "no";
Startup acquisitions = 2;	Phase cycles = 4;	NSA = 4;	NSA = 4;	Startup acquisitions = 2;
NSA = 16;	Frequency stabilization = "yes";	Phase cycles = 4;	Phase cycles = 4;	NSA = 4;
Phase cycles = 16;	Parameter series = "TI";	Frequency stabilization = "yes";	Frequency stabilization = "yes";	Phase cycles = 4;
Frequency stabilization = "yes";	nr TIs = 7;	Parameter series = "TI";	Parameter series = "TI";	Frequency stabilization = "yes";
Parameter series = "TI";	series spacing = "user def.";	nr TIs = 7;	nr TIs = 7;	Parameter series = "TI";
nr TIs = 5;	TI values (ms) = 170, 1000,	series spacing = "user def.";	series spacing = "user def.";	nr TIs = 7;
series spacing = "user def.";	2000, 3000, 5000, 8000, 10000,	TI values (ms) = 170, 1000,	TI values (ms) = 170, 1000,	series spacing = "user def.";
TI values (ms) = 170, 250,	(121) 0;	2000, 3000, 5000, 8000, 10000,	2000, 3000, 5000, 8000, 10000,	TI values (ms) = 170, 1000,
700, 2500, 5400, (123) 0;	inv. bw (Hz) = 1500;	(121) 0;	(121) 0;	2000, 3000, 5000, 8000, 10000,
inv. bw (Hz) = 1500;				

Column 1	Column 2	Column 3	Column 4	Column 5
inv. offset (Hz) = 0;	inv. offset (Hz) = 0;	inv. bw (Hz) = 1500;	inv. bw (Hz) = 300;	(121) 0;
dummy scans = 1;	dummy scans = 0;	inv. offset (Hz) = 0;	inv. offset (Hz) = 400;	inv. bw (Hz) = 1500;
Manual start = "no";	Manual start = "no";	dummy scans = 0;	dummy scans = 0;	inv. offset (Hz) = 0;
Dynamic study = "no";	Dynamic study = "no";	Manual start = "no";	Manual start = "no";	dummy scans = 0;
Arterial Spin labeling = "no";	Arterial Spin labeling = "no";	Dynamic study = "no";	Dynamic study = "no";	Manual start = "no";
Preparation phases = "full";	Preparation phases = "full";	Arterial Spin labeling = "no";	Arterial Spin labeling = "no";	Dynamic study = "no";
Interactive F0 = "no";	Interactive F0 = "no";	Preparation phases = "full";	Preparation phases = "full";	Arterial Spin labeling = "no";
Receiver optimization = "OFF";	Receiver optimization = "ON";	Interactive F0 = "no";	Interactive F0 = "no";	Preparation phases = "full";
Receiver attenuation = 8;	Spectral correction = "yes";	Receiver optimization = "ON";	Receiver optimization = "ON";	Interactive F0 = "no";
Spectral correction = "yes";	spectral correction NSA = 4;	Spectral correction = "yes";	Spectral correction = "yes";	Receiver optimization = "ON";
spectral correction NSA = 16;	fat supp. on correction = "no";	spectral correction NSA = 4;	spectral correction NSA = 4;	Spectral correction = "yes";
fat supp. on correction = "no";	Reference tissue = "White matter";	fat supp. on correction = "no";	fat supp. on correction = "no";	spectral correction NSA = 4;
Reference tissue = "White matter";	PlanScan metabolite = "NAA";	Reference tissue = "White matter";	Reference tissue = "White matter";	fat supp. on correction = "no";
PlanScan metabolite = "NAA";	Shifted metabolite displayed = "H20";	PlanScan metabolite = "NAA";	PlanScan metabolite = "NAA";	Reference tissue = "White matter";
Shifted metabolite displayed = "H20";	Preset window contrast = "soft";	Shifted metabolite displayed = "Lactate/Lipid";	Shifted metabolite displayed = "Lactate/Lipid";	PlanScan metabolite = "Lactate/Lipid";
Preset window contrast = "soft";	Save raw data = "yes";	Preset window contrast = "soft";	Preset window contrast = "soft";	Shifted metabolite displayed = "NAA";
Save raw data = "yes";	Hardcopy protocol = "no";	Save raw data = "yes";	Save raw data = "yes";	Preset window contrast = "soft";
Hardcopy protocol = "no";	Elliptical k-space shutter = "default";	Hardcopy protocol = "no";	Hardcopy protocol = "no";	Save raw data = "yes";
Elliptical k-space shutter = "default";	IF_info_seperator = 1634755923;	Elliptical k-space shutter = "default";	Elliptical k-space shutter = "default";	Hardcopy protocol = "no";
IF_info_seperator = 1634755923;	Total scan duration = "12:19.6";	IF_info_seperator = 1634755923;	Total scan duration = "17:30.0";	Elliptical k-space shutter = "default";
Total scan duration = "18:48.0";	Act. TR/TE (ms) = "10565 / 28";	Total scan duration = "17:30.0";	Act. TR/TE (ms) = "15000 / 28";	Total scan duration = "17:30.0";
Act. TR/TE (ms) = "6000 / 35";	Min. TR/TE (ms) = "10565 / 28";	Act. TR/TE (ms) = "15000 / 28";	Min. TR/TE (ms) = "10597 / 28";	Act. TR/TE (ms) = "15000 / 288";
Min. TR/TE (ms) = "5973 / 34";	Series TI (ms) =	Min. TR/TE (ms) = "10565 / 28";	Series TI (ms) =	Min. TR/TE (ms) = "10825 / 28";
Series TI (ms) = "170/250/700/2500/5400";	"170/1000/2000/3000/5000/8000/10000";	Series TI (ms) =	"170/1000/2000/3000/5000/8000/10000";	Series TI (ms) =
SPAIR TR (ms) = 5983.22266;	SPAIR TR (ms) = 10548.4795;	"170/1000/2000/3000/5000/8000/10000";	SPAIR TR (ms) = 14983.2227;	"170/1000/2000/3000/5000/8000/10000";
SPAIR inv. delay (ms) = "0.00";	SPAIR inv. delay (ms) = "0.00";	SPAIR TR (ms) = 14983.2227;	SPAIR inv. delay (ms) = "0.00";	SPAIR TR (ms) = 14983.2227;
Spectral resolution (Hz/point) = 1.953125;	Spectral resolution (Hz/point) = 1.953125;	SPAIR inv. delay (ms) = "0.00";	Spectral resolution (Hz/point) = 1.953125;	SPAIR inv. delay (ms) = "0.00";
Readout duration (ms) = 512;	Readout duration (ms) = 512;	Spectral resolution (Hz/point) = 1.953125;	Readout duration (ms) = 512;	Spectral resolution (Hz/point) = 1.953125;
SAR / head = "< 4 %";	SAR / head = "< 2 %";	Readout duration (ms) = 512;	SAR / head = "< 1 %";	Readout duration (ms) = 512;
Whole body / level = "0.0 W/kg / normal";	Whole body / level = "0.0 W/kg / normal";	SAR / head = "< 2 %";	Whole body / level = "0.0 W/kg / normal";	SAR / head = "< 2 %";
SED = " 0.0 kJ/kg";	SED = " 0.0 kJ/kg";	Whole body / level = "0.0 W/kg / normal";	SED = " 0.0 kJ/kg";	Whole body / level = "0.0 W/kg / normal";
B1+rms / Coil Power =	B1+rms / Coil Power =	SED = "	B1+rms / Coil Power =	SED = "

"0.46 uT / 4 %"; Max B1+rms = "0.58 uT"; PNS / level = "33 % / normal"; dB/dt = "17.0 T/s"; Sound Pressure Level (dB) = 0;	"0.35 uT / 2 %"; Max B1+rms = "1.04 uT"; PNS / level = "67 % / normal"; dB/dt = "37.6 T/s"; Sound Pressure Level (dB) = 0;	0.0 kJ/kg"; B1+rms / Coil Power = "0.29 uT / 2 %"; Max B1+rms = "1.04 uT"; PNS / level = "67 % / normal"; dB/dt = "37.6 T/s"; Sound Pressure Level (dB) = 0;	"0.25 uT / 1 %"; Max B1+rms = "1.04 uT"; PNS / level = "67 % / normal"; dB/dt = "37.6 T/s"; Sound Pressure Level (dB) = 0;	0.0 kJ/kg"; B1+rms / Coil Power = "0.29 uT / 2 %"; Max B1+rms = "0.90 uT"; PNS / level = "65 % / normal"; dB/dt = "37.6 T/s"; Sound Pressure Level (dB) = 0;

Table 3: Lactate doublet and quadrouplet sequences parameters.

20/05/15		1/06 – 2/06 – 2/06 2th		2/06 3th - 2/06 4th	
SmartSelect =		SmartSelect =		SmartSelect =	
"yes";		"yes";		"yes";	
Coil 1 (exclude) =	"None";	Coil 1 (exclude) =	"None";	Coil 1 (exclude) =	"None";
VOI orientation =		VOI orientation =		VOI orientation =	
"transverse";		"transverse";		"transverse";	
VOI size AP (mm) =	20;	VOI size AP (mm) =	20;	VOI size AP (mm) =	20;
RL (mm) =	20;	RL (mm) =	20;	RL (mm) =	20;
FH (mm) =	20;	FH (mm) =	20;	FH (mm) =	20;
Samples =	1024;	Samples =	1024;	Samples =	1024;
Spectral BW (Hz) =	2000;	Spectral BW (Hz) =	2000;	Spectral BW (Hz) =	2000;
VOI offc. AP (P=+mm) =		VOI offc. AP (P=+mm) =		VOI offc. AP (P=+mm) =	
0;		0;		0;	
RL (L=+mm) =	0;	RL (L=+mm) =	0;	RL (L=+mm) =	0;
FH (H=+mm) =		FH (H=+mm) =		FH (H=+mm) =	
0;		10;		10;	
VOI ang. AP (deg) =	0;	VOI ang. AP (deg) =	0;	VOI ang. AP (deg) =	0;
RL (deg) =	-0;	RL (deg) =	-0;	RL (deg) =	-0;
FH (deg) =	-0;	FH (deg) =	-0;	FH (deg) =	-0;
Chem. shift Dir AP =	"A";	Chem. shift Dir AP =	"A";	Chem. shift Dir AP =	"A";
Chem. shift Dir LR =	"L";	Chem. shift Dir LR =	"L";	Chem. shift Dir LR =	"L";
Chem. shift Dir FH =	"F";	Chem. shift Dir FH =	"F";	Chem. shift Dir FH =	"F";
Large table movement =		Large table movement =		Large table movement =	
"no";		"no";		"no";	
REST slabs =		REST slabs =		REST slabs =	
0;		0;		0;	
Patient position =	"head first";	Patient position =	"head first";	Patient position =	"head first";
orientation =	"supine";	orientation =	"supine";	orientation =	"supine";
Scan type =		Scan type =		Scan type =	
"Spectroscopy";		"Spectroscopy";		"Spectroscopy";	
Scan mode =		Scan mode =		Scan mode =	
"SV";		"SV";		"SV";	
technique =		technique =		technique =	
"ECHO";		"ECHO";		"ECHO";	
VOI selection =		VOI selection =		VOI selection =	
"volume";		"volume";		"volume";	
method =		method =		method =	
"PRESS";		"PRESS";		"PRESS";	
Gradient Spoiling =	"no";	Gradient Spoiling =	"no";	Gradient Spoiling =	"no";
Fast Imaging mode =	"none";	Fast Imaging mode =	"none";	Fast Imaging mode =	"none";
Echo acquisition =	"half";	Echo acquisition =	"half";	Echo acquisition =	"half";
TE =		TE =		TE =	
"shortest";		"shortest";		"user defined";	
Flip angle (deg) =	90;	Flip angle (deg) =	90;	(ms) =	288;
RF pulse set =		RF pulse set =		Flip angle (deg) =	90;
"normal";		"normal";		RF pulse set =	
TR =		TR =		"normal";	
"shortest";		"user defined";		TR =	
RF Shims =		(ms) =	15000;	"user defined";	
"fixed";		RF Shims =		(ms) =	15000;
Shim =		"fixed";		RF Shims =	
"PB-auto";		Shim =		"fixed";	
PB order =		"PB-auto";		Shim =	
"second";		PB order =		"PB-auto";	
Water suppression =		"second";		PB order =	
"excitation";		Water suppression =		"second";	
window (Hz) =	140;	"excitation";		Water suppression =	
second pulse angle =	300;	window (Hz) =	140;	"excitation";	
WS prescan =		second pulse angle =	300;	window (Hz) =	140;
"auto";		WS prescan =		second pulse angle =	300;
BASING pulse =		"auto";		WS prescan =	
"no";		BASING pulse =		"auto";	
Research prepulse =	"no";	"no";		BASING pulse =	
Pre-saturation =	"no";	Research prepulse =	"no";	"no";	
Multi-transmit =	"yes";	Pre-saturation =	"no";	Research prepulse =	"no";
Transmit channels =	"both";	Multi-transmit =	"yes";	Pre-saturation =	"no";
SAR mode =		Transmit channels =	"both";	Multi-transmit =	"yes";
"high";		SAR mode =		Transmit channels =	"both";
B1 mode =		"high";		SAR mode =	
"default";		B1 mode =		"high";	
SAR Patient data =	"auto";	"default";		B1 mode =	
PNS mode =		SAR Patient data =	"auto";	"default";	
"high";		PNS mode =		SAR Patient data =	"auto";

Gradient mode =	
"maximum";	
SofTone mode =	
"no";	
Cardiac synchronization =	"no";
Respiratory compensation =	"no";
Startup acquisitions =	2;
NSA =	
4;	
Phase cycles =	
4;	
Frequency stabilization =	"yes";
Parameter series =	"TI";
nr TIs =	7;
series spacing =	"user def.";
TI values (ms) =	170, 1000,
2000, 3000, 5000, 8000, 10000,	
(121) 0;	
inv. bw (Hz) =	1500;
inv. offset (Hz) =	0;
dummy scans =	0;
Manual start =	
"no";	
Dynamic study =	
"no";	
Arterial Spin labeling =	"no";
Preparation phases =	"full";
Interactive F0 =	"no";
Receiver optimization =	
"ON";	
Spectral correction =	"yes";
spectral correction NSA =	4;
fat supp. on correction =	"no";
Reference tissue =	"White matter";
PlanScan metabolite =	
"NAA";	
Shifted metabolite displayed =	"H20";
Preset window contrast =	"soft";
Save raw data =	"yes";
Hardcopy protocol =	"no";
Elliptical k-space shutter =	"default";
IF_info_seperator =	
1634755923;	
Total scan duration =	
"12:19.6";	
Act. TR/TE (ms) =	"10565 / 28";
Min. TR/TE (ms) =	"10565 / 28";
Series TI (ms) =	
"170/1000/2000/3000/5000/8000/10000";	
SPAIR TR (ms) =	
10548.4795;	
SPAIR inv. delay (ms) =	"0.00";
Spectral resolution (Hz/point) =	1.953125;
Readout duration (ms) =	512;
SAR / head =	
"< 2 %";	
Whole body / level =	"0.0 W/kg / normal";
SED =	" 0.0 kJ/kg";
B1+rms / Coil Power ="0.35 uT / 2 %";	
Max B1+rms =	"1.04 uT";
PNS / level =	
"67 % / normal";	
dB/dt =	"37.6 T/s";
Sound Pressure Level (dB) =	0;

"high";	
Gradient mode =	
"maximum";	
SofTone mode =	
"no";	
Cardiac synchronization =	"no";
Respiratory compensation =	"no";
Startup acquisitions =	2;
NSA =	
4;	
Phase cycles =	
4;	
Frequency stabilization =	"yes";
Parameter series =	"TI";
nr TIs =	7;
series spacing =	"user def.";
TI values (ms) =	170, 1000,
2000, 3000, 5000, 8000, 10000,	
(121) 0;	
inv. bw (Hz) =	1500;
inv. offset (Hz) =	0;
dummy scans =	0;
Manual start =	
"no";	
Dynamic study =	
"no";	
Arterial Spin labeling =	"no";
Preparation phases =	"full";
Interactive F0 =	"no";
Receiver optimization =	
"ON";	
Spectral correction =	"yes";
spectral correction NSA =	4;
fat supp. on correction =	"no";
Reference tissue =	"White matter";
PlanScan metabolite =	
"NAA";	
Shifted metabolite displayed =	"Lactate/Lipid";
Preset window contrast =	"soft";
Save raw data =	"yes";
Hardcopy protocol =	"no";
Elliptical k-space shutter =	"default";
IF_info_seperator =	
1634755923;	
Total scan duration =	
"17:30.0";	
Act. TR/TE (ms) =	"15000 / 28";
Min. TR/TE (ms) =	"10565 / 28";
Series TI (ms) =	
"170/1000/2000/3000/5000/8000/10000";	
SPAIR TR (ms) =	
14983.2227;	
SPAIR inv. delay (ms) =	"0.00";
Spectral resolution (Hz/point) =	1.953125;
Readout duration (ms) =	512;
SAR / head =	
"< 2 %";	
Whole body / level =	"0.0 W/kg / normal";
SED =	" 0.0 kJ/kg";
B1+rms / Coil Power ="0.29 uT / 2 %";	
Max B1+rms =	"1.04 uT";
PNS / level ="67 % / normal";	
dB/dt =	"37.6 T/s";
Sound Pressure Level (dB) =	0;

PNS mode =	
"high";	
Gradient mode =	
"maximum";	
SofTone mode =	
"no";	
Cardiac synchronization =	"no";
Respiratory compensation =	"no";
Startup acquisitions =	2;
NSA =	
4;	
Phase cycles =	
4;	
Frequency stabilization =	"yes";
Parameter series =	"TI";
nr TIs =	7;
series spacing =	"user def.";
TI values (ms) =	170, 1000,
2000, 3000, 5000, 8000, 10000,	
(121) 0;	
inv. bw (Hz) =	1500;
inv. offset (Hz) =	0;
dummy scans =	0;
Manual start =	
"no";	
Dynamic study =	
"no";	
Arterial Spin labeling =	"no";
Preparation phases =	"full";
Interactive F0 =	"no";
Receiver optimization =	
"ON";	
Spectral correction =	"yes";
spectral correction NSA =	4;
fat supp. on correction =	"no";
Reference tissue =	"White matter";
PlanScan metabolite =	
"Lactate/Lipid";	
Shifted metabolite displayed =	"NAA";
Preset window contrast =	"soft";
Save raw data =	"yes";
Hardcopy protocol =	"no";
Elliptical k-space shutter =	"default";
Total scan duration =	
"17:30.0";	
Act. TR/TE (ms) =	"15000 / 288";
Min. TR/TE (ms) =	"10825 / 28";
Series TI (ms) =	
"170/1000/2000/3000/5000/8000/10000";	
SPAIR TR (ms) =	
14983.2227;	
SPAIR inv. delay (ms) =	"0.00";
Spectral resolution (Hz/point) =	1.953125;
Readout duration (ms) =	512;
SAR / head =	"< 2 %";
Whole body / level = "0.0 W/kg / normal";	
SED =	" 0.0 kJ/kg";
B1+rms / Coil Power ="0.29 uT / 2 %";	
Max B1+rms =	"0.90 uT";
PNS / level =	"65 % / normal";
dB/dt =	"37.6 T/s";
Sound Pressure Level (dB) =	0;

Appendix 3

SPIN-ECHO SEQUENCES PARAMETERS FOR T_2 ESTIMATION

Table 1: Water T2 sequences parameters.

7/03/15	20/05/15	1/06-2/06-2/06 2th
SmartSelect = "yes";	SmartSelect = "yes";	SmartSelect = "yes";
Coil 1 (exclude) = "None";	Coil 1 (exclude) = "None";	Coil 1 (exclude) = "None";
VOI orientation = "transverse";	VOI orientation = "transverse";	VOI orientation = "transverse";
VOI size AP (mm) = 20;	VOI size AP (mm) = 20;	VOI size AP (mm) = 20;
RL (mm) = 20;	RL (mm) = 20;	RL (mm) = 20;
FH (mm) = 20;	FH (mm) = 20;	FH (mm) = 20;
Samples = 1024;	Samples = 1024;	Samples = 1024;
Spectral BW (Hz) = 2000;	Spectral BW (Hz) = 2000;	Spectral BW (Hz) = 2000;
VOI offc. AP (P=+mm) = -5;	VOI offc. AP (P=+mm) = 0;	VOI offc. AP (P=+mm) = 0;
RL (L=+mm) = 0;	RL (L=+mm) = 0;	RL (L=+mm) = 0;
FH (H=+mm) =10;	FH (H=+mm) = 0;	FH (H=+mm) = 10;
VOI ang. AP (deg) = 0;	VOI ang. AP (deg) = 0;	VOI ang. AP (deg) = 0;
RL (deg) = -0;	RL (deg) = -0;	RL (deg) = -0;
FH (deg) = -0;	FH (deg) = -0;	FH (deg) = -0;
Chem. shift Dir AP = "A";	Chem. shift Dir AP = "A";	Chem. shift Dir AP = "A";
Chem. shift Dir LR = "L";	Chem. shift Dir LR = "L";	Chem. shift Dir LR = "L";
Chem. shift Dir FH = "F";	Chem. shift Dir FH = "F";	Chem. shift Dir FH = "F";
Large table movement = "no";	Large table movement = "no";	Large table movement = "no";
REST slabs = 0;	REST slabs = 0;	REST slabs = 0;
Patient position = "head first";	Patient position = "head first";	Patient position = "head first";
orientation = "supine";	orientation = "supine";	orientation = "supine";
Scan type ="Spectroscopy";	Scan type = "Spectroscopy";	Scan type = "Spectroscopy";
Scan mode = "SV";	Scan mode = "SV";	Scan mode = "SV";
technique = "ECHO";	technique = "ECHO";	technique = "ECHO";
VOI selection = "volume";	VOI selection = "volume";	VOI selection = "volume";
method ="PRESS";	method = "PRESS";	method = "PRESS";
Gradient Spoiling = "no";	Gradient Spoiling = "no";	Gradient Spoiling = "no";
Fast Imaging mode = "none";	Fast Imaging mode = "none";	Fast Imaging mode = "none";
Echo acquisition = "half";	Echo acquisition = "half";	Echo acquisition = "half";
Flip angle (deg) = 90;	Flip angle (deg) = 90;	Flip angle (deg) = 90;
RF pulse set = "normal";	RF pulse set = "normal";	RF pulse set = "normal";
TR ="user defined";	TR = "user defined";	TR = "user defined";
(ms) = 4000;	(ms) = 3000;	(ms) = 6000;
RF Shims ="fixed";	RF Shims = "fixed";	RF Shims = "fixed";
Shim = "PB-auto";	Shim = "PB-auto";	Shim = "PB-auto";
PB order ="second";	PB order = "second";	PB order = "second";
Water suppression = "no";	Water suppression = "no";	Water suppression = "no";
BASING pulse = "no";	BASING pulse = "no";	BASING pulse = "no";
Fat suppression = "no";	Fat suppression = "no";	Fat suppression = "no";
Research prepulse = "no";	Research prepulse = "no";	Research prepulse = "no";
Pre-saturation = "no";	Pre-saturation = "no";	Pre-saturation = "no";
Multi-transmit = "yes";	Multi-transmit = "yes";	Multi-transmit = "yes";
Transmit channels = "both";	Transmit channels = "both";	Transmit channels = "both";
SAR mode = "high";	SAR mode = "high";	SAR mode = "high";
B1 mode = "default";	B1 mode = "default";	B1 mode = "default";
SAR Patient data = "auto";	SAR Patient data = "auto";	SAR Patient data = "auto";
PNS mode = "low";	PNS mode = "high";	PNS mode = "high";
Gradient mode = "default";	Gradient mode = "maximum";	Gradient mode = "maximum";
SofTone mode = "no";	SofTone mode = "no";	SofTone mode = "no";
Cardiac synchronization ="no";	Cardiac synchronization = "no";	Cardiac synchronization = "no";
Respiratory compensation ="no";	Respiratory compensation = "no";	Respiratory compensation = "no";
Startup acquisitions = 2;	Startup acquisitions = 2;	Startup acquisitions = 2;
NSA = 16;	NSA = 2;	NSA = 2;
Phase cycles = 16;	Phase cycles = 2;	Phase cycles = 2;
Frequency stabilization ="yes";	Frequency stabilization = "yes";	Frequency stabilization = "yes";
Parameter series = "TE";	Parameter series = "TE";	Parameter series = "TE";
nr TEs = 6;	nr TEs = 8;	nr TEs = 9;
series spacing = "user def.";	series spacing = "user def.";	series spacing = "user def.";
TE values (ms) = 35, 100,150, 300, 400, 700, (122) 0;	TE values (ms) = 30, 100, 200, 400, 800, 1200, 1600, 2000, (120) 0;	TE values (ms) = 30, 100, 200, 400, 800, 1200, 1600, 2000, 3000, (119) 0;
dummy scans = 0;	dummy scans = 0;	dummy scans = 0;
Manual start = "no";	Manual start = "no";	Manual start = "no";
Dynamic study = "no";	Dynamic study = "no";	
Arterial Spin labeling ="no";	Arterial Spin labeling = "no";	
Preparation phases = "full";	Preparation phases = "auto";	

Interactive F0 = "no";	Interactive F0 = "no";	Dynamic study = "no";
Receiver optimization ="OFF";	Receiver optimization = "ON";	Arterial Spin labeling = "no";
Receiver attenuation = 8;	Spectral correction = "yes";	Preparation phases = "full";
Spectral correction = "yes";	spectral correction NSA = 2;	Interactive F0 = "no";
spectral correction NSA = 16;	fat supp. on correction = "no";	Receiver optimization = "ON";
fat supp. on correction ="no";	Reference tissue = "White matter";	Spectral correction = "yes";
Reference tissue ="White matter";	PlanScan metabolite = "H20";	spectral correction NSA = 2;
PlanScan metabolite ="H20";	Shifted metabolite displayed = "none";	fat supp. on correction = "no";
Shifted metabolite displayed =	Preset window contrast = "soft";	Reference tissue = "White matter";
"NAA";	Save raw data = "yes";	PlanScan metabolite = "H20";
Preset window contrast ="soft";	Hardcopy protocol = "no";	Shifted metabolite displayed = "Lactate/Lipid";
Save raw data = "yes";	Elliptical k-space shutter = "default";	Preset window contrast = "soft";
Hardcopy protocol = "no";	IF_info_seperator = 1634755923;	Save raw data = "yes";
Elliptical k-space shutter ="default";	Total scan duration = "02:24.0";	Hardcopy protocol = "no";
IF_info_seperator = 1634755923;	Act. TR/TE (ms) = "3000 / 30";	Elliptical k-space shutter = "default";
Total scan duration = "13:36.0";	Min. TR/TE (ms) = "2536 / 28";	IF_info_seperator = 1634755923;
Act. TR/TE (ms) = "4000 / 35";	Series TE (ms) =	Total scan duration = "05:24.0";
Min. TR/TE (ms) = "1236 / 34";	"30/100/200/400/800/1200/1600/2000";	Act. TR/TE (ms) = "6000 / 30";
Series TE (ms)	Spectral resolution (Hz/point) = 1.953125;	Min. TR/TE (ms) = "3536 / 28";
="35/100/150/300/400/700";	Readout duration (ms) = 512;	Series TE (ms) =
Spectral resolution (Hz/point)	SAR / head = "< 5 %";	"30/100/200/400/800/1200/1600/2000/3000";
=1.953125;	Whole body / level = "0.0 W/kg / normal";	Spectral resolution (Hz/point) = 1.953125;
Readout duration (ms) =512;	SED = " 0.0 kJ/kg";	Readout duration (ms) = 512;
SAR / head = "< 4 %";	B1+rms / Coil Power ="0.52 uT / 5 %";	SAR / head = "< 2 %";
Whole body / level = "0.0 W/kg /	Max B1+rms = "0.53 uT";	Whole body / level = "0.0 W/kg / normal";
normal";	PNS / level ="66 % / normal";	SED = " 0.0
SED = " 0.0 kJ/kg";	dB/dt = "37.6 T/s";	kJ/kg";
B1+rms / Coil Power ="0.45 uT / 4	Sound Pressure Level (dB) = 0;	B1+rms / Coil Power = "0.37 uT / 2 %";
%";		Max B1+rms = "0.37 uT";
Max B1+rms = "0.45 uT";		PNS / level = "66 % / normal";
PNS / level ="33 % / normal";		dB/dt = "37.6 T/s";
dB/dt = "17.0 T/s";		Sound Pressure Level (dB) = 0;
Sound Pressure Level (dB) = 0;		

Table 2: Acetate and Lactate sequences parameters.

7/03	20/05	1/06- 2/06 – 2/06 2th	2/06 3th-2/06 4th, Lactate specific sequence
SmartSelect = "yes";	SmartSelect = "yes";	SmartSelect = "yes";	SmartSelect = "yes";
Coil 1 (exclude) = "None";	Coil 1 (exclude) = "None";	Coil 1 (exclude) = "None";	Coil 1 (exclude) = "None";
VOI orientation = "transverse";	VOI orientation = "transverse";	VOI orientation = "transverse";	VOI orientation = "transverse";
VOI size AP (mm) = 20;	VOI size AP (mm) = 20;	VOI size AP (mm) = 20;	VOI size AP (mm) = 20;
RL (mm) = 20;	RL (mm) = 20;	RL (mm) = 20;	RL (mm) = 20;
FH (mm) = 20;	FH (mm) = 20;	FH (mm) = 20;	FH (mm) = 20;
Samples = 1024;	Samples = 1024;	Samples = 1024;	Samples = 1024;
Spectral BW (Hz) = 2000;	Spectral BW (Hz) = 2000;	Spectral BW (Hz) = 2000;	Spectral BW (Hz) = 2000;
VOI offc. AP (P=+mm) = -5;	VOI offc. AP (P=+mm) = 0;	VOI offc. AP (P=+mm) = 0;	VOI offc. AP (P=+mm) = 0;
RL (L=+mm) = 0;	RL (L=+mm) = 0;	RL (L=+mm) = 0;	RL (L=+mm) = 0;
FH (H=+mm) = 10;	FH (H=+mm) = 0;	FH (H=+mm) = 10;	FH (H=+mm) = 10;
VOI ang. AP (deg) = 0;	VOI ang. AP (deg) = 0;	VOI ang. AP (deg) = 0;	VOI ang. AP (deg) = 0;
RL (deg) = -0;	RL (deg) = -0;	RL (deg) = -0;	RL (deg) = -0;
FH (deg) = -0;	FH (deg) = -0;	FH (deg) = -0;	FH (deg) = -0;
Chem. shift Dir AP = "A";	Chem. shift Dir AP = "A";	Chem. shift Dir AP = "A";	Chem. shift Dir AP = "A";
Chem. shift Dir LR = "L";	Chem. shift Dir LR = "L";	Chem. shift Dir LR = "L";	Chem. shift Dir LR = "L";
Chem. shift Dir FH = "F";	Chem. shift Dir FH = "F";	Chem. shift Dir FH = "F";	Chem. shift Dir FH = "F";
Large table movement ="no";	Large table movement = "no";	Large table movement = "no";	Large table movement = "no";
REST slabs =0;	REST slabs = 0;	REST slabs = 0;	REST slabs = 0;
Patient position ="head first"; orientation = "supine";	Patient position = "head first"; orientation = "supine";	Patient position = "head first"; orientation = "supine";	Patient position = "head first"; orientation = "supine";
Scan type ="Spectroscopy";	Scan type = "Spectroscopy";	Scan type = "Spectroscopy";	Scan type = "Spectroscopy";
Scan mode ="SV"; technique = "ECHO";	Scan mode = "SV"; technique = "ECHO";	Scan mode = "SV"; technique = "ECHO";	Scan mode = "SV"; technique = "ECHO";
VOI selection = "volume"; method ="PRESS";	VOI selection = "volume"; method = "PRESS";	VOI selection = "volume"; method = "PRESS";	VOI selection = "volume"; method = "PRESS";
Gradient Spoiling = "no";	Gradient Spoiling = "no";	Gradient Spoiling = "no";	Gradient Spoiling = "no";
Fast Imaging mode = "none";	Fast Imaging mode = "none";	Fast Imaging mode = "none";	Fast Imaging mode = "none";
Echo acquisition = "half";	Echo acquisition = "half";	Echo acquisition = "half";	Echo acquisition = "half";
Flip angle (deg) = 90;	Flip angle (deg) = 90;	Flip angle (deg) = 90;	Flip angle (deg) = 90;
RF pulse set ="normal";	RF pulse set = "normal";	RF pulse set = "normal";	RF pulse set = "normal";
TR ="user defined"; (ms) = 4000;	TR = "user defined"; (ms) = 3000;	TR = "user defined"; (ms) = 6000;	TR = "user defined"; (ms) = 6000;
RF Shims ="fixed";	RF Shims = "fixed";	RF Shims = "fixed";	RF Shims = "fixed";
Shim = "PB-auto"; PB order = "second";	Shim = "PB-auto"; PB order = "second";	Shim = "PB-auto"; PB order = "second";	Shim = "PB-auto"; PB order = "second";
Water suppression ="excitation"; window (Hz) = 140; second pulse angle = 300;	Water suppression = "excitation";	Water suppression = "excitation";	Water suppression = "excitation";
WS prescan = "auto";			
BASING pulse = "no";			
Fat suppression = "no";			
Research prepulse = "no";			

Column 1:

Pre-saturation =
        "no";
Multi-transmit =
        "yes";
Transmit channels =
        "both";
SAR mode ="high";
B1 mode =
        "default";
SAR Patient data =
        "auto";
PNS mode ="low";
Gradient mode =
        "default";
SofTone mode ="no";
Cardiac synchronization =
        "no";
Respiratory compensation ="no";
Startup acquisitions =
        2;
NSA =   16;
Phase cycles =16;
Frequency stabilization =
        "yes";
Parameter series =
        "TE";
  nr TEs =6;
  series spacing =
        "user def.";
  TE values (ms) =35, 100,150,
300, 400, 700, (122) 0;
  dummy scans =0;
Manual start ="no";
Dynamic study ="no";
Arterial Spin labeling =
        "no";
Preparation phases =
        "full";
Interactive F0 ="no";
Receiver optimization =
        "OFF";
Receiver attenuation =
        8;
Spectral correction =
        "yes";
  spectral correction NSA =
        16;
  fat supp. on correction ="no";
Reference tissue ="White matter";
PlanScan metabolite =
        "NAA";
Shifted metabolite displayed
="H20";
Preset window contrast =
        "soft";
Save raw data =
        "yes";
Hardcopy protocol =
        "no";
Elliptical k-space shutter =
        "default";
IF_info_seperator =1634755923;
Total scan duration ="13:36.0";
Act. TR/TE (ms) ="4000 / 35";
Min. TR/TE (ms) ="1396 / 34";
Series TE (ms) =
        "35/100/150/300/400/7
00";
Spectral resolution (Hz/point)
=1.953125;
Readout duration (ms) =
        512;
SAR / head ="< 4 %";
Whole body / level ="0.0 W/kg /
normal";
SED =" 0.0 kJ/kg";
B1+rms / Coil Power ="0.46 uT /

Column 2:

window (Hz) =
        140;
  second pulse angle =
        300;
WS prescan =
        "auto";
BASING pulse =
        "no";
Fat suppression =
        "no";
Research prepulse =
        "no";
Pre-saturation =
        "no";
Multi-transmit =
        "yes";
Transmit channels =
        "both";
SAR mode =
        "high";
B1 mode =
        "default";
SAR Patient data =
        "auto";
PNS mode =
        "high";
Gradient mode =
        "maximum";
SofTone mode =
        "no";
Cardiac synchronization =
        "no";
Respiratory compensation =
        "no";
Startup acquisitions =
        2;
NSA =
        8;
Phase cycles =
        8;
Frequency stabilization =
        "yes";
Parameter series =
        "TE";
  nr TEs =
        8;
  series spacing =
        "user def.";
  TE values (ms) =
        30, 100,

        200, 400, 800, 1200,
1600,

        2000, (120) 0;
  dummy scans =
        0;
Manual start =
        "no";
Dynamic study =
        "no";
Arterial Spin labeling =
        "no";
Preparation phases =
        "full";
Interactive F0 =
        "no";
Receiver optimization =
        "ON";
Spectral correction =
        "yes";
  spectral correction NSA =
        8;
  fat supp. on correction =
        "no";
Reference tissue =
        "White matter";

Column 3:

window (Hz) =
        140;
  second pulse angle =
        300;
WS prescan =
        "auto";
BASING pulse =
        "no";
Fat suppression =
        "no";
Research prepulse =
        "no";
Pre-saturation =
        "no";
Multi-transmit =
        "yes";
Transmit channels =
        "both";
SAR mode =
        "high";
B1 mode =
        "default";
SAR Patient data =
        "auto";
PNS mode =
        "high";
Gradient mode =
        "maximum";
SofTone mode =
        "no";
Cardiac synchronization =
        "no";
Respiratory compensation =
        "no";
Startup acquisitions =
        2;
NSA =
        16;
Phase cycles =
        16;
Frequency stabilization =
        "yes";
Parameter series =
        "TE";
  nr TEs =
        9;
  series spacing =
        "user def.";
  TE values (ms) =
        30, 100,

        200, 400, 800, 1200,
1600,

        2000, 3000, (119) 0;
  dummy scans =
        0;
Manual start =
        "no";
Dynamic study =
        "no";
Arterial Spin labeling =
        "no";
Preparation phases =
        "full";
Interactive F0 =
        "no";
Receiver optimization =
        "ON";
Spectral correction =
        "yes";
  spectral correction NSA =
        16;
  fat supp. on correction =
        "no";
Reference tissue =
        "White matter";

Column 4:

window (Hz) =
        140;
  second pulse angle =
        300;
WS prescan =
        "auto";
BASING pulse =
        "no";
Fat suppression =
        "no";
Research prepulse =
        "no";
Pre-saturation =
        "no";
Multi-transmit =
        "yes";
Transmit channels =
        "both";
SAR mode =
        "high";
B1 mode =
        "default";
SAR Patient data =
        "auto";
PNS mode =
        "high";
Gradient mode =
        "maximum";
SofTone mode =
        "no";
Cardiac synchronization =
        "no";
Respiratory compensation =
        "no";
Startup acquisitions =
        2;
NSA =
        16;
Phase cycles =
        16;
Frequency stabilization =
        "yes";
Parameter series =
        "TE";
  nr TEs =
        9;
  series spacing =
        "user def.";
  TE values (ms) =
        29, 288,

        576, 864, 1152, 1440,
1728,

        2304, 2880, (119) 0;
  dummy scans =
        0;
Manual start =
        "no";
Dynamic study =
        "no";
Arterial Spin labeling =
        "no";
Preparation phases =
        "full";
Interactive F0 =
        "no";
Receiver optimization =
        "ON";
Spectral correction =
        "yes";
  spectral correction NSA =
        16;
  fat supp. on correction =
        "no";
Reference tissue =
        "White matter";

4 %"; Max B1+rms ="0.46 uT"; PNS / level ="33 % / normal"; dB/dt = "17.0 T/s"; Sound Pressure Level (dB) = 0;	PlanScan metabolite = "NAA"; Shifted metabolite displayed = "H20"; Preset window contrast = "soft"; Save raw data = "yes"; Hardcopy protocol = "no"; Elliptical k-space shutter = "default"; IF_info_seperator = 1634755923; Total scan duration = "07:12.0"; Act. TR/TE (ms) = "3000 / 30"; Min. TR/TE (ms) = "2696 / 28"; Series TE (ms) = "30/100/200/400/800/1200/1600/2000"; Spectral resolution (Hz/point) = 1.953125; Readout duration (ms) =512; SAR / head = "< 5 %"; Whole body / level = "0.0 W/kg / normal"; SED = " 0.0 kJ/kg"; B1+rms / Coil Power = "0.53 uT / 5 %"; Max B1+rms = "0.53 uT"; PNS / level ="66 % / normal"; dB/dt = "37.6 T/s"; Sound Pressure Level (dB) = 0;	PlanScan metabolite = "NAA"; Shifted metabolite displayed = "Lactate/Lipid"; Preset window contrast = "soft"; Save raw data = "yes"; Hardcopy protocol = "no"; Elliptical k-space shutter = "default"; IF_info_seperator = 1634755923; Total scan duration = "30:36.0"; Act. TR/TE (ms) = "6000 / 30"; Min. TR/TE (ms) = "3696 / 28"; Series TE (ms) = "30/100/200/400/800/1200/1600/2000/3000"; Spectral resolution (Hz/point) = 1.953125; Readout duration (ms) = 512; SAR / head = "< 3 %"; Whole body / level = "0.0 W/kg / normal"; SED = " 0.0 kJ/kg"; B1+rms / Coil Power = "0.37 uT / 3 %"; Max B1+rms = "0.37 uT"; PNS / level = "66 % / normal"; dB/dt = "37.6 T/s"; Sound Pressure Level (dB) = 0;	PlanScan metabolite = "Lactate/Lipid"; Shifted metabolite displayed = "NAA"; Preset window contrast = "soft"; Save raw data = "yes"; Hardcopy protocol = "no"; Elliptical k-space shutter = "default"; Total scan duration = "30:36.0"; Act. TR/TE (ms) = "6000 / 29"; Min. TR/TE (ms) = "3576 / 28"; Series TE (ms) = "29/288/576/864/1152/1440/1728/2304/2880"; Spectral resolution (Hz/point) = 1.953125; Readout duration (ms) = 512; SAR / head = "< 3 %"; Whole body / level = "0.0 W/kg / normal"; SED = " 0.0 kJ/kg"; B1+rms / Coil Power = "0.37 uT / 3 %"; Max B1+rms = "0.37 uT"; PNS / level = "66 % / normal"; dB/dt = "37.6 T/s"; Sound Pressure Level (dB) = 0;

Appendix 4

SEQUENCES PARAMETERS FOR METABOLITES QUANTITATION OF SIEMENS PHANTOM AT MEYER

Table 1: PRESS sequences for quantitation of metabolites in the Siemens phantom.

Water		Metabolites	
Data file name: DBIEX_6_2_RAW_act.sdat		Data file name: DBIEX_7_2_RAW_act.sdat	
SmartSelect =	"yes";	SmartSelect =	"yes";
Coil 1 (exclude) =	"None";	Coil 1 (exclude) =	"None";
VOI orientation =	"transverse";	VOI orientation =	"transverse";
VOI size AP (mm) =	20;	VOI size AP (mm) =	20;
RL (mm) =	20;	RL (mm) =	20;
FH (mm) =	20;	FH (mm) =	20;
Samples =	1024;	Samples =	1024;
Spectral BW (Hz) =	2000;	Spectral BW (Hz) =	2000;
VOI offc. AP (P=+mm) =	-5;	VOI offc. AP (P=+mm) =	-5;
RL (L=+mm) =	0;	RL (L=+mm) =	0;
FH (H=+mm) =	10;	FH (H=+mm) =	10;
VOI ang. AP (deg) =	0;	VOI ang. AP (deg) =	0;
RL (deg) =	-0;	RL (deg) =	-0;
FH (deg) =	-0;	FH (deg) =	-0;
Chem. shift Dir AP =	"A";	Chem. shift Dir AP =	"A";
Chem. shift Dir LR =	"L";	Chem. shift Dir LR =	"L";
Chem. shift Dir FH =	"F";	Chem. shift Dir FH =	"F";
Large table movement =	"no";	Large table movement =	"no";
REST slabs =	0;	REST slabs =	0;
Patient position =	"head first";	Patient position =	"head first";
orientation =	"supine";	orientation =	"supine";
Scan type =	"Spectroscopy";	Scan type =	"Spectroscopy";
Scan mode =	"SV";	Scan mode =	"SV";
technique =	"ECHO";	technique =	"ECHO";
VOI selection =	"volume";	VOI selection =	"volume";
method =	"PRESS";	method =	"PRESS";
Gradient Spoiling =	"no";	Gradient Spoiling =	"no";
Fast Imaging mode =	"none";	Fast Imaging mode =	"none";
Echo acquisition =	"half";	Echo acquisition =	"half";
TE =	"user defined";	TE =	"user defined";
(ms) =	35;	(ms) =	35;
Flip angle (deg) =	90;	Flip angle (deg) =	90;
RF pulse set =	"normal";	RF pulse set =	"normal";
TR =	"user defined";	TR =	"user defined";
(ms) =	4000;	(ms) =	4000;
RF Shims =	"fixed";	RF Shims =	"fixed";
Shim =	"PB-auto";	Shim =	"PB-auto";
PB order =	"second";	PB order =	"second";
Water suppression =	"no";	Water suppression =	"excitation";
BASING pulse =	"no";	window (Hz) =	140;
Fat suppression =	"no";	second pulse angle =	300;
Research prepulse =	"no";	WS prescan =	"auto";
Pre-saturation =	"no";	BASING pulse =	"no";
Multi-transmit =	"yes";	Fat suppression =	"no";
Transmit channels =	"both";	Research prepulse =	"no";
SAR mode =	"high";	Pre-saturation =	"no";
B1 mode =	"default";	Multi-transmit =	"yes";
SAR Patient data =	"auto";	Transmit channels =	"both";
PNS mode =	"low";	SAR mode =	"high";
Gradient mode =	"default";	B1 mode =	"default";
SofTone mode =	"no";	SAR Patient data =	"auto";
Cardiac synchronization =	"no";	PNS mode =	"low";
Respiratory compensation =	"no";	Gradient mode =	"default";
Startup acquisitions =	2;	SofTone mode =	"no";
NSA =	16;	Cardiac synchronization =	"no";
Phase cycles =	16;	Respiratory compensation =	"no";
Frequency stabilization =	"yes";	Startup acquisitions =	2;
Parameter series =	"no";	NSA =	16;
Manual start =	"no";	Phase cycles =	16;
Dynamic study =	"no";	Frequency stabilization =	"yes";
Arterial Spin labeling =	"no";	Parameter series =	"no";
Preparation phases =	"full";	Manual start =	"no";

```
Interactive F0 =                "no";            Dynamic study =                      "no";
Receiver optimization =              "OFF";      Arterial Spin labeling =        "no";
Receiver attenuation =            8;             Preparation phases =            "full";
Spectral correction =        "yes";             Interactive F0 =                "no";
   spectral correction NSA =  16;               Receiver optimization =              "OFF";
   fat supp. on correction =  "no";             Receiver attenuation =            8;
Reference tissue =           "White matter";    Spectral correction =        "yes";
PlanScan metabolite =            "H20";             spectral correction NSA =  16;
Shifted metabolite displayed =  "NAA";             fat supp. on correction =  "no";
Preset window contrast =     "soft";            Reference tissue =           "White matter";
Save raw data =                  "yes";         PlanScan metabolite =                "NAA";
Hardcopy protocol =          "no";              Shifted metabolite displayed =  "H20";
Elliptical k-space shutter = "default";         Preset window contrast =     "soft";
IF_info_seperator =          1634755923;        Save raw data =                      "yes";
Total scan duration =        "02:16.0";         Hardcopy protocol =          "no";
Act. TR/TE (ms) =            "4000 / 35";        Elliptical k-space shutter = "default";
Min. TR/TE (ms) =            "571 / 34";         IF_info_seperator =          1634755923;
Spectral resolution (Hz/point) = 1.953125;      Total scan duration =        "02:16.0";
Readout duration (ms) =           512;          Act. TR/TE (ms) =            "4000 / 35";
SAR / head =                 "<  4 %";          Min. TR/TE (ms) =            "731 / 34";
Whole body / level =         "0.0 W/kg / normal"; Spectral resolution (Hz/point) = 1.953125;
SED =                        "  0.0 kJ/kg";     Readout duration (ms) =           512;
B1+rms / Coil Power =        "0.45 uT / 4 %";   SAR / head =                 "<  4 %";
Max B1+rms =                 "0.45 uT";         Whole body / level =         "0.0 W/kg / normal";
PNS / level =                "33 % / normal";   SED =                        "  0.0 kJ/kg";
dB/dt =                      "17.0 T/s";        B1+rms / Coil Power =        "0.46 uT / 4 %";
Sound Pressure Level (dB) =  0;                 Max B1+rms =                 "0.46 uT";
                                                PNS / level =                "33 % / normal";
                                                dB/dt =                      "17.0 T/s";
                                                Sound Pressure Level (dB) =  0;
```

ABOUT THE AUTHORS

Andrea Barucci received his degree in Physics from the University of Florence in September 2006, and in 2011 he received the PhD in Electronic Engineering Systems. At the moment he is a researcher at the "Nello Carrara" Institute of Applied Physics (IFAC, Via Madonna del Piano 10, 50019 Sesto F.no – Firenze, Italy) that is part of the National Research Council (CNR). From 2010 to 2015 he has worked on applications of biosensors to nanomedicine, focusing on fabrication techniques and computer modeling. In July 2015 he received the title of Medical Physicist from the School on Medical Physics at the faculty of Medicine and Surgery (University of Florence).

He is actually working on biomolecular functional Nuclear Magnetic Resonance Imaging (MRS, DWI, DTI, FMRI, TBSS) in clinical practice.

Roberto Carpi, Clinician Radiologist, Director of Radiologia Santa Maria Nuova (Piazza S.Maria Nuova, 1 - 50123 Firenze), USL Toscana Centro.

Antonio Ciccarone, Medical Physicist, Qualified Radiation Protection Expert II° and MR Safety Expert, expert in advanced MRI tecniques and part of the Medical Physics Unit at the Meyer Children University Hospital (Viale Pieraccini 24, 50139 Firenze – Italy).

Marco Espostito, Medical Physicist, expert in MRI advanced techniques and clinical radiotherapy, he is actually working at the "Ospedale Santa Maria Annunziata" (Via dell'Antella, 58 - 50012 Ponte a Niccheri - Bagno a Ripoli - Firenze), as a part of the regional structure of "Fisica Sanitaria", Piazza S.Maria Nuova, 1 - 50123 Firenze, USL Toscana Centro

Maristella Olmastroni, Clinician Radiologist, expert in clinical MRI and UltraSound techniques, he is actually working at the "Ospedale Santa Maria Nuova" (Piazza S.Maria Nuova, 1 - 50123 Firenze), USL Toscana Centro.

Giovanna Zatelli, Medical Physicist, Director of the structure " SOC Fisica Sanitaria" (Piazza S.Maria Nuova, 1 - 50123 Firenze), USL Toscana Centro.